

OPTIMAL AND ROBUST SWITCHING CONTROL STRATEGIES:
THEORY, AND APPLICATIONS IN TRAFFIC MANAGEMENT

**OPTIMAL AND ROBUST SWITCHING CONTROL STRATEGIES:
THEORY, AND APPLICATIONS IN TRAFFIC MANAGEMENT**

Proefschrift

ter verkrijging van de graad van doctor
aan de Technische Universiteit Delft,
op gezag van de Rector Magnificus prof. ir. K.C.A.M. Luyben,
voorzitter van het College voor Promoties,
in het openbaar te verdedigen op maandag 20 April 2015 om 10:00 uur

door

Mohammadreza HAJIAHMADI

Master of Science in Electrical Engineering,
Amirkabir University of Technology,
geboren te Isfahan, Iran.

This dissertation has been approved by the promotor:

Prof. dr. ir. B. De Schutter
Prof. dr. ir. J. Hellendoorn

Composition of the doctoral committee:

Rector Magnificus	voorzitter
Prof. dr. ir. B. De Schutter	Technische Universiteit Delft, promotor
Prof. dr. ir. J. Hellendoorn	Technische Universiteit Delft, promotor
Prof. dr. J. Daafouz	Institut National Polytechnique de Lorraine
Prof. dr. N. Geroliminis	École Polytechnique Fédérale de Lausanne
Prof. dr. ir. W.P.M.H Heemels	Technische Universiteit Eindhoven
Prof. dr. ir. J.H. van Schuppen	Technische Universiteit Delft
Prof. dr. ir. S.P. Hoogendoorn	Technische Universiteit Delft

disc

This dissertation has been completed in partial fulfillment of the requirements of the Dutch Institute of Systems and Control (DISC) for graduate studies. The support of the BSIK project “Next Generation Infrastructure (NGI)” is gratefully acknowledged, as well as the support of the European Union COST Actions TU1102 and TU0702, and the European Union 7th Framework Network of Excellence “Highly-complex and networked control systems (HYCON2)”.

ISBN: 978-94-6186-442-0

Copyright © 2015 by Mohammad Hajiahmadi

All rights reserved. No part of the material protected by this copyright notice may be reproduced or utilized in any form or by any means, electronics or mechanical, including photocopying, recording or by any information storage and retrieval system, without written permission of the author.

Printed in the Netherlands

Author's email: mohamadreza.ha@gmail.com

PREFACE

This thesis is the result of my four years of work in the Delft Center for Systems and Control. Despite all the ups and downs, I must say I have enjoyed most of my time and looking from outside, it has been probably the most productive and fruitful period of my life. And this has not been possible without the help and support I have received from many people during these four years.

The first person I wish to thank is Bart, to whom I am grateful for being my promotor and supervisor and for giving me the trust, support and the freedom in choosing my own way of doing research and for giving me the opportunity to go on research visits. Also, Bart, I am thankful for being allowed to occasionally violate your *first things first* rule and work on my favorite topics. Also, I admire your availability to discuss research problems even past midnight on Sundays.

I would also like to thank my second promotor Hans Hellendoorn. I appreciate your help in having a vision, a sense of the bigger picture, viewing the whole and not just focusing on small parts. Also, I am very grateful for your confidence in me and for keeping me motivated through these 4 years. Furthermore, I am thankful to you and Bart for spending your valuable time on reviewing my thesis draft.

I do extend my appreciation to Prof. Nikolas Geroliminis at EPFL, Switzerland, for hosting me for about four months. I would like to thank you for your advices and support during my stay in EPFL and also for accepting to be my committee member. Moreover, I am grateful for our valuable scientific collaboration we had together with Dr. Jack Haddad. I learned a lot from you guys.

I am also grateful to Prof. Chris Tampère and Dr. Ruben Corthout for arranging my short visits to the Katholieke Universiteit Leuven (KU Leuven). Also, I would like to thank Goof van de Weg and Dr. Andreas Hegyi who have helped me a lot to finish the LTM project initiated in my first year of PhD in Leuven and successfully led to nice results which are presented in this thesis. Particularly, Goof, I highly appreciate your technical support and your patience and perseverance in this project. Furthermore, I would also like to thank Dr. Victor Knoop for the nice collaboration we had. Unfortunately, I kept being occupied with other tasks which prevented me from extending our work. Hopefully, now I can refresh my mind and explore more in our joint work.

I would like to thank my committee members, Prof. Jan van Schuppen, Prof. Jamal Daafouz, Prof. Maurice Heemels, Prof. Nikolas Geroliminis and Prof. Serge Hoogendoorn for their constructive comments and suggestions that helped me to improve my dissertation in the final stage.

I am truly grateful to all my friends and colleagues at DCSC, especially to Yashar, Amir, Farid, Alfredo, Bart, Dieky, Edwin, Elisabeth, Hans V., Ilya, Jia, Le, Marco, Max, Noor, Reinier, Renshi, Ruxandra, Subo, Sachin, Sadegh, Samira, Yue, Zhe, and Zhou for letting me have unforgettable great memories during our badminton sessions, table football competitions, road trips, game nights, and surprise birthday parties ;). Moreover, I especially thank Bart for translating my summary and propositions into Dutch,

Le and Yashar for accepting to present my work at conferences, Subo, Sadegh, Amir and Yashar for helping me with moving to my new house. Here I would also like to thank our secretaries (Kitty, Heleen, Esther, Marieke, Saskia) for being very kind and helpful.

I would like to use this opportunity to thank my parents and my brother and sister, for all the love and for supporting my decision of a life far from home. Last but not least, my special thanks to my beloved wife Mahya, for her unreserved love and care.

Mohammad Hajiahmadi
Den Haag, April 2015

CONTENTS

1	Introduction	1
1.1	Motivation of the Research	1
1.2	Research Goals and Main Contributions	5
1.3	Structure of the Thesis	6
	Part I: Modeling and Control of Traffic Networks	9
2	Background on Traffic Flow Modeling and Control	11
2.1	Control Objectives and Challenges	12
2.2	Freeway Traffic Networks	13
2.2.1	Basic Concepts and Elements of Modeling.	13
2.2.2	Overview of Existing Control Approaches	16
2.3	Urban Traffic Networks	20
2.3.1	Basic Concepts and Elements of Modeling.	20
2.3.2	Overview of Existing Control Approaches	22
2.4	Summary	25
3	Integrated Predictive Freeway Control Using the Link Transmission Model	27
3.1	Introduction	28
3.2	Link Transmission Model	28
3.2.1	Link Model.	29
3.2.2	Node Models.	29
3.2.3	Update Equations	31
3.3	Extensions of the LTM.	31
3.3.1	Ramp Metering	31
3.3.2	Variable Speed Limit Control.	32
3.4	Predictive Hybrid Freeway Traffic Control.	36
3.4.1	Nonlinear Model Predictive Control Formulation	36
3.4.2	Reformulation of the Link Transmission Model	37
3.4.3	Mixed Integer Linear Optimization Problem	41
3.5	Case Study	41
3.5.1	Set-Up	41
3.5.2	Identification and Calibration of the LTM	43
3.5.3	Micro-Simulation and Predictive Control of the Leuven Corridor	44
3.6	Concluding Remarks	53
4	Optimal Hybrid Control for Urban Traffic Networks	55
4.1	Introduction	56
4.2	MFD-Based Modeling of Urban Regions	57
4.3	Optimal Hybrid Control for a Multi-Region Urban Network.	58
4.3.1	Hybrid Control: Perimeter and Switching Controllers	58

4.3.2	Hybrid Multi-Region Model	58
4.3.3	Optimal Control Problem Formulation	59
4.4	Approximation of the Hybrid Multi-Region Model	61
4.4.1	First Approach: PWA Approximation Plus Forward Simulation.	62
4.4.2	Second Approach: Recasting 2-Dimensional PWA Approximation	64
4.5	Reformulation as a Mixed Integer Linear Optimization Problem	65
4.6	Case Studies	67
4.6.1	Set-up	68
4.6.2	Performance Evaluation of Nonlinear Approach	69
4.6.3	Performance Evaluation of Approximation Approaches	70
4.6.4	Robustness to Measurement Errors and Uncertain Demands	73
4.7	Concluding Remarks	80
5	Optimal Dynamic Region-Based Route Guidance	83
5.1	Introduction	84
5.2	Multi-Region Macroscopic Modeling	84
5.3	Multi-Level Optimal Route Guidance	87
5.3.1	Objective Function and Constraints	87
5.3.2	Model Predictive Control for High-Level Route Guidance	88
5.4	Case Study	89
5.4.1	Set-Up	90
5.4.2	Results and Discussion.	91
5.5	Concluding Remarks	92
	Part II: Robust Stabilization of Switched Systems	95
6	Background on Analysis and Control of Switched Systems	97
6.1	Definition and Classification of Switched Systems	98
6.2	Stability Analysis for Continuous-Time Switched Linear Systems	99
6.2.1	Stability under Arbitrary Switching.	99
6.2.2	Stability Analysis under Dwell Time Constraint	100
6.2.3	Robust Stabilization of Switched Linear Systems.	102
6.3	Stability Analysis and Stabilization of Switched Nonlinear Systems	105
6.4	Summary	108
7	Stabilization and Robust H_∞ Control for Switched Nonlinear Systems	109
7.1	Introduction	110
7.2	Problem Statement	110
7.3	Stabilization in the Absence of Disturbances	111
7.4	Disturbance Attenuation via State-Based Switching.	114
7.4.1	L_2 -gain.	114
7.4.2	Robust H_∞ Switching Control Design	115
7.5	Case Study	117
7.5.1	Set-Up	117
7.5.2	Results and Discussion.	119
7.6	Concluding Remarks	120

8	Robust Control for Sector-Bounded Switched Nonlinear Systems	123
8.1	Introduction	124
8.2	Problem Statement	125
8.3	Stability Analysis under Arbitrary Switching.	126
8.4	Stability Analysis with Average Dwell Time	128
8.5	Design of Robust Stabilizing Switching Laws	129
8.5.1	Stabilization Using Multiple Lyapunov Functions	130
8.5.2	Robust H_∞ Switching Control Design	131
8.6	Case Studies	137
8.6.1	Example 1	137
8.6.2	Example 2	138
8.7	Concluding Remarks	141
9	Stabilization and Robust Control for Mixed Switching Affine Systems	143
9.1	Introduction	144
9.2	Problem Statement	145
9.3	Stabilization Using State-Based Switching	146
9.4	Robust Switching Control Design for L_2 -gain Minimization.	153
9.5	Stabilization of the Original Switched Nonlinear System	158
9.6	Case Studies	160
9.6.1	Example 1	160
9.6.2	Example 2	161
9.6.3	Example 3	163
9.7	Concluding Remarks	168
10	Conclusions and Recommendations	169
10.1	Conclusions.	169
10.2	Recommendations for Future Research	171
	Bibliography	177
	Summary	197
	Samenvatting	199
	List of Publications	201
	Curriculum Vitæ	203

1

INTRODUCTION

The main aim of this dissertation is to develop efficient optimal and robust control strategies for stabilization and disturbance attenuation of hybrid and switched systems in general and for control and management of freeway and urban traffic networks, as particular cases of hybrid systems. This introductory chapter presents the motivation of this research starting from the congestion control problem in traffic networks. We further briefly sketch our approaches and the main contributions, which will be extensively elaborated throughout the thesis. Finally, we conclude this chapter with the explanation of the organization of other chapters.

1.1. MOTIVATION OF THE RESEARCH

THIS thesis is divided into two parts, macroscopic modeling and control of traffic networks and robust control of switched systems. The two parts are closely connected via the traffic models we develop in the first part and the traffic control objectives.

1.1.1. MACROSCOPIC MODELING AND CONTROL OF TRAFFIC NETWORKS

With an increasing number of vehicles and limited infrastructure, government authorities, transportation companies, and traffic researchers have concentrated their efforts on using the currently available resources in order to improve the travel conditions. The aim of almost all the traffic control research projects has been developing efficient control strategies to reduce congestion and to improve travel time in the one of the most complex physical systems, i.e. traffic networks.

Over the past hundred years, traffic control has been developed from fixed-time control approaches to traffic-responsive methods [159, 203], from model-free [18, 48, 186] to model-based control [104, 138, 187], from heuristic solutions [18, 219] to more advanced mathematical approaches such as optimization-based control schemes [3, 71, 138]. The traffic control goals have been extended from controlling isolated urban intersections [84] or individual freeway on-ramps [184] to larger urban areas with multiple intersections [2] or long freeway stretches with several on-ramps and off-ramps [187].

As a first solution for the traffic management problem, fixed-time signal control was used at individual intersections [232]. The fixed duration for the green phase was obtained using historical traffic data. However, since the fixed-time control approach does not use any feedback traffic data, it cannot adapt itself to the altering traffic conditions. Therefore, the focus was turned towards traffic-responsive control methods. Taking advantage of traffic measurement devices such as loop detectors, GPS data and video cameras, feedback control strategies started to develop and become popular. The feedback structure allows the traffic-responsive approaches to adapt their control actions based on the current traffic conditions.

Nevertheless, the traffic-responsive control methods relied only on historical data and the current traffic situation. There was no future traffic perspective and prediction that would help with more effective decisions. Therefore, traffic experts started developing traffic control methods that take advantage of models describing the traffic behavior. Various models to represent the traffic phenomena, from the travel behavior of individual vehicles to the flow dynamics of groups of vehicles traveling in freeway or urban networks have been proposed [156, 156, 220]. The traffic models can be used to simulate a network and to predict the future traffic states.

Model-based methods that utilize optimization algorithms to make optimal control decisions have been developed in recent years [2, 12, 19, 96, 104, 139, 140, 153, 187]. Optimal control theory along with accurate enough traffic flow models can be used to search for the best performing sequence of control decisions for a desired time horizon. However, since the traffic network is a complex system with several sources of uncertainties and affecting disturbances, the performance of the optimal control strategies may deteriorate. The main reasons for this could be measurement errors, future disturbance prediction errors, inaccuracy in models, and unpredictable incidents in the traffic network.

One promising solution is the receding-horizon optimization-based control approach known as Model Predictive Control (MPC) [160, 198]. Basically, MPC incorporates an optimization algorithm along with a prediction model in order to find the optimal control inputs at each control time step. The optimization problem is solved at next control time steps with new information gathered from the system under control, i.e. the traffic network in our case. Due to its rolling horizon feature and its a priori knowledge about the nominal time profile of disturbances, MPC has shown to be effective in response to disturbances.

Moreover, MPC has an adaptive structure, which means it can incorporate many traffic objective functions (or even a combination of multiple objectives, such as reducing travel delays, reducing emissions and fuel consumptions, etc.), it can handle constraints on the system states and on the control inputs, and it can adjust or replace the prediction model to fulfill the traffic control requirements. Moreover, all kinds of traffic control measures such as ramp metering, variable speed limits (VSLs), and traffic signals can be integrated in the MPC framework.

Nonetheless, there are challenges in using MPC for large-scale networks. The size of the optimization problem of the MPC scheme increases when the size of the traffic network under control grows. There has been a trend towards network control rather than local independent control of isolated intersections (or on-ramps in the freeway traffic framework). The main reason is that reducing local traffic delay might result in more

travel delays and congestion somewhere else in the network. Therefore, network control and coordination approaches have been developed [159, 183, 187, 203]. However, model predictive control for large-scale traffic networks might not be real-time feasible due to the increasing size of the optimization problem. On the other hand, since most traffic flow models are nonlinear [41, 156, 168, 238], the optimization problems integrated in the MPC scheme would be nonlinear and thus in general hard to solve.

Therefore, in the first part of this thesis, we focus on finding solutions for real-time predictive control of freeway and urban networks. In this process, there are three approaches to investigate:

- Reducing the computational complexity of the traffic flow models,
- Reformulating the optimization problems so that they can be solved more efficiently,
- Using hierarchical and distributed coordination and control techniques along with proper network partitioning.

In this thesis, we will consider a combination of all three approaches to reduce the on-line computation time of the MPC optimization problems for both the freeway and the urban networks case. Thereby:

- ✓ For the first point, we aim to use less computationally complex traffic flow models that still yield an acceptable level of accuracy. For both freeway and urban networks, we develop and extend models in order to make them ready to use in the MPC framework.
- ✓ Regarding the second point, since the models we have developed are still nonlinear, we also investigate approximation and transformation techniques to reformulate the nonlinear optimization problems into more efficient mixed integer linear optimization problems.
- ✓ For the last point, we introduce a multi-level control and management structure. In the urban traffic context, we assume that the network is properly partitioned into multiple subnetworks. The traffic congestion problem along with route guidance in the network are divided among local controllers, one for each subnetwork, while a centralized model predictive controller efficiently provides optimal traffic control inputs (controlling flows between neighboring subnetworks, switching between timing plans for intersections inside subnetworks, and destination-dependent traffic flow splitting rates) using an aggregate modeling approach.

MPC requires a traffic flow model that can accurately predict the traffic states. Moreover, a good estimation of the disturbances affecting the system is also crucial. However, since unpredictable incidents, mismatch between models and reality, and disturbance estimation errors always exist in traffic networks, the performance of MPC may deteriorate. Therefore, one can choose either to improve the robustness of MPC approach or to shift to an alternative approach. In the second part of this thesis, we focus on the latter option and we aim to tackle the issues with uncertain disturbances affecting the system (traffic network) and also with the online computational effort required to determine control decisions.

1.1.2. ROBUST CONTROL OF SWITCHED SYSTEMS

As pointed out in [92, 96], many traffic flow models have a hybrid nature in the sense that they incorporate both continuous-time and discrete-time variables. For instance, in the freeway traffic control context, the variable speed limit signs normally take only discrete values (e.g. 50, 70, 90, 100, and 120 km/h), while the traffic state variables (flow, density, and average speed) are continuous-time. Therefore, a dynamical model representing a freeway traffic network equipped by VSL signs would have a hybrid structure. On the other hand, for urban traffic networks, switching between a number of pre-defined timing plans for multiple intersections in order to control congestion and to improve the travel time is common in practice [137, 159, 202]. Therefore, a hybrid model can be developed to describe the urban traffic network under switching control [96].

The traffic flow models discussed before can be treated as a special class of hybrid systems known as switched systems. A switched system comprises of multiple dynamical subsystems and a switching signal that determines the active subsystem governing the dynamics of the system over time. To be more precise, our traffic flow models (especially the ones presented in the first part of this thesis) can be included in the category of switched systems with nonlinear subsystems (some reformulations may be required).

Stability analysis and control synthesis for various classes of switched system have been addressed in the literature in recent years [6, 40, 73, 113, 149]. Switched systems may show surprising behavior. For instance, a switched linear system that consists of stable linear subsystems may have unstable behavior under certain switching patterns. On the other hand, a particular switching rule can stabilize a switched system with unstable subsystem. Therefore, stability analysis and design of stabilizing controllers for these systems is challenging and is different from the non-switched case. Nevertheless, for the switched linear systems case, effective tools and methods in the literature have been proposed for stability analysis under arbitrary or restricted switching [74, 112, 152], for controllability and observability [14, 218, 229], and for the design of various types of controllers that ensure different performance criteria such as H_2 and H_∞ [74, 208, 240, 245]. However, switched nonlinear systems have not gained much attention and so far, no concrete procedure for the analysis and control of the general forms of these systems have been proposed. Most of the research has been devoted to the particular classes of these systems [4, 55, 127, 236].

In the second part of this thesis, we concentrate on analyzing and designing robust stabilizing controllers for more general types of switched nonlinear systems, inspired by our proposed traffic models. The specific problems that we deal with are:

- Stability analysis for switched nonlinear systems under arbitrary switching,
- Design of robust controllers that minimize the effects of disturbances on the output of switched nonlinear systems,
- Development of control design conditions and procedures that can be efficiently implemented and checked using available convex optimization tools.

In order to perform stability analysis and design robust controllers for switched nonlinear systems, we use the properties of the nonlinearities in the system to develop structured stability conditions that can be evaluated efficiently. More specifically:

- ✓ For the first point, we use multiple Lyapunov functions along with a dwell time constraint on the consecutive switching instants, in order to formulate less conservative (compared to a single Lyapunov function approach) asymptotic stability conditions under arbitrary switching.
- ✓ Regarding the second point, we investigate a robust control design approach that minimizes an upper bound on the L_2 -gain of the switched system from the disturbance input to the output of the system. The procedure provides an integrated design of a robust stabilizing switching law and state feedback control inputs.
- ✓ For the last point, we aim to use the characteristics of the nonlinear functions governing the dynamics of the switched system to formulate the stability conditions in the form of linear or least complex bilinear matrix inequalities. The main properties that we use are the possibility of fitting the functions in sector sets with arbitrary bounds and the smoothness of the functions.

In the next section, we will present our main contributions regarding the problems that we have discussed for both parts of this thesis.

1.2. RESEARCH GOALS AND MAIN CONTRIBUTIONS

The main aim of this PhD dissertation is to present efficient optimal and robust control strategies for hybrid and switched systems and for our particular applications, urban and freeway networks. In this process, the following major contributions have been obtained:

- **Efficient integrated predictive control framework for freeway networks**

In order to construct an efficient model predictive framework for large-scale freeway networks, we propose two extensions for the recently developed Link Transmission Model in order to represent the effects of ramp metering and variable speed limits. Using the extended model and taking advantage of mathematical transformation techniques, an integrated predictive ramp metering and variable speed limits control scheme is proposed in which mixed integer linear optimization problems are solved in a receding horizon fashion.

- **Optimal hybrid perimeter and switching timing plans control for urban networks**

We propose a multi-region hybrid urban traffic model developed based on the notion of Macroscopic Fundamental Diagram (MFD) [69]. Using the hybrid model, we develop a model predictive control scheme that is able to efficiently control network flows inside urban regions and between neighboring regions. Furthermore, using a high-level modeling approach based on the MFD, we also propose a multi-level predictive route guidance scheme. In this scheme, the complex routing problem for large-scale urban areas is relaxed by decomposing the problem into multiple layers and by defining regional origins and destinations.

- **Stability analysis and robust control of sector-bounded switched nonlinear systems**

Based on multiple Lyapunov functions that contain the nonlinearities in the

switched system, we propose a robust control design approach in the form of an optimization problem that can be efficiently solved using a combination of convex optimization techniques and line search methods. Solving the optimization problem results in the minimum upper bound on the L_2 -gain of the closed-loop switched nonlinear system along with the matrices for the stabilizing switching laws and state feedback control inputs.

- **Robust control of switched nonlinear systems via approximate switched affine systems**

We propose a robust H_∞ control scheme for switched nonlinear systems that can be approximated by switched affine systems with mixed autonomous and controlled switching types. We develop two control design procedures formulated in the form of bi-level optimization problems that can be efficiently solved using line search along with convex optimization algorithms. Furthermore, sufficient conditions for stability of the original switched nonlinear system using the proposed methodologies are presented.

1.3. STRUCTURE OF THE THESIS

A road map of the thesis is illustrated in Fig. 1.1. The thesis has two main parts which are connected through the modeling approach and the urban traffic control problem presented in Chapter 4. The chapters in Part I mainly present traffic flow models and control approaches for both urban and freeway networks. The chapters in Part II deal with the stability analysis and the design of robust stabilizing controllers for different types of switched nonlinear systems. Chapters 2 and 6 are devoted to the background knowledge required for better understanding the main contributing chapters.

The contents and contributions per chapter can be summarized as follows:

CHAPTER 3

This chapter presents the extensions of the link transmission model for ramp metering and variable speed limits control. Using the extended model, an integrated model predictive freeway traffic control scheme is developed. Further, to improve the efficiency, a reformulation of the model is proposed. Using the reformulated model, we establish a mixed integer linear optimization problem that is solved in the receding horizon manner.

Parts of this chapter have been partially presented in [88, 90, 98].

CHAPTER 4

Macroscopic multi-region modeling of urban networks using the concept of Macroscopic Fundamental Diagram (MFD) is presented in this chapter. Furthermore, using the proposed MFD-based hybrid model, a model predictive control scheme is developed in order to reduce the travel delay in large-scale urban networks partitioned into multiple subnetworks. Moreover, in order to improve the computational complexity of the approach, multiple approximation methods are proposed to transform the nonlinear MPC approach into more efficient MPC schemes with mixed integer linear optimization problems.

The contents of this chapter have been presented in [95, 96].

CHAPTER 5

Proceeding with the MFD-based modeling of urban networks, another multi-region macroscopic model is proposed in this chapter for the purpose of decomposing the route guidance problem for large networks into a multi-level less computationally complex scheme. The proposed dynamic optimal route guidance approach consists of two levels and incorporates an MPC approach. At the higher level, the optimal splitting rates for destination-dependent flows towards neighboring regions are determined. At the lower level, local controllers realize the optimal splitting rates sent from the higher level MPC controller.

Parts of this chapter have been published in [97].

CHAPTER 7

Stability analysis and design of robust H_∞ switching controllers for general switched nonlinear systems with a constraint on the feedback control input are discussed in this chapter. A model reformulation is used to relax the constraint on the control input. The design procedure for a stabilizing switching law with H_∞ performance is presented using a multiple Lyapunov functions approach.

The contents of this chapter have been presented in [91].

CHAPTER 8

This chapter mainly presents stability results for switched systems with nonlinear functions characterizing the dynamics of the system and bounded in sector sets with asymmetric slopes. Stability analysis under arbitrary switching with and without the average dwell time constraint is presented. Moreover, using a multiple Lyapunov functions approach along with linear matrix inequalities (LMI) techniques, the design procedure for robust H_∞ switching laws and state feedback controllers is formulated as an optimization problem. The optimization problem can be solved using a combination of a convex optimization algorithm along with a line search method.

Parts of this chapter have been published in [92, 93].

CHAPTER 9

In this chapter, we consider approximating a switched nonlinear system by a switched affine system with mixed switching types. Based on the approximate switched system, two procedures for the design of stabilizing switching laws are proposed. The proposed methods are further extended for joint design of switching laws and state feedback controllers that fulfill the H_∞ performance criterion. The design procedures are formulated as optimization problems that minimize upper bound on the L_2 -gain of the switched system. In order to solve the optimization problems, combined line search and convex optimization techniques can be used. Moreover, the sufficient conditions for stabilizing the original switched nonlinear system using the proposed methodologies are also presented in this chapter.

The contents of this chapter have been partially presented in [94].

Finally, Chapter 10 concludes the thesis with the main contributions and directions for future research.

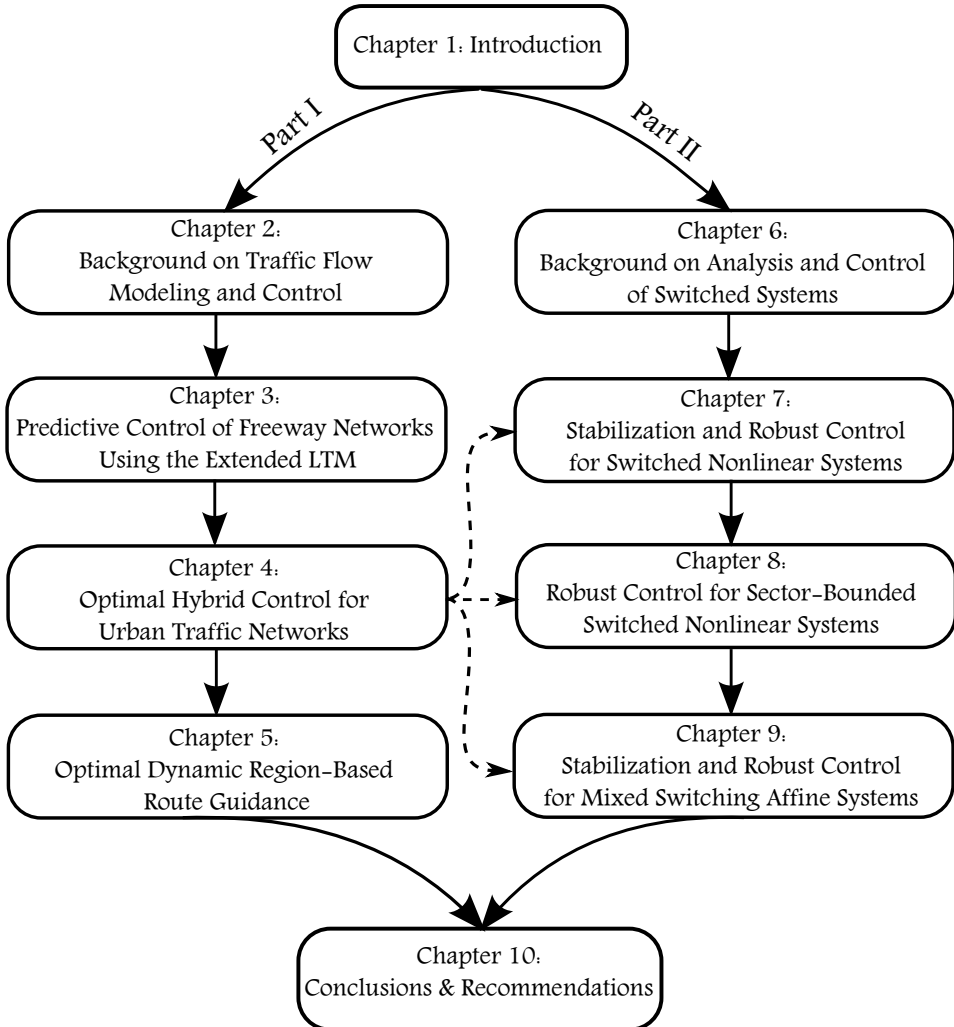


Figure 1.1: Structure of the thesis.

PART I:
MODELING AND CONTROL OF
TRAFFIC NETWORKS

2

BACKGROUND ON TRAFFIC FLOW MODELING AND CONTROL

This chapter provides some background knowledge on traffic flow modeling and control. First, we present common traffic control objectives, issues, and challenges in traffic network control. Next, we focus on freeway traffic flow models starting from different model categories based on the level of detail. We discuss more elaborately macroscopic flow modeling since it is the basis for our approach in Chapter 3. Next, we give an overview of the existing freeway control schemes ranging from heuristic and rule-based methods to model-based optimal and optimization-based approaches.

In the second part, we focus on the urban traffic modeling and control. First, we introduce multiple urban traffic flows and next, we elaborate more on the concept of aggregate and high-level modeling, since it will be extensively used in Chapters 4 and 5. Next, we present several existing urban traffic control approaches. We end this part with more discussion on control using the aggregate modeling approach and the benefits one achieves from this methodology.

2.1. CONTROL OBJECTIVES AND CHALLENGES

FOR a properly designed traffic management and control scheme, the following objectives could be taken into account.

SAFETY

The traffic control schemes should never cause unsafe situations. However, the efficiency in controlling or preventing congestion automatically increases safety. Moreover, ensuring safety prevents incidents to happen and consequently, provides higher traffic flows. On the other hand, simultaneous high speeds and densities negatively have impact on the safety [103].

2

NETWORK RELIABILITY

It may not be possible to prevent all congestions, but it is useful to predict the travel time of drivers heading to their destinations. In other words, accurate estimation of the arrival times helps drivers to choose proper departure times. A traffic control scheme can provide good estimation of realizable travel times for drivers. Moreover, it can also optimize the network to realize the estimated travel times. This can be achieved by optimal distribution of the traffic flows over the network.

TRAFFIC NETWORK FLOW PERFORMANCE

The traffic flow performance can be described using different criteria. As a result, the objectives of traffic control schemes can be different. The performance criteria can be the throughput, travel times, homogeneity of the traffic flows, or the safety level both over space and time. The total time spent in the network (on the mainstream road and at the on-ramps queues) is often considered as performance criterion [71, 90, 104, 155].

FUEL CONSUMPTION, EMISSIONS AND NOISE POLLUTION

The main aim of any traffic controller is to improve the performance of the traffic network. However, the performance could vary depending on the desire of different users of the network, the operation time of the network, and the location of the network. For example, environmentalists would like reduced dispersion of emissions and propagation of sound pollution to a protected target zone, while transport authorities could be interested to improve traffic throughput and safety. Moreover, in urban areas, the density of the population is relatively high. People living in big cities usually suffer from air pollution. One of the biggest sources of the environmental pollution in cities comes from the emissions of congested traffic flows. A well-designed traffic management system that can control both travel delays and traffic emissions effectively is highly desired. After all, one can define three performance criteria; emissions, fuel consumption, and dispersion of emissions to target zones [241].

COMPUTATIONAL EFFICIENCY

The calculation time required to compute the traffic control inputs (e.g. the ramp metering rates or the variable speed limits) should be small enough to make real-time control of freeway networks possible. For the heuristic-based and rule-based approaches this is not a concern, but e.g. for more advanced control schemes such as model-based

predictive control [103, 187, 198] computation of the optimal control inputs should be performed in a small period of time such that real-time traffic management is possible. As the computational complexity of model-based predictive control and its associated optimization problem grows, for larger freeway networks, research has been oriented either towards using simpler but faster models to represent the network [41, 238, 239] or on the decentralized and distributed implementation of the traffic control schemes [59, 162, 187].

VARIATION IN TRAFFIC CONTROL MEASURES

In general, frequent fluctuations and sudden jumps in the values of the control measures such as ramp metering rates and variable speed limits are not desired from the safety and the drivers' comfort point of view. Since it is also possible to have different optimal traffic control settings that can result in the same traffic performance, priority is usually given to attain the same performance level with a minimal fluctuation in the traffic control measures.

A perfect traffic control scheme would be the one that can take into account and fulfill nearly all the traffic objectives and criteria mentioned above. In the next section, we introduce some of the proposed freeway traffic control schemes in the literature that address some of the traffic concerns mentioned here.

2.2. FREEWAY TRAFFIC NETWORKS

This section provides background on freeway traffic flow modeling, traffic objectives and challenges, and an overview of traffic control methods proposed in the literature and in practice. As for the traffic flow modeling, we first introduce the main concepts and the classification of existing models. Next, we focus on a particular class of traffic flow models, the so-called macroscopic flow models. In the next subsection, freeway traffic objectives and environmental concerns are discussed. Finally, existing solutions and control approaches from heuristic and rule-based methods to advanced model-based control schemes are briefly reviewed.

2.2.1. BASIC CONCEPTS AND ELEMENTS OF MODELING

For traffic networks, a wide range of traffic flow models has been developed [116, 165, 214, 216]. They can be used for the design of traffic control strategies, for the development of new infrastructure, and for the education of traffic operators and traffic managers [103, 116, 215].

Traffic flow models can be classified in several ways. The nature of traffic flow models can differ based on their specific application, their level of detail, the describing time domain (discrete-time or continuous-time), and their stochastic or deterministic behavior in describing the traffic states [116]. Based on their level of detail, they can be categorized as microscopic, macroscopic, and mesoscopic traffic flow models [116]. Traffic flow models that represent the behavior of individual vehicles in a traffic network are included in the category of microscopic traffic flow models. Microscopic traffic flow models can be also categorized into different classes based on the concepts they use [116], e.g. the car-following models [194, 196], cellular automaton-based models [175], and so on. Moreover, microscopic simulators such as AIMSUN [9] and VISSIM [58] use microscopic traffic flow models.

On the other hand, macroscopic traffic models describe the aggregate dynamics in terms of the spatial vehicle density, the average flow, and the average speed. Since in the microscopic traffic models each car is characterized by its own motion dynamics, the computation time required for traffic simulations grows large as the number of simulated cars increases [106, 116]. Therefore, these types of models are mostly suitable for off-line traffic simulations, detailed investigations, or numerical evaluation of collective traffic variables such as the density-dependent velocity distribution, the distribution of headway distances [174]. Moreover, on some occasions, macroscopic modeling approaches may provide better results than modeling approaches with a higher details [116]. Hence, although the microscopic models and simulators are able to reproduce the detailed effects of traffic flows, most traffic researchers prefer macroscopic traffic flow models [105, 133, 151, 185].

Macroscopic traffic flow models deal with traffic flow in terms of aggregate variables (such as average speed, flow, and density). Macroscopic traffic models do not distinguish the behavior of individual vehicles in a traffic stream. Therefore, macroscopic traffic flow models are suited for faster than real-time traffic simulations [106, 116]. Most often macroscopic models are derived from the analogy between vehicular flow and flow of continuous media (e.g. fluids or gases) [141], resulting in traffic flow models with a limited number of equations that are relatively easy to handle [116]. The first macroscopic traffic models were reported in [151, 200]. These models established the basis for the development of the more accurate traffic flow models presented in [41, 168, 185, 189, 238].

The independent variables of a continuous macroscopic traffic flow model are location x and time t . Most macroscopic traffic flow models describe the dynamics of the density denoted by ρ , the average speed denoted by v , the flow q and the relation between these variables. Basically, all macroscopic traffic models are based on the continuity equation [108]

$$\frac{\partial \rho(x, t)}{\partial t} + \frac{\partial (\rho(x, t)v(x, t))}{\partial x} = d(x, t), \quad (2.1)$$

where $d(x, t)$ denotes the rate of vehicles entering the freeway at an on-ramp or the rate of vehicles leaving the freeway at an off-ramp. Moreover, most macroscopic models define the relation between the density ρ , the flow q , and the average speed v as

$$q(x, t) = \rho(x, t)v(x, t), \quad (2.2)$$

where the density ρ is per single lane. However, (2.1) and (2.2) do not completely describe the traffic dynamics as the number of unknown variables is more than the number of equations. Consequently, to obtain a more complete description of the traffic flow dynamics, extra equations are required. As a third equation, most first-order macroscopic traffic flow models (like the cell transmission model [41] and the link transmission model [238], Payne model [189], and Fastlane [226]) assume a static speed-density relation. But for the description of emergent traffic jams and stop-and-go traffic, one needs a dynamic speed equation [108, 241]. Therefore, for most higher-order macroscopic models, the third equation that describes the dynamics of the average speed can

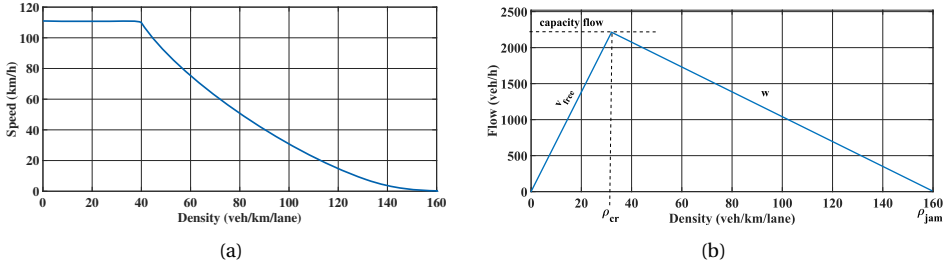


Figure 2.1: Triangular fundamental diagram: (a) speed-density plot, (b) flow-density plot.

be written in the following general form [108]:

$$\frac{\partial v(x, t)}{\partial t} + v(x, t) \frac{\partial v(x, t)}{\partial x} = - \frac{1}{\rho(x, t)} \frac{\partial P(\rho(x, t) v(x, t))}{\partial x} + \frac{1}{\tau} (V(\rho(x, t)) - v(x, t)), \quad (2.3)$$

where $V(\rho(x, t))$ is the generalized equilibrium speed given by the fundamental diagram relationship between $v(x, t)$ and $\rho(x, t)$ (will be explained shortly), τ is the relaxation time and $P(\rho(x, t), v(x, t))$ is the traffic pressure. The traffic pressure is a quantity that describes the degree to which drivers interact with each other [193]. The third dynamic equation (2.3) results in a second-order traffic flow model. The difference between the various existing macroscopic traffic flow models mainly concern the expressions used for the traffic pressure $P(\rho(x, t), v(x, t))$, the relaxation time τ , and the generalized equilibrium speed $V(\rho(x, t))$, which results in different equations for the average speed $v(x, t)$.

To explain the models constructed on (2.3), we first start with the relation between the speed v and the density ρ . When the density on the road is very low and the average distance headway is large, the drivers travel at the free-flow speed. This is called the free-flow driving. As the density starts to increase to a critical point ρ_{cr} (i.e. the density at which the maximum capacity of the network is used), the speed starts decreasing until a traffic jam occurs. When the density is at its maximum ρ_{max} , the speeds of vehicles approach zero. These relations can be graphically illustrated using the so-called fundamental diagram. A fundamental diagram that is obtained using real data from a freeway network has a lot scattering, particularly in the congested part. However, one can fit a function to the data and use the fitted function to build up a traffic flow model. One way to approximate the fundamental diagram is to use straight lines to obtain the so-called triangular fundamental diagram is illustrated in Fig. 2.1. Based on the triangular fundamental diagram, first-order models such as the cell transmission model [41, 42] and the link transmission model [89, 90, 115, 239] have been developed. These models are relatively accurate for reproducing congestion phenomena and the propagation of jams. The relatively simple traffic dynamics allows us to study traffic route assignment and also to design efficient and relatively fast control algorithms.

Another approximation for the fundamental diagram is to use higher-degree polynomials or exponential functions. The relation between the equilibrium speed V and

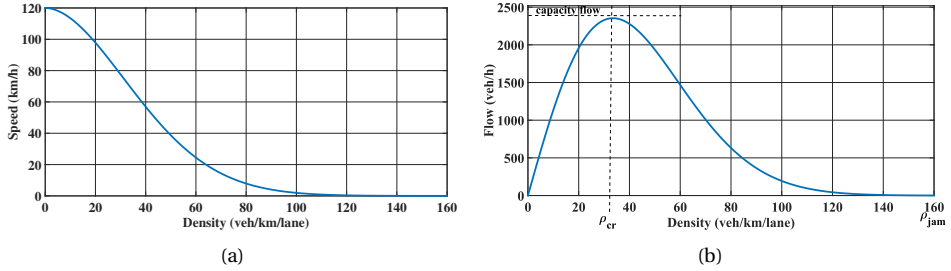


Figure 2.2: Fundamental diagram: (a) speed-density plot, (b) flow-density plot.

2

the density ρ can be formulated as

$$V(\rho) = v_{\text{free}} \exp \left[-\frac{1}{\alpha} \left(\frac{\rho}{\rho_{\text{cr}}} \right)^\alpha \right], \quad (2.4)$$

where ρ_{cr} is the critical density, v_{free} is the free-flow speed, and α is a parameter. The relation formulated in (2.4) can be also illustrated in Fig. 2.2(a) for speed versus density and in Fig. 2.2(b) for flow versus density. Based on this fundamental relation, second-order models such as METANET [168] are developed. The METANET can represent the evolution of density, flow and average speed of freeway links. The interested reader is referred to [104, 168] for more details about the METANET and its extensions.

While second-order traffic models can be more accurate than first-order models to represent traffic dynamics, they suffer from additional complexity that makes the model calibration difficult. Moreover, model-based control schemes constructed on second-order models such as METANET are not efficient for large-scale networks. On the other hand, the cell transmission model and the link transmission model are relatively simpler and keep acceptable level of accuracy. But some traffic phenomena such as capacity drop cannot be accurately represented by these models in their original formulations. It has been observed that in some cases there is a drop in the maximum flow (capacity) of a freeway link depending on whether the link is in free-flow or congestion. Such drop in the capacity of a link is usually a result of congestion in the downstream links of the link [144].

2.2.2. OVERVIEW OF EXISTING CONTROL APPROACHES

There are various methods in the literature for control of freeway networks using different traffic measures. Among them we discuss a number of heuristic and rule-based approaches and some more advanced methods that are based on optimal control [138] and the model predictive control theory [160, 198].

HEURISTIC AND RULE-BASED CONTROL STRATEGIES

Rule-based systems solve problems using if-then rules [100, 205]. These rules are usually built up using expert knowledge and stored in an inference engine. The inference engine has a memory that stores rules and information about the problem, a pattern matcher, and a rule applier. The pattern matcher searches through the memory to find

out which rules are appropriate for the problem and next, the rule applier selects the rule to apply. However, these systems work only with pre-defined rules and in their basic implementation learning is not involved.

When the congestion is imported from downstream, local ramp metering almost has no effect. Therefore, coordinated control strategies are crucial. HERO (HEuristic Ramp metering coOrdination) [186] is a simple rule-based coordinated ramp-metering scheme that applies ALINEA (Asservissement LINéaire d'Entrée Autoroutière) for the local regulators. ALINEA is a local proportional feedback ramp metering control strategy [184]. The coordination principle of HERO is as follows. First, it receives the real-time detected ramp queue lengths and mainstream densities from the local controllers. Next, it checks whether the ramp queue length exceeds a certain activation threshold, and whether the merge density is close to the critical density. If both conditions are satisfied, this ramp is defined as master ramp. Next, it defines a minimum ramp queue length for the slave ramps, which is updated according to the real-time changing of the master ramp queue length. By real-time tuning the minimum queue length based on the traffic state of the master ramp, the queue lengths of the slave ramps are increased to approach the queue length of the master ramp. When the queue of the master ramp decreases beneath a certain threshold or the mainstream density becomes under critical, the coordination procedure stops.

ACCEZZ (Adaptive and Coordinated Control of Entrance Ramps with Fuzzy Logic) [18] is a rule-based algorithm for coordinated ramp metering. The core of ACCEZZ is a fuzzy controller. The control rules are expressed by a number of fuzzy sets that are identified and obtained from heuristics, expert knowledge or simulation. The inputs of the fuzzy controller are measured on the mainstream and on-ramps, i.e. the average speed, average traffic flow, and average occupancy at the upstream and the downstream links of the on-ramp. The output of the fuzzy controller, the metering rate, is calculated based on the real-time measured and historical traffic data.

Case-based reasoning solves a problem using the knowledge that is gained from previously experienced or simulated similar cases [201]. In this way, this technique learns how to solve a new problem and saves the new solution in a database. A disadvantage of this approach is that it may not be clear what must be done for a case that is not yet integrated in the database. To improve the existing traffic management systems, BSES (Boss Scenario Evaluation System) [48, 117] is proposed based on fuzzy multi-agent case-based reasoning. The main features of the system are 1) its case-based structure, i.e. it uses examples of control scenarios under different real traffic conditions, 2) the fuzzy logic inference system that identifies the similarity of the current situation to other cases stored in the database, and 3) the agent-based structure, i.e. combining the predictions of the effects of different traffic control strategies for small networks. The main advantages of the BSES scheme are the computation speed (with respect to the cases in which we use traffic flow models), the ability to use actual knowledge (rather than general information or simulated data), and the ability to learn from previous experiences.

MODEL-BASED CONTROL STRATEGIES

Freeway network modeling and control with the goal of reducing the travel time, reducing the fuel consumption and emissions, increasing the throughput of the network have been extensively investigated in the literature [5, 28, 104, 138, 187, 241]. In model-based traffic control, an efficient and accurate model for the evolution of the traffic is required.

This model has to be accurate and also computationally efficient for real-time simulation and control of a large-scale network.

The main idea of optimal control is to find the optimal control measures for the whole freeway network by optimizing a cost function based on a network model for a certain future time horizon. The optimal control approach can coordinate the freeway network in a centralized structure. It not only can coordinate different space locations and different time instants in the future, but also it can coordinate different kinds of traffic measures (e.g. ramp metering, speed limits, and route guidance) [140, 186].

AMOC (Advanced Motorway Optimal Control) [139, 140] and OASIS (Optimal Advanced System for Integrated Strategies) [138] are two control schemes based on optimal control theory. They both adopt the macroscopic freeway traffic model METANET [168] as optimization model. However, because the freeway network model is nonlinear, one of the challenges is to find an efficient algorithm to solve the large-scale optimization problem. A numerical solution algorithm that is based on a feasible-direction nonlinear optimization method, is proposed to solve this problem [138, 140]. The AMOC approach has been applied to the Amsterdam ring-road [139], and has shown good performance and effectiveness. However, due to the open-loop structure of AMOC, the obtained optimal control actions may get deteriorated by all kinds of errors, such as estimation error of the initial state, future disturbance prediction error, model parameter mismatch error, and unpredictable incident errors.

Model predictive control (MPC) is a model-based control approach that is based on the optimization of control inputs that improve a given performance criterion (objective function) over some prediction horizon. The performance criterion of MPC is formulated as a cost function of the predicted system states, outputs, or inputs. The MPC approach can be used for non-linear and time-variant systems. In addition, it can incorporate constraints on the inputs, states, and outputs of the system. Since the core control strategy in Chapters 3, 4 and 5 is MPC, we will explain the basic concepts of the MPC framework here. For more detailed information on MPC, we refer the interested reader to [160, 198].

The MPC, in general, computes online optimal control solutions of an optimization problem that is formulated to reflect the desired performance of a system. All MPC-based control approaches have five main concepts:

- *System and disturbance modeling:* MPC relies on the prediction of the system states and outputs in the future, and on the evolution of either already known disturbances or of the probabilistic properties (or known bounds) of the unknown disturbances.
- *Performance criterion* In the MPC framework, a performance criterion is defined as a cost function over a (finite or infinite) prediction horizon.
- *Constraints:* The constraints can be linear or non-linear. MPC can treat both equality and inequality constraints on the system states, outputs, and inputs. The constraints can be related to the operational limits of the system, economic concerns, environmental demands, safety requirements.
- *Optimization:* MPC uses optimization techniques to optimize the control inputs in such a way that the value of the given cost function is minimal. Depending on

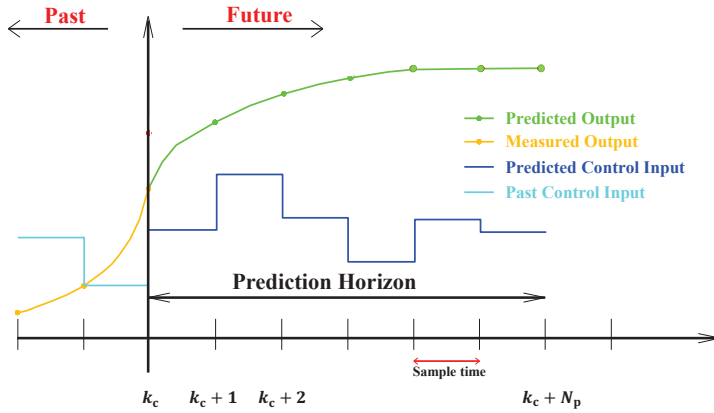


Figure 2.3: The main concept of the MPC scheme.

the system's model, the constraints, and the cost function, the solutions obtained can be optimal or sub-optimal. In principle MPC uses online optimization to design optimal control inputs. But to gain computational speeds it is also possible in some cases, to design MPC based on off-line optimization (such MPC is known as explicit MPC [13]).

- *Receding horizon principle*: This means that after computation of the optimal future control sequence, only the first control sample is implemented. Subsequently, the horizon is shifted for one sample period and the optimization is re-executed with new information from the system. This is illustrated in Fig. 2.3. At every control time step k_c , the MPC controller determines the optimal control input that minimizes a given performance criterion over the prediction period $[k_c \cdot T_c, (k_c + N_p - 1) \cdot T_c]$, where T_c is the control sample time and N_p is the prediction horizon.

On the other hand, the main disadvantage of MPC for non-linear systems originates from the nonlinear and non-convex optimization problem involved. Such optimization problems do not only bring difficulty in computing optimal solutions, but also the computation time required to get even suboptimal solutions may become very high. Usually, the computation time exponentially increases as the number of control inputs (optimization variables) or the prediction horizon increase.

DISTRIBUTED MPC

Due to its high computational demand, conventional MPC for traffic systems is not tractable in practice [12, 47, 104, 154, 162]. There are many advancements in the literature to address the computational complexity problems of MPC [13, 154, 162, 231]. A distributed control structure can be developed to avoid the exponential growth of the computational complexity for the centralized MPC, when the network scale keeps on in-

creasing. The large-scale freeway traffic network is then decomposed into subproblems, each of which is controlled by a local MPC controller [63, 162, 187].

As an example of decentralized MPC, [187] proposed an MPC approach based on the AMOC algorithm using a hierarchical control scheme. The hierarchical control structure consists of three basic layers: the estimation/prediction layer, the optimization layer, and the direct control layer. The estimation/prediction layer receives historical information and real-time detected traffic states to generate the current state estimation and future predictions of the disturbances for the next layer. The optimization layer (AMOC) optimizes the state trajectory over a time interval based on the initial states and future disturbance prediction obtained from the upper layer. Next, in the local direct layer, local ALINEA controllers are adapted using the optimized traffic set points or trajectories obtained from the upper optimization layer.

In Chapter 3, we will further discuss the model-based control approaches and present an efficient integrated model predictive scheme developed based on the first-order, fast yet accurate, link transmission model [115, 238, 239].

2.3. URBAN TRAFFIC NETWORKS

This section concentrates on traffic flow modeling and control strategies for urban traffic networks. In the modeling section, we first briefly discuss different types of urban traffic flow models and next, we focus on the concept of Macroscopic Fundamental Diagram (MFD), which is the basis for our modeling and control approaches developed in Chapters 4 and 5. Next, we review some of the existing urban traffic control schemes ranging from rule-based and open loop optimal control approaches to model predictive control schemes and recent MFD-based methods.

2.3.1. BASIC CONCEPTS AND ELEMENTS OF MODELING

For different traffic applications, we have to select proper traffic models with good level of modeling accuracy and less computational effort. Both microscopic models and macroscopic models provide various levels of modeling power. Essentially, more detailed modeling of traffic dynamics leads to higher computational complexity of the model. Therefore, a criterion for selecting a proper model for a particular traffic network would be that the model should be able to represent all important behaviors, and meanwhile, the simulation speed of the model is fast enough [182].

The store-and-forward model [1] was proposed to describe the stop-and-go urban traffic flow dynamics controlled by traffic lights. The store-and-forward model later used for control purposes in [2], is a simple model with a low computational complexity but it is particularly useful for the saturated traffic condition. In the saturated condition, the vehicle queues added up from the red phase cannot be completely discharged at the end of the next green phase. The model proposed in [10] and extended in [52] can describe queues and calculates time delays for vehicles reaching the queues in a link and it is capable of describing different traffic scenarios.

The cell transmission model [41] and the link transmission model [115, 238] are both models derived based on the kinematic wave theory [151], [200]. The extensions of these models for urban traffic flow modeling can be found in [80, 238]. The model proposed in [131] has a lower modeling power, but it cannot describe traffic scenarios other than the saturated case. The models proposed in [154, 223] are able to describe the traffic flow

dynamics (including vehicle queues) in all traffic scenarios (unsaturated, saturated, and over-saturated traffic conditions) by updating the model in small time steps.

Essentially, all macroscopic urban traffic models mentioned above are spatiotemporally discrete models. This means that they are sampled into road segments spatially and are sampled temporally with a sampling period. In [153, 154], a discrete-time urban traffic model, known as the S-model, with a variable sampling time interval is proposed for model-based predictive control, which provides a balance between modeling accuracy and computational complexity. Nevertheless, for larger networks, the model becomes extremely complex. Specially if it is used in the MPC framework for prediction of traffic states, the associated optimization problem would need a very large computation time which means that the modeling and methodology proposed in [153] is not feasible in real-time.

Large-scale urban networks need efficient traffic management and control schemes. In fact, modeling a large urban network would be a complex task if one wants to study and model the traffic dynamics of each element (i.e. each link and each intersection, including route choice of travelers). This has been performed in the modeling approaches in [1, 151, 153, 154, 200, 223]. On the other hand, centralized control of an urban network with such detailed modeling approach would be computationally complex and makes its implementation in real-time infeasible. Hence, instead of adopting a detailed modeling approach, researchers are investigating alternative possibilities for deriving an aggregate model for the whole traffic network.

MODELING USING THE MACROSCOPIC FUNDAMENTAL DIAGRAM

The idea of macroscopic fundamental diagram (MFD) was first proposed in [77] and similar approaches were introduced later in [43, 109, 161]. Investigation on the MFD with dynamic features is recently performed in [70]. The MFD captures macroscopically (at a network level) the traffic flow characteristics and dynamics of an urban region. It relates the number of vehicles (accumulation) in the region and its production, defined as the trip completion rate (flows of vehicles reaching their destination), see Chapter 4. The underlying assumption in these works is that the network is homogeneously or evenly congested, which is not always the case. Homogeneous networks with a small variance on link densities have a *well-defined* MFD, i.e. there is a low scatter of flows for the same densities (or accumulations) [72, 166]. A well-defined MFD is schematically shown in Fig. 2.4. The shape of the MFD can be approximated by a non-symmetric unimodal curve skewed to the right, i.e. the critical accumulation, n_{cr} (veh), that maximizes network flow is smaller than half the jammed accumulation n_{max} . Note that the network topology, the signal timing plans of the signalized intersections, and the infrastructure characteristics affect the shape of the MFD, see e.g. [45, 68, 107]. Other investigations of the MFD using empirical or simulated data can be found in [27, 44, 206], while routing strategies based on the MFD can be found in [87, 136].

As can be observed in Fig. 2.4, as the accumulation or density is increasing (the network operates with free flow condition), the traffic flow increases up to the area where the capacity of the network is reached. Going beyond the critical density, the network gets congested and enters the over-saturated region. The main goal is then to maintain the overall traffic state in the capacity state (saturated region), by applying traffic management and control schemes (e.g. traffic signal optimization, gating [135], route guidance) and further, to avoid spillover and gridlock situation.

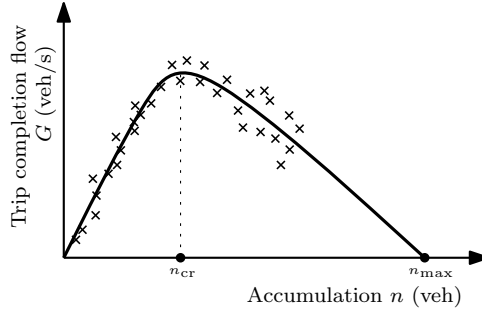


Figure 2.4: Macroscopic fundamental diagram.

2

Heterogeneous networks might not have a well-defined MFD, mainly in the congestion (decreasing) part of the MFD, and the scatter usually becomes higher as accumulation increases, see [27, 72, 166]. The principal requirement for a well-defined MFD is the homogeneity of the area-wide traffic conditions. In order to further clarify the necessity for a well-defined MFD, [166] have figured out that the spatial distribution of link densities has the key influence on the shape of the MFD. The obtained results suggest that the MFD can be applied for unevenly congested network if the network can be partitioned into homogeneous regions [123].

Therefore, based on the concept of MFD and a proper partitioning of a large urban network, we can determine a multi-region aggregate model that can represent the traffic flow inside and between urban regions. Using this model, efficient control strategies can be developed to control flows in the network on the high level [71, 87, 95–97]. This idea can be further extended for the design of a multi-level urban traffic modeling and control approach in which at the top level aggregate models based on the MFD are used while at the lower levels, more detailed models are used as basis for the design of local controllers [11].

In the next section, some of the well-known urban traffic control approaches are discussed.

2.3.2. OVERVIEW OF EXISTING CONTROL APPROACHES

At the beginning of the development of traffic signal control on 1914, fixed-time control was used at intersections [232]. In this framework, the length of the green time duration is always fixed or at least fixed during multiple time intervals during the whole day. The fixed-time control actions are predefined according to the historical traffic information. However, fixed-time control is open-loop and hence, it cannot adapt the control actions to the current traffic condition. Therefore, traffic-responsive control has been emerged, along with the application of a variety of detectors (loop detectors, video cameras, etc.) to get feedback from the traffic network.

Traffic-responsive control falls into the feedback control category that can adjust the control actions base on the currently measured traffic states. Both for fixed-time control or for traffic-responsive control, the control strategies are not constructed on traffic models, but on the historical traffic information or the measured traffic information. These control strategies can only consider the past and the current traffic condition. In

order to avoid this, traffic models are used in traffic control schemes to predict the future traffic states, which results in model-based traffic control strategies. Model-based coordinated control strategies [2, 3, 20, 52, 71, 96, 183] do not introduce the feedback control only to adjust the control actions to the current detected traffic states, but also to use the feedback data along with a prediction model to make effective decisions in a long term run.

In the following subsections, we present some of the well-known urban traffic control approaches.

RULE-BASED CONTROL STRATEGIES

Similar to ACCEZZ for freeway networks, fuzzy-logic controllers with genetic algorithms or neural network algorithms are also applied in urban traffic systems. In [114], an urban traffic control scheme is proposed. It applies a fuzzy-logic controller as local intersection controller, and heuristic technique to coordinate the control results obtained from fuzzy-logic controllers and to derive the green time for each phase in a traffic signal cycle. In each fuzzy-logic controller, an evolutionary algorithm is applied to learn and update in real-time the fuzzy sets.

A more complex urban network control with a hierarchical architecture is given in [34] based on a fuzzy neural decision support concept. The architecture has three layers. The lowest layer includes intersection agents that control individual intersections in the traffic network. The middle layer consists of zone agents that control several pre-assigned intersection agents. The highest level includes one regional control agent managing all zone agents. In each layer, every agent can obtain traffic data and makes decisions independently. Both lower and upper layer agents can cooperate with each other. For zone agents, the fuzzy rules are adjusted using an evolutionary algorithm. Several techniques including reinforcement learning, weight adjustment, and tuning the fuzzy relations have been used to adapt the dynamics of the agents.

OPTIMAL CONTROL APPROACHES

In recent years, a number of model-based optimization control strategies based on simple traffic models have been proposed, e.g. PRODYN [57], CRONOS [19, 20], OPAC [66], RHODES [210], and MOTION [17]. They can predict the traffic behavior of the network. However, the models used in these control schemes are relatively simple traffic flow models. This in fact limits the performance.

UTOPIA/SPOT [164] is a hierarchical system with simple local intersection controllers and a central controller for an area of an urban network. The central controller optimizes the control actions for the whole area based on a simple model of the network. The local controller makes decisions based on only the local information, but with a penalty term to guarantee that the local decisions are not too far from the decisions made by the central controller. Therefore, UTOPIA/SPOT partially avoids the online computational effort but on the other hand, may result in suboptimal solutions.

A linear quadratic optimal control approach, Traffic-responsive Urban Control (TUC) [1, 137], is developed based on a store-and-forward model [2]. Instead of optimizing the control inputs (i.e. green times), TUC optimizes a linear multi-variable feedback regulator off-line, where the feedback gain matrices are solutions of the corresponding algebraic Riccati equation. Therefore, the TUC strategy reduces the online computational complexity significantly by moving the time-consuming optimization to

the off-line part. However, when the real traffic conditions change, the feedback control law needs to be re-designed according to the new current traffic conditions, which is also computationally complex if it occurs frequently.

Dynamic Intersection Signal Control Optimization (DISCO) [157] is a dynamic urban traffic optimization-based control approach developed using the cell transmission model. It considers the fundamental diagram and can capture traffic phenomena such as shock waves and queue dynamics. The timing plans of urban traffic networks are determined by solving an optimization problem using a genetic algorithm. Despite all advantages, this optimal control approach is open-loop. It solves the optimization problem based on the approximation of the future disturbances, which can be inaccurate (specially if unpredictable incidents occur). Moreover, mismatches between the model and the real world and inaccuracies in estimating initial traffic states can always happen. Under these circumstances, the control results obtained from optimal control methods are not the best control actions anymore.

SCOOT (Split Cycle Offset Optimization Technique) [203], which is an adaptive system that responds automatically to fluctuations in traffic flow, is the most common traffic control system used in the United Kingdom. However, widely used strategies like SCOOT and SCATS [159], although applicable to large-scale networks, are less efficient under saturated traffic conditions [135]. On the other hand, more advanced traffic-responsive strategies like OPAC [66], PRODYN [57], and RHODES [210] use optimization algorithms with exponential increase of complexity, which do not permit a central network-wide application. Thus, most available strategies face limitations when it comes to saturated traffic conditions that are frequently occurred in traffic networks. [30] proposed a dynamic method to control an oversaturated traffic network by using a bang-bang control method for the oversaturated intersections. In [2], the problem of network-wide signal control is formulated as a quadratic-programming problem that aims at balancing the link queues in order to minimize the risk of queue spillback. Furthermore, multiple control approaches have been proposed that use computationally inefficient optimization algorithms, such as genetic algorithms [157], and ant colony optimization [36]. However, because of their high computational demands, the real-time and network-wide implementation of these methods might not be feasible.

MODEL PREDICTIVE CONTROL

Model predictive control known also as receding horizon control has been in the traffic control context recently [52, 65, 71, 96, 223]. The MPC method proposed in [52] is computationally intensive and it can describe different traffic scenarios. It needs historical data to estimate the traffic flow rate of each intersection.

An MPC scheme is proposed in [223] based on an extended model of [131], which is capable of simulating the traffic dynamics in all traffic scenarios (unsaturated, saturated, and over-saturated traffic conditions). The MPC controller gives effective performance but it is not applicable to large-scale urban networks.

On the other hand, a distributed control structure can be developed to avoid the exponential growth of the computation time of centralized MPC, when the network scale increases. The problem of finding optimal signal timing plans for a large number of traffic lights is a challenging problem because of the exponential growth of joint timing plans that need to be taken care of as the network size grows. However, if we decompose the problem into smaller subproblems, we may be able to find a sufficiently

good solution in a reasonable amount of time. The decomposition of the problem can be performed by assuming that each traffic signal is an independent decision maker. To coordinate the decision makers (traffic signals), game theory [167, 171] is applied in [32].

VFC-OPAC (Virtual-Fixed-Cycle Optimized Policies for Adaptive Control) [65] is a hierarchical control scheme, which consists of a three-layer control architecture. The local control layer implements an optimization in the rolling horizon procedure, i.e. it continuously calculates and shifts optimal switching sequences for the prediction horizon, subject to the some fixed-cycle constraints communicated from the upper synchronization layer. The coordination layer optimizes the offsets (the offset is the time between the start of the green light at one intersection and the start of green light at another intersection) at each intersection (once per cycle). The synchronization layer calculates the network-wide virtual-fixed-cycle (once every few minutes). The VFC allows the cycle time to start or terminate within a flexible range at each intersection. The cycle length can be calculated separately for groups of intersections. Over time, the flexible cycle length and offsets are updated as the system adapts to traffic conditions.

MFD-BASED CONTROL

As mentioned in the previous sections, the MFD can be used to establish efficient strategies to control network flows. Among them is the perimeter control, i.e. limiting the inflow of a network to ensure a high production [43, 71, 134, 237]. In [71], optimal perimeter control for a two-region urban city is formulated by using the notion of MFD. For stability analysis of perimeter control, the reader can refer to [86], while optimal control for mixed urban freeway networks utilizing MFDs is found in [87]. Perimeter control for single or multiple-region homogeneous networks has been analyzed with linear multi-variable feedback regulators in [134] and [3].

It should be noted that changes in the network topology, the signal timing plans of the signalized intersections, and the infrastructure characteristics affect the shape of the MFD. In [95, 96] this issue has been addressed and the authors have introduced another level of control inside urban networks with taking into account the variability of the MFD. More details on this method will be presented in Chapter 4.

As other examples of using the MFD, [148] introduced fixed-time signal timing perimeter control. In [3], a feedback control approach is applied to multiple subnetworks with separate individual MFDs in a heterogeneous urban network. In [67] a three-dimensional MFD relating the accumulations (cars and public transports) with the total flow in the network is proposed. The obtained results may be applied for perimeter control to maximize the network capacity or the passenger capacity in urban networks. Finally, [85] has proposed a robust perimeter control design to handle uncertainties in the MFD.

In the next chapter, we will show how we can extend the idea of perimeter control using the MFD towards timing plans control inside urban regions. We will propose a generic multi-region MFD-based model that provides the basis for the design of perimeter and switching controllers (to switch between timing plans of urban regions).

2.4. SUMMARY

In this chapter, we have given an overview of traffic flow modeling and control for both freeway and urban networks. First, we have reviewed traffic control objectives and chal-

lenges. Next, in the first part, we have started with the modeling concepts and classifications for freeway networks. The focus has been on macroscopic flow models. Next, existing control solutions from model-free and heuristic approaches to model-based optimal and predictive control schemes have been briefly introduced.

In the next part, we have turned the attention towards modeling of urban networks. Multiple models for individual intersections in the literature, such the store-and-forward model and the S-model have been reviewed. Next, the concept of aggregate modeling using the macroscopic fundamental diagram has been explained. Next, we have categorized some of existing solutions in the literature for urban traffic control. Rule-based and heuristics approaches were first introduced. Next, several optimal control-based methods for large-scale networks have been presented. In the end, some of the methods recently developed based on the notion of MFD have been described and some remaining challenges have been mentioned. In the next chapters, we will use the modeling elements and the control structures (specially the MPC framework) that have been presented in this chapter.

3

INTEGRATED PREDICTIVE FREEWAY CONTROL USING THE LINK TRANSMISSION MODEL

In this chapter, we use the recently developed link transmission model (LTM) in an on-line hybrid model-based predictive control (MPC) framework. We first extend the model for ramp metering and variable speed limit control. Next, we present an integrated freeway traffic control approach based on the new model in order to minimize the total time spent in the network. The integrated scheme has the capability of controlling large-scale freeway networks in real-time as the model is computationally efficient and it is yet accurate enough for our control purposes. In addition, we reformulate the extended model as a system of linear inequalities with mixed binary and real variables. The reformulated model along with the linearized objective function establish a mixed integer linear optimization problem that is more tractable and even faster than the original optimization problem integrated in the MPC scheme. Finally, to investigate the performance of the proposed approaches (nonlinear MPC and the mixed integer linear optimization counterpart), we choose a freeway network layout based on the Leuven Corridor in Belgium. First, we calibrate the extended LTM for this network using micro-simulation data and next, we use the calibrated LTM as prediction model inside an MPC controller. Closed-loop results using a microscopic simulation model show that the two proposed MPC methods are able to efficiently improve the total travel time.

3.1. INTRODUCTION

THE link transmission model (LTM) proposed in [238] is a first-order traffic flow model for freeway networks. It was originally developed for dynamic traffic assignment [230]. Results presented and discussed in [115, 238, 239] show the capability of the LTM for fast modeling of large-scale networks. However, this model needs to be extended in order to include effects of traffic measures (ramp metering and variable speed limits (VSLs)) and for using it in model-based traffic control schemes. In the following sections, we will present our proposed modifications of the original LTM for ramp metering and VSL control.

Furthermore, using the extended model, we develop a hybrid model predictive control scheme for freeway network control. In the proposed framework, the extended LTM is used as prediction model. Network modeling and predictive control using the extended LTM is expected to be fast compared to e.g. the METANET-based and CTM-based approaches [104, 195, 241]. However, further steps towards reaching *real-time* and efficient control for large-scale freeway networks is crucial and will be also addressed in this chapter.

In order to achieve real-time control of large-scale freeway networks, we first reformulate the nonlinear LTM. We utilize some mathematical techniques for piecewise affine systems [217] along with the simplifying assumption that the number of VSL values is finite (which is consistent with reality), to transform the extended LTM into a linear model composed of linear equations and inequalities with mixed real and integer variables.

Having transformed the model, the nonlinear optimization in the MPC framework can be replaced by a mixed integer linear optimization problem if the objective function is linearized. The mixed linear optimization problem can be solved faster and in a more tractable way compared to the nonlinear case.

The chapter is organized as follows. In Section 3.2, we define the LTM components and review the original mathematical formulations. In Section 3.3, we elaborately present our extensions for ramp metering and variable speed limits. Section 3.4 first discusses the main concepts, objectives and structure of the proposed predictive ramp metering and VSL control scheme, and next, presents the approximation and reformulation of the extended LTM towards achieving a more efficient and fast control scheme. In the case study section, we evaluate the performance of the integrated ramp metering and VSL control scheme using a real network layout, the Leuven Corridor. First, we present the set-up and results of the identification and the calibration of the LTM. Next, we discuss and compare the closed-loop control results using two MPC methods (non-linear and mixed integer linear programming approaches). Finally, the chapter ends with concluding remarks and future research directions.

3.2. LINK TRANSMISSION MODEL

In this section, the original LTM is introduced using [238] and [239]. The LTM is capable of determining time-dependent link volumes, link travel times, and route travel times in traffic networks. To this aim, the LTM uses the so-called cumulative number of vehicles to represent the traffic evolution. The cumulative numbers of vehicles are updated using flow functions of links and nodes defined in the following subsections.

3.2.1. LINK MODEL

In the LTM framework, the traffic network is characterized by links that are connected via different types of nodes, as depicted in Fig. 3.1. A link i starts at an upstream boundary denoted by x_i^0 and ends at a downstream boundary denoted by x_i^L . The length of the link is denoted by L_i .

The cumulative number of vehicles $N(x, k)$ is defined only for the upstream and downstream boundaries of each link at the time step k , with sample time T_s . In order to obtain the update equations for the cumulative number of vehicles we need to define two quantities for each link: the sending and the receiving number of vehicles. The sending number of vehicles for link i is the maximum number of vehicles that can potentially leave the downstream end of this link during the time interval $[k \cdot T_s, (k+1) \cdot T_s)$ and is defined as

$$S_i(k) = \min \left[N \left(x_i^0, k+1 - \frac{L_i}{v_{\text{free},i} \cdot T_s} \right) - N(x_i^L, k), q_{M,i} \cdot T_s \right], \quad (3.1)$$

where $v_{\text{free},i}$ and $q_{M,i}$ are the free-flow speed and the capacity of link i , respectively. Note that we have assumed a triangular fundamental diagram [41] (which considers that all vehicles have the same free-flow speed regardless of the flow). Moreover, in this chapter, we assume that the fraction $\frac{L_i}{v_{\text{free},i} \cdot T_s}$ has integer values and if not, we round it off towards the closest integer value (in the original LTM formulation, interpolation between grid points is used instead). The sending number is constrained by the boundary conditions at the upstream end of the link. If the downstream link boundary at time step $k+1$ is in the free-flow traffic condition, then this state must have been originated from the upstream boundary $\frac{L_i}{v_{\text{free},i} \cdot T_s}$ time steps earlier. Note that the sample time must be selected as $T_s \leq \frac{L_i}{v_{\text{free}}}$ in order to prevent vehicles from traversing a link within one sampling period.

Similarly, the receiving number of vehicles $R_i(k)$ is the maximum number of vehicles that can enter the upstream end of link i during the time interval $[k \cdot T_s, (k+1) \cdot T_s)$ and it is formulated as

$$R_i(k) = \min \left[N \left(x_i^L, k+1 - \frac{L_i}{w_i \cdot T_s} \right) + \rho_{\text{max},i} L_i - N(x_i^0, k), q_{M,i} \cdot T_s \right], \quad (3.2)$$

where w_i and $\rho_{\text{max},i}$ are the maximum speed of the congestion wave propagating backward, and the jam density of link i , respectively. Similar to the previous case, the fraction $\frac{L_i}{w_i \cdot T_s}$ is also rounded towards the nearest integer value.

3.2.2. NODE MODELS

In the LTM framework, links are connected to each other through different types of nodes. For each node, the transition number of vehicles is defined and determined using the sending and receiving numbers of vehicles of its connected links. Basically, the transition number of vehicles represents the maximum number of vehicles that can travel from incoming links to outgoing links of a node during the time interval $[k \cdot T_s, (k+1) \cdot T_s)$. Moreover, we denote the set of the incoming and the outgoing links of each type of node with ℓ_{in} and ℓ_{out} , respectively. In the following, we define the transition number of vehicles for various types of nodes, starting with the simplest case.

In order to represent a difference in the characteristics of a road such as capacity, speed limits, lane change, etc., an inhomogeneous node n_{nh} can be defined. For the

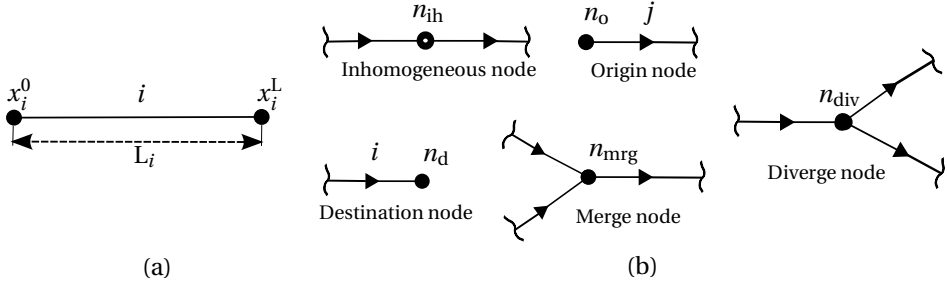


Figure 3.1: (a) Link model, (b) Different node types.

simplest case with one input and one output link, the transition number $G_{ij}(k)$ is formulated as

$$G_{ij}(k) = \min [S_i(k), R_j(k)], \quad i \in \ell_{in}(n_{nh}), j \in \ell_{out}(n_{nh}), \quad (3.3)$$

where i is the unique incoming link and j is the unique outgoing link of the given node.

For each origin in the network, the corresponding origin node n_o is defined and the transition number of vehicles is determined as follows:

$$G_{oj}(k) = \min [N_o(k+1) - N(x_j^0, k), R_j(k)], \quad j \in \ell_{out}(n_o), \quad (3.4)$$

where j is the index of the link connected to the origin (we assume that there is only one link connected to an origin or a destination) and N_o denotes the traffic demand in origin o in terms of the cumulative number of vehicles. A simple queue model for origin o is defined as

$$\omega_o(k) = N_o(k) - N(x_j^0, k), \quad (3.5)$$

where $\omega_o(k)$ and $N(x_j^0, k)$ denote the number of vehicles standing in the queue at origin o and the cumulative number of vehicles that already entered the network at time step k , respectively.

For a destination in the network, the corresponding destination node n_d is defined and the transition number of vehicles is determined based on the sending number of vehicles of the incoming link i and possible restrictions of the destination. If the destination accepts all the flows, the transition number of vehicles will be defined as

$$G_{id}(k) = S_i(k), \quad i \in \ell_{in}(n_d), \quad (3.6)$$

with i the index of the unique incoming link of destination d . Otherwise, if the destination is treated as a bottleneck with a user-defined constrained outflow R_d , the $G_{id}(k)$ would be the minimum of the sending number of vehicles of the incoming link i and the maximum receiving number of vehicles of the destination d :

$$G_{id}(k) = \min [S_i(k), R_d(k)], \quad i \in \ell_{in}(n_d). \quad (3.7)$$

For merging of links and/or on-ramps in traffic networks, a merge node is defined. Multiple models have been proposed for the merge of links, [42, 125, 143, 178, 220]. We choose one of the priority-based merge models for two incoming links proposed in [42].

To this aim, the transition number of vehicles from an incoming link i of a merge node to the unique outgoing link j is formulated as follows:

$$\begin{cases} G_{ij}(k) = S_i(k) & \text{if } R_j(k) \geq S_i(k) + S_{i'}(k), \\ G_{ij}(k) = \text{median} \left[S_i(k), R_j(k) - S_{i'}(k), \alpha_{ij} R_j(k) \right] & \text{otherwise,} \end{cases} \quad (3.8)$$

$$\alpha_{ij} = \frac{q_{M,i}}{q_{M,i} + q_{M,i'}}, \quad (3.9)$$

where $j \in \ell_{\text{out}}(n_{\text{mrg}})$, $i, i' \in \ell_{\text{in}}(n_{\text{mrg}})$, $i \neq i'$. The distribution fractions α_{ij} reflect priorities that are proportional to the capacities of the incoming links $q_{M,i}$. Note that the sum $\sum_{i \in \ell_{\text{in}}(n_{\text{mrg}})} \alpha_{ij}$ is equal to 1. The reader is referred to [220] for a general merge model with more than two incoming links.

A diverge node connects one incoming link i to its outgoing links $j \in \ell_{\text{out}}(n_{\text{div}})$. For the two outgoing links case, the following model for transition numbers of vehicles has been proposed in [177]:

$$G_{ij}(k) = \min \left[\beta_{ij} S_i(k), R_j(k), \frac{\beta_{ij}}{\beta_{ij'}} R_j(k) \right], \quad (3.10)$$

for $j \in \ell_{\text{out}}(n_{\text{div}})$. The outflow of the incoming link is divided over the outgoing links according to the turning fractions β_{ij} ($\sum \beta_{ij} = 1$). For the general case with more than two outgoing and/or incoming links and other types of nodes (e.g. intersection nodes) the interested reader is referred to [220].

3.2.3. UPDATE EQUATIONS

Having determined the transition number of vehicles of all nodes, the cumulative number of vehicles for the upstream and downstream boundaries of links can be updated using the following equations:

$$N(x_i^1, k+1) = N(x_i^1, k) + \sum_{j \in \ell_{\text{out}}(n)} G_{ij}(k), \quad \text{for all } i \in \ell_{\text{in}}(n), \quad (3.11)$$

$$N(x_j^0, k+1) = N(x_j^0, k) + \sum_{i \in \ell_{\text{in}}(n)} G_{ij}(k), \quad \text{for all } j \in \ell_{\text{out}}(n), \quad (3.12)$$

for each node n .

3.3. EXTENSIONS OF THE LTM

In this section, the LTM model is extended to include traffic control signals. First we investigate the possibility of extending the LTM for metering of on-ramps. Next, variable speed control using the LTM is discussed and required modifications of the model are explained.

3.3.1. RAMP METERING

An on-ramp can be treated as a combination of an origin node and a merge node connected by a virtual link with a link length that is equal to 0. We place an origin node for the metered ramp with a constraint on its outflow to a virtual link. Thus, the transition

number of vehicles of the on-ramp o to the virtual link i' can be determined as follows (based on (3.4)):

$$G_{oi'}(k) = \min \left[N_o(k+1) - N(x_{i'}^0, k), r_o(k) \cdot q_{M,i'} \cdot T_s \right], \quad (3.13)$$

where $q_{M,i'}$ is the capacity of the virtual link i' (veh/h), T_s is the sample time, and $r_o(k) \in [0, 1]$ is the metering rate. Moreover, $N_o(k+1)$ denotes the traffic demand in the on-ramp o and $N(x_{i'}^0, k)$ is the cumulative number of vehicles that already entered the virtual link i' .

Next, the transition numbers of vehicles from the virtual link to the outgoing link of the merge node can be determined by (3.8) using $G_{oi'}(k)$, as the sending number of vehicles of the on-ramp, and the sending number of vehicles of the mainstream incoming link.

Note that using the metering rate $r_o(k)$, one can limit the outflow of an on-ramp in order to prevent traffic congestion on the mainstream road.

3

3.3.2. VARIABLE SPEED LIMIT CONTROL

According to [213], [146], [224], [5], there are two aspects of using VSL in practice. The first view is about reducing the speed differences to homogenize the traffic densities on the road in order to have more stable flow of vehicles. The second idea is to reduce densities and prevent congested situations by introducing lower speed limits. The latter view of VSL control is considered in this chapter. In the following, we elaborate on the LTM modifications required in order to emulate the effects of variable speed limit signs.

Basically, a VSL can be used to modify the time that vehicles spend to reach the downstream boundary of a link. By looking at the LTM model, it can be inferred that manipulating the travel time can be realized using a time-varying speed v_{free} in the model. From now on, we denote the time-varying speed v_{free} with $\bar{v}(k)$, the speed that holds for all vehicles entering the link during $[k \cdot T_s, (k+1) \cdot T_s)$. In addition to this modification, different traffic conditions that can occur in reality should be investigated and the resulting cases should be integrated in the extended model. In Fig. 3.2(a) and 3.2(b), the results of changing the value of the VSL in the free-flow condition are shown for two cases. Before proceeding, note that without loss of generality, the VSL is assumed to be implemented at the upstream boundary of a link.

We start with the case that the speed limit increases at time step k^* to a higher value, as depicted in Fig. 3.2(a). In this case, the vehicles are supposed to reach the downstream boundary faster. However, after the value of the speed limit is changed, there may exist some vehicles still traveling in the link that were not confronted with the new speed limit. These vehicles reach the downstream boundary of the link without following the new speed limit. Therefore, in order to obtain a better update for the cumulative number of vehicles, these vehicles should also be taken into account.

On the other hand, when the speed limit is lowered at time step k^* , the evolution of the cumulative number of vehicles may look similar to Fig. 3.2(b) (if a free-flow condition is applied, otherwise in congested situations the influence of VSL may not be as apparent as what is depicted here). Vehicles that enter the link after the time instant at which the VSL value is altered, are affected by the new speed limit and will follow the new speed restriction. However, for the vehicles that are already in the link, the

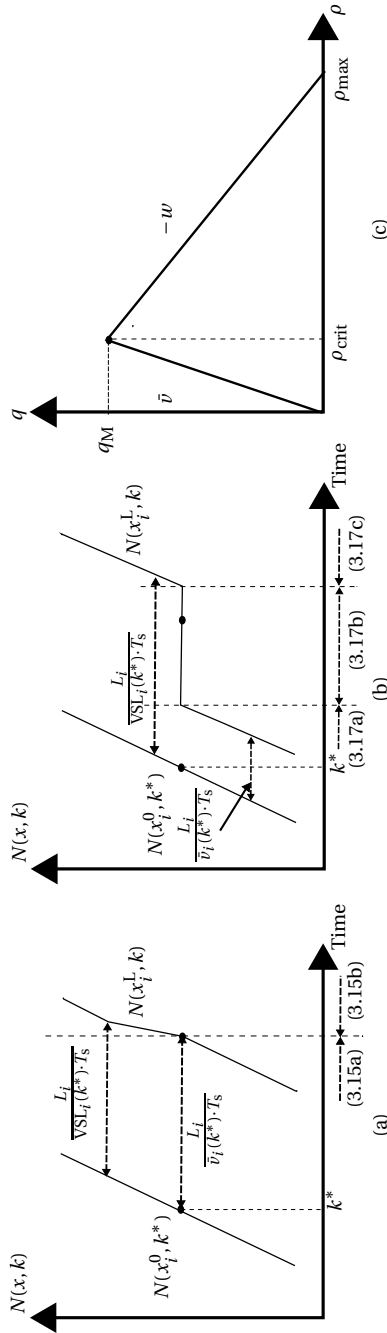


Figure 3.2: (a) Increase in the value of VSL (see conditions (3.15a) and (3.15b)), (b) Decrease in the value of VSL (see conditions (3.18a)–(3.18c)) (c) Triangular fundamental diagram.

new speed limit is not applicable. They reach the upstream boundary with their previously assigned speed limit or the free-flow speed of the freeway. Moreover, since the new speed limit is lower, there will be a time interval in which the cumulative number of vehicles remains constant (this means that no vehicle departs from the downstream end). With this information, we now mathematically formulate these conditions.

INCREASE IN THE VALUE OF VSL

As shown in Fig. 3.2(a), it takes some time for the vehicles that did not experience the new speed limit to leave the link. Before this time, the sending number of vehicles should be determined using the old value of \bar{v} . Moreover, the capacity of the road $q_{M,i}$ is calculated using a triangular fundamental diagram constructed on the old \bar{v} (we assume that the speed of the backward propagating congestion wave remains unchanged). From Fig. 3.2(c), the capacity $q_{M,i}$ can be determined as follows:

$$q_{M,i} = \rho_{\max,i} \cdot \frac{\bar{v}_i \cdot w_i}{\bar{v}_i + w_i}. \quad (3.14)$$

If the value of the VSL increases at time step k^* , the speed \bar{v} and the capacity of link i will be changed according to the following conditions (for $k \geq k^*$):

$$\left\{ \begin{array}{l} \text{if } N(x_i^L, k) < N(x_i^0, k^*) : \left\{ \begin{array}{l} N(x_i^L, k+1) = N(x_i^0, k+1 - \frac{L_i}{\bar{v}_i(k^*-1) \cdot T_s}), \\ \bar{v}_i(k) = \bar{v}_i(k^* - 1), \\ q_{M,i}(k) = \rho_{\max,i} \cdot \frac{\bar{v}_i(k^*-1) \cdot w_i}{\bar{v}_i(k^*-1) + w_i}, \end{array} \right. \end{array} \right. , \quad (3.15a)$$

$$\left\{ \begin{array}{l} \text{if } N(x_i^L, k) \geq N(x_i^0, k^*) : \left\{ \begin{array}{l} N(x_i^L, k+1) = N(x_i^0, k+1 - \frac{L_i}{\text{VSL}_i(k^*) \cdot T_s}), \\ \bar{v}_i(k) = \text{VSL}_i(k^*), \\ q_{M,i}(k) = \rho_{\max,i} \cdot \frac{\text{VSL}_i(k^*) \cdot w_i}{\text{VSL}_i(k^*) + w_i}, \end{array} \right. \end{array} \right. \quad (3.15b)$$

where $\text{VSL}_i(k^*)$ is the value at the time step k^* of the VSL installed at the upstream boundary of link i . In the case (3.15a), the vehicles that are being confronted by the new VSL value has not reached the end of the link. Therefore, the value of $N(x_i^L, k+1)$ must be related to the value of $N(x_i^0)$ with a travel delay that is calculated based on the old value of the VSL, i.e. $\frac{L_i}{\bar{v}_i(k^*-1) \cdot T_s}$. Once the first vehicle reaches the downstream end of the link, the condition (3.15b) holds and the value of $N(x_i^L, k+1)$ must be calculated based on the new travel delay $\frac{L_i}{\text{VSL}_i(k^*) \cdot T_s}$.

Now the sending number of vehicles for link i can be determined using $N(x_i^L, k+1)$ and $q_{M,i}(k)$ obtained from (3.15a)–(3.15b):

$$S_i(k) = \min \left[N(x_i^L, k+1) - N(x_i^L, k), q_{M,i}(k) \cdot T_s \right]. \quad (3.16)$$

On the other hand, in order to determine the receiving number of vehicles $R_i(k)$, the capacity $q_{M,i}$ should be altered *immediately* after the VSL value is changed. This means that the capacity should be always calculated using $\text{VSL}_i(k)$, as follows:

$$R_i(k) = \min \left[N \left(x_i^L, k+1 - \frac{L_i}{w_i \cdot T_s} \right) + \rho_{\max,i} L_i - N(x_i^0, k), \rho_{\max,i} \cdot \frac{\text{VSL}_i(k) \cdot w_i}{\text{VSL}_i(k) + w_i} \cdot T_s \right], \quad (3.17)$$

This is due to the fact that for predecessor links of link i , the capacity of link i is changed when a new speed limit is introduced. But for the sending number of vehicles at the downstream boundary of link i , the capacity remains unchanged until all the vehicles that did not experience the new speed limit pass the end of link i , which is exactly the criterion distinguishing (3.15a) from (3.15b).

DECREASE IN THE VALUE OF VSL

In order to formulate the problem in this case, we note that every vehicle that reaches the downstream end of a link must have entered the link either $\frac{L_i}{\bar{v}_i(k^*-1)}$ or $\frac{L_i}{\text{VSL}_i(k^*)}$ time steps earlier (note that $\text{VSL}_i(k^*) < \bar{v}_i(k^*-1)$). Hence for $k \geq k^*$, $N(x_i^L, k+1)$ can be equal to $N(x_i^0, k+1 - \frac{L_i}{\bar{v}_i(k^*-1)})$, $N(x_i^0, k+1 - \frac{L_i}{\text{VSL}_i(k^*)})$ or $N(x_i^0, k^*)$. In (3.18a)–(3.18c), different conditions that may occur and the corresponding changes in the model are presented.

$$\left\{ \begin{array}{l} \text{if } N(x_i^0, k^*) > N\left(x_i^0, k+1 - \frac{L_i}{\bar{v}_i(k^*-1) \cdot T_s}\right): \\ \quad \left\{ \begin{array}{l} N(x_i^L, k+1) = N\left(x_i^0, k+1 - \frac{L_i}{\bar{v}_i(k^*-1) \cdot T_s}\right), \\ \bar{v}_i(k) = \bar{v}_i(k^*-1), \\ q_{M,i}(k) = \rho_{\max,i} \cdot \frac{\bar{v}_i(k^*-1) \cdot w_i}{\bar{v}_i(k^*-1) + w_i}, \end{array} \right. \end{array} \right. \quad (3.18a)$$

$$\left\{ \begin{array}{l} \text{if } N\left(x_i^0, k+1 - \frac{L_i}{\bar{v}_i(k^*-1) \cdot T_s}\right) \geq N(x_i^0, k^*) \geq N\left(x_i^0, k+1 - \frac{L_i}{\text{VSL}_i(k^*) \cdot T_s}\right): \\ \quad \left\{ \begin{array}{l} N(x_i^L, k+1) = N(x_i^0, k^*), \\ \bar{v}_i(k) = \bar{v}_i(k^*-1), \\ q_{M,i}(k) = \rho_{\max,i} \cdot \frac{\bar{v}_i(k^*-1) \cdot w_i}{\bar{v}_i(k^*-1) + w_i}, \end{array} \right. \end{array} \right. \quad (3.18b)$$

$$\left\{ \begin{array}{l} \text{if } N\left(x_i^0, k+1 - \frac{L_i}{\text{VSL}_i(k^*) \cdot T_s}\right) > N(x_i^0, k^*): \\ \quad \left\{ \begin{array}{l} N(x_i^L, k+1) = N\left(x_i^0, k+1 - \frac{L_i}{\text{VSL}_i(k^*) \cdot T_s}\right), \\ \bar{v}_i(k) = \text{VSL}_i(k^*), \\ q_{M,i}(k) = \rho_{\max,i} \cdot \frac{\text{VSL}_i(k^*) \cdot w_i}{\text{VSL}_i(k^*) + w_i}, \end{array} \right. \end{array} \right. \quad (3.18c)$$

The first case (3.18a) pertains to vehicles reaching the downstream boundary that were not confronted with the new (lower) speed limit. Hence, the update for the cumulative number of vehicles $N(x_i^L, k+1)$ should be calculated based on the old speed $\bar{v}_i(k^*-1)$. In the second case (3.18b), due to the lower VSL value for the link, there is no vehicle passing the downstream end for a short period. Thus, $N(x_i^L, k+1)$ should be equal to the cumulative number of vehicles at the upstream boundary by the time step that the VSL sign is changed (k^*). The last case (3.18c) describes the situation that vehicles reach the downstream end while they did encounter the new value of the VSL. Therefore, the cumulative number $N(x_i^L, k+1)$ should be calculated based on the new speed limit $\bar{v}_i(k) = \text{VSL}_i(k^*)$.

The sending number of vehicles is calculated using $N(x_i^L, k+1)$ and $q_{M,i}(k)$ obtained from the conditions (3.18a)–(3.18c) and (3.16). However, as mentioned in the previous

section, in order to determine the receiving number of vehicles $R_i(k)$, the capacity $q_{M,i}$ should be altered right after the new speed limit is announced (this means that for $k \geq k^*$, $q_{M,i}(k) = \rho_{\max,i} \cdot \frac{VSL_i(k^*) \cdot w_i}{VSL_i(k^*) + w_i}$ for use in the receiving number of vehicles equation (3.17)).

Furthermore, all the aforementioned equations in the current section and in the previous section are valid until a new speed limit is introduced. Whenever a new limit is announced, based on its new value (which could be lower or higher than the old one), the evolution equations should be updated as prescribed in this section. However, it should be noted that in our framework, the VSL values should not be updated rapidly. In fact the VSL updating interval must be bigger than the largest free-flow travel time in the link.

In the next section, the extended LTM will be utilized in the model predictive control framework for ramp metering and VSL control of freeway traffic networks.

3.4. PREDICTIVE HYBRID FREEWAY TRAFFIC CONTROL

Model Predictive Control (MPC) [160] is an advanced control method originally developed for control of industrial processes and recently for traffic networks [12, 59, 104, 187]. The main concept is to use a prediction model of the system and an objective function that assesses the desired performance over a given prediction horizon, and next, to find the optimal control inputs using an optimization algorithm. The optimization algorithm finds a sequence of optimal control inputs for the whole prediction horizon, but only the first control input sample is applied to the system and the procedure is repeated for the next control step but with a shift in the prediction period.

3.4.1. NONLINEAR MODEL PREDICTIVE CONTROL FORMULATION

For a traffic network, one can define different objective functions based on travel time, fuel consumption of vehicles, emissions, etc. The objective function we choose here is the total time spent (TTS) in the traffic network, consisting of the time vehicles spend in queues at mainstream origins and on-ramps and the travel time on the freeway. The TTS objective function in the MPC framework is formulated as follows:

$$J_{TTS}(k_c) = T_s \cdot \sum_{k=Mk_c}^{M(k_c+N_p)-1} \left[\sum_{o \in O_{\text{all}}} \omega_o(k) + \sum_{i \in \ell_{\text{all}}} (N(x_i^0, k) - N(x_i^1, k)) \right], \quad (3.19)$$

where T_s is the simulation sample time, k_c is the controller time step counter, and k is the model time step counter. In fact, we assume that the controller sample time T_c is an integer multiple of the simulation sample time: $T_c = MT_s$. In the time intervals between consecutive control time steps, the control inputs are not altered. Moreover, N_p is the prediction horizon, ω_o is the queue length at origin o , and ℓ_{all} and O_{all} are the set of all links and the set of all origins, respectively. Moreover, the optimal control inputs obtained from the MPC controller may in general have undesired fluctuations over time. Note that the control inputs are in fact the metering rate and the values shown on the VSL signs. Therefore, to avoid large fluctuations a penalty term on the control input deviations is introduced and added to the objective function. The penalty term on the

ramp metering input is formulated as

$$\zeta_r \sum_{l=k_c}^{k_c+N_p-1} \sum_{o \in O_{\text{ramp}}} |r_o(l) - r_o(l-1)|, \quad (3.20)$$

where r_o is the metering signal, O_{ramp} is the set of indices of metered ramps¹, and ζ_r is a weighting factor. Similarly, penalizing the VSL input can be formulated as

$$\zeta_v \sum_{l=k_c}^{k_c+N_p-1} \sum_{i \in \ell_{\text{vsl}}} |\text{VSL}_i(l) - \text{VSL}_i(l-1)|, \quad (3.21)$$

where VSL_i is the VSL input, ℓ_{vsl} is the set of indices of links equipped with VSL signs, and ζ_v is a weighting factor.

Moreover, to reduce the complexity, control variables are sometimes taken constant after passing a predefined control horizon N_c . Taking this into account, N_p in (3.20) and (3.21) can be replaced by N_c . Moreover, to take into account the physical limitation of queues at on-ramps, we use a hard constraint on the queue lengths. The total objective function along with the queue length constraint and the LTM as prediction model constitute a nonlinear nonconvex optimization problem that has to be solved at every control step in the MPC framework to find the optimal control signals. There is no guarantee to find a unique global solution for the optimization problem and furthermore, solving the nonlinear optimization may take considerable time. In the next section, a solution to this problem is proposed. More specifically, we will transform the nonlinear nonconvex optimization problem into a mixed integer linear programming (MILP) problem.

Using the methods proposed in [188, 234], one can transform the model and the objective function into a system of linear equations and inequalities involving real and integer variables and formulate an MILP problem. The MILP problem can be efficiently solved using existing MILP solvers like CPLEX or GLPK (see [7]). Note that MILP solvers can find the *global* optimum of the MILP problem.

3.4.2. REFORMULATION OF THE LINK TRANSMISSION MODEL

In order to obtain an MILP problem, we first transform the extended LTM into a system of linear inequalities with mixed real and binary variables, inspired by the method proposed in [188]. Compared to the mixed logical dynamical form proposed in [15], this system of linear inequalities is less complex, as it needs less and less inequalities to model the system.

In the following, we present the transformation approach for different parts of the LTM. First, we consider the parts of the model that are not affected by the VSL extension, and next, we present the reformulation of the proposed VSL extensions into the linear form.

For links that are not equipped with VSL signs, the delays $\frac{L_i}{v_{\text{free},i} \cdot T_s}$ and $\frac{L_i}{w_i \cdot T_s}$ would be constant over time. Moreover, the transition number of vehicles (3.3) for a homogeneous

¹It should be noted that outflows of mainstream origins can also be controlled in some cases (mainstream metering), so in that case they can also be included in the set O_{ramp} .

node is the minimum of the following three affine functions (based on the formulations in (3.1) and (3.2)):

$$f_{G_{ij},1}(k) = N\left(x_i^0, k + 1 - \frac{L_i}{v_{\text{free},i} \cdot T_s}\right) - N(x_i^I, k), \quad (3.22)$$

$$f_{G_{ij},2}(k) = q_{M,i}(k) \cdot T_s, \quad (3.23)$$

$$f_{G_{ij},3}(k) = N\left(x_i^I, k + 1 - \frac{L_i}{w_i \cdot T_s}\right) + \rho_{\max,i} L_i - N(x_i^0, k). \quad (3.24)$$

The minimum operation over three functions can be represented by the following logical sentence:

$$\begin{aligned} & \left\{ (f_{G_{ij},1}(k) \leq f_{G_{ij},2}(k)) \wedge (f_{G_{ij},1}(k) \leq f_{G_{ij},3}(k)) \Leftrightarrow (G_{ij}(k) = f_{G_{ij},1}(k)) \right\} \\ \vee & \left\{ (f_{G_{ij},2}(k) \leq f_{G_{ij},1}(k)) \wedge (f_{G_{ij},2}(k) \leq f_{G_{ij},3}(k)) \Leftrightarrow (G_{ij}(k) = f_{G_{ij},2}(k)) \right\} \\ \vee & \left\{ (f_{G_{ij},3}(k) \leq f_{G_{ij},1}(k)) \wedge (f_{G_{ij},3}(k) \leq f_{G_{ij},2}(k)) \Leftrightarrow (G_{ij}(k) = f_{G_{ij},3}(k)) \right\} \end{aligned} \quad (3.25)$$

We introduce two binary variables $\delta_{G_{ij},1}$ and $\delta_{G_{ij},2}$, and we also define the constraint $\delta_{G_{ij},1}(k) + \delta_{G_{ij},2}(k) \leq 1$ so that we can have only three combinations for $(\delta_{G_{ij},1}, \delta_{G_{ij},2})$. The transformation of (3.25) to a set of linear inequalities is [188]:

$$\delta_{G_{ij},1}(k) + \delta_{G_{ij},2}(k) \leq 1, \quad (3.26)$$

$$(\delta_{G_{ij},1}(k) + \delta_{G_{ij},2}(k)) \cdot M^- \leq G_{ij}(k) - f_{G_{ij},1}(k) \leq 0, \quad (3.27)$$

$$(1 - \delta_{G_{ij},1}(k) + \delta_{G_{ij},2}(k)) \cdot M^- \leq G_{ij}(k) - f_{G_{ij},2}(k) \leq 0, \quad (3.28)$$

$$(1 + \delta_{G_{ij},1}(k) - \delta_{G_{ij},2}(k)) \cdot M^- \leq G_{ij}(k) - f_{G_{ij},3}(k) \leq 0, \quad (3.29)$$

where M^- is a negative number with a large absolute value that ensures

$$|M^-| > \left| \min_{n \in \{1,2,3\},k} [G_{ij}(k) - f_{G_{ij},n}(k)] \right|. \quad (3.30)$$

The equivalence of (3.3) and (3.26)–(3.29) is validated as follows:

$$f_{G_{ij},1}(k) \leq f_{G_{ij},2}(k) \text{ and } f_{G_{ij},1}(k) \leq f_{G_{ij},3}(k) \Leftrightarrow \begin{cases} G_{ij}(k) = f_{G_{ij},1}(k), \\ (\delta_{G_{ij},1}(k), \delta_{G_{ij},2}(k)) = (0, 0) \end{cases} \quad (3.31)$$

$$f_{G_{ij},2}(k) \leq f_{G_{ij},1}(k) \text{ and } f_{G_{ij},2}(k) \leq f_{G_{ij},3}(k) \Leftrightarrow \begin{cases} G_{ij}(k) = f_{G_{ij},2}(k), \\ (\delta_{G_{ij},1}(k), \delta_{G_{ij},2}(k)) = (1, 0) \end{cases} \quad (3.32)$$

$$f_{G_{ij},3}(k) \leq f_{G_{ij},1}(k) \text{ and } f_{G_{ij},3}(k) \leq f_{G_{ij},2}(k) \Leftrightarrow \begin{cases} G_{ij}(k) = f_{G_{ij},3}(k), \\ (\delta_{G_{ij},1}(k), \delta_{G_{ij},2}(k)) = (0, 1) \end{cases} \quad (3.33)$$

The same procedure can be applied to origin and destination nodes.

The transition number of vehicles for merging nodes can also be transformed into

linear inequalities. Consider the merging of two incoming links i and i' :

$$\begin{cases} G_{ij}^{\text{mrg}}(k) = S_i(k), & G_{i'j}^{\text{mrg}}(k) = S_{i'}(k) & \text{if } R_j(k) \geq S_i(k) + S_{i'}(k), \\ \left\{ \begin{array}{l} G_{ij}^{\text{mrg}}(k) = \text{median} \left[S_i(k), R_j(k) - S_{i'}(k), \alpha_{ij} R_j(k) \right], \\ G_{i'j}^{\text{mrg}}(k) = \text{median} \left[S_{i'}(k), R_j(k) - S_i(k), \alpha_{i'j} R_j(k) \right] \end{array} \right. & \text{otherwise,} \end{cases} \quad (3.34)$$

with $\alpha_{ij} = \frac{q_{M,i}}{q_{M,i} + q_{M,i'}}$, $\alpha_{i'j} = \frac{q_{M,i'}}{q_{M,i} + q_{M,i'}}$.

We consider the transformation of the transition number of vehicles from link i to the outgoing link j , $G_{ij}^{\text{mrg}}(k)$ (a similar approach can be applied to $G_{i'j}^{\text{mrg}}(k)$). First of all, for condition $R_j(k) \geq S_i(k) + S_{i'}(k)$, we can define a binary variable $\delta_{\text{mrg}}(k)$. We assume that the binary variable is set to 1 whenever the condition holds. Now the condition can be transformed to a linear form using the following basic rule [15]:

$$[f(x) \leq 0] \Leftrightarrow [\delta = 1], \quad \text{iff} \quad \begin{cases} f(x) \leq M \cdot (1 - \delta), \\ f(x) \geq \epsilon + (m - \epsilon) \cdot \delta, \end{cases} \quad (3.35)$$

with f an affine function defined over a bounded set \mathcal{X} of the input variable x , m and M the lower and upper bounds of f over \mathcal{X} , $\epsilon > 0$ a small tolerance namely the machine precision². The transformed condition is formulated as follows:

$$S_i(k) + S_{i'}(k) - R_j(k) \leq M^{\text{mrg}} \cdot (1 - \delta_{\text{mrg}}(k)), \quad (3.36)$$

$$S_i(k) + S_{i'}(k) - R_j(k) \geq \epsilon + (m^{\text{mrg}} - \epsilon) \cdot \delta_{\text{mrg}}(k), \quad (3.37)$$

where M^{mrg} and m^{mrg} denote the upper and the lower bounds of $S_i(k) + S_{i'}(k) - R_j(k)$. Note that an estimation of the bounds m^{mrg} , M^{mrg} can be obtained based on the trajectories of $S_i, R_j, S_{i'}$ obtained from simulation and historical data from the traffic network. Note that a tight upper/lower bound estimation is not crucial, although it is better from a computational point of view.

Moreover, we include the following constraint:

$$(1 - \delta_{\text{mrg}}(k)) \cdot m_{ij} \leq G_{ij}^{\text{mrg}}(k) - S_i(k) \leq (1 - \delta_{\text{mrg}}(k)) \cdot M_{ij}, \quad (3.38)$$

with m_{ij} and M_{ij} the lower and the upper bounds of $G_{ij}^{\text{mrg}}(k) - S_i(k)$, respectively. Now if $\delta_{\text{mrg}} = 1$, then $G_{ij}^{\text{mrg}}(k) = S_i(k)$.

Now for simplicity, we assign new names for the affine functions in the argument of the median operator, as follows:

$$g_1(k) = S_{i'}(k), \quad (3.39)$$

$$g_2(k) = R_j(k) - S_{i'}(k), \quad (3.40)$$

$$g_3(k) = \alpha_{ij} R_j(k). \quad (3.41)$$

Moreover, three binary variables $\delta_{\text{med},1}(k)$, $\delta_{\text{med},2}(k)$, $\delta_{\text{med},3}(k)$ are defined. Six combinations may occur and therefore we add the following two constraints:

$$\delta_{\text{med},1}(k) + \delta_{\text{med},2}(k) + \delta_{\text{med},3}(k) \geq 1, \quad (3.42)$$

$$\delta_{\text{med},1}(k) + \delta_{\text{med},2}(k) + \delta_{\text{med},3}(k) \leq 2, \quad (3.43)$$

²It is mainly used to change a strict inequality into a non-strict inequality.

to cover all the possible conditions. It can be verified that the constraints³

$$g_1 - g_3 \leq (1 - \delta_{\text{med},1} + \delta_{\text{med},3}) \cdot M^+, \quad (3.44)$$

$$g_3 - g_1 \leq (1 - \delta_{\text{med},3} + \delta_{\text{med},1}) \cdot M^+, \quad (3.45)$$

$$g_2 - g_1 \leq (1 - \delta_{\text{med},1} + \delta_{\text{med},2}) \cdot M^+, \quad (3.46)$$

$$g_1 - g_2 \leq (2\delta_{\text{med},1} + \delta_{\text{med},2} + \delta_{\text{med},3} - 1) \cdot M^+, \quad (3.47)$$

$$g_3 - g_2 \leq (3 - 2\delta_{\text{med},1} - \delta_{\text{med},2} - \delta_{\text{med},3}) \cdot M^+, \quad (3.48)$$

$$g_2 - g_3 \leq (1 + \delta_{\text{med},1} - \delta_{\text{med},2}) \cdot M^+, \quad (3.49)$$

$$(\delta_{\text{med},1} + 2\delta_{\text{med},2} + \delta_{\text{med},3} - 1) \cdot M^- + \delta_{\text{mrg}} \cdot M^- \leq G_{ij}^{\text{mrg}} - g_1 \leq (\delta_{\text{med},1} + 2\delta_{\text{med},2} + \delta_{\text{med},3} - 1) \cdot M^+ + \delta_{\text{mrg}} \cdot M^+, \quad (3.50)$$

$$(1 + \delta_{\text{med},1} - \delta_{\text{med},2} + \delta_{\text{med},3}) \cdot M^- + \delta_{\text{mrg}} \cdot M^- \leq G_{ij}^{\text{mrg}} - g_2 \leq (1 + \delta_{\text{med},1} - \delta_{\text{med},2} + \delta_{\text{med},3}) \cdot M^+ + \delta_{\text{mrg}} \cdot M^+, \quad (3.51)$$

$$(2 - \delta_{\text{med},1} + \delta_{\text{med},2} - \delta_{\text{med},3}) \cdot M^- + \delta_{\text{mrg}} \cdot M^- \leq G_{ij}^{\text{mrg}} - g_2 \leq (2 - \delta_{\text{med},1} + \delta_{\text{med},2} - \delta_{\text{med},3}) \cdot M^+ + \delta_{\text{mrg}} \cdot M^+, \quad (3.52)$$

$$(3 - \delta_{\text{med},1} - 2\delta_{\text{med},2} - \delta_{\text{med},3}) \cdot M^- + \delta_{\text{mrg}} \cdot M^- \leq G_{ij}^{\text{mrg}} - g_3 \leq (3 - \delta_{\text{med},1} - 2\delta_{\text{med},2} - \delta_{\text{med},3}) \cdot M^+ + \delta_{\text{mrg}} \cdot M^+, \quad (3.53)$$

along with (3.36)–(3.38) and (3.42)–(3.43) are an equivalent representation of (3.34). Note that $M^- \ll 0$ and $M^+ \gg 0$ in (3.44)–(3.53) should be chosen in a similar way as in (3.30).

Now we consider the links that have speed limit signs installed and activated at their upstream boundary. According to Section 3.3.2, the delay term in the sending number of vehicles is time-varying (note that the congestion wave speed w is assumed not to be altered. Hence, the delay term $\frac{L_i}{w_i \cdot T_s}$ is constant). Therefore, the function (3.22) is no longer affine. Moreover, in the presence of speed limits, the conditions introduced in Section 3.3.2 need to be taken into account in order to determine the correct delay in (3.1) and also the capacity $q_{M,i}(k)$.

In order to simplify the transformation, we assume that the VSL can take values only from a finite set. This is a realistic assumption since the VSL signs on roads typically show only 3-5 discrete numbers for the speed limit (e.g. 50, 70, 100, 120 km/h). Therefore, the sending number of vehicles can be reformulated as sum of cumulative number of vehicles with different discrete delays:

$$S_i(k) = \min \left[q_{M,i}, \sum_{n=1}^{N_{\text{speed}}} \delta_n(k) \cdot N \left(x_i^0, k + 1 - \frac{L_i}{\text{VSL}_{i,n} \cdot T_s} \right) - N(x_i^L, k) \right], \quad (3.54)$$

with N_{speed} the total number of discrete VSL values. On the other hand, we can define two binary variables $\delta_{i,\text{inc}}$ and $\delta_{i,\text{dec}}$, as follows:

$$\text{VSL}_i(k) - \text{VSL}_i(k-1) - \epsilon \geq 0 \iff \delta_{i,\text{inc}}(k) = 1, \quad (3.55)$$

$$\text{VSL}_i(k) - \text{VSL}_i(k-1) + \epsilon \leq 0 \iff \delta_{i,\text{dec}}(k) = 1. \quad (3.56)$$

Hence, we can capture and store the value $N(x_i^0, k^*)$ in $Z_{N,i}$, formulated as

$$Z_{N,i}(k) = [\delta_{i,\text{inc}}(k) + \delta_{i,\text{dec}}(k)] \cdot N(x_i^0, k). \quad (3.57)$$

Similarly, we can store the VSL value in an auxiliary variable $Z_{\text{VSL},i}$:

$$Z_{\text{VSL},i}(k) = [\delta_{i,\text{inc}}(k) + \delta_{i,\text{dec}}(k)] \cdot \text{VSL}_i(k). \quad (3.58)$$

³The time index k is dropped for the ease of readability.

If $k = k^*$, then $Z_{VSL,i}(k^*) = VSL_i(k^*)$, otherwise $Z_{VSL,i}(k) = 0$. Now we review two basic rules adopted from [15]. The product of two binary variables δ_1 and δ_2 can be replaced by an auxiliary binary variable $\delta_3 \triangleq \delta_1 \cdot \delta_2$. It can be verified that

$$\delta_3 = \delta_1 \cdot \delta_2 \text{ iff } \begin{cases} -\delta_1 + \delta_3 \leq 0, \\ -\delta_2 + \delta_3 \leq 0, \\ \delta_1 + \delta_2 - \delta_3 \leq 1. \end{cases} \quad (3.59)$$

Moreover, multiplication of a binary variable δ with an affine function $f(\cdot)$ defined over a bounded set \mathcal{X} of the variable x can be replaced by an auxiliary variable $z \triangleq \delta \cdot f(x)$, meaning that $z = 0$ when $\delta = 0$ and $z = f(x)$ in case $\delta = 1$. It can be proved that

$$z = \delta \cdot f(x) \text{ iff } \begin{cases} z \leq M \cdot \delta, \\ z \geq m \cdot \delta, \\ z \leq f(x) - m \cdot (1 - \delta), \\ z \geq f(x) - M \cdot (1 - \delta), \end{cases} \quad (3.60)$$

with m and M the lower and upper bounds of $f(\cdot)$ over the set \mathcal{X} , respectively. Using the equivalent forms (3.35), (3.59), (3.60), we can transform (3.54)–(3.58) and subsequently, the VSL conditions (3.15a)–(3.15b) and (3.18a)–(3.18c) into a system of linear equations and inequalities.

3.4.3. MIXED INTEGER LINEAR OPTIMIZATION PROBLEM

After transforming the LTM into a linear form, the total objective function should also be reformulated. The TTS objective function is already linear. But the penalty terms (3.20) and (3.21) are piecewise affine. It can be transformed into a mixed-integer linear form by defining additional binary and auxiliary variables. However, there exists a more efficient way to recast the penalty terms as linear problems without introducing binary variables. It can be easily proved that the following optimization problems have the same optimal solution:

$$\min_{\theta} \sum |\theta_i| \iff \begin{cases} \min_{\theta, \beta} \sum \beta_i \\ \beta_i \geq \theta_i \\ \beta_i \geq -\theta_i \end{cases}$$

Using this technique along with the reformulated model, the final MILP problem can be constructed.

3.5. CASE STUDY

This section describes the evaluation of the proposed integrated ramp metering and variable speed limit control scheme. First, the benchmark network and the selected traffic scenario will be described. Next, identification and calibration of the LTM for the benchmark network is presented. Finally, closed-loop control results of the freeway network using the proposed model predictive control schemes will be presented.

3.5.1. SET-UP

The South-North direction of the A2 freeway near Leuven, Belgium, is taken as the benchmark network. Fig. 3.3 shows a Google maps illustration of this freeway. The

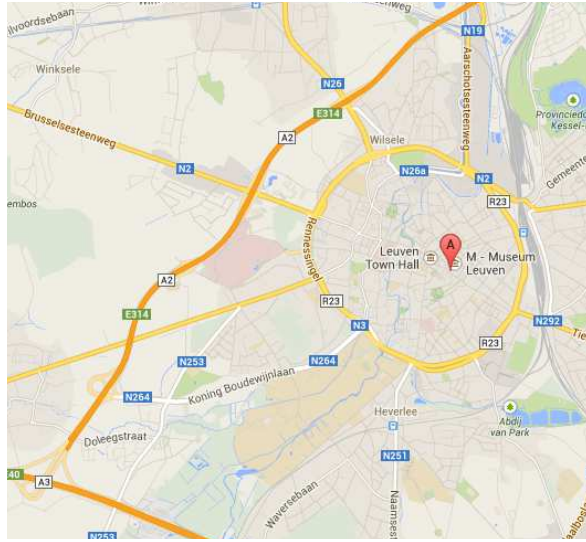


Figure 3.3: Google maps illustration of the A2 freeway in Leuven, Belgium. The South-North direction is used for the evaluation.



Figure 3.4: Schematic representation of the network.

freeway consists of 4 on-ramps and 4 off-ramps and congestion is triggered at the most downstream on-ramp. Ramp metering installations are placed at every on-ramp and variable speed limits are placed directly downstream of every off-ramp. Fig. 3.4 shows a schematic representation of the freeway network. The freeway is divided up into 11 links with two lanes which have the following lengths in kilometers, ordered from upstream to downstream: 1, 1.18, 0.42, 1.03, 0.53, 0.52, 0.72, 0.82, 0.4, 1.8, and 1.0 km. Inductive loop detectors measuring the number of vehicles that have passed, and their average speed are located at the upstream and downstream end of every link.

The four off-ramps are located at positions 2.18, 3.63, 4.68, and 6.22 km. The end of the merging section is considered as the off-ramp location. The on-ramps are located at positions 2.6, 4.16, 5.4, and 6.86 km. The beginning of the merging section is taken as the on-ramp location. At every on-ramp, the stop-line of the ramp metering installation is located 150 meters upstream of the merging area. The on-ramp queue has a storage space of 900 meters. Loop detectors are placed at the stop-line, and at the maximum queue length, 900 meters upstream of the stop-line.

The freeway is simulated using the microscopic simulation software package VISSIM 5.30. The following parameters of VISSIM have been altered from the default settings: CC0 3.50 m, CC1 1.1 s, CC2 8.00 m, CC3 -8.00 (-), CC4 -0.50 (-), CC5 0.60 (-), CC6 6.00 (-), CC7 -0.25 (m/s²), CC8 1.00 (m/s²), and CC9 1.50 m/s². Using these parameters, a capacity flow of 1800 veh/h/lane, and a queue discharge rate of 1800 veh/h/lane are

obtained, thus, there is no capacity drop present. The sampling time in VISSIM is 0.2 seconds. Furthermore, the demand profiles for the mainstream road and the on-ramps are presented in Table 3.1. The (fixed) split fractions are 28.09% of the mainstream flow for off-ramp 1, 6.79% for off-ramp 2, 12.90% for off-ramp 3, and 10.26% for off-ramp 4. Note that the demand of on-ramp 4 has an increase to 1000 (veh/h) for a short period and then it decreases to a lower level. This high on-ramp demand causes congestion on the mainstream road that propagates all the way back to the upstream end of the freeway (as also illustrated in Fig. 3.6(a)).

Table 3.1: Mainstream and on-ramps demands (veh/h)

Timing	Main	Ramp 1	Ramp 2	Ramp 3	Ramp 4
0-900 s	2225	240.5	223	265	250
900-1800 s	4450	750	446	530	500
1800-2100 s	4450	750	446	530	1000
2100-2400 s	4450	750	446	530	250
2400-6300 s	4450	750	446	530	500
6300-7200 s	2225	240.5	223	265	250

MATLAB is used to compute the optimal ramp metering and VSL signals. The simulation sample time in MATLAB is 5 seconds. The MPC controller determines the optimal control inputs every 60 seconds using the TOMLAB optimization toolbox (the *patternsearch* solver is used to solve the nonlinear optimization problem, and the *CPLEX* solver inside the TOMLAB toolbox is used to solve the MILP problem) in MATLAB on a computer with a 3.6 GHz processor and 8Gb RAM.

3.5.2. IDENTIFICATION AND CALIBRATION OF THE LTM

Using simulation data from VISSIM, the LTM is calibrated. The identification procedure for estimation of the LTM parameters is formulated as a nonlinear optimization problem solved using the global optimization solver *patternsearch*. The objective is to minimize the difference between the real densities and the estimated densities from the LTM, formulated as follows:

$$\mathcal{J} = \frac{1}{n_d n_\ell} \sum_{i=1}^{n_\ell} \sum_{k=1}^{n_d} (\rho_i(k) - \hat{\rho}_i(k))^2, \quad (3.61)$$

where n_d , n_ℓ , ρ_i , and $\hat{\rho}_i$ denote the number of data samples, the number of links, the real flow and the flow predicted by the LTM, respectively. The density of links can be calculated using the cumulative number of vehicles for upstream and downstream boundaries of links, as follows:

$$\rho_i(k) = \frac{N(x_i^0, k) - N(x_i^1, k)}{L_i}. \quad (3.62)$$

The nonlinear optimization problem is solved using the function *patternsearch* from the *Global Optimization* toolbox of MATLAB. The optimization algorithm is run 10 times for different random initial points in order to prevent reaching a local optimum only. The

Table 3.2: Estimated parameters for each link

Link	v_{free} (km/h)	w (km/h)	ρ_{max} (veh/km)	q_M (veh/h)
1	119.00	23.00	290.34	5596
2	119.84	24.00	271.24	5423
3	115.00	22.37	219.78	4115
4	114.06	24.00	263.23	5219
5	110.50	23.97	213.65	4208
6	116.96	20.25	289.23	4992
7	114.01	18.87	232.76	3777
8	112.34	22.28	268.53	4992
9	118.25	23.00	218.15	4200
10	120.00	20.00	288.41	4944
11	118.91	22.90	283.33	5440

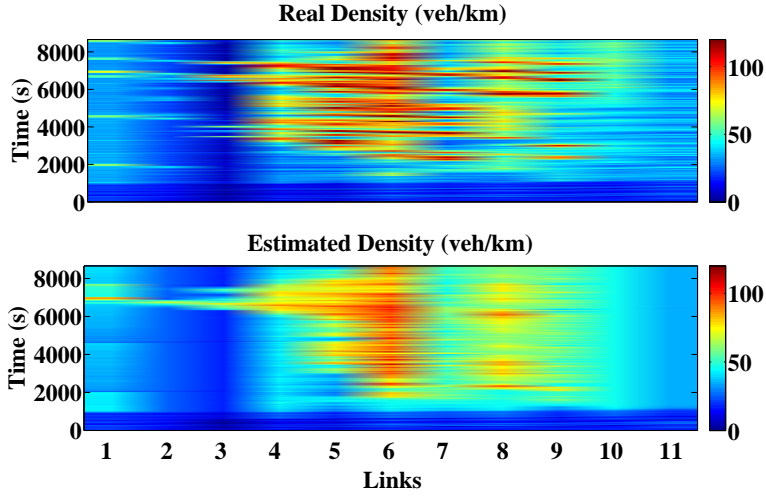
obtained parameters of the LTM are presented in Table 3.2. The links are numbered from upstream to downstream. Note that in the network layout, there are extra lanes from 200 m before the off-ramps and also for 200 m after the on-ramps. However, we do not define extra links in the LTM to model these small parts, but we take into account the cumulative number of vehicles leaving (entering) these links to fit 2-lane LTM links to the data. This is consistent with having different maximum densities for different links in Table 3.2.

Moreover, results presented in Fig. 3.5 verify that the calibrated LTM is able to estimate traffic densities close to the ones obtained from the simulation data.

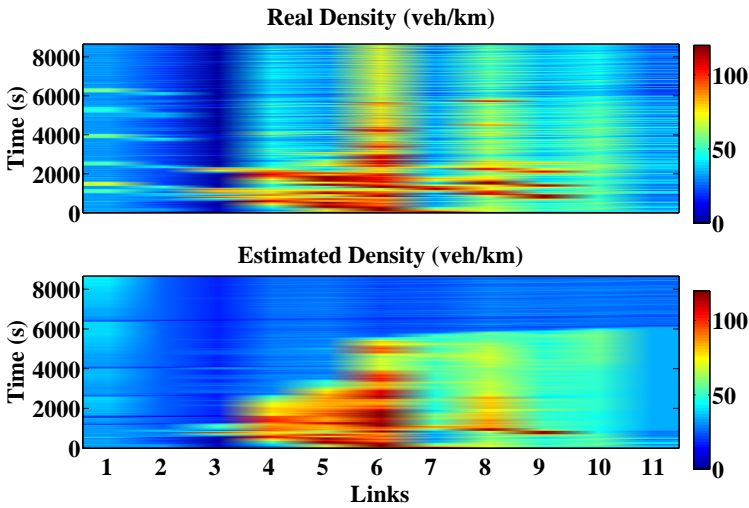
3.5.3. MICRO-SIMULATION AND PREDICTIVE CONTROL OF THE LEUVEN CORRIDOR

Fig. 3.6(a) shows an illustration of the uncontrolled situation. It can be observed that congestion forms near the most downstream on-ramp and propagates upstream. Once it reaches the most upstream on-ramp, the congestion increases close to this on-ramp. The total time spent, which is the sum of the mainstream traveling time and the time spent in queues at on-ramps is 1115.63 (veh · h). The total time spent on the mainstream road only is 1061.41 (veh · h).

Now the uncontrolled case is compared with the cases in which predictive ramp metering and VSL control is applied. Two proposed methods are implemented, nonlinear MPC based on the original formulation of the extended LTM, and MILP-MPC. The optimization problems integrated in both methods have a queue length constraint of 100 vehicles for all on-ramps. The improvement in the TTS values for the nonlinear MPC and the MILP case along with the average computation time (required for solving each optimization step) are compared in Table 3.3. As can be inferred, the control approaches are able to provide approximately 10 – 14% reduction in the TTS value. Moreover, the MPC approaches provide a significant reduction in the total time spent on the mainstream road (around 44% less than the uncontrolled case). Although this comes at the price of having longer queues at the on-ramps, the overall TTS is considerably lower than the



(a)



(b)

Figure 3.5: Calibration of the LTM: real and estimated densities of all links for two traffic scenarios with different demand profiles: (a) congestion starts in the middle of the simulation period, (b) network is already congested at the beginning of the simulation period.

uncontrolled case.

Results of closed-loop simulation using the nonlinear MPC method with $N_p = 5$, $N_c = 2$ are illustrated in Fig. 3.6(b) and Fig. 3.8. Moreover, the results of the MILP-MPC approach are presented in Fig. 3.7 and Fig. 3.9. Comparing Fig. 3.6(a) and Fig. 3.6(b), it can be observed that the MPC controller is able to resolve the congestion caused by the high demand in the most downstream on-ramp. In fact, the MPC controller (in both

Table 3.3: Comparison of TTS (veh · h) and CPU time (s) for two approaches, nonlinear MPC and MILP-MPC. The percentages show the reduction in the TTS with respect to the uncontrolled case. The CPU times for N-MPC are multiplied by 5 to express that the nonlinear optimization is solved 5 times in each control time step.

Control parameters	Total time spent (TTS) (veh · h)		Average CPU time (s)		Time spent on mainstream road (veh · h)	
	N-MPC	MILP-MPC	N-MPC	MILP-MPC	N-MPC	MILP-MPC
$N_p = 3, N_c = 2$	1036.14 (-7.1%)	1032.19 (-7.5%)	26.88 × 5	7.32	597.25 (-43.73%)	595.91 (-43.85%)
$N_p = 5, N_c = 2$	987.53 (-11.4%)	994.84 (-10.8%)	43.29 × 5	10.51	590.62 (-44.36%)	592.91 (-44.13%)
$N_p = 7, N_c = 3$	972.81 (-12.7%)	963.90 (-13.6%)	124.33 × 5	21.79	588.99 (-44.51%)	585.12 (-44.87%)

the nonlinear and the MILP case) achieves this by limiting the outflow of the on-ramps (especially the first 3 on-ramps, as also shown in Fig. 3.8(a)) and by imposing the speed limit mostly for the first links of the freeway, as depicted in Fig. 3.8(b).

Moreover, the queue lengths at the on-ramps for both uncontrolled and controlled (ramp metering) cases are shown in Fig. 3.10. As can be seen, the queue lengths in the controlled case are considerably higher than in the uncontrolled condition. However, they do not exceed the 100 (veh) constraint on the queue length. In addition, using the MPC schemes, the total time spent in the network is improved and moreover, the congestion (with reduced mean speed and high densities of vehicles in several links) is significantly attenuated, as illustrated in Fig. 3.6(b) and Fig. 3.7. Note that because the micro-simulation has a stochastic nature, it is possible that sometimes the nonlinear MPC approach performs better than the MILP-MPC method and vice versa. It should be noted that in both methods we use rounding approximations to make the delays integer variables. Moreover, in the MILP-MPC approach, we just reformulate the LTM. Therefore, we expect that the performance of both methods should be close to each other. As can be observed in Fig. 3.6(b) and Fig. 3.7, in this run of the closed-loop simulation, the congestion level is less in the MILP-MPC control case. Instead, the queue lengths in the nonlinear MPC case are a bit smaller than in the MILP-MPC case. Furthermore, as discussed in Section 3.4, we use a penalty term in the total objective function to reduce fluctuations in the control inputs, as can be seen in Fig. 3.8 and Fig. 3.9. The penalty term and the TTS objective function are normalized by their nominal values (the uncontrolled case) in the total objective function. In addition, the penalty term is weighted by 0.2.

Regarding the computation time, as can be inferred from Table 3.3, the nonlinear optimization problem is solved for several random initial points in each MPC control step, since there may exist multiple local optimal solutions. On the contrary, the MILP approach is more efficient and it provides the global solution of the reformulated problem. Moreover, due to the stochastic nature of the micro-simulation, the performance of nonlinear MPC is sometimes worse than the MILP approach (note that both N-MPC and MILP-MPC use rounding approximations for the delays in the model). Furthermore, experiments for $N_p > 7$ and $N_c > 3$ show that the computation time (particularly for the nonlinear approach) grows exponentially, while the reduction in the TTS is not significant. Moreover, for small N_p the queues are not dissolved until the end of the simulation period. One way to prevent this is to increase N_p . However, for large values of N_p , it might be the case that MPC focuses more optimizing the future behavior rather than the current conditions. One can also increase N_c to prevent this, but this comes at the price of computational complexity and also more fluctuations in the control inputs. Another solution is therefore to add an end-point penalty function to the total objective function (as it is also performed in [155]). The end-point term expresses the time required for vehicles present in the network by the end of the prediction horizon to exit the network. For our case study setup, a prediction horizon between 7 and 9 is enough as by reducing the demands, the queues start to discharge before the end of simulation period (as can be observed from Fig. (3.10)).

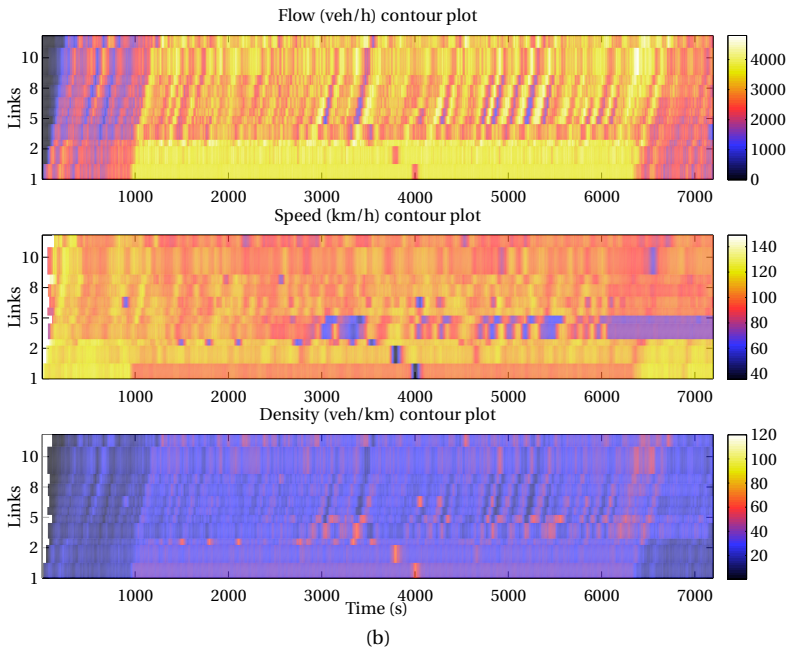
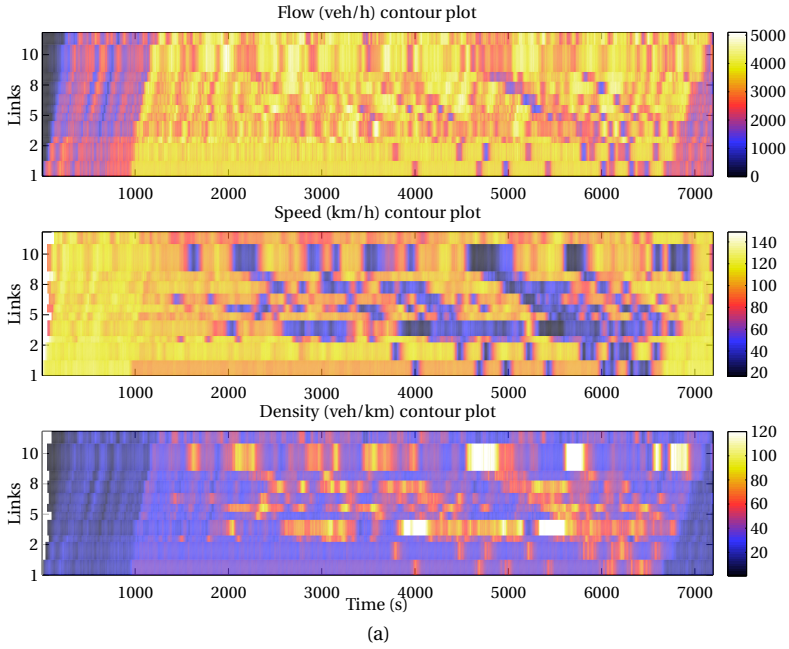


Figure 3.6: Flow, speed and density plots for all links over time: (a) uncontrolled case, (b) controlled using nonlinear MPC.

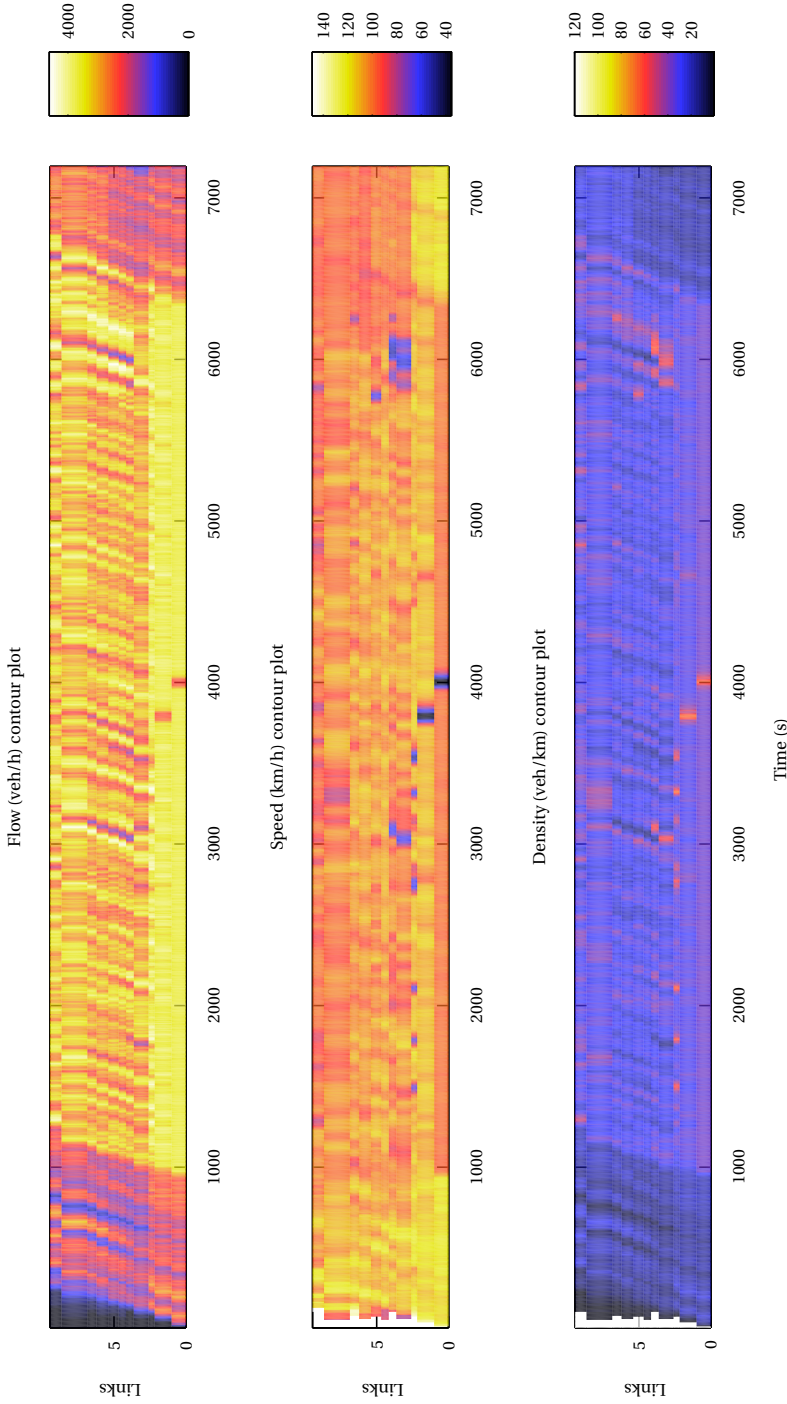
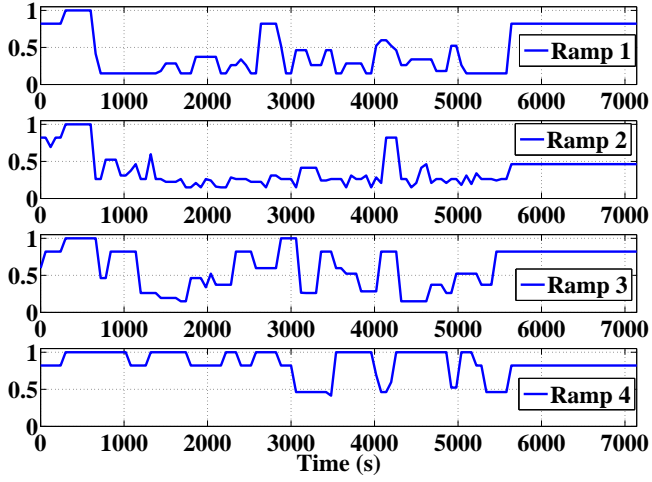
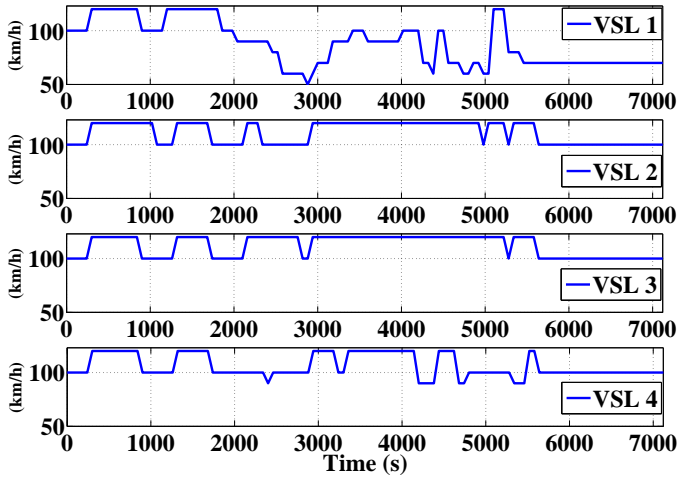


Figure 3.7: Flow, speed and density plots for all links over time: MILP-MPC approach.

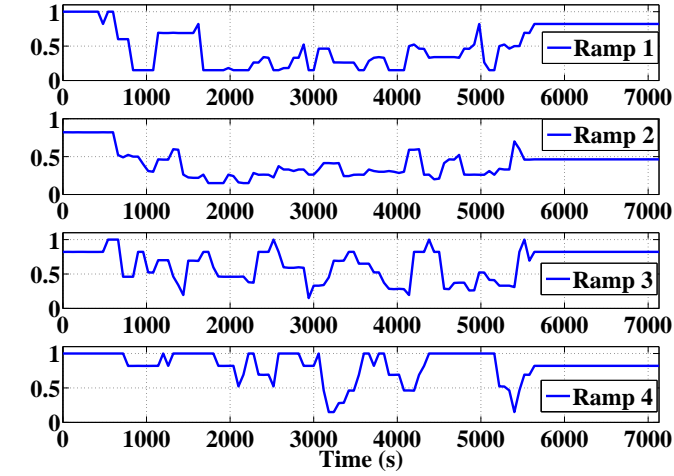


(a)

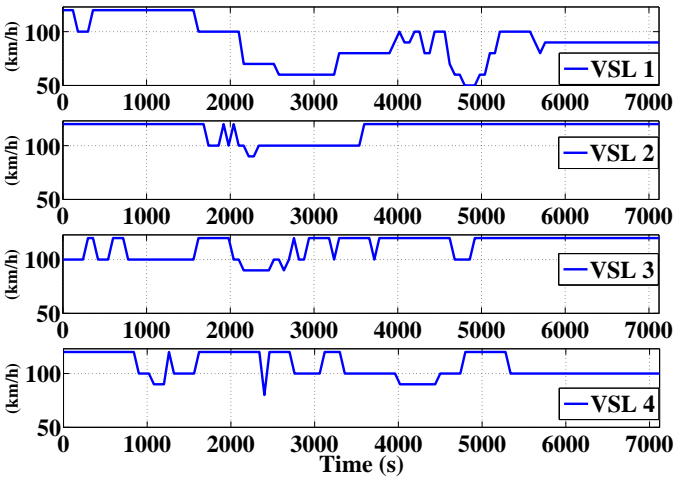


(b)

Figure 3.8: Nonlinear MPC control inputs: (a) Ramp metering signals, (b) VSL signals.

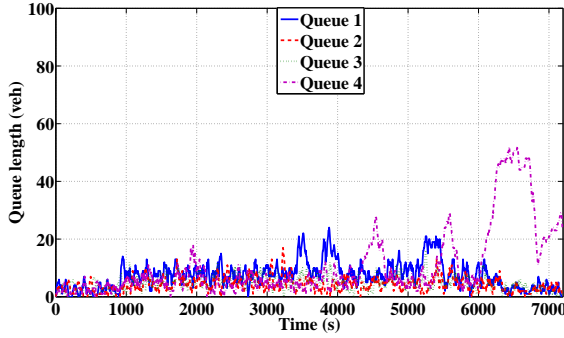


(a)

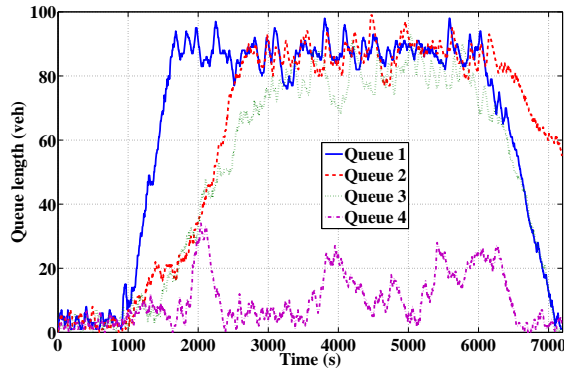


(b)

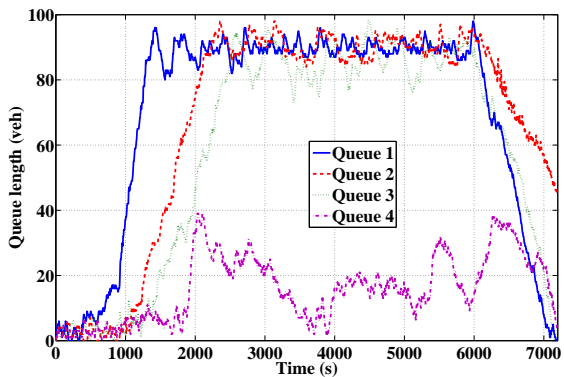
Figure 3.9: MILP-MPC control inputs: (a) Ramp metering signals, (b) VSL signals.



(a)



(b)



(c)

Figure 3.10: Queues at on-ramps: (a) uncontrolled, (b) controlled by nonlinear MPC, (c) controlled using MILP-MPC.

3.6. CONCLUDING REMARKS

The link transmission model has been extended, reformulated and utilized in a model predictive control framework. We first modified the model in order to incorporate the effects of traffic control measures, ramp metering and variable speed limits. Next, we established two integrated predictive ramp metering and VSL control schemes, non-linear MPC based on the extended LTM, and a mixed integer linear programming approach based on the transformed LTM. Finally, the performance of the proposed control schemes was evaluated using micro-simulation for the Leuven Corridor. The obtained results show that the MPC schemes are able to achieve considerable improvement in the total time spent in the network, and moreover, the computation time required for control of such network with several links, on/off-ramps and control inputs is reasonably low (specially for the mixed integer linear programming method).

Possible research directions in addition to the current work would be, 1) further extending the LTM to include the effects of possible capacity drop at merge nodes, and 2) incorporating robust model predictive techniques in order to better cope with uncertainties in demand profiles and incidents, 3) field implementation of the proposed LTM-based predictive control schemes.

4

OPTIMAL HYBRID CONTROL FOR URBAN TRAFFIC NETWORKS

In this chapter, we present an optimal hybrid control scheme for multi-region urban networks. In this scheme, we have two types of control inputs: (i) perimeter control inputs, and (ii) binary control inputs for switching between timing plans. The perimeter controllers are located at the border between the regions, as they manipulate the transfer flows between regions, while the switching controllers influence the dynamics of the urban regions, and as a result affect the internal flows within each region. The optimal control inputs are determined using a mixed integer nonlinear optimization problem that is solved in a receding horizon fashion. Moreover, to decrease the computational complexity due to the nonlinear and non-convex nature of the optimization problem, we reformulate the problem as a mixed integer linear programming (MILP) problem utilizing piecewise affine approximation techniques. We present two different approaches for transformation of the original model and building up the MILP problems, and we evaluate and compare the performance of the approximate methods along with the original problem formulation for different traffic scenarios of a two-region urban case study.

4.1. INTRODUCTION

THE idea of perimeter control using the concept of MFD was discussed in Chapter 2. In this chapter, we introduce an extra level of control that can manipulate the flow dynamics of each urban region by switching between signal timing plans. Changing timing plans for signalized intersections within regions might alter the shape of the MFD, which will affect the network flow dynamics. Therefore, instead of assuming one MFD for each region, we introduce a set of MFDs, where each MFD corresponds to a certain collection of timing plans for the intersections inside the region.

Combining switching timing plans and perimeter control might significantly increase the network performance, as it gives the ability to control both inside and on the border of urban regions, and to adjust to a vast variety of demands and traffic conditions. However, combining these two controllers is not straightforward, as a mixture of discrete and continuous control inputs is introduced that might have different effects on the flow dynamics. The model of an urban region will be a nonlinear state space model based on the MFD and it has both continuous perimeter control inputs and binary variables for switching the timing plans. Moreover, model predictive control (MPC) [160] is used to solve the optimal control problem. Since we deal with a hybrid system, the resulting open-loop optimization problem is a mixed integer nonlinear problem. Solving nonlinear and nonconvex optimization problems can be time-consuming and finding a global solution is not guaranteed. If the problem is solved multiple times for different initial points, chances are high that a reasonably optimal solution is found. While multi-start optimization algorithms or global optimization techniques can be used to overcome this issue, one can try to approximate and transform the model into a mixed integer affine form and formulate the optimization problem as a mixed integer linear programming (MILP) problem. The computation time will decrease significantly and one global optimum solution for the MILP problem will be obtained.

To summarize, the chapter contributes in three ways. First, a novel hybrid MFD-based model is proposed that is capable of modeling the effect of switching between timing plans on the MFD of an urban network. Second, a model predictive control scheme is constructed based on the proposed hybrid model and further simplifying mathematical techniques are presented in order to decrease the computational complexity of the associated optimization problem. Among the techniques are avoiding 2-dimensional piecewise affine approximation and using two simpler approaches instead, and quantization of the perimeter control input to solve the problem with input/states multiplications. Finally, we consider practical issues regarding measuring the traffic variables, trip demands and also the scattered MFDs observed in real networks and therefore we add three types of uncertainties into our hybrid model in order to make simulation of a multi-region urban network more realistic.

The rest of this chapter is organized as follows. In Section 4.2, a hybrid MFD-based model of an R -region urban network is presented, while in Section 4.3 the optimal hybrid control problem is formulated. Two mixed linear models based on the piecewise affine approximation of the original model are proposed in Section 4.4 and the corresponding mixed integer linear optimization problem is formulated in Section 4.5. The performance of the predictive hybrid controllers (linear and nonlinear) are tested for several case study examples with different scenarios in Section 4.6. The chapter concludes with a discussion about the results and ideas for further research.

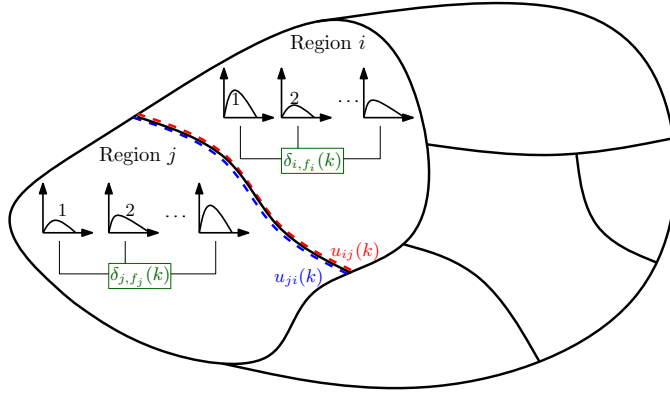


Figure 4.1: Hybrid multi-region system with perimeter and switching timing plans control inputs $u_{ij}(k)$ and $\delta_{i,f_i}(k)$ for region i , and $u_{ji}(k)$ and $\delta_{j,f_j}(k)$ for region j .

4.2. MFD-BASED MODELING OF URBAN REGIONS

Let us assume that a heterogeneous urban traffic network can be partitioned into R homogeneous regions, each having a well-defined MFD (later we will assume that each homogeneous region can have a set of different MFDs corresponding to the activated signal timing plans), see Fig. 4.1. In this chapter, the model time step counter and the sampling period are denoted by k (–) and T (s), respectively, where $t = k \cdot T$ and $k \in \{0, 1, 2, \dots, K-1\}$. Let $q_{ij}(k)$ (veh/s) be the traffic flow demand generated in region $i \in \{1, \dots, R\}$ at time step k with final destination in region $j \in \mathcal{N}_i$, where \mathcal{N}_i is the set of regions that are directly reachable from region i . Corresponding to the traffic demands, accumulation states are defined to model the dynamic equations: $n_{ij}(k)$ (veh) denotes the total number of vehicles in region i with destination to region j at time step k . Let us denote $n_i(k)$ (veh) as the accumulation or the total number of vehicles in region i at time step k , i.e. $n_i(k) = n_{ii}(k) + \sum_{j \in \mathcal{N}_i} n_{ij}(k)$. The MFD is defined by $G_i(\cdot)$ (veh/s) which is the trip completion flow for region i . The trip completion flow for region i is the sum of transfer flows, i.e. trips from i with destination j , $j \in \mathcal{N}_i$, plus the internal flow, i.e. trips from i with destination i . The *transfer flow* from i with destination to j , denoted by $M_{ij}(k)$ (veh/s), is calculated corresponding to the ratio between accumulations, i.e. $M_{ij}(k) = (n_{ij}(k)/n_i(k)) \cdot G_i(n_i(k))$, $j \in \mathcal{N}_i$, while $M_{ii}(k)$ is the *internal flow* from i with destination to i and is calculated by $M_{ii}(k) = (n_{ii}(k)/n_i(k)) \cdot G_i(n_i(k))$. Furthermore, we use a third-degree polynomial of $n_i(k)$ to describe the MFD, e.g. $G_i(n_i(k)) = a_i \cdot n_i^3(k) + b_i \cdot n_i^2(k) + c_i \cdot n_i(k)$, where a_i , b_i , and c_i are estimated parameters (of course, one can approximate the MFD using higher-degree polynomials or exponential functions).

The vehicle conservation equations (without including control measures) of the multi-region MFD-based model are

$$n_{ii}(k+1) = n_{ii}(k) + T \cdot \left(q_{ii}(k) + \sum_{j \in \mathcal{N}_i} M_{ji}(k) - M_{ii}(k) \right), \quad (4.1)$$

$$n_{ij}(k+1) = n_{ij}(k) + T \cdot \left(q_{ij}(k) - M_{ij}(k) \right) \quad (4.2)$$

for $i \in \{1, 2, \dots, R\}$ and for $j \in \mathcal{N}_i$. These equations are a generalized (R regions instead

of two) and discretized form of the equations presented in [71]. Note that route choice modeling is not included in the dynamic equations.

4.3. OPTIMAL HYBRID CONTROL FOR A MULTI-REGION URBAN NETWORK

In the previous section, the MFD-based model (4.1)–(4.2) was introduced without any control measure. In the following, two types of controllers are introduced in Section 4.3.1 and included in the dynamic equations (4.1) and (4.2) in Section 4.3.2, while in Section 4.3.3 the optimal hybrid control problem for the multi-region urban network is formulated.

4.3.1. HYBRID CONTROL: PERIMETER AND SWITCHING CONTROLLERS

Two types of controllers are introduced in the hybrid control problem: (i) perimeter controllers, and (ii) binary controllers for switching between signal timing plans. The perimeter controllers are located at the border between regions, as they manipulate the *transfer flows* between regions, while the switching controllers influence the dynamics of the urban regions, as they define the shape of the MFDs. Note that the switching controllers and the perimeter controllers might affect each other, but we assume that these effects are negligible.

The signal timing plans alter the shape of the MFD, see [68]. In this chapter, it is assumed that each urban region has a predefined library of signal fixed-timing plans for the signalized intersections inside the region, e.g. fixed-timing plans for the morning and evening peak hours and a typical uncongested hour, where each plan in the library has different green, red, cycle, and offset settings for the intersections. It is also assumed that for each activated timing plan (each plan consists of different fixed cycle ratio for different intersections inside a region), the region will have a different MFD, i.e. a non-symmetric unimodal curve skewed to the right, but with different values of the maximum output, and critical accumulations, see e.g. the different MFDs for regions i and j in Fig. 4.1. Therefore, the timing plan library employs a library of MFDs for each region. The switching controller of the region activates one MFD from the library by switching from one signal plan to another.

The optimal perimeter and switching plans decisions are obtained by minimizing the total time spent in the R urban regions. The total time spent (veh · s) is defined as follows:

$$J = T \cdot \sum_{k=0}^{K-1} \sum_{i=1}^R n_i(k). \quad (4.3)$$

4.3.2. HYBRID MULTI-REGION MODEL

Let us denote the perimeter control inputs by $u_{ij}(k)$ ($-$), $i \in \{1, \dots, R\}$, $j \in \mathcal{N}_i$, and the switching timing plans control inputs by $\delta_{i,f_i}(k) \in \{0, 1\}$, where $f_i \in \mathcal{F}_i$ and \mathcal{F}_i is the set of MFDs in the library for region i . The control inputs $u_{ij}(k)$, $\delta_{i,f_i}(k)$, and $u_{ji}(k)$, $\delta_{j,f_j}(k)$ are associated with regions i and j , respectively.

The perimeter control inputs $u_{ij}(k)$ and $u_{ji}(k)$ are introduced at the border between the regions i and j as shown in Fig. 4.1, where the purpose is to control the transfer

flows between the two regions. The transfer flow $M_{ij}(k)$, $i = \{1, \dots, R\}$, $j \in \mathcal{N}_i$, is controlled such that only a fraction of the flow actually transfers from region i to region j , i.e. $u_{ij}(k) \cdot M_{ij}(k)$, where $0 \leq u_{ij}(k) \leq 1$. Hence, the MFD-based model (4.1) and (4.2) is altered by replacing $M_{ij}(k)$ and $M_{ji}(k)$ by $u_{ij}(k) \cdot M_{ij}(k)$ and $u_{ji}(k) \cdot M_{ji}(k)$, respectively. It is also assumed that these controllers will not change the shape of the MFDs.

Since the perimeter controllers exist only at the border between the regions, the internal flows cannot be controlled nor restricted. However, the internal flows are determined by the MFDs of the regions. The switching controllers can indirectly manipulate the internal flows by switching the MFDs (or more precisely by switching between the signal timing plans of the signalized intersections). Recall that the vehicle conservation equations (4.1) and (4.2) assume that each region has only one MFD. Let us now assume that each region i has a predefined MFD library (or set of MFDs denoted by \mathcal{F}_i) that corresponds to a signal timing plans library for the signalized intersections. The switching control signal $\delta_{i,f_i}(k)$ activates the MFD $f_i \in \mathcal{F}_i$, i.e. $G_{i,f_i}(\cdot)$, if $\delta_{i,f_i}(k) = 1$ and $\delta_{i,r_i}(k) = 0$, $\forall r_i \in \mathcal{F}_i \setminus \{f_i\}$ (so only one $\delta_{i,f_i}(k) = 1$ at any time step, i.e. $\sum_{f_i \in \mathcal{F}_i} \delta_{i,f_i}(k) = 1$). Therefore, the multi-region MFD-based model (4.1) and (4.2) is modified to include the switching controllers, as the term $G_i(n_i(k))$ is changed to¹ $\sum_{f_i \in \mathcal{F}_i} \delta_{i,f_i}(k) \cdot G_{i,f_i}(n_i(k))$. The new hybrid multi-region MFD-based model is formulated as

$$n_{ii}(k+1) = n_{ii}(k) + T \cdot (q_{ii}(k) + \sum_{j \in \mathcal{N}_i} u_{ji}(k) \cdot M_{ji}(k) - M_{ii}(k)) \quad (4.4)$$

$$n_{ij}(k+1) = n_{ij}(k) + T \cdot (q_{ij}(k) - u_{ij}(k) \cdot M_{ij}(k)) \quad (4.5)$$

$$M_{ii}(k) = \frac{n_{ii}(k)}{n_i(k)} \cdot \left[\sum_{f_i \in \mathcal{F}_i} \delta_{i,f_i}(k) \cdot G_{i,f_i}(n_i(k)) \right] \quad (4.6)$$

$$M_{ij}(k) = \frac{n_{ij}(k)}{n_i(k)} \cdot \left[\sum_{f_i \in \mathcal{F}_i} \delta_{i,f_i}(k) \cdot G_{i,f_i}(n_i(k)) \right] \quad (4.7)$$

$$n_i(k) = n_{ii}(k) + \sum_{j \in \mathcal{N}_i} n_{ij}(k). \quad (4.8)$$

4.3.3. OPTIMAL CONTROL PROBLEM FORMULATION

After defining and including the controllers in the hybrid multi-region MFD-based model, we formulate the optimal hybrid control problem. The scheme of the optimal control problem is presented in Fig. 4.2. The aim is to minimize the total time spent (4.3) by manipulating the perimeter controller and by switching between the timing plans of the libraries.

In reality, homogeneous regions have an MFD with some scatter, particularly in the congested regime. Therefore, errors are expected between the hybrid R -region MFD model (assuming well-defined MFDs) and the real network. Therefore, a closed-loop optimal control scheme is needed in order to take into account the errors between the plant and the model and also the disturbances, e.g. variations in the expected demands, that might affect the system (the differences between the model and the plant will be discussed in details later in Section 4.6). Among these schemes is the model predictive control (MPC) framework, which has been widely used for different traffic control

¹Since one and only one $\delta_{i,f_i}(k)$ is equal to 1 at the same time, we can replace one of the binary variables denoted by $\delta_{i,f_i}(k)$, with $1 - \sum_{f_i \in \mathcal{F}_i \setminus \{f_i\}} \delta_{i,f_i}(k)$ and thus reduce the number of variables.

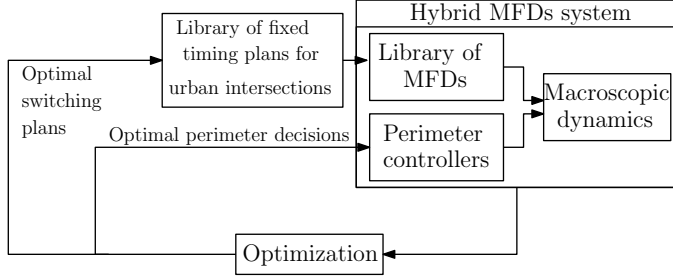


Figure 4.2: Optimal hybrid perimeter and switching plans control scheme.

purposes [2, 12, 104, 129, 154, 187]. The MPC controller determines the optimal control inputs in a receding horizon manner, meaning that at each time step an objective function is optimized over a prediction horizon of N_p steps and a sequence of optimal control inputs is derived. Then the first sample of the control inputs is applied to the system and the procedure is repeated with a shifted horizon.

We directly formulate the problem in the MPC framework. Let k_c (–) and T_c (s) be the control time step and the control sample time, respectively. It is assumed that the controller time step length is an integer multiple of the model time step length, i.e. $T_c = M \cdot T$. Then, the overall optimization problem is formulated as follows:

$$\min_{\tilde{u}_{ij}(k_c), \tilde{\delta}_{i,f_i}^c(k_c), \bar{n}_{ii}(k_c), \bar{n}_{ij}(k_c), i \in \{1, \dots, R\}, j \in \mathcal{N}_i} T \cdot \sum_{k=M \cdot k_c}^{M \cdot (k_c + N_p) - 1} \sum_{i=1}^R n_i(k) \quad (4.9)$$

subject to:

$$\text{Model equations (4.4) – (4.8)} \quad (4.10)$$

$$0 \leq n_i(k) \leq n_{i,\text{jam}} \quad (4.11)$$

$$u_{ij,\text{min}} \leq u_{ij}^c(k_c) \leq u_{ij,\text{max}} \quad (4.12)$$

$$u_{ij}(k) = u_{ij}^c(k_c) \text{ if } k \in \{M \cdot k_c, \dots, M \cdot (k_c + 1) - 1\} \quad (4.13)$$

$$\delta_{i,f_i}(k) = \delta_{i,f_i}^c(k_c) \text{ if } k \in \{M \cdot k_c, \dots, M \cdot (k_c + 1) - 1\} \quad (4.14)$$

$$\delta_{i,f_i}^c(k_c) \in \{0, 1\}, \forall f_i \in \mathcal{F}_i \quad (4.15)$$

for $i \in \{1, \dots, R\}$ and for all $j \in \mathcal{N}_i$, where $n_{i,\text{jam}}$ (veh) is the jam accumulation for region i , and $u_{ij,\text{min}}$ and $u_{ij,\text{max}}$ (–) are respectively the lower and upper bounds for the perimeter control signals for regions i and j . The optimization variables defined over the prediction horizon N_p are $\bar{n}_{ij}(k_c) = [n_{ij}(M \cdot k_c), \dots, n_{ij}(M \cdot (k_c + N_p) - 1)]^T$, $\bar{n}_{ii}(k_c) = [n_{ii}(M \cdot k_c), \dots, n_{ii}(M \cdot (k_c + N_p) - 1)]^T$, $\tilde{u}_{ij}(k_c) = [u_{ij}^c(k_c), \dots, u_{ij}^c(k_c + N_p - 1)]^T$ and $\tilde{\delta}_{i,f_i}^c(k_c) = [\delta_{i,f_i}^c(k_c), \dots, \delta_{i,f_i}^c(k_c + N_p - 1)]^T$, where $u_{ij}^c(k_c + l)$ and $\delta_{i,f_i}^c(k_c + l)$ for $l = 0, \dots, N_p - 1$ are the perimeter and switching control inputs at every control time step k_c , respectively.

The current model does not directly consider downstream restrictions, e.g. the boundary capacity. One more term can be added to the model, the boundary capacity, which is a function of the accumulation in the receiving region and it restricts the

transfer flow if the receiving region is highly congested. We have not considered this constraint in our optimization problem, main because (i) the boundary capacity only starts to decrease when the accumulation increases beyond the critical accumulation (see [69]), and (ii) the control inputs will not allow the system to get close to gridlock .

Moreover, one can add a penalty term to the objective function (4.9), in order to prevent undesired fluctuations in the perimeter control inputs and the decision switching variables. The penalty on the perimeter control inputs can be defined as follows:

$$\sum_{l=1}^{N_p-1} |u_{ij}^c(k_c + l) - u_{ij}^c(k_c + l - 1)|. \quad (4.16)$$

Moreover, to reduce the computation time, control variables are sometimes taken constant after passing a predefined control horizon $N_c \leq N_p$. More precisely, we have $u_{ij}^c(k_c + l) = u_{ij}^c(k_c + N_c - 1)$ and $\delta_{i,f_i}^c(k_c + l) = \delta_{i,f_i}^c(k_c + N_c - 1)$ for $l = N_c, \dots, N_p - 1$.

Overall, the problem (4.9)–(4.15) is a mixed integer nonlinear optimization problem (MINLP) and it can be solved using mixed integer nonlinear optimization algorithms [21]. However, since here we deal with both real and binary decision variables and also since the model equations have nonlinear terms, the optimization problem could have multiple (local) optimal points. Moreover, as will be demonstrated in Section 4.6, the optimization algorithm takes considerable time. This is mainly because the MINLP algorithm is executed for several random initial points, in order to find a sufficiently low value of the objective function. Thus, in the next section we simplify and reformulate the problem in order to eventually establish a mixed integer *linear* optimization problem.

4.4. APPROXIMATION OF THE HYBRID MULTI-REGION MODEL

Solving the nonlinear and non-convex (the non-convexity is because of having a hybrid nonlinear model with a mixture of continuous perimeter control inputs and binary decision variables to switch between MFDs) optimization problem (4.9)–(4.15) can be time-consuming and not tractable for real-time implementation. In the following two subsections, we will recast the problem into a mixed integer *linear* optimization problem. The nonlinear model in the MPC framework (4.9)–(4.15) is replaced by an approximate model following piecewise affine (PWA) approximation techniques and some mathematical simplifications. The idea of PWA approximation of MFDs was also presented in a hierarchical control framework for intelligent vehicle highway systems in [11].

Basically, the nonlinearity in the dynamic equations is present in: (i) the internal and transfer trip completion flows, see $M_{ii}(k)$ in (4.6) and $M_{ij}(k)$ in (4.7), respectively, and (ii) the product between the perimeter controllers and the transfer trip completion flows, see (4.4) and (4.5). In the following, we address these nonlinearities and obtain two different approximate models. The first model is less computationally complex but less accurate than the second one. In the case study section, we present the performance evaluation of two control methods built up on the two approximate models along with a control approach designed based on the original nonlinear model.

4.4.1. FIRST APPROACH: PWA APPROXIMATION PLUS FORWARD SIMULATION

In this method, we use combined approximation of the nonlinearities in the MFD-based model along with a forward simulation technique that will be described shortly. The multiplication of $n_{ii}(k)$ (or $n_{ij}(k)$) with the other variables in the square brackets in (4.6) (or (4.7)) results in multiple products of real variables. In principle, each product needs to be approximated by a PWA function [8, 217]. A function $f : \Omega \rightarrow \mathbb{R}^m$ is PWA if there exists a polyhedral partition $\{\Omega_i\}_{i \in \mathcal{I}}$ ($\cup_{i \in \mathcal{I}} \Omega_i = \Omega$, $\Omega_i \neq \emptyset$, $\text{int}(\Omega_i) \cap \text{int}(\Omega_j) = \emptyset$, $\forall i \neq j$) of $\Omega \subseteq \mathbb{R}^n$ such that f is affine on each polyhedron Ω_i . One can approximate a nonlinear function by a PWA function with arbitrary accuracy and by considering a sufficiently large number of regions. However, for our particular case (bivariate function of accumulations) the PWA approximation is a tedious task as more parameters have to be introduced (see e.g. [60]). In other words, we have to deal with a two-dimensional PWA approximation [24, 60] and in order to get enough accuracy in the modeling, the resulting PWA function would need a large number of affine pieces. This may add more complexity to the associated optimization problem. Therefore, as a main consideration in the PWA approximation, the number of affine functions should be kept small while providing a close match to the original nonlinear function.

Hence, in order to simplify the approximation, we estimate the variables $n_{ii}(k)$ and $n_{ij}(k)$ in the transfer flows by forward simulation as follows: we first simulate the multi-region MFD-based model based on the formulation presented in (4.4) and (4.5) over a prediction horizon with control inputs and initial accumulations obtained from the previous time step, and subsequently the variables $n_{ii}(k)$ and $n_{ij}(k)$ in $M_{ii}(k)$ and $M_{ij}(k)$ are replaced with the values obtained from the simulation. Hence, we no longer deal with multiplication of variables but only with multiplication with time-varying but known parameters.

PWA APPROXIMATION OF THE TRIP COMPLETION FLOWS

The nonlinearity in the internal trip completion flows $M_{ii}(k)$ is approximated as follows (a similar procedure is applied to the transfer flows $M_{ij}(k)$). Substituting the third-degree polynomial $G_{i,f_i}(n_i(k)) = a_{i,f_i} \cdot n_i^3(k) + b_{i,f_i} \cdot n_i^2(k) + c_{i,f_i} \cdot n_i(k)$ into (4.6), one can re-write the internal flows $M_{ii}(k)$ for $i = 1, 2, \dots, R$ as follows:

$$M_{ii}(k) = n_{ii}(k) \cdot \left[\sum_{f_i \in \mathcal{F}_i} \delta_{i,f_i}(k) \cdot (a_{i,f_i} \cdot n_i^2(k) + b_{i,f_i} \cdot n_i(k) + c_{i,f_i}) \right]. \quad (4.17)$$

The function $P_{i,f_i}(n_i(k)) = a_{i,f_i} \cdot n_i^2(k) + b_{i,f_i} \cdot n_i(k) + c_{i,f_i}$ (inside the parentheses in (4.17)) defined on the interval $[n_{i,\min}, n_{i,\max}]$ can be approximated by a continuous PWA function $\hat{P}_{i,f_i}(n_i(k))$ with three intervals as follows:

$$\hat{P}_{i,f_i}(n_i(k)) = \begin{cases} \gamma_{i,f_i} + \frac{n_i(k) - n_{i,\min}}{a_{i,f_i} - n_{i,\min}} \cdot (\xi_{i,f_i} - \gamma_{i,f_i}) & \text{for } n_{i,\min} \leq n_i(k) < \alpha_{i,f_i}, \\ \xi_{i,f_i} + \frac{n_i(k) - \alpha_{i,f_i}}{\beta_{i,f_i} - \alpha_{i,f_i}} \cdot (\epsilon_{i,f_i} - \xi_{i,f_i}) & \text{for } \alpha_{i,f_i} \leq n_i(k) < \beta_{i,f_i}, \\ \epsilon_{i,f_i} + \frac{n_i(k) - \beta_{i,f_i}}{n_{i,\max} - \beta_{i,f_i}} \cdot (\zeta_{i,f_i} - \epsilon_{i,f_i}) & \text{for } \beta_{i,f_i} \leq n_i(k) < n_{i,\max}, \end{cases} \quad (4.18)$$

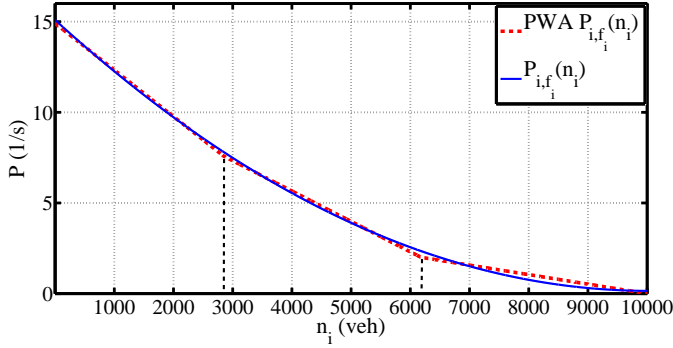


Figure 4.3: PWA approximation of a 2nd-degree polynomial P_{i,f_i} .

where the tuple $\theta_{i,f_i} = \{\gamma_{i,f_i}, \alpha_{i,f_i}, \beta_{i,f_i}, \xi_{i,f_i}, \epsilon_{i,f_i}, \zeta_{i,f_i}\}$ can be estimated by solving the following nonlinear least-squares optimization problem:

$$\min_{\theta_{i,f_i}} \int_{n_{i,\min}}^{n_{i,\max}} (P_{i,f_i}(n_i(k)) - \hat{P}_{i,f_i}(n_i(k)))^2 dn_i. \quad (4.19)$$

This optimization problem can be solved by multi-start nonlinear optimization algorithms [62]. An example of PWA approximation of a 2nd-degree polynomial $P_{i,f_i}(n_i)$ is shown in Fig. 4.3.

APPROXIMATION OF THE PRODUCT BETWEEN THE PERIMETER CONTROL INPUTS AND THE TRANSFER FLOWS

The transfer flows are multiplied with the perimeter controller inputs in (4.4) and (4.5). These products cannot be replaced with values obtained from simulation as the optimal perimeter inputs should be determined from the optimization algorithm. As discussed before, the perimeter control inputs determine the percentage of flows that are allowed to transfer between regions and thus they take values in the interval $[0, 1]$. In reality, the perimeter control is realized by changing the signal settings of intersections. As an approximation, we assume that the perimeter input take values from a finite set in the interval $[0, 1]$. This means that we can make the control inputs $u_{ij}(k)$ quantized as follows [15]:

$$u_{ij}(k) = u_{ij,0} \cdot \left(\sum_{l=0}^r 2^l \cdot \omega_{ij,l}(k) \right), \quad (4.20)$$

where $u_{ij,0}$ are a priori given constants and $\omega_{ij,l}(k) \in \{0, 1\}$ are the optimization variables. The set of possible input values is then finite and its cardinality is 2^{r+1} , while the difference between two consecutive values is determined by $u_{ij,0}$. Having a sum of weighted binary variables for each perimeter control input, the problem with multiplication of control inputs with transfer flow functions will be simplified, since multiplication with binary variables can be easily handled with the techniques presented in Section 4.5.

²Note that in this way we have equal steps of change in the value of the control input. However, one can define proper constant coefficients in order to get non-equal jumps in the value of u_{ij} over its domain.

Remark 4.1. Another way to tackle the problem with the multiplication of perimeter control input and the transfer flow function is to introduce a new variable \tilde{M}_{ji} and rewrite (4.4) as

$$n_{ii}(k+1) = n_{ii}(k) + T \cdot \left(q_{ii}(k) + \sum_{j \in \mathcal{N}_i} \tilde{M}_{ji}(k) - M_{ii}(k) \right), \quad (4.21)$$

with the additional constraint

$$0 \leq \tilde{M}_{ji}(k) \leq M_{ji}(k). \quad (4.22)$$

This method is more accurate than quantizing the perimeter control input. However, if the control input u_{ji} explicitly appears in the objective function (e.g. we can use the penalty term (4.16) to attenuate the fluctuations of the control inputs over time. This penalty term is added to the objective function.), this method would not be applicable.

4.4.2. SECOND APPROACH: RECASTING 2-DIMENSIONAL PWA APPROXIMATION

In the previous section, we have presented one way to tackle the problem with multiplication of real variables: using forward simulation. This method can deliver satisfactory results for some cases. However, in order to achieve more accuracy one can iterate the forward simulation and the optimization inside each MPC control step, which would introduce additional computation time. Instead of using forward simulation to estimate the multiplication terms $n_{ii}(k)$ and $n_{ij}(k)$ with the square brackets in (4.6) and (4.7), one can directly approximate the bilinear functions following two-dimensional PWA approximation methods in the literature, e.g. the one in [60]. However, there are methods to reduce the two-dimensional PWA approximation to a one-dimensional problem. In the sequel, we treat the nonlinear terms in the model by using the reducing methods proposed in [15] and [234]. We give detailed descriptions only for the nonlinear terms in $M_{ii}(k)$ (see (4.17)), but a similar explanation holds for $M_{ij}(k)$. According to (4.17), we have to deal with two nonlinear terms: $n_{ii}(k) \cdot n_i(k)$ and $n_{ii}(k) \cdot n_i^2(k)$.

PWA APPROXIMATION OF $n_{ii}(k) \cdot n_i(k)$

The term $n_{ii}(k) \cdot n_i(k)$ can be rewritten as [234]

$$n_{ii}(k) \cdot n_i(k) = \frac{1}{4} \left[\left(n_i(k) + n_{ii}(k) \right)^2 - \left(n_i(k) - n_{ii}(k) \right)^2 \right]. \quad (4.23)$$

Defining two new auxiliary variables

$$y_{1,i}(k) = n_i(k) + n_{ii}(k), \quad y_{2,i}(k) = n_i(k) - n_{ii}(k), \quad (4.24)$$

one gets $n_{ii}(k) \cdot n_i(k) = \frac{1}{4} (y_{1,i}^2(k) - y_{2,i}^2(k))$. Instead of performing a two-dimensional PWA approximation, we now have to deal with the PWA approximation of two separate single-variable functions $y_{1,i}^2(k)$ and $y_{2,i}^2(k)$. The function $f(y_i) = y_i^2$ can be approximated by a PWA function using a nonlinear least-squares optimization formulation as in (4.18). Thereby, the domain of the function should be defined properly and according to the domain of the original variable. For instance, the domain of $f(y_{1,i}) = y_{1,i}^2$ is $[y_{1,i,\min}, y_{1,i,\max}]$ with $y_{1,i,\min} = \min\{n_i + n_{ii} \mid n_{i,\min} \leq n_i \leq n_{i,\max}, n_{ii,\min} \leq n_{ii} \leq n_{ii,\max}\}$ and $y_{1,i,\max} = \max\{n_i + n_{ii} \mid n_{i,\min} \leq n_i \leq n_{i,\max}, n_{ii,\min} \leq n_{ii} \leq n_{ii,\max}\}$.

PWA APPROXIMATION OF $n_{ii}(k) \cdot n_i^2(k)$

We follow the same procedure as above. Defining two variables $y_{3,i}(k)$ and $y_{4,i}(k)$, $n_{ii}(k) \cdot n_i^2(k)$ can be rewritten as $\frac{1}{4}(y_{3,i}^2(k) - y_{4,i}^2(k))$ with

$$y_{3,i}(k) = n_i^2(k) + n_{ii}(k), \quad y_{4,i}(k) = n_i^2(k) - n_{ii}(k). \quad (4.25)$$

However, there is still a nonlinear term in $y_{3,i}(k)$ and $y_{4,i}(k)$. The simple solution for that is to approximate the term $n_i^2(k)$ with a set of affine functions determined from an identification procedure like in (4.18) with an appropriate domain for $n_i(k)$ and next replace $n_i^2(k)$ with its PWA approximation in $y_{3,i}(k)$ and $y_{4,i}(k)$.

MULTIPLICATION WITH CONTROL INPUTS $u_{ij}(k)$

As discussed before, the transfer flows are multiplied by the perimeter control inputs. One can use the procedure explained in Section 4.4.2 for approximation of the multiplication of $u_{ij}(k)$ with $n_{ij}(k) \cdot n_i^2(k)$ and $n_{ij}(k) \cdot n_i(k)$. However, this would introduce more variables and make the model more complicated for optimization use. In this case, we assume that the perimeter control inputs are quantized and defined as in (4.20). Hence, instead of having multiplication of real variables, we deal with multiplication of binary decision variables and PWA-approximated transfer flow functions. In the next section, a way for dealing with this type of multiplications is presented.

Remark 4.2. *As a comparison of the two approximation methods, the second approach is expected to give results closer to those of the original nonlinear approach, provided that the approximations are performed with enough accuracy. This is because in the first method, we replace some variables with simulated data and the values will remain unchanged during the optimization. However, the computation time required in the second approach is expected to be higher than the first one since in the second approach more auxiliary variables are defined. These expectations will be confirmed in the case studies section.*

4.5. REFORMULATION AS A MIXED INTEGER LINEAR OPTIMIZATION PROBLEM

The approximate models cannot be directly used in a linear or piecewise affine MPC framework (4.9)–(4.15). This is due to the fact that in the approximate models two sets of binary variables are introduced; one set is associated with switching between the intervals of the PWA functions, and the other set contains the switching signals for both the timing plans and also the perimeter control inputs (as we quantized them). On the other hand, due to the large number of regions that the combination of different affine pieces in the model introduces, the repeated evaluation of the approximate models as a part of the optimization algorithm inside the MPC scheme, is not efficient. Therefore, we make a conversion of the approximate models to a system of the following form:

$$\begin{aligned} x(k+1) &= A \cdot x(k) + B_1 \cdot u(k) + B_2 \cdot \delta(k) + B_3 \cdot z(k) + b, \\ y(k) &= C \cdot x(k) + D_1 \cdot u(k) + D_2 \cdot \delta(k) + D_3 \cdot z(k), \\ E_1 \cdot x(k) + E_2 \cdot u(k) + E_3 \cdot \delta(k) + E_4 \cdot z(k) &\leq d, \end{aligned} \quad (4.26)$$

where $x(k) \in \mathbb{R}^{n_x}$ and $y(k) \in \mathbb{R}^{n_y}$ respectively represent the state and output vectors, while $\delta(k) \in \{0, 1\}^{n_\delta}$ and $z(k) \in \mathbb{R}^{n_z}$ are auxiliary binary and real-valued variables, resulting from a procedure explained subsequently. Further, b and d are constant vectors that along with the system matrices A, B_i, C, D_i, E_i specify a mixed logical dynamic model [15]. In this model representation, the binary (defined for the PWA functions, the switching between MFDs, and the quantization of the perimeter control signals) and auxiliary variables required to define the regions are directly included in model through additional constraints. Compared with the models derived in the previous section, one large but tractable model results that is composed by stacking the individual linear and affine equations along with auxiliary linear inequalities, thus resulting in a model size that grows linearly with increasing the number of regions.

In this section, we transform the approximate models presented in the previous sections to the form (4.26). Consider an affine function $f(\cdot)$ defined over a bounded set \mathcal{X} of the variable x , with upper and lower bounds M and m over \mathcal{X} . Having a binary decision variable $\delta \in \{0, 1\}$, it can be proved that the following statement holds (from a numerical point of view) [15, 234]:

$$[f(x) \leq 0] \Leftrightarrow [\delta = 1] \text{ is equivalent to } \begin{cases} f(x) \leq M \cdot (1 - \delta), \\ f(x) \geq \epsilon + (m - \epsilon) \cdot \delta, \end{cases} \quad (4.27)$$

with ϵ being a very small tolerance (known as the machine precision) used to change a strict inequality into a non-strict inequality. Moreover, the product of two binary variables δ_1 and δ_2 can be replaced by an auxiliary binary variable $\delta_3 \triangleq \delta_1 \cdot \delta_2$. Next, it can be verified that [15, 234]

$$\delta_3 = \delta_1 \cdot \delta_2 \text{ is equivalent to } \begin{cases} -\delta_1 + \delta_3 \leq 0, \\ -\delta_2 + \delta_3 \leq 0, \\ \delta_1 + \delta_2 - \delta_3 \leq 1. \end{cases} \quad (4.28)$$

Finally, multiplication of a binary variable δ with an affine function $f: \mathbb{R}^n \rightarrow \mathbb{R}$ can be replaced by an auxiliary variable $z \triangleq \delta \cdot f(x)$, meaning that $z = 0$ when $\delta = 0$ and $z = f(x)$ in case $\delta = 1$. It is easy to verify that [15, 234]

$$z = \delta \cdot f(x) \text{ is equivalent to } \begin{cases} z \leq M \cdot \delta, \\ z \geq m \cdot \delta, \\ z \leq f(x) - m \cdot (1 - \delta), \\ z \geq f(x) - M \cdot (1 - \delta). \end{cases} \quad (4.29)$$

Using the above rules, one can rewrite the approximate models presented in the previous section into the form of (4.26). For instance, the PWA function (4.18) can be rewritten as

$$\hat{P}_{i,fi}(n_i(k)) = \sum_{j=1}^3 (\mathcal{A}_{i,fi}^j \cdot n_i(k) + \mathcal{B}_{i,fi}^j) \cdot \delta_{i,fi}^j, \quad (4.30)$$

where the $\delta_{i,fi}^j$ variables correspond to the intervals defined in (4.18) ($\delta_{i,fi}^j = 1$ when $n_i(k)$ is in the j th interval) and $\mathcal{A}_{i,fi}^j, \mathcal{B}_{i,fi}^j$ can be calculated from the formulation presented in (4.18). Then, it is straightforward to rewrite (4.30) into the form of (4.26) with the help of (4.27) and (4.29).

After reformulation of the approximate models presented in Section 4.4, we obtain a system of linear equations and linear inequality constraints including real and integer variables. Returning to the optimization problem, the selected performance index (total time spent) is already in the linear form. However, the penalty on the control inputs (4.16) is nonlinear. This objective function can be transformed into a linear form by defining auxiliary variables as follows:

$$\sum_{l=1}^{N_p-1} q_l \quad \text{subject to} \quad \begin{cases} q_l \geq u_{ij}^c(k_c + l) - u_{ij}^c(k_c + l - 1), \\ q_l \geq -(u_{ij}^c(k_c + l) - u_{ij}^c(k_c + l - 1)). \end{cases} \quad (4.31)$$

It can be easily proved that minimizing (4.31) over u_{ij}^c and q_l would result in the same optimal solution as in case of minimizing (4.16) over u_{ij}^c .

All in all, the problem of minimizing the total time spent in the network subject to the obtained mixed linear model of the system and other linear constraints on the inputs and states is formulated as a mixed integer linear optimization problem (MILP), which has to be solved in the MPC framework. This problem is more tractable and can be solved using advanced solvers [7].

4.6. CASE STUDIES

In this section, we implement and evaluate the performance of the proposed hybrid schemes using simulation. We stick to the macroscopic level to investigate and highlight the performance of our proposed control methods. We use a simulation model to represent the urban traffic network and a prediction model to estimate the traffic states inside the MPC framework. We start with a low mismatch between the simulation model and the prediction model in Section 4.6.2, to evaluate how the proposed control algorithms deal with the general traffic congestion control problem. Next, we perform several extensive tests with the introduction of different types of uncertainties in the simulation model, in order to better represent reality and to evaluate our control approaches under more realistic scenarios. In Section 4.6.2, we investigate the performance of the hybrid perimeter and switching timing plans control (the original MINLP approach) and show that additional improvements are obtained, compared with perimeter control or switching timing plans only, if both control entities are coordinated and considered in the mixed integer nonlinear optimization. The performance of the proposed hybrid scheme is further compared with a greedy feedback perimeter controller. In Section 4.6.3, the two approximation methods are implemented and their performance is compared with that of the mixed integer nonlinear programming approach in terms of computation time and total cost. Two different demand profiles are selected in the examples to show that the proposed hybrid scheme is able to handle different traffic scenarios. Finally, we present the results of evaluating our proposed methods for different types of uncertainties (in state measurements, MFDs, trip demands) introduced in the simulation model. In the following, we describe in full detail the urban network under study and different types of uncertainties that might exist in reality and that need to be modeled in the network simulation model.

4.6.1. SET-UP

We consider an urban network partitioned into two homogeneous regions (i.e. $R = 2$): the periphery (region 1) and the city center (region 2). The library of the signal timing plans and MFDs is given a priori for each region. In Section 4.6.2, a set of 5 MFDs is defined for the periphery (region 1) and the city center (region 2) as depicted in Fig. 4.5(a) and (b), respectively. In Fig. 4.5(b) the set consists of $\text{MFD}_{1,3}$ adopted from [70] with maximum trip completion flow 6.3 (veh/s) corresponding to critical accumulation 3400 (veh), jam accumulation 10000 (veh) (thus the parameters of the 3rd-degree polynomial would be $a = 4.13 \times 10^{-11}$ (1/(veh² · h)), $b = -8.28 \times 10^{-7}$ (1/(veh · h)), $c = 4.192 \times 10^{-3}$ (1/h)) and 4 other MFDs that are obtained based on varying from the critical accumulation and the maximum trip completion flow of $\text{MFD}_{1,3}$. The percentages of the deviations are $\pm 10\%$ and $\pm 5\%$ for the critical accumulation and the maximum trip completion flow, respectively. Moreover, it is assumed that the sizes of the two regions are different; hence, the MFDs of the city center (region 2) are equal to the periphery MFDs multiplied by 1.4, as shown in Fig. 4.5(a). In practice, these MFDs can be obtained by changing the signal settings of intersections and can be estimated by the methods proposed in [45, 68].

In Sections 4.6.3 and 4.6.4, each region is assumed to have 3 MFDs (the same $\text{MFD}_{1,2}$, $\text{MFD}_{1,3}$, and $\text{MFD}_{1,4}$ as in Fig. 4.5(b)).

4

UNCERTAINTIES IN MFDs

The dynamic equations of the simulation model (used to represent the network) differ from the prediction model used in the MPC framework as they contain different types of error explained in the following. Note that the presented MFDs in Fig. 4.5(a)-(b) are utilized for the MPC prediction model, while the network is assumed to include errors in the MFDs following the error formulation in [71]. In reality, an MFD is extracted based on several data collection experiments in the network. Based on the level of homogeneity of the network, the MFD will exhibit scattering. By scattering, we mean that in general corresponding to each accumulation there exist multiple trip production points. The level of scattering increases when the accumulation grows. Therefore, there is no explicit mathematical equation for the MFD. In the following, we approximate the MFD using a 3rd-degree polynomial but to take into account the scattering we assume a uniformly distributed additive noise with zero mean and a variance that is proportional to the accumulation level. For all simulation scenarios, we add the error e_i (veh/s) to the MFDs of the simulation model as follows:

$$e_i(k) \sim \mathcal{U}(-C_i \cdot n_i(k), C_i \cdot n_i(k)), \quad (4.32)$$

$$\tilde{G}_{i,f_i}(n_i(k)) = G_{i,f_i}(n_i(k)) + e_i(k), \quad (4.33)$$

with $C_i = 0.2/3600$. Hence, we get a model where the scattering increases with the increase in the level of accumulations. The MFDs \tilde{G}_{i,f_i} used to simulate the urban network are depicted in Fig. 4.4.

Note that there also exist other uncertainties in the urban network modeling. The errors in the measurement of the accumulations and uncertainties in the estimation of the trip demands are among them that will be extensively discussed in Section 4.6.4. In Sections 4.6.2 and 4.6.3, we only consider the errors in the MFDs, while in the last section (robustness evaluation) we investigate the effects of all possible uncertainties

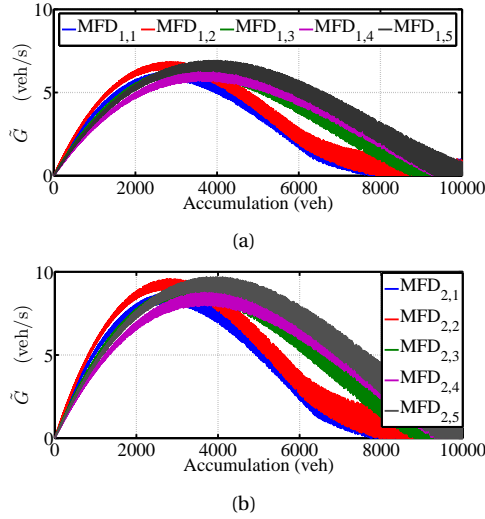


Figure 4.4: Uncertain MFDs representing the urban network under control, (a) MFDs of the periphery, and (b) MFDs of the center.

(uncertainties in MFDs, error in the state measurements, uncertainties in the estimation of trip demands) on the performance of the hybrid control approaches.

SIMULATION PARAMETERS

For simulation of the system, we choose the sample time as $T = 30$ s. Moreover, the control sample time is selected as $T_c = 60$ s in Sections 4.6.2 and 4.6.3, while it varies for Section 4.6.4 (robustness to measurement noise). The hybrid model predictive controllers (the MINLP approach and the PWA-MILP methods) use the prediction horizon $N_p = 20$ (which corresponds to 20 min, since $T_c = 60$ s) and the control horizon³ $N_c = 2$ (corresponds to 2 min). Moreover, the penalty term (4.16) is added to the objective function with a weight of 10 (this choice is obtained based on the nominal values of the total time spent objective function and the penalty term; more discussions about finding proper weights are provided in [71]). Furthermore, the lower and upper bounds of the perimeter input are selected as $u_{ij,\min} = 0.1$ and $u_{ij,\max} = 0.9$. Therefore, the flows between regions are neither completely allowed, nor fully blocked.

4.6.2. PERFORMANCE EVALUATION OF NONLINEAR APPROACH

The demand profiles for trips inside each region and between them are illustrated in Fig. 4.5(d). There is a high demand for trips inside the periphery, see $q_{11}(\cdot)$ in the figure. Further, both regions are initially congested, i.e. the initial accumulations are larger than the critical accumulations ($n_{11}(0) = 3700$ (veh), $n_{12}(0) = 2300$ (veh), $n_{21}(0) = 2000$ (veh), $n_{22}(0) = 2000$ (veh)).

The hybrid controller finds the optimal perimeter control inputs along with the optimal timing plans, as shown in Fig. 4.5(e) and (f), for each region using the mixed integer nonlinear optimization. The switching between the MFDs that occurs during the

³The current choice for these parameters are based on the tuning procedure in [71].

Table 4.1: Performance evaluation for different control schemes in Section 4.6.2.

Control scheme	Total time spent (veh · s)
Uncontrolled	Gridlock
Greedy feedback controller	Gridlock
Perimeter control with MFD _{1,5} and MFD _{2,1}	3.47×10^7
Perimeter control with MFD _{1,5} and MFD _{2,2}	3.42×10^7
Perimeter control with MFD _{1,5} and MFD _{2,3}	3.38×10^7
Perimeter control with MFD _{1,5} and MFD _{2,4}	3.37×10^7
Perimeter control with MFD _{1,5} and MFD _{2,5}	3.36×10^7
Perimeter control with other MFD combinations	Gridlock
Switching timing plans only	Gridlock
Hybrid controller (MINLP approach)	2.78×10^7

simulation period is graphically displayed in Fig. 4.5(a) and (b). For Region 1, MFD_{1,5} is selected for the whole simulation period, while for Region 2 switching between MFDs occurs multiple times.

In the absence of control or having only perimeter control, one or both regions would get into a gridlock situation. But with optimal switching between timing plans and assisted by perimeter control, both regions will escape from high-level congestion and they will be eventually uncongested by the end of the simulation interval, as depicted in Fig. 4.5(c).

In order to evaluate the MPC hybrid controller results, the total time spent for the whole period of simulation (1 hour) is compared for several control schemes as shown in Table 4.1: (i) only perimeter control (the timing plans for both regions are fixed during the entire simulation period. Since there exist 5 MFDs (timing plans) in each of the libraries, 25 combinations are possible), (ii) switching timing plans control only, and (iii) a greedy feedback perimeter controller. The greedy perimeter controller is a simple state-feedback *perimeter* controller with the policy of protecting regions with high accumulations and high trip destinations. The control law of the greedy controller is as follows: if both regions are uncongested, the perimeter control inputs are maximized and if both regions are congested, the perimeter control inputs $u_{i,j}$ and $u_{j,i}$ are respectively set to the maximum and minimum values if region j is more congested than region i and vice versa. Note that the greedy control has been tested for all 25 combinations of MFDs.

The results shown in Table 4.1 imply that the MPC hybrid controller is superior for all control schemes in the sense that at least 17% improvement in total time spent is achieved when both controllers are applied jointly instead of only perimeter control. Also note that applying only switching timing plan control or using the greedy feedback controller still leads to gridlock situations in one or both regions.

4.6.3. PERFORMANCE EVALUATION OF APPROXIMATION APPROACHES

In this subsection, we provide a scenario to evaluate the performance of the proposed approximate methods and the original mixed integer nonlinear optimization approach. Moreover, in order to have a better performance evaluation of the approximation ap-

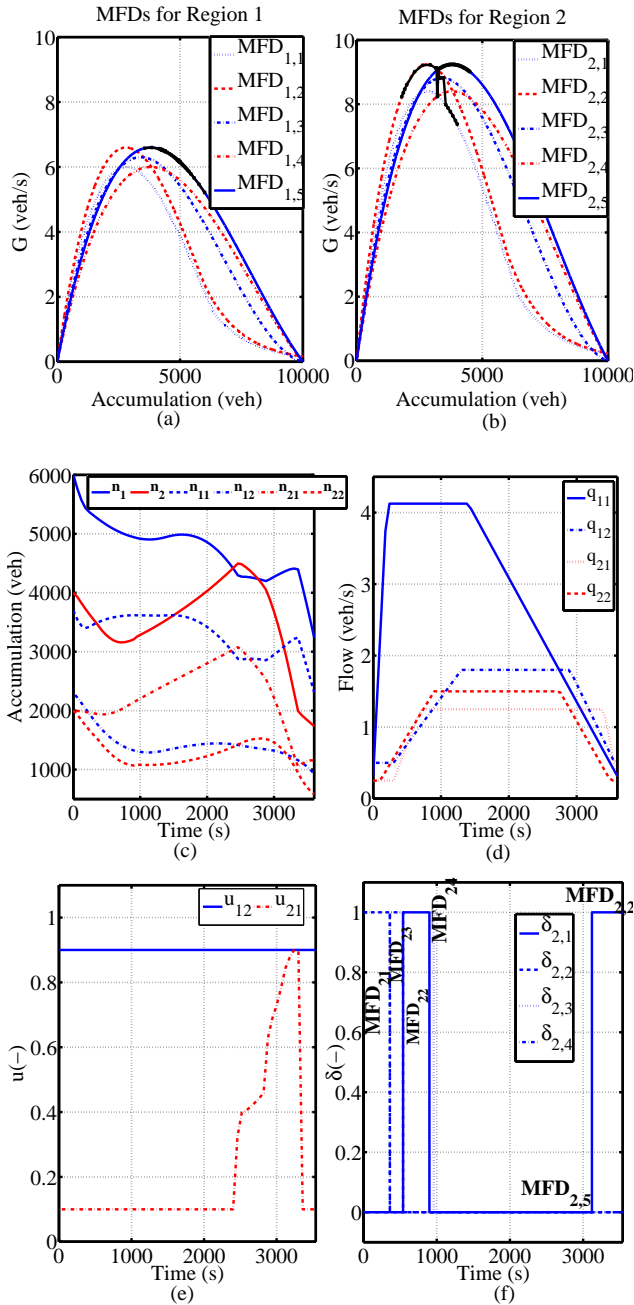


Figure 4.5: Performance overview of the nonlinear hybrid scheme, a,b) MFDs used in the prediction model along with the illustration of the switching between MFDs (black curves), c) accumulations, d) average demand profiles used in MPC, e) optimal perimeter control input, e) optimal switching signals for region 2 (the controller always chooses $MFD_{1,5}$ for region 1 in this case).

proaches, the results are compared with the greedy perimeter controller as well.

The demand profile simulates a peak morning hour with high demand $q_{12}(\cdot)$ for trips from region 1 (the periphery) to region 2 (the city center), as shown in Fig. 4.7(d). The closed-loop system is simulated for a period of 1 hour. The initial accumulations are $n_{11}(0) = 2700$ (veh), $n_{12}(0) = 2700$ (veh), $n_{21}(0) = 2000$ (veh), $n_{22}(0) = 2000$ (veh). The accumulations of the regions are measured and fed to the MPC controller. There are 3 cases of MPC controllers; one with embedded MINLP optimization based on the non-linear prediction model, one with MILP optimization based on the first approximate model as prediction model (we call it PWA-MILP1), and one with MILP optimization based on the second approximate model as prediction model (we call it PWA-MILP2). The quantized perimeter input is formulated as

$$u_{ij}(k) = 0.26 \cdot (0.5 + 2^0 \cdot \omega_{ij,1}(k) + 2^1 \cdot \omega_{ij,2}(k)). \quad (4.34)$$

Therefore, in the PWA-MILP cases, the perimeter control input takes values from the set $\{0.13, 0.4, 0.65, 0.9\}$.

The evolution of the accumulations over time corresponding to the MINLP approach, the first approximation method PWA-MILP1, the second approximation method PWA-MILP2, and the greedy controller are depicted in Fig. 4.6(a), 4.6(b), 4.6(c), and 4.6(d), respectively. These figures demonstrate the effectiveness of the control measures as they show that the control inputs prevent the two regions from moving forward towards gridlock (as all accumulations are less than the jam accumulations). In the absence of control, gridlock would occur. The MINLP approach results in a better performance compared to both PWA-MILP approaches, in particular for the accumulations of region 2. For the PWA-MILP1 approach, this can be explained by the fact that we have approximated the second-degree polynomials with two affine functions, see (4.18), and also because of the forward simulation method that has been introduced to overcome the multiplication of variables. Hence, the performance of the PWA-MILP1 method can be improved by approximating the polynomials with a larger number of affine functions and by using more iterations in each control time step.

Nevertheless, a more accurate way to tackle the problem with multiplication of variables was proposed in the second approximation method PWA-MILP2. Therefore, the performance of the PWA-MILP2 method is closer to the MINLP approach in terms of the sum of accumulations over the whole simulation period. Moreover, in order to further verify the advantage of the MILP formulation of the problem, the greedy perimeter controller results are compared with the results of the hybrid approaches. Comparing with Fig. 4.6(d), the greedy perimeter controller's performance is much worse than each of the 3 hybrid approaches. With the greedy controller, the accumulations of both regions will exceed 7000 vehicles at the end of the simulation time, and the total time spent is much higher.

The optimal perimeter control inputs for the MINLP, PWA-MILP1, PWA-MILP2 approaches, and the greedy controller are shown in Fig. 4.6(e), 4.6(f), 4.6(g), and 4.6(h), respectively. The perimeter inputs u_{12} of the MINLP approach are close to the maximum to allow more vehicles to leave region 1 while u_{21} varies more over time. Moreover, the optimal switching timing plans for the MINLP, PWA-MILP1, and PWA-MILP2 approaches are respectively illustrated in Fig. 4.7(a), 4.7(b), and 4.7(c), for both regions 1 and 2. It can be observed in this scenario that the optimization algorithms mostly

choose the MFD with the highest flow rate. This is more clear in the MINLP and PWA-MILP2 approaches while in the PWA-MILP1 case, the switching between MFDs occurs more often.

The computation time and total time spent are compared for different proposed algorithms and for different values of prediction horizon in Table 4.2. The average computation time for the scenario $N_p = 20$ is 51.52 (s) for one run of the MINLP algorithm⁴, while it is 1.143 (s) and 5.3934 (s) for the PWA-MILP1 and PWA-MILP2 approaches. Note that the MINLP algorithm has been executed 10 times in each control time step for different random initial points in order to prevent reaching a locally optimal solution. The CPU times reported for the MINLP algorithm are the average over all control time steps in which the nonlinear optimization is executed 10 times.

It can be inferred from Table 4.2 that the PWA-MILP2 method has a better performance in terms of the total time spent (veh · s) compared to the PWA-MILP1 approach but slightly worse than the MINLP case. The computation time of the PWA-MILP2 approach is larger than PWA-MILP1 approach but much smaller than nonlinear case. Furthermore, using each of the two PWA-MILP approaches results in less total time spent than the greedy perimeter controller (3.75×10^7 (veh·s)). Only in the case $N_p = 10$, the first approximation method gives a slightly larger time spent compared to the one achieved from the greedy controller.

Moreover, as mentioned before in Remark 4.1, the quantization of the perimeter control input can be prevented by introducing an auxiliary variable \tilde{M} and by adding some extra inequality constraints, provided that the perimeter control input is not penalized. Results of using this technique are presented in Table 4.2, under the name PWA-MILP3. In fact, we follow the same approach as in PWA-MILP2, but without quantizing the perimeter input and without considering the penalty term on the perimeter input. The obtained results show a slight decrease in the computation time and an improvement in the total objective function (compared to the other approximation methods). So if one prefers to penalize the control input (e.g. to prevent instability or other undesired behaviors due to oscillations in the control input), PWA-MILP1 or PWA-MILP2 are suggested. However, if penalizing the control input is not deemed necessary, clearly PWA-MILP3 is the best choice.

4.6.4. ROBUSTNESS TO MEASUREMENT ERRORS AND UNCERTAIN DEMANDS

In this section, we first study the effects of measurement errors on the performance of the proposed schemes and propose a solution for the drawbacks caused by these errors. Next, we study the impacts of unbiased and biased noise in trip demands. The selected scenario is similar to Section 4.6.3 but with addition of the two new types of uncertainties introduced in the simulation model. The prediction horizon is $N_p = 20$ (corresponding to 20 min), the control horizon is $N_c = 2$ (corresponding to 2 min), simulation sample time 30 s, and the total simulation time is 1 hour.

⁴These CPU times were obtained adopting the functions `minlpBB` and `Cplex` inside the *Tomlab* toolbox of Matlab 7.12.0 (R2011a), on a 64-bit Windows PC with a 2.8GHz Intel Core i7 processor and 8Gb RAM.

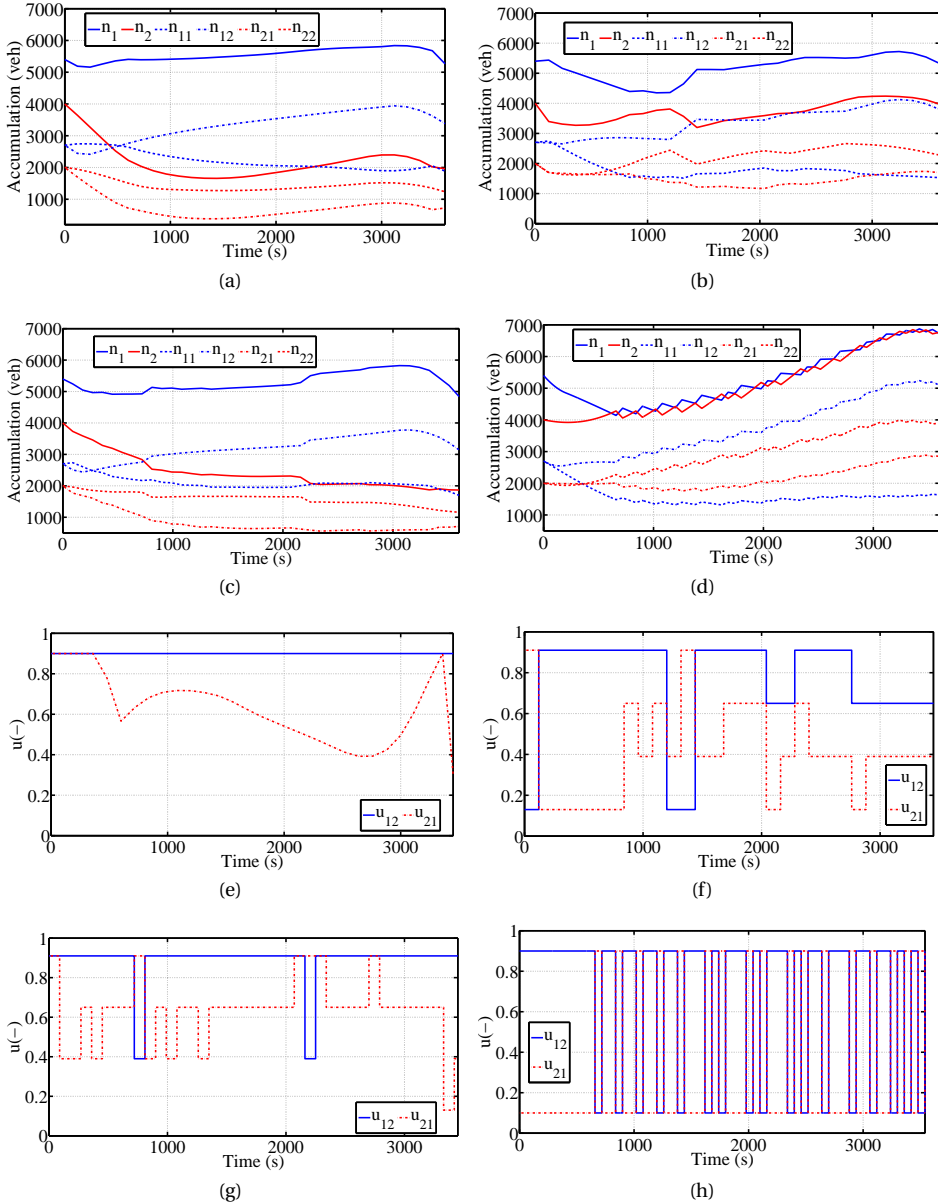


Figure 4.6: The results obtained from the MINLP approach, PWA-MILP1, PWA-MILP2 methods, and the greedy perimeter controller: accumulations are presented in 4.6(a), 4.6(b), 4.6(c), and 4.6(d), respectively. perimeter control inputs are presented in 4.6(e), 4.6(f), 4.6(g), and 4.6(h), respectively.

Table 4.2: Performance evaluation for the methods of Section 4.6.3

Prediction horizon N_p	Total time spent (veh · s)			Average computation time (s)				
	MINLP	PWA-MILP 1	PWA-MILP 2	PWA-MILP 3	MINLP	PWA-MILP 1	PWA-MILP 2	PWA-MILP 3
10 min	3.35×10^6	3.91×10^6	3.47×10^6	3.42×10^6	20.33×10	0.527	1.1323	1.0165
20 min	2.85×10^6	3.31×10^6	2.87×10^6	2.85×10^6	51.52×10	1.143	5.3934	3.5341
30 min	2.79×10^6	3.18×10^6	2.84×10^6	2.80×10^6	164.12×10	4.103	9.3129	7.8275

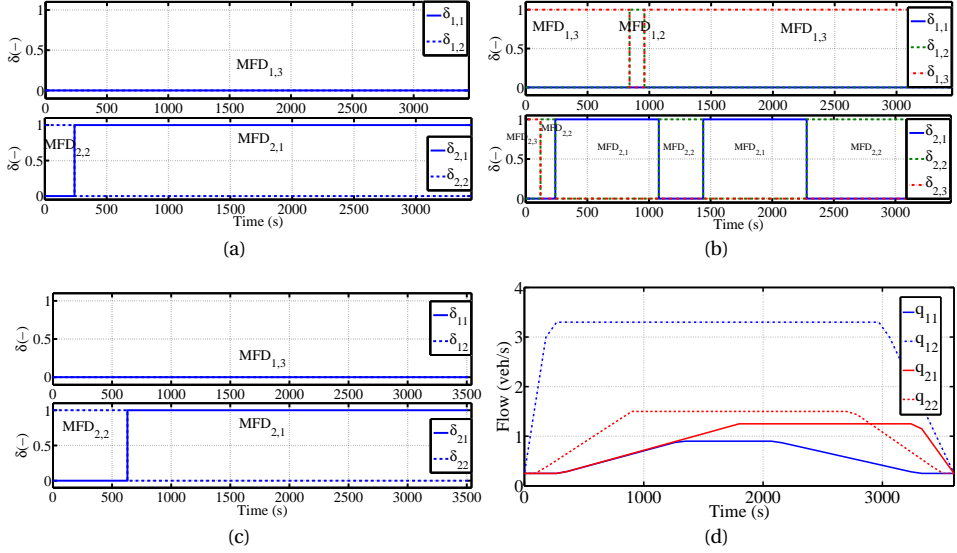


Figure 4.7: The results obtained from the MINLP approach, PWA-MILP1, PWA-MILP2 methods, and the greedy perimeter controller: switching between timing plans are presented in 4.7(a), 4.7(b), and 4.7(c), respectively. The nominal trip demand profiles used in the prediction model are illustrated in 4.7(d).

4

STATE MEASUREMENTS ERRORS

In reality, there is uncertainty about the measured states of the network, specially in the estimation of the number of vehicles with destinations inside regions or across the regions (n_{ii} and n_{ij}). Hence, the effects of errors in the measured states should be taken into account. However, to be consistent with reality, one should expect larger errors in the n_{ij} than in the total number of vehicles inside the region, i.e. n_i . This is due to the fact that estimating the total number of vehicles inside a region is easier to obtain than estimating the number of vehicles with certain destinations that can be inside a region or in neighboring regions (e.g. n_i can be estimated with fixed sensors in certain locations of the network, while n_{ij} would require tracking the on-board navigation devices of vehicles to identify their destinations). Therefore, we model the error in the states as follows:

$$\tilde{n}_{ii}(k) = n_{ii}(k) + \omega_{ii} \cdot n_{ii}(k) \cdot \varepsilon_{ii}(k), \quad (4.35)$$

$$\tilde{n}_{ij}(k) = n_{ij}(k) + \omega_{ij} \cdot n_{ij}(k) \cdot \varepsilon_{ij}(k), \quad (4.36)$$

where the values for ω_{ii} and ω_{ij} are first set to 0.05 and then to 0.1, to simulate a 5% and a 10% error in the measurements, respectively. Moreover, the error vector $\varepsilon(k) = (\varepsilon_{ii}(k), \varepsilon_{ij}(k))^T$ has a normal distribution with the mean value of zero and the covariance matrix as

$$\text{Cov}(\varepsilon) = \begin{bmatrix} 1 & -0.75 \\ -0.75 & 1 \end{bmatrix}. \quad (4.37)$$

To motivate the elements of the covariance matrix, note that the total number of vehicles inside the region i ($\tilde{n}_i(k) = \tilde{n}_{ii}(k) + \tilde{n}_{ij}(k)$) will contain the sum of the elements of the

error vector $\varepsilon(k)$. On the other hand, the variance of the sum of two correlated variables $\text{Var}(X + Y)$ is $\text{Var}(X) + \text{Var}(Y) + 2\text{Cov}(X, Y)$. Therefore, the variance of the error in the estimation of n_i is 0.5 if the variance of the errors in estimating n_{ij} and n_{ii} is 1. This is consistent with our previous discussion on the difficulty of measuring the destination-dependent accumulations.

By adding measurement errors to the simulation model, as in (4.35)–(4.36), the performance of the hybrid controller gets affected by introducing fluctuations in the perimeter control inputs and by slightly increasing the number of switchings between MFDs. Simulation results in case of having 10% error in the measured n_{ij} are depicted in Fig. 4.8(a). The perimeter control inputs show considerable jumps, and therefore not useful for practical situations. Traffic operators expect more stable control profiles with smaller changes in the pattern. In order to overcome this problem, we propose, in addition to penalizing the control input variations, to select a control sample time larger than the simulation sample time while keeping the obtained control inputs constant between two consecutive control time steps. By performing this, the perimeter control inputs will have a smoother behavior over time, as can be observed in Fig. 4.8(b), while the total time spent in the network is not altered significantly.

Results for simulations with different T_c are presented in Table 4.3. Note that due to the addition of errors in the system, we expect different total time spent values for different runs with the same set of control inputs. Thus, the values presented in the table are the average over 10 runs for each case of the control sample time. It can be observed that for less frequent calls to the controller, we achieve around the same result but with less oscillations in the control inputs. However, for the ratio $T_c/T = 6$ and higher the performance will get worse. Furthermore, the obtained results show that the PWA-MILPI approach yields worse results compared to the other two approaches due to the forward simulation technique.

UNCERTAINTIES IN TRIP DEMANDS

Furthermore, we also take into account the uncertainty in trip demands. The prediction model in the MPC framework takes the average profile as e.g. shown in Fig. 4.5(d), while the network simulation model assumes noisy demand profiles to represent uncertain variations in demands from day to day and also to include incidents that temporarily affect the demand profiles. For the first case, the unbiased demand is assumed to have an additive white Gaussian noise, as follows:

$$\varrho_{ij} \sim \mathcal{N}(0, \sigma_{ij}^2), \quad (4.38)$$

$$\tilde{q}_{ij}(k) = q_{ij}(k) + \varrho_{ij}, \quad (4.39)$$

with $i, j = 1, 2$ and σ_{ij}^2 (veh²/s²) the variance of the noise. For the simulations, we consider a large noise with⁵ $\sigma = 0.5$. On the other hand, in the biased case, the demand profile has a sudden jump, as well as an additive nonzero mean Gaussian noise. This jump is not known to the MPC controller and only included in the network simulation model. In Fig. 4.9(a), the demand profile corrupted with unbiased noise is shown, while the biased demand with a sudden jump of 5 veh/s for a period of 10 min is depicted in

⁵In order to ensure that the total demand variable \tilde{q}_{ij} is always larger than or equal to zero, we clip the negative values to zero.

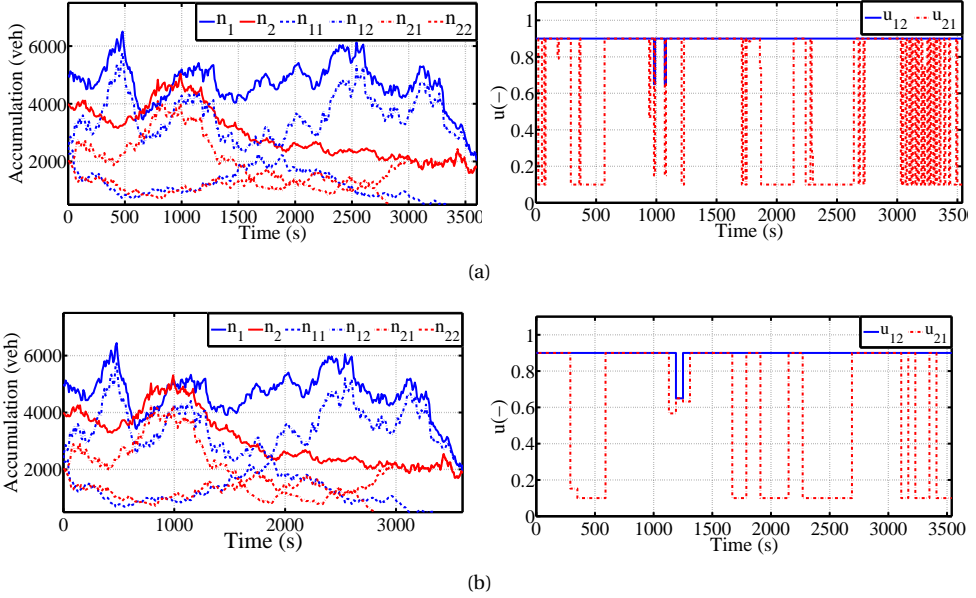


Figure 4.8: (a) Effect of measurement errors on states and perimeter control inputs, and (b) smoothing the perimeter control inputs (MINLP approach).

4

Fig. 4.9(b). Note that since we deal with aggregated region-based trip demands, these demands suffer less from the effects of fluctuations that exist in regular OD demand estimations. Furthermore, the level of the noise added to the trip demands is consistent with the results of practical experiments presented in the literature ([145, 211]).

Now we study the effects of adding noise in the trip demands in the simulation model (note that the prediction model still uses the average demand profile). In the first case the demand profile depicted in Fig. 4.9(a) is selected. Simulation results are presented in Fig. 4.10 for two control strategies MINLP and PWA-MILP2. The numerical results for other cases are presented in Table 4.3. As can be observed, the hybrid control strategies are able to handle the unbiased noise in the demands. Only small size fluctuations in the control inputs occur, which can be prevented by penalizing the control inputs and also by increasing the control sample time. It should be noted that increasing the control sample time more than 3 times the simulation sample time affects the performance.

Next, we use the biased noise in the demand profile of the simulation model. We have added Gaussian noise with a mean of 10% of the average profile and a variance $\sigma_{ij}^2 = 0.2^2$, and a jump in q_{22} as depicted in Fig. 4.9(b). Simulation results for the PWA-MILP2 approach are illustrated in Fig. 4.11, while numerical results for all approaches are presented in Table 4.3. Overall, it can be inferred that the proposed hybrid control strategies are robust to different types of uncertainties in the urban network (reality). When comparing all modeling errors, we notice that the approaches are most sensitive to measurement errors in the states since an error changes the initial condition and subsequently, also the predicted state evolution in a significant way. However, note

Table 4.3: TTS values ($\times 10^7$ (veh · s)) for the methods of Section 4.6.3, in the presence of measurement error and noise in demands (in addition to errors in the MFDs).

Noise in trip demands	T_c T	No measurement error			Measurement error (5%)			Measurement error (10%)		
		MINLP	PWA-MILP 1	PWA-MILP 2	MINLP	PWA-MILP 1	PWA-MILP 2	MINLP	PWA-MILP 1	PWA-MILP 2
no noise	2	2.85	3.31	2.87	2.87	3.42	2.92	3.26	3.76	3.28
	3	-	-	-	2.90	3.46	2.99	3.28	3.78	3.29
	6	-	-	-	3.43	3.86	3.48	3.62	3.97	3.66
unbiased	2	2.88	3.22	2.86	2.94	3.45	3.01	3.15	3.81	3.18
	3	-	-	-	2.97	3.53	3.13	3.19	4.01	3.21
	6	-	-	-	3.56	3.78	3.64	3.73	gridlock	3.91
biased	2	3.14	3.97	3.20	3.32	4.21	3.30	3.45	gridlock	3.55
	3	-	-	-	3.36	4.35	3.38	3.56	gridlock	3.61
	6	-	-	-	3.74	gridlock	3.86	3.88	gridlock	4.02

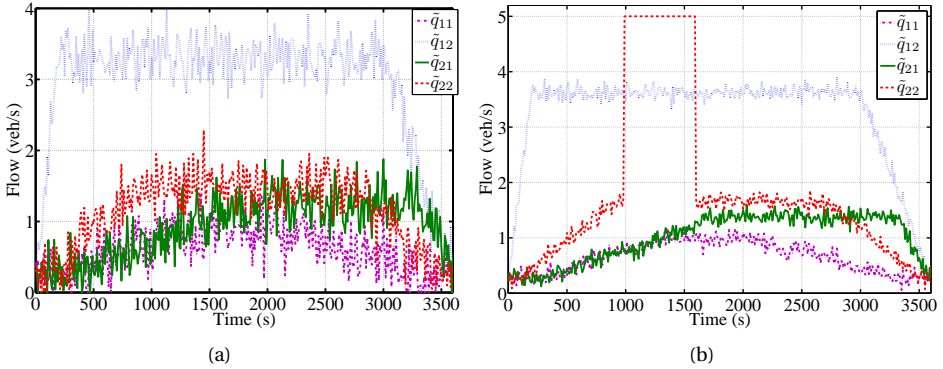


Figure 4.9: Noisy demand profiles used in the simulation model (network); (a) high unbiased noise in demand, and (b) biased noise (sudden jump in q_{22}).

that the 10% error in the measurements, in the order of $0.1 \times 5000 = 500$ vehicles, is consistent with recent findings in the literature on the estimation of accumulations and MFDs [145, 181]. As can be inferred from Table 4.3, the PWA-MILP1 approach yields poor performance when combined MFD, measurement, and demand noise exist in the simulation model. The MINLP approach has impressive and robust performance under different conditions, only it suffers from high computation time for large scale problems. Hence, for small-scale cases in which the computation time is not crucial, the multi-start MINLP approach is suggested, while for larger problems, either one of the three approximation methods can be chosen based on the structure of the network, the type and level of uncertainties, and the acceptable level of oscillation in the control inputs. For instance, PWA-MILP1 is the fastest method and but it is applicable in cases where there are not much uncertainty and measurement errors. The PWA-MILP2 method has better performance but it is slower than the first approximation method. The PWA-MILP3 approach maintains good performance and it is faster than PWA-MILP2 (in general) but the control inputs may have fluctuations since it is not possible to penalize them in the optimization problem of this method.

4.7. CONCLUDING REMARKS

Within the hierarchical multi-level approach for control of large-scale urban traffic networks, we have introduced a new control scheme that combines switching between timing plans and perimeter control to manage and control a large-scale urban network.

The optimal control solutions are obtained in a model predictive control scheme for two different open-loop optimization problems: mixed integer nonlinear and mixed integer linear programming. The mixed integer linear programming problem is based on the piecewise affine approximation of the nonlinear model. The results of the case studies have shown the significant reduction of the computation time using the approximate MILP approaches. The computation times for solving the MILP problems have been much lower than for solving the MINLP problem. This is very crucial for real-time implementation in networks with a large number of regions, as the MINLP approach might not be tractable. Furthermore, it should be noted that the MILP results only devi-

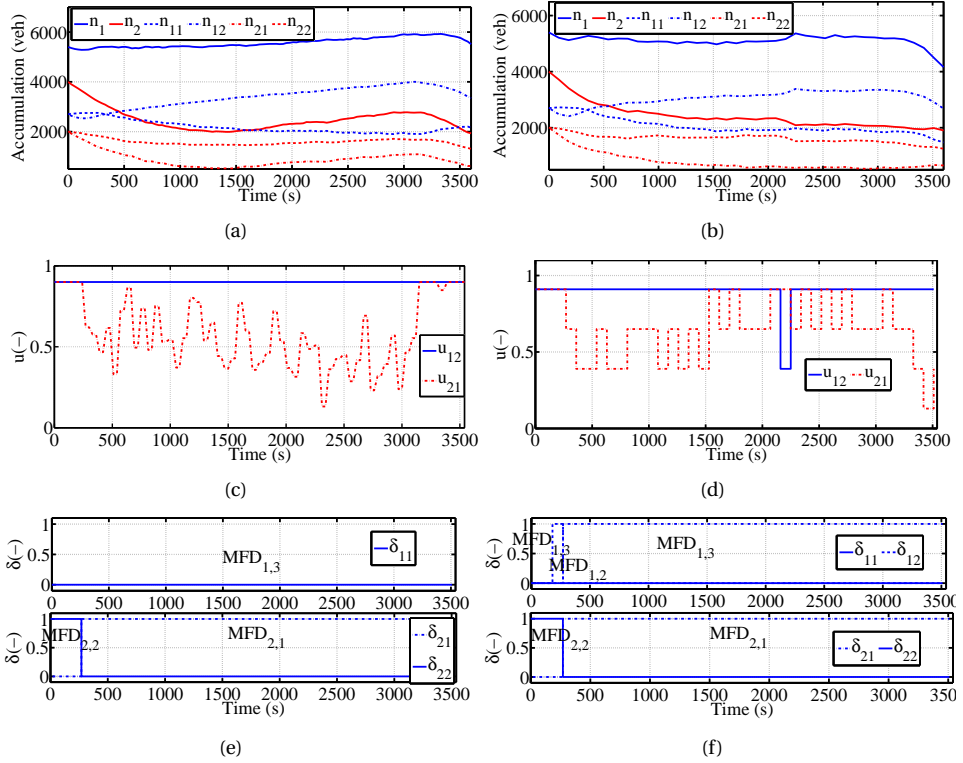


Figure 4.10: Robustness to unbiased noise in demand: Accumulations, (a) MINLP approach, (b) PWA-MILP2 approach. Perimeter input, (c) MINLP approach, (d) PWA-MILP2 approach. Switching between timing plans, (e) MINLP approach, (f) PWA-MILP2 approach.

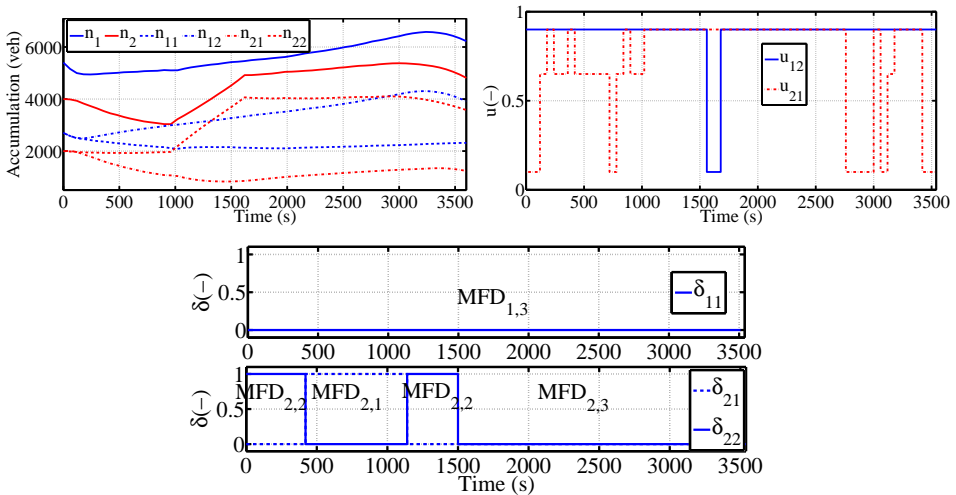


Figure 4.11: Biased noise (peak in q_{22}), control using PWA-MILP2.

ate a little (specially for the second approach) compared to the MINLP results.

The effectiveness of hybrid (perimeter and timing plan switching) control has been compared quantitatively with perimeter control only. It is apparent that the switching timing plan controllers can enhance the network performance when they collaborate with the perimeter controllers, as they can more efficiently utilize the network capacity to decrease the total time spent in the network. However, several research questions are still open in this direction, e.g. investigation of other approximation methods that might enhance the MILP approach. Simulation of the closed-loop system using micro-simulation software packages and field implementation of the proposed methods would shed more light on how these controllers can change the spatial distribution of congestion. In the hierarchical framework of this chapter, lower-level local controllers must be properly designed in order to realize the optimal control inputs determined by the high-level schemes. The effect of control decisions in the route choice of users is also a research direction. Monitoring techniques [145, 181, 211] for different types of sensors and penetration rates to decrease the measurement errors in the state variables and in the demands should be studied as well.

5

OPTIMAL DYNAMIC REGION-BASED ROUTE GUIDANCE

In this chapter, we use an aggregate modeling approach based on the macroscopic fundamental diagram (MFD) in order to find dynamic optimal routing strategies. An urban area can be divided into homogeneous regions each modeled by a (set of) macroscopic fundamental diagram. Thus, we can solve the route guidance problem in a regional fashion by using model predictive control and the high-level MFD-based prediction model. The optimal routing advices obtained from the high-level controller can be used as references (to track) for lower-level local controllers installed at the borders of the regions. Hence, using the proposed hierarchical scheme, the complexity of solving the route guidance problem in a large network will be decreased significantly with respect to other methods that are based on detailed models and routes. We evaluate the performance of the proposed approach using a multi-origin multi-destination grid network. The obtained results show significant performance of the optimal dynamic route guidance over other static routing methods.

5.1. INTRODUCTION

As discussed in Chapters 2 and 4, the MFD can be utilized for high-level and aggregated traffic network modeling. The key advantages of the MFD-based modeling approach are the small number of parameters that need to be calibrated, and also the computational efficiency in simulation and control. Therefore, in this chapter we aim at using the MFD-based modeling technique for solving another challenging problem, viz., dynamic route guidance in urban traffic networks.

Dynamic route guidance has been an interesting topic in the traffic management context [122, 136, 185, 190, 207, 227, 228, 228]. The main concept of dynamic routing is to guide the traffic towards alternative routes in the network in order to reduce the imbalance in the distribution of traffic flows, to improve the overall travel time, and/or to minimize other traffic objectives such as emissions or total fuel consumption. In this chapter, we address the route guidance problem using a multi-level scheme. We use the aggregate modeling approach based on the MFD for describing the flow of vehicles traveling in a multi-region urban network. The high-level traffic flow model is then used in an optimal dynamic route guidance framework. The framework is developed based on the theory of model predictive control (MPC) [160, 198] and its main goal is to determine optimal references for guiding the traffic of vehicles between urban regions in order to achieve minimum delays in reaching the destinations.

Basically, the proposed route guidance scheme consists of two levels. At the higher level, a central MPC controller uses the MFD-based traffic flow model in order to find optimal splitting rates for traffic flows heading towards specific destinations. The obtained optimal splitting rates will be communicated to the lower level controllers that are installed at the borders of urban regions. These local controllers have the task to realize the reference splitting rates by manipulating the signaled intersections and/or by adapting the dynamic route guidance information. A major advantage of this approach is that the necessity of establishing pre-defined routes in the network and searching for the optimal ones is relaxed by finding the destination-dependent splitting fractions towards the neighboring regions of a region. Hence, we shift from the link-level splitting rates to region-level splitting of traffic flows. Another main advantage of this scheme is that the computational complexity is much less than that of the usual route assignment problems that deal with a huge collection of roads and intersections.

The chapter is organized as follows. In Section 5.2, we present the high-level modeling of multi-region urban networks based on the concept of the MFD and macroscopic traffic flow modeling. Next, in Section 5.3, we introduce a multi-level scheme for optimal dynamic route guidance and formulate the corresponding optimization problem. Section 5.4 presents a case study that illustrates the proposed route guidance approach and evaluates and compares the performance of the proposed scheme with a static routing method.

5.2. MULTI-REGION MACROSCOPIC MODELING

The modeling method starts by splitting the network into several regions, which are as homogeneous as possible in the sense of distribution of congestion. For heterogeneous networks, it might be possible to partition them into more homogeneous regions such that each region has a well-defined MFD, see [123]. The traffic dynamics are modeled in these regions, using the extracted MFD for each region (as depicted in Fig. 5.1).

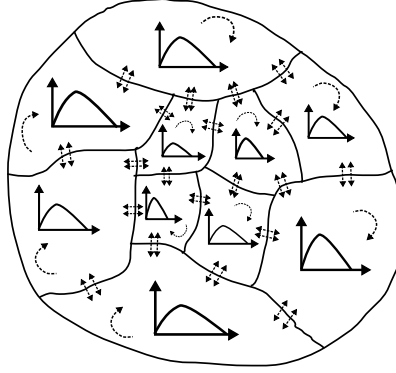


Figure 5.1: Schematic multi-region urban network.

In each region $i \in \mathcal{R}$, with \mathcal{R} the set of all regions, the accumulation is defined as the weighted density of all links in region i and is formulated as follows:

$$n_i(k) = \sum_{\lambda \in \Lambda_i} (\kappa_\lambda \cdot L_\lambda \cdot \rho_\lambda(k)), \quad (5.1)$$

where Λ_i contains all links in region i and κ_λ , L_λ , and ρ_λ are the number of lanes, the length, and the density of link λ , respectively.

The set of neighboring regions of region i is defined as \mathcal{J}_i . The flow from region i to region $j \in \mathcal{J}_i$ is determined by the minimum of three elements [97, 136]:

1. The capacity of the boundary between region i and region j , $C_{i,j}$.
2. The demand from region i to region j , $D_{i,j}$.
3. The supply in region j , S_j .

The demand from region i to region j is determined based on the MFD, a function we indicate as $P_i(n_i)$. In fact, we can construct a demand and supply scheme similar to the cell transmission model [42]. The supply can be determined in the same way as in the cell transmission model; the supply is equal to the critical production $P_{j,\text{cr}}$ for accumulations lower than the critical accumulation n_{cr} and is equal to the value given by the MFD for higher accumulations:

$$S_j(k) = \begin{cases} P_{j,\text{cr}} & \text{if } n_j(k) \leq n_{j,\text{cr}} \\ P_j(n_j(k)) & \text{if } n_j(k) > n_{j,\text{cr}} \end{cases} \quad (5.2)$$

Contrary to the cell transmission model, the demand in a region starts decreasing when the accumulation exceeds the critical accumulation. This is because there might be internal traffic jams in the region, limiting the potential outflow. This is graphically shown in Fig. 5.2.

The fraction of accumulations in each region i heading towards destination $d \in \mathcal{D}$ is known (using historical data and also information from on-board navigation devices) and is denoted by $n_{i,d}$. Moreover, the routing from region i to a destination d is coded by

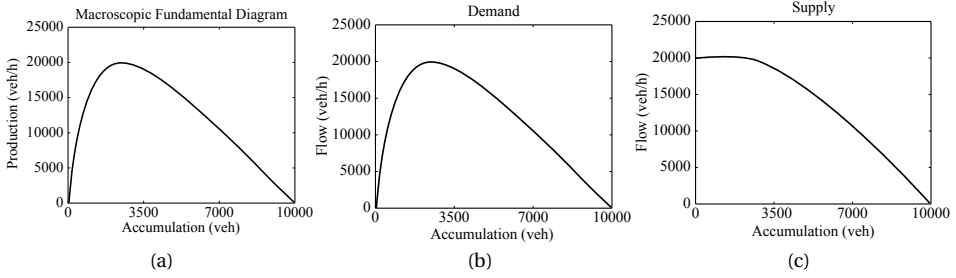


Figure 5.2: The factors determining the flow, (a) Macroscopic Fundamental Diagram, (b) demand, and (c) supply.

the next neighboring region j in the so called destination-specific splitting rates $\alpha_{i,j,d}$. Therefore, the total demand from region i towards region j is formulated as

$$D_{i,j}(k) = \sum_{d \in \mathcal{D}} \left(\alpha_{i,j,d}(k) \cdot \frac{n_{i,d}(k)}{n_i(k)} \cdot P_i(n_i(k)) \right), \quad (5.3)$$

where \mathcal{D} is the set of all destinations. This demand is limited by the capacity of the boundary of regions i and j , giving the effective demand $\tilde{D}_{i,j}$ as

$$\tilde{D}_{i,j}(k) = \min \{ D_{i,j}(k), C_{i,j} \}. \quad (5.4)$$

The fraction of traffic allowed over the boundary between i and j is indicated by $\frac{\tilde{D}_{i,j}(k)}{D_{i,j}(k)}$. As an intermediate step, we now have the demand from region i to destination d via region j , formulated as follows:

$$\tilde{D}_{i,j,d}(k) = \alpha_{i,j,d}(k) \cdot \frac{n_{i,d}(k)}{n_i(k)} \cdot P_i(n_i(k)) \cdot \frac{\tilde{D}_{i,j}(k)}{D_{i,j}(k)}. \quad (5.5)$$

The total demand towards region j determined by adding up all effective demands towards region j is

$$D_j(k) = \sum_{i \in \mathcal{J}_j} \tilde{D}_{i,j}(k). \quad (5.6)$$

This value is compared with the supply in region j . If the supply is larger, the flow is unrestricted. However, if the supply is lower, the fraction of the flow that can travel into region j is determined as

$$\psi_j(k) = \min \left\{ \frac{S_j(k)}{D_j(k)}, 1 \right\}. \quad (5.7)$$

If the supply restricts the flow, the actual flow to cell j is proportional to the demands towards the cell. Now, the flow is set as the minimum of demand and supply.

Now, for region i we consider those neighboring regions $j \in \mathcal{J}_i$ which there are nonzero demands $\tilde{D}_{i,j}(k) > 0$ from region i to them. The outflow from region i to region $j \in \mathcal{J}_i$ can be calculated using $\tilde{D}_{i,j}(k)$ and the fraction of flows that can enter region j , derived in (5.7). The result is formulated as

$$q_{i,j}(k) = \psi_j(k) \cdot \tilde{D}_{i,j}(k). \quad (5.8)$$

The flow can be separated per destination. So, similar to reducing the overall flow (5.8), we can modulate the flow per destination (5.5) as follows:

$$q_{i,j,d}(k) = \psi_j(k) \cdot \tilde{D}_{i,j,d}(k). \quad (5.9)$$

Therefore, the accumulation in any region i towards destination d can now be updated as follows:

$$n_{i,d}(k+1) = n_{i,d}(k) + T_s \left(\sum_{j \in \mathcal{B}} q_{j,i,d}(k) - \sum_{j \in \mathcal{B}} q_{i,j,d}(k) \right), \quad (5.10)$$

with T_s the sample time. Hence, the total accumulation in region i will be

$$n_i(k+1) = \sum_{d \in \mathcal{D}} n_{i,d}(k+1). \quad (5.11)$$

In the next section, we use the presented model for prediction of accumulations in the network in order to determine the optimal splitting rates.

5.3. MULTI-LEVEL OPTIMAL ROUTE GUIDANCE

In this section, we develop a route guidance scheme based on the high-level MFD-based model derived in the previous section. In the proposed framework, we solve the dynamic routing problem on a macroscopic level. This means that instead of taking into account individual roads and intersections, we deal with regional destinations and the way that traffic flow should be split towards the neighboring regions in order to avoid congestion in regions, to decrease the overall travel time and consequently, to improve the arrival rates at the destinations. We assume a two-level structure as depicted in Fig. 5.3. At the top level, the optimal route guidance problem is solved based on the aggregate model presented in the previous section. At the lower level, the optimal variables (the splitting rates) that are obtained from the high-level optimization problem are taken as references, i.e. local controllers in the lower level aim at realizing the optimal splitting rates for (destination-dependent) flows of vehicles that want to travel across the regions. In the following, we elaborate on the type of optimization problem that has to be solved in order to achieve the aforementioned goals.

5.3.1. OBJECTIVE FUNCTION AND CONSTRAINTS

In order to formulate the routing problem, an objective needs to be defined. The major aim in an urban network could be maximizing the arrival rate, i.e. the number of vehicles that complete their trips and reach their destinations, or similarly minimizing the total travel delays. Over the (discrete) simulation interval $[0, K T_s]$, the total delay criterion J_{TD} (veh·s) is formulated as

$$J_{TD} = T_s \cdot \sum_{i \in \mathcal{R}} \sum_{k=0}^{K-1} (n_i(k)). \quad (5.12)$$

Note that in some cases reducing the accumulations of certain regions is more important and therefore, additional weights can be assigned to the accumulations of those regions in (5.12).

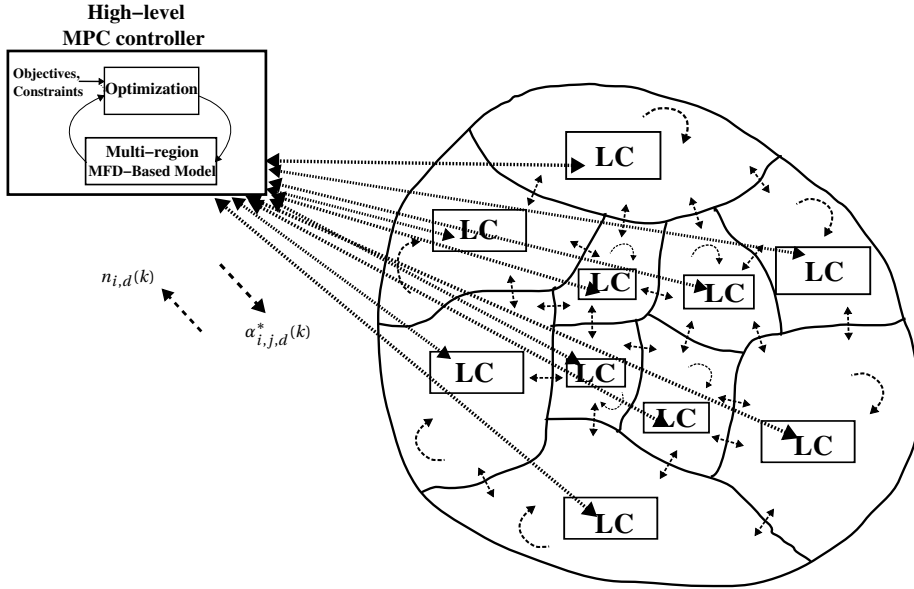


Figure 5.3: Two-level optimal dynamic route guidance (LC: local controller).

5.3.2. MODEL PREDICTIVE CONTROL FOR HIGH-LEVEL ROUTE GUIDANCE

5

Model Predictive Control (MPC) [160, 198] is an advanced control method originally developed for industrial processes and now for broader applications such as traffic networks. In the traffic control framework, the main idea is to use a prediction model of the network (e.g. the aggregate model obtained in Section 5.2) and an objective function assessing the desired performance of the urban traffic network, in order to find the optimal inputs through an optimization algorithm. In our case, the optimization variables are the optimal splitting rates for flows of vehicles heading towards multiple destinations. The overall optimization variables include splitting rates of all destination-dependent flows in all regions of the network. In order to formulate the problem of finding optimal splitting rates in the MPC framework, we define k_c and T_c as control time step and control sample time, respectively. Here we assume that the control sample time is an integer multiple of the simulation sample time, i.e. $T_c = M \cdot T_s$. The optimization algorithm assumes a prediction horizon N_p for the evolution of the network variables and minimizes the objective function over the horizon. The obtained optimal variables constitute a sequence of optimal splitting rates for the whole prediction horizon. In the MPC context, only the first sample of the obtained values is used and afterwards the prediction horizon is shifted one step forward. At the new control time step k_c , the prediction and optimization procedure over the shifted horizon are repeated using new observations from the network. Moreover, to reduce the number of optimization variables, usually a control horizon $N_c < N_p$ is introduced and from the control step $k_c + N_c - 1$ to the last step of the prediction horizon $k_c + N_p - 1$, the control inputs (splitting rates) are taken to be constant.

Furthermore, the optimal splitting rates are communicated to the lower level local

controllers as references to track. Basically, the local controllers try to achieve the optimal splitting rates by manipulating the timing plans of the signalized intersections placed at the borders of regions. Communication and coordination between the local controllers placed at different borders of a region is crucial. Note that control is carried out only at the borders and thus the MFDs of regions are expected to be unchanged. Nevertheless, we can take advantage of the approach proposed in Chapter 4 in order to extend our control to inside regions and hence to distribute the congestion in a more uniform way. This can be done by defining several timing plans for intersections inside each region and hence having a set of MFDs obtained for that region. By proper switching between the pre-defined timing plans, we will be able to balance the congestion inside regions in addition to the determination of splitting rates for flows traveling to neighboring regions.

In order to formulate the MPC optimization problem, we define $J_{\text{TD}}^{\text{MPC}}$ as

$$J_{\text{TD}}^{\text{MPC}} = T_s \cdot \sum_{i \in \mathcal{R}} \sum_{k=M \cdot k_c}^{M \cdot (k_c + N_p) - 1} (n_i(k)). \quad (5.13)$$

The overall optimization problem will be formulated as follows:

$$\min_{\tilde{\alpha}_{i,j,d}(k_c), \tilde{n}_{i,d}(k_c)} J_{\text{TD}}^{\text{MPC}}, \quad (5.14)$$

subject to:

model equations (5.10), (5.11),

$$0 \leq \alpha_{i,j,d}(k_c) \leq 1, \quad \forall i \in \mathcal{R}, \forall j \in \mathcal{J}_i, \forall d \in \mathcal{D}, \quad (5.15)$$

$$\sum_{j \in \mathcal{J}_i} \alpha_{i,j,d}(k_c) = 1, \quad \forall i \in \mathcal{R}, \forall d \in \mathcal{D}, \quad (5.16)$$

$$\alpha_{i,j,d}(k) = \alpha_{i,j,d}^c(k_c), \quad \text{if } k \in \{M \cdot k_c, \dots, M \cdot (k_c + 1) - 1\}, \\ \forall i \in \mathcal{R}, \forall j \in \mathcal{J}_i, \forall d \in \mathcal{D}, \quad (5.17)$$

The optimization variables defined over the prediction horizon N_p are $\tilde{\alpha}_{i,j,d}(k_c) = [\alpha_{i,j,d}^c(k_c), \dots, \alpha_{i,j,d}^c(k_c + N_p - 1)]^T$ and $\tilde{n}_{i,d}(k_c) = [n_{i,d}(M \cdot k_c), \dots, n_{i,d}(M \cdot (k_c + N_p) - 1)]^T$, where $\alpha_{i,j,d}^c(k_c + l)$ for $l = 0, \dots, N_p - 1$, is the splitting rate corresponding to the fraction of the flow towards destination d that travels from region i to region j at control time step $k_c + l$. The sum of the splitting rates for the flows heading towards a certain destination should be equal to 1, as in (5.16).

The nonlinear optimization problem (5.14)–(5.17) can be solved using either global optimization algorithms or multi-start local optimization methods.

In the next section, the proposed optimal route guidance approach is implemented on an urban network case study.

5.4. CASE STUDY

This section describes modeling and optimal routing for an urban network case study. The aim is to show the performance of the proposed high-level modeling and optimal dynamic route guidance approach. In the first part, the set-up of the case study is described and in the second part, the obtained results together with the discussions are presented.

5.4.1. SET-UP

In order to implement the model presented in Section 5.2, we consider a grid network. The network is a 4×4 regional network, with regions of 5×5 km, as shown in Fig. 5.4. The regions are homogeneous, with a critical accumulation $n_{cr}=3200$ (veh) and 40 km of road length in the region. The free flow speed is assumed to be $V_{free}=80$ km/h. The capacity of the borders is set to 2000 veh/h/lane. For each region, an MFD is assumed and it is approximated with an exponential function as follows:

$$P_i = n_i \cdot V_{free,i} \cdot \exp\left(-\frac{1}{2}\left(\frac{n_i}{n_{cr}}\right)^2\right). \quad (5.18)$$

For each region i , the neighboring regions are defined as the ones that are in the same column or row as region i . For instance, for region 7 the set of neighboring regions is $\{3, 6, 8, 11\}$. As illustrated in Fig. 5.4, the origins are indicated by blue squares and the destination are marked as red circles. The demand (veh/h) for each origin-destination pair is selected as in Table 5.1.

Table 5.1: Origin-destination demands (veh/h)

Destinations Origins	Region 2	Region 8	Region 9	Region 14
Region 1	1000	1800	1750	3000
Region 4	1900	1400	1000	1400
Region 11	1700	1200	1300	1300
Region 16	2000	1000	1000	1800

The constant demand values of Table 5.1 are multiplied by time-varying factors in order to consider the uncertainty in the demand profiles and also to make the simulation of the network under control more realistic. At each time step, the demand values in Table 5.1 are multiplied by a uniformly distributed random number with mean value 1 and variance 0.1.

The optimal route guidance is carried out first by a static shortest-path algorithm and next by the model predictive scheme described in Section 5.3. The shortest-path algorithm determines the shortest routes (in time) based on the average speeds of all regions. First the costs of traveling between neighboring regions are obtained based on the current state of the network. Next the shortest path (in time) between each pair of regions in the network is calculated using the Floyd-Warshall algorithm [199].

For the MPC scheme, we choose the prediction model similar to the simulation model but without the noise in the demands. Moreover, we select the prediction and control horizons $N_p = 6$ and $N_c = 2$, respectively. Using simulations for different horizons, these values have proved to be sufficient for our case (in general, the prediction interval should be long enough to include important dynamics of the system under control) while the computation time of the optimization algorithm is still acceptable. It has been observed that with increasing prediction and/or control horizons, there are small improvements in the results while the computational complexity will grow exponentially.

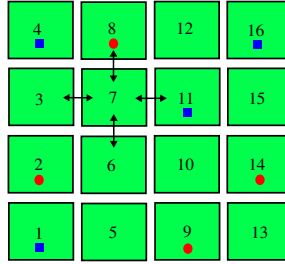


Figure 5.4: Layout of the 4x4 urban network.

The simulation sample time is chosen as $T_s = 10$ s. The control sample time (for both static and dynamic schemes) is selected to be $T_c = 60$ s.

Furthermore, in order to take into account the uncertainty in modeling, the updated accumulations in the network model (simulation model) are corrupted with additive white Gaussian noises that have zero mean value and 2% of the measured accumulations as variance. Note that the prediction model in the MPC framework is taken to be free of noise, but it is supplied with actual accumulations as initial values for the prediction model.

The nonlinear optimization problem inside the MPC scheme is solved using the *snopt* algorithm integrated in the *Tomlab* toolbox of MATLAB. This optimization algorithm tries to find the (global) optimal value for the objective function (5.14) subject to the model equations and the linear constraints on the splitting rates. In order to escape from the local optima, we use a multi-start technique with 10 random points.

5.4.2. RESULTS AND DISCUSSION

Results for simulation of the urban network for a period of 3000 s are depicted in Fig. 5.5. In the first column, the time evolution of the fixed-routing case is presented. By fixed-routing we mean that the shortest routes in time are determined a priori using the shortest-path algorithm and are fixed during the simulation period. As time progresses, congestion builds up in the regions that are located in the center. This is due to the fact that the center regions are the intermediate regions for many routes between the origin and destination regions, and if no routing policy is considered, the accumulation would grow especially in these regions till it reaches the critical point. From then, the inflow to these regions is constrained and instead the congestion forms upstream of these regions. The total delay in the network for the whole simulation interval is $3315 \cdot 10^4 \pm 4.32\%$ (veh-s) (for 5 times running with the same initial conditions).

In column (b) of Fig. 5.5, the results of using the shortest-path algorithm are presented (every 6 simulation time steps, the shortest-path algorithm recalculates the shortest routes). As can be observed, the congestion level is lower than for the fixed-routing case. However, the route advices in this approach are determined based on the current situation of network. Therefore, this approach is unable to take into account the future impacts of the trip demands on the accumulation and hence it cannot prevent the congestion from occurring in the intermediate regions. Nevertheless, by rerouting the traffic, the level of congestion reduces a bit (as can be observed from columns (a) and (b) of Fig. 5.5) as a result of preventing the traffic from entering the congested regions. The

overall delay in the network for the whole simulation period is $2431 \cdot 10^4 \pm 8.45\%$ (veh-s) (again for 5 times running with the same initial conditions).

The best performance is achieved by the MPC scheme as shown in the third column of Fig. 5.5. The congestion level is significantly reduced in the destination and intermediate regions. The total delay in the network for the whole simulation interval is $1820 \cdot 10^4 \pm 9.87\%$ (veh-s). The achieved number is again the average over 5 simulations of the whole system. The total delay obtained using MPC is much lower than the two other approaches meaning that the arrival rates are high in the proposed framework.

Note that another major advantage of using the proposed high-level routing scheme is that the computation time is reasonable compared to other routing methods in the literature which are based on detailed modeling [36, 83].

5.5. CONCLUDING REMARKS

We have presented a multi-level scheme for optimal dynamic route guidance in urban traffic networks using the macroscopic fundamental diagram (MFD). On the high level, the dynamics of the urban regions and the flows of vehicles traveling towards multiple destinations in the network are described using an aggregate traffic flow model based on the MFD. The presented model have enabled us to efficiently model and control urban networks that can be partitioned into a number of homogeneous regions. Next, we have formulated an optimization problem solved in the receding horizon fashion in order to find the optimal splitting rates towards neighboring regions. Taking into account that the modeling approach does not depend on the shape of the regions, we have developed a high-level model for a grid network and have implemented the MPC route guidance scheme to reduce the total time spent in the network. The obtained results have shown significant performance of the proposed predictive scheme over an existing shortest-path method.

Note that the optimal splitting rates are realized using local controllers installed at the borders of regions and therefore the MFDs will not be altered much. However, as an extension to the current work, we can use the idea of having multiple timing plans inside regions (and consequently defining multiple MFDs for each region), as presented in Chapter 4, to control the traffic inside the urban regions. Furthermore, since the routing problem is solved on the high level, the computational complexity of the proposed scheme is expected to be low compared to other existing dynamic approaches that are based on detailed modeling. This should be investigated using extensive numerical experiments based on layouts of real networks and by comparing with other dynamic methods. Also, in order to reduce the computation time even more, we can approximate and reformulate the model in order to achieve mixed integer linear optimization problems (as was done for the MFD-based model in Chapter 4).

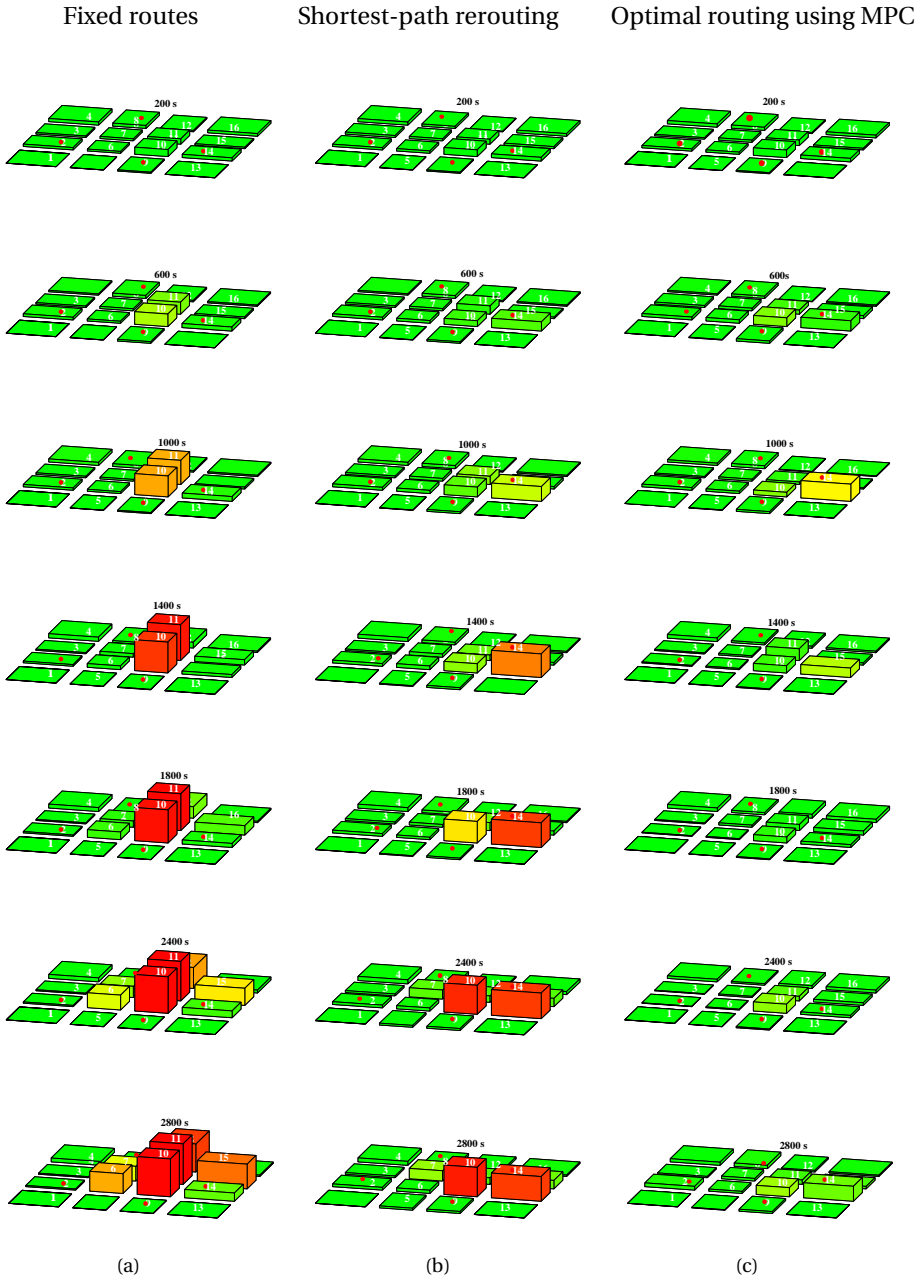


Figure 5.5: Results for a 4×4 network, (a) Uncontrolled (fixed routes), (b) Shortest-path algorithm, (c) Optimal dynamic routing using MPC

PART II:
ROBUST STABILIZATION OF
SWITCHED SYSTEMS

6

BACKGROUND ON ANALYSIS AND CONTROL OF SWITCHED SYSTEMS

This chapter gives an overview of switched systems that will help with better understanding our contributions in the next chapters. In the first section, we present the general definition of switched systems, while in the next sections, we briefly discuss stability analysis and robust control of switched linear and switched nonlinear systems.

6.1. DEFINITION AND CLASSIFICATION OF SWITCHED SYSTEMS

SWITCHED systems are a class of hybrid systems characterized by a set of linear and/or nonlinear subsystems and a switching signal selecting the active subsystems [149]. Switched systems and switched multi-controller systems arise in cases in which several dynamical models are required to represent a system due to e.g. uncertainty in parameters, changing environmental factors, or specific applications that utilize switching between a set of controllers in order to achieve a higher performance [40, 74, 112, 149, 150]. These systems have numerous applications in the control of mechanical systems, process control, automotive industry, power systems, aircraft and traffic control, and many other fields. Additionally, control using switching between multiple controllers has emerged in recent years, especially for systems that cannot be stabilized by any continuous static state feedback control law [26].

Mathematically speaking, these systems are often characterized by a set of differential or difference equations. One way to categorize switched systems is based on the dynamics of their subsystems, e.g. continuous-time or discrete-time, linear or nonlinear. A continuous-time switched nonlinear system can be formulated as

$$\dot{x}(t) = f_{\sigma}(x(t)), \quad (6.1)$$

with $x = (x_1, \dots, x_n)^T$ the state vector, $\{f_i : i \in \mathcal{N}\}$ a set of vector functions from \mathbb{R}^n to \mathbb{R}^n , \mathcal{N} a finite index set and $\sigma : \mathbb{R}^+ \rightarrow \mathcal{N}$ a piecewise constant function called the switching signal that orchestrates switching between the subsystems and determines the active subsystem for each time instant. By piecewise constant we mean that the switching signal has a finite number of changes on any finite time interval.

Moreover, the value of σ may be determined based on time or on states or a combination of both, or may be generated by a more complex procedure (e.g. by involving memory). In case all the subsystems are linear, we obtain a continuous-time switched linear system formulated as

$$\dot{x}(t) = A_{\sigma}x(t). \quad (6.2)$$

Similarly, we can formulate a discrete-time switched system as a set of difference equations as follows:

$$x(k+1) = f_{\sigma}(x(k)), \quad (6.3)$$

where k denotes the discrete time step counters. For the discrete-time switched linear counterpart we have

$$x(k+1) = A_{\sigma}x(k). \quad (6.4)$$

Furthermore, the switching between subsystems may occur autonomously or in a controlled manner (or a combination of both, as discussed later in Chapter 9). In the controlled case, state- and/or time-dependent switching rules can be designed in order to e.g. stabilize an unstable switched system. As an example of autonomous switching behavior, we draw the attention to the piecewise affine systems (as introduced in Chapter 4, Section 4.4). A piecewise affine system is in fact a switched system with affine subsystems and autonomous state-based switching behavior (when the state of the system crosses the boundaries of polyhedral regions).

Research on switched systems has been revolving around stability analysis [73, 74, 112, 112, 152], controllability and observability [14, 218, 229], and stabilizing controller design with guaranteed performance criteria [6, 50, 55, 74, 208, 240, 245]. From now on, through the following sections and the next 3 chapters, we mainly focus on the stability analysis problem and the design of robust stabilizing controllers for continuous-time switched systems.

6.2. STABILITY ANALYSIS FOR CONTINUOUS-TIME SWITCHED LINEAR SYSTEMS

In this section, we focus on stability of continuous-time switched linear systems, the subsystems of which are continuous-time linear time-invariant systems. Our main concern here is to provide the conditions that can guarantee the asymptotic stability of the switched linear system. Such switched systems may exhibit some surprising behavior. For instance, even when all subsystems are exponentially stable, the states of the switched system may grow unboundedly for certain switching signals [149]. Another interesting fact is that by proper switching between unstable subsystems, one may be able to make the switched system exponentially stable [149, 152]. Therefore, the stability of switched systems depends both on the dynamics of each subsystem and on the switching behavior. The stability of switched systems can be investigated for two main cases. One is the stability analysis of switched systems under given switching signals (e.g. for arbitrary switching or for time-based switching patterns with restricted dwell time) and the other one is the synthesis of stabilizing switching signals for a switched system composed of several dynamical subsystems.

We will briefly review some results on the stability and stabilizability of switched systems from these two perspectives. In particular, we focus on stability analysis for switched linear systems under arbitrary switching in Section 6.2.1. Next, we introduce the concepts of dwell time and average dwell time [110, 150] and we review stability under time-based switching with average dwell time. For the synthesis of stabilizing switching signals for switched linear systems, we present the well-known multiple Lyapunov functions approach using piecewise quadratic functions.

6.2.1. STABILITY UNDER ARBITRARY SWITCHING

For stability analysis, we first consider whether the switched system is asymptotically stable when there is no restriction on the switching signal. This problem is often referred to as stability analysis under arbitrary switching. For this case, it is necessary that all subsystems are asymptotically stable. However, even when all subsystems of a switched system are exponentially stable, it is possible to have unbounded trajectories from any initial state for such a switched system. Therefore, in general, the asymptotic stability of all subsystems is not sufficient to ensure stability for the switched system under arbitrary switching. Nevertheless, for particular cases (e.g. if the A_i matrices of the switched linear system are pairwise commutative [176]) we can conclude asymptotic stability of the switched system from the stability of its subsystems.

On the other hand, if there exists a common Lyapunov function (CLF) for all subsystems, then the stability of the switched system is guaranteed under arbitrary switching. The existence of a common quadratic Lyapunov function for all subsystems ensures the

quadratic stability of the switched linear system. Quadratic stability is a particular case of exponential stability [152]. The conditions for the existence of a common quadratic Lyapunov function for switched system (6.2) can be formulated as linear matrix inequalities of the following form:

$$PA_i + A_i^T P < 0, \quad \forall i \in \mathcal{N}, \quad (6.5)$$

with $P \in \mathbb{R}^{n \times n}$ a positive definite symmetric matrix. Note that existence of a common quadratic Lyapunov function is only sufficient for the stability of switched systems with arbitrary switching (in contrast to the non-switched case, where the existence of quadratic Lyapunov functions is necessary and sufficient for the asymptotic stability of the linear systems).

So far we have considered the existence of a CLF in order to conclude asymptotic stability of the switched system. Now the question is whether the converse holds, i.e. whether asymptotically stable switched systems with arbitrary switching admit a CLF or not. The following theorem presents a converse Lyapunov theorem.

Theorem 6.1. [46] *If the switched system (6.2) is globally uniformly asymptotically stable and moreover, if its subsystems are uniformly exponentially stable, there exists a common Lyapunov function for this system.*

The converse Lyapunov theorem was extended in [163] to switched nonlinear systems that are globally uniformly asymptotically stable. References [46, 163] suggest that the common Lyapunov function does not require to be quadratic. Therefore, using non-quadratic Lyapunov functions for stability analysis has been addressed in the literature [118, 243]. An example of a non-quadratic common Lyapunov function is presented in the following theorem.

Theorem 6.2. [170] *The switched linear system (6.2) is exponentially stable under arbitrary switching if and only if there exists a strictly convex common Lyapunov function of a quasi-quadratic form formulated as follows:*

$$V(x) = x^T P(x)x, \quad (6.6)$$

with $P^T(x) = P(x) = P(ax)$, $\forall x \neq 0$, $a \in \mathbb{R}$, $a \neq 0$.

Finally, finding conditions to assure stability under all possible switching signals is also important. For example, multi-controller schemes are often used to realize different performance requirements. When one designs multiple controllers for a system, a desired feature is that the switching between controllers does not result in instability. It is possible to guarantee this property for multiple-controller design in some specific cases [113].

6.2.2. STABILITY ANALYSIS UNDER DWELL TIME CONSTRAINT

Switched systems might not be able to preserve stability under arbitrary switching, but may be stable under restricted switching patterns. Basically, restricted switching may emerge from the physical constraints on the system. Furthermore, there might be the case that one has some information about possible switching patterns in a switched system, e.g. for a piecewise affine system (as a particular case of switched systems) partitioning of the state space and the resulting switching rules (autonomous in this case) are

pre-determined. As another example of restricted switching, it might be desired to have a certain limit on the time interval between two consecutive switching time instants. The reason might be related to the fact that the state trajectories have to stay for some time interval in a certain set before traveling to another sets. With this a priori information about the switching signal and the restrictions, we may be able to obtain stronger stability results for a given switched system rather than in the arbitrary switching case where we in fact, consider the worst case scenarios [150].

This section will present stability analysis of the switched systems under the restricted switching signals. Having this problem solved, we will be able to find out appropriate restrictions that must be imposed on the switching signals in order to ensure the stability of switched systems. The restrictions on switching signals may be in the time domain (e.g. dwell time and average dwell time between switching signals) or in the state space (e.g. abstractions from partitions of the state space).

In case of stable subsystems, fast enough switching may lead to instability. This might be explained by failing to absorb the energy increase caused by the switching [51]. On the other hand, when there is an unstable subsystem, if the system stays too long or switches too frequently to this subsystem, the stability may be destroyed. Therefore, if the system dynamics are governed by the stable subsystems long enough and it switches less frequently, then the system may be able to attenuate the energy increase resulted from switching or from staying in unstable modes and preserve the stability. This idea is mathematically formulated in the concepts of dwell time and average dwell time switching proposed in [110, 173].

Definition 6.1. A positive constant T_D is called the dwell time of a switching signal if the time interval between any two consecutive switchings is not smaller than T_D .

It can be proved that it is always possible to preserve stability when all subsystems are stable and the switching is slow enough, meaning that T_D is sufficiently large [173]. On the other hand, if occasionally the time interval between two successive switching becomes smaller than the dwell time T_D , provided this does not occur too frequently, overall stability may be preserved. This idea is captured by the concept of *average dwell time* in [110].

Definition 6.2. A positive constant T_{AD} is called the average dwell time for a switching signal σ if

$$N_\sigma(t_0, t) \leq N_0 + \frac{t - t_0}{T_{AD}} \quad (6.7)$$

holds for all $t \geq t_0$ and a constant parameter $N_0 \geq 0$. The value $N_\sigma(t_0, t)$ denotes the number of switchings that occur over the interval (t_0, t) .

It can be inferred from (6.7) that on average the dwell time between any two consecutive switching instants is not smaller than T_{AD} . It is proved in [110] that if all subsystems are exponentially stable, then the switched system is exponentially stable provided that the average dwell time is sufficiently large. Moreover, it can be shown that using the average dwell time notion, we will be able to characterize a larger class of stable switching signals than by using the fixed dwell time concept as in Definition 6.1. Interested readers may refer to [33, 35, 53, 112, 130, 242] for further details and recent applications of the concept of average dwell time for stability and stabilization of switched systems.

6.2.3. ROBUST STABILIZATION OF SWITCHED LINEAR SYSTEMS

In the previous two sections, we have discussed stability properties of switched systems under given switching signals, which may be restricted or arbitrary. The problem studied was under what conditions on the dynamics of the subsystems and/or on the switching signals the switched system is stable. Another interesting problem for switched systems is the synthesis of stabilizing switching signals for a given set of dynamical subsystems, called the switching stabilization problem.

The stability analysis and design of stabilizing switching laws have been usually performed in the framework of multiple Lyapunov functions (MLF). The main idea is that multiple Lyapunov-like functions each corresponding to a single subsystem or a certain region in the state space, are concatenated to make a global Lyapunov function. The MLF might not monotonically decrease along the state trajectories and may have discontinuities and therefore, be piecewise differentiable. However, often the only requirement is that the MLF must have nonpositive Lie-derivatives for particular subsystems in particular regions of the state space, instead of having globally negative derivative. There are several results regarding the MLF concept in the literature [56, 73, 208]. The MLF approach in [51] corresponds to the case in which the Lyapunov-like function is decreasing whenever the corresponding subsystem becomes active and its value does not increase at each switching instant. However, one may be able to obtain less conservative results. For instance, the switching signals may be constrained such that at every time when the system switches away from a subsystem, the value of the corresponding Lyapunov function must be smaller than its value at the previous switching time instant. Hence, the switched system would be asymptotically stable [23]. In other words, for each subsystem the values of the corresponding Lyapunov-like function at switching time instants in which the subsystems is inactivated, construct a monotonically decreasing sequence. Moreover, as a different approach, the Lyapunov-like function may increase its value during a time interval, only if the increment is bounded by a certain type of continuous-time functions [119].

In the switching stabilization literature, most of the papers focus on the quadratic stabilization. A system is quadratically stable if there exists a quadratic Lyapunov function $V(x) = x^T P x$ with a quadratic bound on the derivative of the Lyapunov function with respect to time of the form $\dot{V}(x) \leq -\epsilon \|x\|^2$ for some $\epsilon > 0$. A necessary and sufficient condition for a switched system composed of two linear subsystems to be quadratically stabilizable is the existence of a stable convex combination of the two A_i matrices [233]. A generalization to more than two linear subsystems is proposed in [192] by using a min-projection strategy, as presented in the following theorem.

Theorem 6.3. [192] *If there exist a positive definite matrix $P > 0$ and constants $\alpha_i \in [0, 1]$, $\sum_{i \in \mathcal{N}} \alpha_i = 1$ such that $\sum_{i \in \mathcal{N}} \alpha_i A_i$ is stable, i.e.:*

$$\sum_{i \in \mathcal{N}} \alpha_i (A_i^T P + P A_i) < 0 \quad (6.8)$$

then the min projection scheme

$$\sigma(t) = \arg \min_{i \in \mathcal{N}} x(t)^T P A_i x(t) \quad (6.9)$$

makes the switched system (6.2) asymptotically stable.

A necessary and sufficient condition for the quadratic stabilizability of switched linear systems is presented in the following theorem.

Theorem 6.4. [212] *The switched system (6.2) is quadratically stabilizable if and only if there exists a positive definite matrix P such that the set of matrices $\{A_i P + P A_i^T\}$ is strictly complete, i.e. for any $x \in \mathbb{R}^n$, $x \neq 0$, there exists $i \in \mathcal{N}$ such that $x^T(A_i P + P A_i^T)x < 0$. Consequently, a stabilizing switching signal can be selected as*

$$\sigma(t) = \arg \min_{i \in \mathcal{N}} x^T(t)(A_i P + P A_i^T)x(t). \quad (6.10)$$

Other examples of stabilizing approaches in the literature are the probabilistic algorithm proposed in [120] using a piecewise quadratic Lyapunov function, the exponentially stabilizing switching laws designed based on solving extended LQR optimal problems proposed in [37], the max-switching strategy of [191], and the min-switching scheme using composite quadratic functions presented in [243].

Furthermore, using multiple quadratic Lyapunov functions and the so-called Lyapunov-Metzler inequalities, a min-switching stabilizing law is proposed in [73]. A class of Metzler matrices that is used for the design of the switching rule is denoted by \mathcal{M} and it consists of all $M \in \mathbb{R}^{N \times N}$ matrices with elements μ_{ij} that have the following properties:

$$\mu_{ij} \geq 0 \quad \forall i \neq j, \quad \sum_{i=1}^N \mu_{ij} = 0 \quad \forall j. \quad (6.11)$$

The following theorem states sufficient conditions for the design of a stabilizing switching law for (6.2) with N subsystems.

Theorem 6.5. [73] *Assume there exist positive definite matrices P_i , $i = 1, \dots, N$, and a Metzler matrix M that satisfy the Lyapunov-Metzler inequalities*

$$A_i^T P_i + P_i A_i + \sum_{j=1}^N \mu_{ji} P_j < 0, \quad i = 1, \dots, N, \quad (6.12)$$

then the switching law

$$\sigma(t) = \arg \min_{i=1, \dots, N} x^T(t) P_i x(t) \quad (6.13)$$

makes the system (6.2) globally asymptotically stable.

The Lyapunov-Metzler conditions provide stability even in the presence of possible sliding modes [73]. The main idea behind the Lyapunov-Metzler conditions is to guarantee the negativity of the Lyapunov function associated to the active subsystem. Moreover, each subsystem is activated whenever the value of its associated Lyapunov function is the minimum among all Lyapunov functions. Therefore, the overall decrease of the global Lyapunov function is ensured using conditions (6.12).

Since the inequalities (6.12) are nonlinear and involve multiplication of matrix variables, more relaxed conditions based on (6.12) have been proposed in the literature to obtain more computationally efficient feasibility checking problems [33, 50, 74, 76].

Moreover, in order to avoid chattering, modified Lyapunov-Metzler conditions have been proposed in [54] and combined with the average dwell time switching as in [6, 53].

Besides the switching stabilization literature as described above, feedback stabilization of switched systems and piecewise affine systems with state or output feedback (continuous-variable) control laws has also been a point of interest for researchers [31, 38, 56, 99, 101, 204]. For piecewise affine system where autonomous switching occurs at boundaries between partitions of the state space, feedback controllers have been designed in order to stabilize the PWA system [99, 204]. For simultaneous design of stabilizing switching laws and state or output feedback controllers, we refer to [6, 49, 50, 53, 54].

In addition to the asymptotic stabilization, other performance criteria have also been taken into account in the synthesis of control schemes for switched systems. Among them is the minimization of the L_2 -gain [111, 225, 245], which will be extensively used in the next chapters. We consider the more general switched system formulated as follows:

$$\dot{x}(t) = A_\sigma x(t) + B_\sigma u(t) + H_\sigma \omega(t) \quad (6.14)$$

$$y(t) = C_\sigma x(t) + D_\sigma u(t) + G_\sigma \omega(t), \quad (6.15)$$

with y the output, u the state feedback control input, ω the disturbance input that is assumed to have a bounded L_2 norm, defined as follows:

$$\|\omega\|_{L_2[0,T]}^2 = \int_0^T \|\omega(t)\|^2 dt < \infty, \quad \forall T \geq 0. \quad (6.16)$$

Now system (6.14)–(6.15) has an L_2 -gain bounded above by $\gamma > 0$ under some switching law σ if

$$\|y\|_{L_2[0,T]} \leq \gamma \|\omega\|_{L_2[0,T]} \quad (6.17)$$

for all nonzero $\omega \in L_2[0, T]$ ($0 \leq T < \infty$) and for initial condition $x(0) = 0$. It follows that:

$$\|y\|_{L_2[0,T]} \leq \gamma \|\omega\|_{L_2[0,T]} \Rightarrow \int_0^T \left(\|y(t)\|^2 - \gamma^2 \|\omega(t)\|^2 \right) dt \leq 0 \quad (6.18)$$

for any $T \geq 0$ when $x(0) = 0$. Taking this definition into account, stabilizing control schemes can be designed such that the upper bound on the L_2 -gain of the switched system satisfies a desired level or is even minimized. The following theorem presents a design procedure for a switching law that asymptotically stabilizes the switched system in the absence of disturbances and moreover, it guarantees a desired upper bound for the L_2 -gain of the system exposed to disturbances that have bounded L_2 norms.

Theorem 6.6. [49] Assume there exist positive definite matrices P_i , a Metzler matrix M and a positive scalar γ such that the inequalities

$$\begin{bmatrix} P_i A_i + A_i^T P_i + \sum_{j=1}^N \mu_{ji} P_j & \star & \star \\ H_i^T P_i & -\gamma I & \star \\ C_i & G_i & -I \end{bmatrix} < 0, \quad \forall i \in \{1, \dots, N\} \quad (6.19)$$

hold. Then the switching law (6.13) makes the the switched system (6.14)–(6.15) with $u \equiv 0$ globally asymptotically stable and moreover, guarantees the upper bound γ for the L_2 -gain of the system from the input ω to the output y .

Furthermore, an optimization problem can be formulated with minimizing γ as the objective function and the inequalities (6.19) as constraints [50, 74].

Other performance criteria can also be integrated into the control design procedure. For instance, we refer to [74, 76] for switching H_2 control for switched linear systems.

As mentioned before, state or output feedback controllers can be designed together with the switching laws. More specifically, a switching rule can be designed jointly with a set of dynamic state or output feedback controllers to assure global asymptotic stability of the closed-loop switched system and also a desired upper bound on the L_2 gain from the disturbance input to the controlled output [54, 74, 124, 245]. For switched system (6.14)–(6.15), a joint design of state feedback controllers $u = K_i x$ and a switching rule can be realized by simply replacing A_i, E_i matrices in (6.19) by $(A_i + B_i K_i)$ and $(E_i + F_i K_i)$ (design of output feedback switching controllers is more complicated. We refer to [50, 209] for more insights.). Further, an optimization problem can be formulated to minimize the upper bound on the actual L_2 -gain of the closed-loop system. However, the resulting optimization problem involves bilinear matrix inequalities. In [49, 50] more computationally efficient conditions are proposed using linear matrix inequalities (LMI) techniques and by taking the diagonal elements of the Metzler matrix equal to each other. The last assumption is conservative in general and may lead to infeasibility of the reformulated optimization problem.

As a final remark, sliding mode can occur as a result of using switching control schemes. In some approaches, it has been proved that the possible sliding modes would be stable and would not affect their analysis and control schemes [73]. However, for the general case, possibility of having sliding modes must be studied by checking the direction of the vector fields along the switching surfaces, and the equivalent dynamics of sliding modes should be integrated in the model of the switched system, as an additional mode as a combination of current modes of the system [61]. Afterwards, we can start with stability analysis and control synthesis for the switched system.

6.3. STABILITY ANALYSIS AND STABILIZATION OF SWITCHED NONLINEAR SYSTEMS

In contrast to the switched linear systems case, stability analysis of switched nonlinear systems has not been widely addressed in the literature. Nevertheless, we can refer to the survey papers [78, 150, 235] for an overview on the analysis of switched nonlinear systems. As can be inferred from the literature, there is no concrete procedure for analysis and control of general switched nonlinear systems. Most of the works are related to particular classes of these systems. For instance, [244] presents quadratic stability for switched nonlinear systems with generalized homogeneous mappings. Stabilization of a class of cascade switched nonlinear systems with non-minimum phase modes is discussed in [236]. For switched nonlinear cascade systems, [179] proposes a stabilization approach based on multiple Lyapunov functions. The approach presented in [55] provides a systematic way to design stabilizing controllers for switched nonlinear systems that are input/output linearizable. The method is based on the existence of control Lya-

punov functions, which however are not easy to find for most cases of switched nonlinear systems. For switched systems with smooth nonlinear vector functions that are bounded in symmetric sector sets, [4, 93, 127] have presented stability analysis and robust H_∞ control design procedures. Moreover, a different approach based on equivalent polynomial representation and the sum of squares decomposition is proposed in [169].

The obtained results in almost all these papers have roots in two main stability notions, the multiple Lyapunov functions technique [23, 35, 119] and the dwell-time approach [110, 173]. Reference [23] proposes that stability can be achieved if the value of each Lyapunov function does not increase when the corresponding subsystem is active. In [119] this condition is relaxed by allowing the Lyapunov function to occasionally increase its value during the activating period of the corresponding subsystem. The recent work [245] extends the idea of [119] to a more general case that allows a bounded increase of the Lyapunov function over the multiple subsequent time instants in which the corresponding subsystem becomes active.

On the other hand, as mentioned before for the switched linear systems case, [110, 173] introduce the concepts of dwell time and average dwell time to conclude that slow switching can lead to stability under arbitrary switching patterns, provided that the subsystems are individually stable. The references [25, 221] have extended this concept to the mode-dependent dwell time.

Among the existing works on switched nonlinear systems, [35, 245] have presented more general results. In [35], a multiple Lyapunov functions approach is pursued for time-based stability analysis and state-based stabilization of switched nonlinear systems. For stability analysis under arbitrary switching, [35] proposes a generalization of the minimum dwell time concept. The results are determined based on the computation of an upper bound on the dwell time, using multiple Lyapunov functions. As in the switched linear case, stability of individual subsystems is a necessary condition.

For state-based stabilization of switched nonlinear systems with unstable subsystems, [35] has generalized the Lyapunov-Metzler inequalities (6.12). In the proposed approach in [35], a global Lyapunov function is constructed as the minimum over a number of functions each associated to one subsystem. The following theorem presents the main result.

Theorem 6.7. [35] *Assume there exist functions V_1, \dots, V_N , that are all differentiable, positive definite, radially unbounded, and zero at zero. Furthermore, assume there exists a Metzler matrix with elements μ_{ij} that satisfies the Lyapunov-Metzler inequalities:*

$$\frac{\partial V_i(x)}{\partial x} f_i(x) + \sum_{j=1}^N \mu_{ji} V_j(x) < 0, \quad \forall i \in \{1, \dots, N\} \quad (6.20)$$

for all $x \neq 0$. Then the switching rule

$$\sigma(t) = \arg \min_{i=1, \dots, N} V_i(x(t)) \quad (6.21)$$

makes the equilibrium point $x = 0$ of (6.1) globally asymptotically stable.

The stability conditions (6.20) involve determination of Lyapunov functions. Note that in the switched linear case (6.12), the main problem is the multiplication of unknown matrices. But in (6.20), the structure of the Lyapunov functions is unknown.

Therefore, checking the feasibility of (6.20) is a hard task in general and it may involve solving multi-parametric optimization problems and/or gridding techniques. Therefore, in this thesis, we aim at tackling the stability problem for switched nonlinear using a different method that is not as computationally complex as the conditions in (6.20). This method is extensively discussed in Chapter 9.

Moreover, the disturbance attenuation problem for switched systems has also attracted attention of researchers in recent years. L_2 -gain analysis and H_∞ control have been developed for switched linear systems based on the extension of algebraic Riccati inequalities [158]. For the particular cases of switched nonlinear systems, the H_∞ control problem is proposed based on the Hamilton-Jacobi inequalities for nonlinear systems [111, 225, 245].

In [245], L_2 -gain analysis and H_∞ control for switched nonlinear systems is addressed. The approach is basically a generalization of the well-known min-switching strategy [150]. For the general model

$$\dot{x}(t) = f_\sigma(x(t)) + g_\sigma(x(t))u(t) + p_\sigma(x(t))\omega(t), \quad (6.22)$$

$$y(t) = h_\sigma(x(t)), \quad (6.23)$$

with $f_i, g_i, p_i, i \in \{1, \dots, N\}$, nonlinear vector functions of states, [245] proposes the following results.

Theorem 6.8. [245] *Suppose there exist positive definite and smooth functions $V_i(x)$, with $V_i(0) = 0$, continuous functions $\mu_i(x) \leq 0$, smooth functions $\beta_{ij}(x)$ with $\beta_{ij}(0) = 0$ and $\beta_{ii}(x) = 0$, such that*

$$\begin{aligned} \frac{\partial V_i}{\partial x} f_i + \frac{1}{2} \frac{\partial V_i}{\partial x} \left(\frac{1}{\gamma^2} p_i p_i^T - g_i g_i^T \right) \frac{\partial^T V_i}{\partial x} + \frac{1}{2} h_i^T h_i + \\ \sum_{j=1}^m \mu_{ij}(x) (V_i(x) - V_j(x) + \beta_{ij}(x)) \leq 0, \quad \forall i \in \{1, \dots, N\}, \end{aligned} \quad (6.24)$$

$$\frac{\partial \beta_{ij}}{\partial x} \left(f_i(x) - g_i(x) g_i^T(x) \frac{\partial^T V_i}{\partial x}(x) \right) \leq 0, \quad \forall i, j \in \{1, \dots, N\}, \quad (6.25)$$

$$\beta_{ij}(x) + \beta_{jk}(x) \leq \min \{0, \beta_{ik}(x)\}, \quad \forall i, j, k \in \{1, \dots, N\}, \quad (6.26)$$

$$\frac{\partial \beta_{ij}}{\partial x} p_i = 0, \quad \forall i, j \in \{1, \dots, N\}. \quad (6.27)$$

Then, the feedback controllers

$$u_i(x) = -g_i^T(x) \frac{\partial^T V_i}{\partial x} \quad (6.28)$$

along with the switching law

$$\sigma(t) = i \quad \text{if } \sigma(t^-) = i \text{ and } x(t) \in \text{int}(\Omega_i), \quad (6.29)$$

$$\sigma(t) = j \quad \text{if } \sigma(t^-) = i \text{ and } x(t) \in \tilde{\Omega}_{ij}, \quad (6.30)$$

where Ω_i and $\tilde{\Omega}_{ij}$ are defined as

$$\Omega_i = \{x \mid V_i(x) - V_j(x) + \beta_{ij}(x) \leq 0, j = 1, 2, \dots, m\}, \quad (6.31)$$

$$\tilde{\Omega}_{ij} = \{x \mid V_i(x) - V_j(x) + \beta_{ij}(x) = 0\}, \quad j \neq i, \quad (6.32)$$

make the closed-loop system globally asymptotically stable when $\omega \equiv 0$. Also the overall L_2 -gain from ω to y on any finite time interval $[0, T]$ will be less than or equal to γ .

Compared to the conventional min-switching scheme as in Theorem 6.7, conditions of Theorem 6.8 and the consequently the switching law (6.29) allow the Lyapunov functions V_i to grow during the periods in which their corresponding subsystems are active.

6.4. SUMMARY

In this chapter we have presented the general definition of switched systems as a class of hybrid systems. Several categories of these systems based on the dynamics of the subsystems and the nature of the switching signals have been introduced. Moreover, from Section 6.2 to the end of this chapter, we have focused on the stability analysis and control synthesis for continuous-time switched linear systems and their nonlinear counterparts. First, we have discussed the concept of common Lyapunov function to conclude stability of switched linear systems under arbitrary switching patterns. Next, we have introduced the multiple Lyapunov functions approach and the notions of the minimum and the average dwell times in order to conclude that with arbitrary but slow switching between stable subsystems we can maintain global stability. Furthermore, we have utilized the multiple Lyapunov functions approach for the design of state-based stabilizing switching laws. Multiple methods from the literature have been briefly explained. Among them, we have presented the Lyapunov-Metzler approach [35, 73] in more detail as we will use the main concept of this method in the next chapters. Moreover, we have defined the L_2 -gain for switched systems and further, have discussed some robust H_∞ switching control schemes from the literature. Finally, we have presented stability analysis and control of switched nonlinear systems. As mentioned before, most of the literature deals with particular cases of these systems. We have briefly discussed some of them and further, we have presented the main results from [35, 245] for stabilization and H_∞ control of more general cases of switched nonlinear systems. Methods from these two papers along with the ones from [4, 110] will be more elaborately addressed in the next chapters.

7

STABILIZATION AND ROBUST H_∞ CONTROL FOR SWITCHED NONLINEAR SYSTEMS

This chapter presents robust switching control strategies for switched nonlinear systems with constraints on the control inputs. First, a model transformation is proposed such that the constraint on the continuous control inputs is relaxed. Next, the effect of disturbances is taken into account and the L_2 -gain analysis and the H_∞ control design problem for switched nonlinear systems are formulated. Furthermore, in the case study section, the robust switching control approach is utilized for urban network control using the MFD-based modeling framework discussed in Chapter 4.

7.1. INTRODUCTION

THE disturbance attenuation problem for switched systems has attracted attention of researchers in recent years [124, 147, 158]. L_2 -gain analysis and H_∞ control have been developed for switched linear systems based on the extension of algebraic Riccati inequalities [158]. For the particular cases of switched nonlinear systems, the H_∞ control problem has been proposed based on the Hamilton-Jacobi inequalities for nonlinear systems [111, 225, 245]. As an example, in [245] a nonlinear switched system is considered that is affine both in the control input and the disturbance input. The model contains a set of nonlinear subsystems each controlled with an unconstrained continuous control input. Further, a switching signal determines the active subsystem. However, the design procedure for the switching rule and the continuous feedback control is based on the fact that the control input is not constrained. In this chapter, we study the stabilization problem for switched nonlinear systems that are affine in the control and disturbance inputs. The aim is to extend the current results on stabilization and H_∞ control to the constrained control case.

The chapter is organized as follows. First, we present the problem formulation along with a model transformation in Section 7.2. Next, we discuss stability analysis and stabilization in the absence of disturbances Section 7.3. In Section 7.4 the effect of disturbances is taken into account and the L_2 -gain is defined for the switched nonlinear system. Further, we present H_∞ control via switching between modes. Next, we evaluate the performance of the H_∞ switching controller for an urban network case study. Finally, Section 7.6 contains the concluding remarks.

7.2. PROBLEM STATEMENT

Consider the following switched nonlinear system

$$\dot{x}(t) = f_{\sigma(t)}(x(t)) + g_{\sigma(t)}(x(t)) \cdot u(t) + p_{\sigma(t)}(x(t))\omega(t), \quad x(0) = x_0, \quad (7.1)$$

where $x \in \mathbb{R}^{n_x}$ is the state, $u \in \mathbb{R}^{n_u}$ is the control input, and $\omega \in \mathbb{R}^{n_\omega}$ is the disturbance input. The switching signal is denoted by $\sigma(t)$ and is assumed to be piecewise constant. The variable σ takes values from a pre-defined index set $\{1, \dots, N\}$, and for each value that $\sigma(t)$ assumes, the state space model (7.1) is governed by a different set of vector functions f_i , g_i , and p_i from the following sets:

$$f_{\sigma(t)} \in \{f_1, \dots, f_N\}, \quad (7.2)$$

$$g_{\sigma(t)} \in \{g_1, \dots, g_N\}, \quad (7.3)$$

$$p_{\sigma(t)} \in \{p_1, \dots, p_N\}. \quad (7.4)$$

The vector functions f_i , g_i , and p_i are continuous functions of states such that $f_i(0) = 0$, $g_i(0) = 0$, and $p_i(0) = 0$. Moreover, the control input u is constrained as follows:

$$u(t) \in [0, 1]^{n_u}. \quad (7.5)$$

This constraint on the control input is common in particular applications such as urban traffic control. As presented in Chapter 4, the perimeter control input u is in fact the ratio of green and red phases of a traffic signal.

The aim is to design a state feedback controller together with a switching rule in order to stabilize the system and to reduce the effects of disturbances. However, the constraint (7.5) on the control input limits the design freedom.

The problem at hand cannot be easily tackled based on the current literature about stabilization of switched nonlinear systems. For instance, the approach presented in [55] provides a systematic way for designing stabilizing control inputs for switched nonlinear systems that are input/output-linearizable. The method is based on the existence of the control Lyapunov functions, which however are not easy to find for the general system (7.1). Moreover, the design procedures proposed in [147, 179] do not handle any constraint on the control input. Further, having a relative degree¹ $r = 1$ is crucial for some approaches like the one of [55, 179]. Essentially, in the approaches of [55, 179], a state coordinate transformation is used that is not easy to obtain for the general model (7.1).

As mentioned before, we assume that the control input $u(t)$ is constrained in $[0, 1]$. For specific applications (e.g. the urban traffic control presented in Chapter 4), the sensitivity to small variations of the control input is relatively low and therefore, a finite number of values is enough for controlling the system. To be more precise, we assume that $u(t)$ is quantized and hence it can be rewritten as

$$u(t) = u_0 \cdot \left(\sum_{l=0}^r 2^l \cdot \delta_l(t) \right), \quad (7.6)$$

with $u_0 \in \mathbb{R}$ a constant and $\delta_l(t) \in \{0, 1\}^{n_u}$. The set of possible input values is then finite and its cardinality is 2^{r+1} , while the difference between two consecutive values is determined by u_0 . By quantizing the control input u as in (7.6) new modes are introduced and therefore we denote the total number of modes by N' with a new set of vector functions $\{f'_1, \dots, f'_{N'}\}$ that are determined using the functions f_i and g_i and the values that the quantized input u can take.

As a result, the system in (7.1) can be reformulated as

$$\dot{x}(t) = f'_{\sigma'(t)}(x(t)) + p_{\sigma'(t)}(x(t))\omega(t), \quad x(0) = x_0, \quad (7.7)$$

where $f'_{\sigma'(t)} \in \{f'_1, \dots, f'_{N'}\}$.

The current formulation helps to have a concise design procedure as we reflect the effects of the continuous control input u in the switching signal σ' and hence, we have to deal only with one type of control input (switching).

7.3. STABILIZATION IN THE ABSENCE OF DISTURBANCES

In this section, the stability problem is formulated for system (7.7) in the absence of disturbances. The resulting model is

$$\dot{x}(t) = f'_{\sigma'(t)}(x(t)), \quad x(0) = x_0. \quad (7.8)$$

¹The system (7.1) with $\omega \equiv 0$ has relative degree r at point x_0 if

$$\begin{aligned} L_g L_f^k h(x) &= 0, \text{ for all } x \text{ in a neighborhood of } x_0, \text{ and for } k = 1, \dots, r-2, \\ L_g L_f^{r-1} h(x_0) &\neq 0, \end{aligned}$$

where L denotes the Lie derivative [121].

It is assumed that the state vector $x(t)$ is available for feedback for all $t \geq 0$, and the aim is to determine a piecewise constant function $r(\cdot) : \mathbb{R}^{n_x} \rightarrow \{1, \dots, N'\}$, such that the switching law

$$\sigma'(t) = r(x(t)) \quad (7.9)$$

guarantees that the equilibrium $x = 0$ is globally asymptotically stable for (7.8). It should be noted that we do not assume that any of the vector fields in the set $\{f'_1, \dots, f'_{N'}\}$ is either locally or globally asymptotically stable.

The candidate Lyapunov function $\vartheta(\cdot)$ is constructed as follows:

$$\vartheta(x) := \min_{i=1, \dots, N'} V_i(x), \quad (7.10)$$

where $V_1, \dots, V_{N'}$ are differentiable, positive definite, and radially unbounded functions of x . However, this function might not be differentiable everywhere even if the functions V_i are all differentiable. To overcome this issue, the notion of Metzler matrices [16, 73] is used. A Metzler matrix is a matrix in which all the off-diagonal components are non-negative. For our goal, we limit the attention to a subclass of Metzler matrices denoted by \mathcal{M} and containing all matrices $M \in \mathbb{R}^{N' \times N'}$ with elements μ_{ij} , such that

$$\mu_{ij} \geq 0 \quad \forall i \neq j, \quad \sum_{i=1}^{N'} \mu_{ij} = 0, \quad \forall j. \quad (7.11)$$

The following theorem provides the design procedure for the stabilizing switching rule (recall from Theorem 6.7).

Theorem 7.1. [35] *Assume there exist functions $V_1, \dots, V_{N'}$, which are all differentiable, positive definite, radially unbounded, and zero at zero. Furthermore, assume there exists matrix $M \in \mathcal{M}$ with elements μ_{ij} that satisfies the Lyapunov-Metzler inequalities*

$$\frac{\partial V_i(x)}{\partial x} f'_i(x) + \sum_{j=1}^{N'} \mu_{ji} V_j(x) < 0, \quad i \in \{1, \dots, N'\} \quad (7.12)$$

for all $x \neq 0$. Then the switching rule (7.9) with

$$r(x(t)) = \arg \min_{i=1, \dots, N'} V_i(x(t)) \quad (7.13)$$

makes the equilibrium point $x = 0$ of (7.8) globally asymptotically stable.

Proof. For instructive reasons, we present the proof from [35]. The Lyapunov function (7.10) is piecewise differentiable, which means that it is not differentiable for all $x \in \mathbb{R}^{n_x}$. Therefore, we need to define the following derivative (see [35, 64, 102]):

$$\mathbf{D}(\vartheta(x(t))) = \limsup_{\Delta t \rightarrow 0^+} \frac{\vartheta(x(t + \Delta t)) - \vartheta(x(t))}{\Delta t}. \quad (7.14)$$

Assume that at an arbitrary $t \geq 0$, the state switching control is given by $\sigma(t) = r(x(t)) = i$ for some $i \in I(x(t)) = \{i : \vartheta(x) = V_i(x)\}$. Hence, from (7.14) and (7.8), we have (using Theorem 1 in [142])

$$\mathbf{D}(\vartheta(x(t))) = \min_{i \in I(x(t))} \frac{\partial V_i}{\partial x} f'_i \leq \frac{\partial V_i}{\partial x} f'_i. \quad (7.15)$$

Since (7.12) is valid for any $M \in \mathcal{M}$ and $V_j \geq V_i$ for all $j \in \{1, \dots, N'\} \setminus \{i\}$, using the fact that $i \in I(x(t))$ and by rewriting the Lyapunov-Metzler inequality (7.12) as

$$\frac{\partial V_i}{\partial x} f'_i < - \sum_{j=1}^{N'} \mu_{ji} V_j, \quad i \in \{1, \dots, N'\}, \quad \text{for all } x \neq 0, \quad (7.16)$$

one can obtain

$$\mathbf{D}(\vartheta(x(t))) \leq \frac{\partial V_i}{\partial x} f'_i < - \sum_{j=1}^{N'} \mu_{ji} V_j \leq - \left(\sum_{j=1}^{N'} \mu_{ji} \right) V_i = 0, \quad \text{for all } x \neq 0. \quad (7.17)$$

Thus, the switching law (7.13) makes the equilibrium point $x = 0$ of the switched nonlinear system (7.8) globally asymptotically stable. \square

Note that when all vector fields are globally asymptotically stable, the simplest choice for the Metzler matrix, $M = 0$, would be possible.

In order to design and implement the switching law (7.13), one would need to search for appropriate positive definite *functions* V_i and a Metzler matrix that satisfy the Lyapunov-Metzler inequalities (7.12) for all $x \neq 0$. Unfortunately, this is a very hard task in general. In case of quadratic Lyapunov functions sometime it is possible to recast the problem as a Bilinear Matrix Inequality (BMI) problem [222] and thus, take advantage of the existing solvers for BMIs. But the general case would involve multiplication of matrices and state variables and therefore, in order to check the feasibility of (7.12), multi-parametric optimization techniques can be employed. Nonetheless, one can use a simpler but less accurate approach to tackle the problem of finding the parameters of V_i along with the elements of the Metzler matrix M . By gridding the domain of the state x , one can formulate the Lyapunov-Metzler inequalities for each vertex of the grid. Depending on the characteristics of the system under study and the objectives, one can make grids with different levels of accuracy in a uniform or non-uniform way. Next, the remaining task is to find solutions for the parameters of V_i and the Metzler matrix in order to satisfy all Lyapunov-Metzler inequalities for all grid points. This is a nonlinear optimization problem in which the feasibility of all nonlinear inequality constraints has to be checked. Of course, there might exist multiple solutions for this problem, but any feasible solution would work for finding the stabilizing switching law.

The aforementioned feasibility problem includes determination of *all* elements of a Metzler matrix. In order to simplify the implementation procedure and speed up the computation of feasible solutions, we could limit the choice of the Metzler matrices. For a Metzler matrix $M \in \mathcal{M}$, assume that the diagonal elements μ_{ii} are all equal to $-\bar{\mu}$, with $\bar{\mu}$ a positive constant. Thus, the sum over the remaining elements of each column of the matrix is

$$\sum_{j=1, j \neq i}^{N'} \mu_{ji} = \bar{\mu} \quad (7.18)$$

for all $i = 1, \dots, N'$. Substitution of this matrix in the Lyapunov-Metzler equation (7.12) results in the following corollary [35, 49].

Corollary 7.1. *Suppose that there exist positive definite, differentiable, radially unbounded and zero at zero functions $V_1, \dots, V_{N'}$, and a positive constant $\bar{\mu}$, such that*

$$\frac{\partial V_i}{\partial x} f'_i + \bar{\mu}(V_j - V_i) < 0, \quad j \in \{1, \dots, N'\} \setminus \{i\}, \quad \forall x \neq 0 \tag{7.19}$$

for $i = 1, \dots, N'$. Then, the switching rule (7.13) makes the equilibrium point $x = 0$ of the system (7.8) globally asymptotically stable.

In order to check the validity of (7.19), one can multiply (7.19) by μ_{ji} and sum up for all $j = 1, \dots, N', j \neq i$ and next, multiply the result by $1/\bar{\mu}$ and finally, reach the Lyapunov-Metzler inequalities (7.12).

It should be noted that (7.19) is a more conservative condition than (7.12). However, it is more convenient to determine a feasible solution of (7.19). Instead of searching for a Metzler matrix with all unknown elements, we would simply have to find a positive constant $\bar{\mu}$. Thus, the overall feasibility problem consists in finding the parameters of the functions V_i and a positive value for $\bar{\mu}$. In order to solve this, we can first fix $\bar{\mu}$ and then check the feasibility of the inequalities using a combined gridding technique and a nonlinear optimization algorithm.

7.4. DISTURBANCE ATTENUATION VIA STATE-BASED SWITCHING

In this section, we present an approach to tackle the disturbance attenuation problem mentioned in Section 7.2. The model of the system under control is as follows:

$$\dot{x}(t) = f'_{\sigma'(t)}(x(t)) + p_{\sigma'(t)}(x(t))\omega(t), \quad x(0) = x_0, \tag{7.20}$$

$$y(t) = h_{\sigma'(t)}(x(t)), \tag{7.21}$$

with $y \in \mathbb{R}^{n_y}$ the output vector and $h_{i'}$, $i' \in \{1, \dots, N'\}$, continuous vector functions with $h_{i'}(0) = 0$. Moreover, we assume that the disturbance vector ω belongs to the space of square integrable functions, L_2 space. The disturbance ω belongs to the L_2 -space if

$$\|\omega\|_{L_2[0,T]} = \left(\int_0^T \omega^T(t)\omega(t)dt \right)^{1/2} < \infty, \quad \forall T \geq 0. \tag{7.22}$$

where $\|\cdot\|_{L_2[0,T]}$ denotes the L_2 -norm on $[0, T]$.

7.4.1. L_2 -GAIN

System (7.20) has an L_2 -gain bounded above by $\gamma > 0$ under some switching law σ' if $\|y\|_{L_2[0,T]} \leq \gamma \|\omega\|_{L_2[0,T]}$ for all nonzero $\omega \in L_2[0, T]$ ($0 \leq T < \infty$) and for initial condition $x(0) = 0$. It follows that

$$\begin{aligned} \|y\|_{L_2[0,T]} \leq \gamma \|\omega\|_{L_2[0,T]} &\iff \int_0^T \left(\|y(t)\|^2 - \gamma^2 \|\omega(t)\|^2 \right) dt \leq 0 \\ &\iff \int_0^T \left(\|h_{\sigma'(t)}(x(t))\|^2 - \gamma^2 \|\omega(t)\|^2 \right) dt \leq 0 \end{aligned} \tag{7.23}$$

for any $T > 0$ when $x(0) = 0$. The aim is to design a switching strategy σ' such that the L_2 -gain of system (7.20) is upper bounded by γ .

7.4.2. ROBUST H_∞ SWITCHING CONTROL DESIGN

The approach for H_∞ control of switched nonlinear systems proposed in [245] is not applicable for control of (7.1), as the input u is constrained in the box $[0, 1]^{n_u}$. Nevertheless, we transformed the model using quantization of the input variable and obtained the model in (7.7). For this model, the following problem is defined. Assume that a constant $\gamma > 0$ is given, the goal is to design a switching law σ' , such that the origin of the closed-loop system is globally asymptotically stable when $\omega(t) = 0, \forall t \geq 0$, and the overall L_2 -gain from ω to $y = h_{\sigma'(t)}(x)$ on any finite time interval $[0, T]$ is less than or equal to γ , i.e.

$$\int_0^T \left(\gamma^2 \|\omega(t)\|^2 - \|h_{\sigma'(t)}(x(t))\|^2 \right) dt \geq 0. \quad (7.24)$$

The following theorem provides the design procedure for the switching law (inspired by [245] and the linear case in [158]).

Theorem 7.2. *Consider the switched system (7.7). Assume that there exist positive definite, differentiable, and radially unbounded functions $V_i, i \in \{1, \dots, N'\}$, a Metzler matrix M with elements μ_{ij} and a scalar $\gamma > 0$, such that the following Lyapunov-Metzler inequalities are satisfied:*

$$\frac{\partial V_i}{\partial x} f'_i + \frac{1}{2\gamma^2} \frac{\partial V_i}{\partial x} p_i p_i^T \frac{\partial^T V_i}{\partial x} + \frac{1}{2} h_i^T h_i + \sum_{j=1}^{N'} \mu_{ji} V_j < 0 \quad (7.25)$$

for $i = 1, \dots, N'$. Then, the system (7.20) under the switching law

$$\sigma'(t) = r(x(t)) = \arg \min_{i=1, \dots, N'} V_i(x(t)) \quad (7.26)$$

has L_2 -gain bounded above by γ . Subsequently, in case $\omega \equiv 0$, the system is asymptotically stable.

Before proceeding with the proof, we emphasize again that the switching signal is assumed to be piecewise constant. In other words, one can define a switching sequence as $\{(t_k, r(x(t_k)))\}_{k=1}^\infty$ with $r(x(t_k)) \in \{1, \dots, N'\}$, while the switching rule remains unchanged in the interval $[t_k, t_{k+1})$.

Proof. Assume that the switching sequence in the interval $[0, T]$ is defined as

$$\left\{ (t_k, r(x(t_k))) \mid r(x(t_k)) \in \{1, \dots, N'\}, k = 1, 2, \dots, l \right\}, \quad (7.27)$$

with $t_1 = 0$ and $t_l \leq T$. Under the switching law (7.13) in each time interval $[t_k, t_{k+1})$ we have

$$\frac{\partial V_i}{\partial x} f'_i + \frac{1}{2\gamma^2} \frac{\partial V_i}{\partial x} p_i p_i^T \frac{\partial^T V_i}{\partial x} + \frac{1}{2} h_i^T h_i < - \sum_{j=1}^{N'} \mu_{ji} V_j \leq \left(- \sum_{j=1}^{N'} \mu_{ji} \right) V_i = 0. \quad (7.28)$$

Now following a similar procedure as in [158, 225], we define

$$J = \int_0^T \left(\frac{1}{2} \|h_{\sigma'(t)}(x(t))\|^2 - \frac{\gamma^2}{2} \|\omega(t)\|^2 + \mathbf{D}(\vartheta(x(t))) \right) dt. \quad (7.29)$$

According to the definition of $\mathbf{D}(\vartheta(x))$ in (7.15) and taking into account the switching sequence (7.27), we obtain

$$\begin{aligned} J \leq & \sum_{k=1}^{l-1} \int_{t_k}^{t_{k+1}} \left(\frac{1}{2} \|h_{r(x(t_k))}(x)\|^2 - \frac{\gamma^2}{2} \|\omega\|^2 + \dot{V}_{r(x(t_k))}(x) \right) dt \\ & + \int_{t_l}^T \left(\frac{1}{2} \|h_{r(x(t_l))}(x)\|^2 - \frac{\gamma^2}{2} \|\omega\|^2 + \dot{V}_{r(x(t_l))}(x) \right) dt. \end{aligned} \quad (7.30)$$

The derivative $\dot{V}_{r(x(t_k))}$ is

$$\dot{V}_{r(x(t_k))}(x(t)) = \frac{\partial V_{r(x(t_k))}(x(t))}{\partial x} \cdot \left[f'_{r(x(t_k))}(x(t)) + p_{r(x(t_k))}(x(t)) \cdot \omega(t) \right]. \quad (7.31)$$

Substitution of (7.31) in (7.30) along with adding and subtracting the term

$$\frac{1}{2\gamma^2} \frac{\partial V_{r(x(t_k))}}{\partial x} p_{r(x(t_k))} p_{r(x(t_k))}^T \frac{\partial^T V_{r(x(t_k))}}{\partial x} \quad (7.32)$$

and completing the squares yields (the arguments of the functions are dropped for reducing the complexity)

$$\begin{aligned} & \sum_{k=1}^{l-1} \int_{t_k}^{t_{k+1}} \left(\frac{\partial V_{r(x(t_k))}}{\partial x} f'_{r(x(t_k))} + \frac{1}{2} \|h_{r(x(t_k))}\|^2 \right. \\ & \quad \left. + \frac{1}{2\gamma^2} \frac{\partial V_{r(x(t_k))}}{\partial x} p_{r(x(t_k))} p_{r(x(t_k))}^T \frac{\partial^T V_{r(x(t_k))}}{\partial x} - \left\| \frac{\gamma}{\sqrt{2}} \omega - \frac{1}{\sqrt{2}\gamma} \frac{\partial V_{r(x(t_k))}}{\partial x} p_{r(x(t_k))} \right\|^2 \right) dt \\ & + \int_{t_l}^T \left(\frac{\partial V_{r(x(t_l))}}{\partial x} f'_{r(x(t_l))} + \frac{1}{2} \|h_{r(x(t_l))}\|^2 \right. \\ & \quad \left. + \frac{1}{2\gamma^2} \frac{\partial V_{r(x(t_l))}}{\partial x} p_{r(x(t_l))} p_{r(x(t_l))}^T \frac{\partial^T V_{r(x(t_l))}}{\partial x} - \left\| \frac{\gamma}{\sqrt{2}} \omega - \frac{1}{\sqrt{2}\gamma} \frac{\partial V_{r(x(t_l))}}{\partial x} p_{r(x(t_l))} \right\|^2 \right) dt. \end{aligned} \quad (7.33)$$

Referring to (7.28), we can conclude that (7.33) is smaller or equal to zero. Hence,

$$J = \int_0^T \left(\frac{1}{2} \|h_{\sigma'(t)}\|^2 - \frac{\gamma^2}{2} \|\omega\|^2 + \mathbf{D}(\vartheta) \right) dt \leq 0. \quad (7.34)$$

Note that V_i are positive definite functions with zero value at zero. Thus,

$$\int_0^T \left(\|h_{\sigma'(t)}\|^2 - \gamma^2 \|\omega\|^2 \right) dt \leq -2V_i(x(T)) \leq 0, \quad \forall i. \quad (7.35)$$

Hence, the L_2 -gain of the system is bounded above by γ . Moreover, it is easy to show (by utilizing Lemma 3.2.6 of [225]) that the system is asymptotically stable when $\omega \equiv 0$. \square

Similar to the procedure explained in Section 7.3, a feasibility problem has to be solved in order to find the parameters of the functions V_i along with μ_{ij} . Moreover, the upper bound on the L_2 -gain, γ , can be set either as an unknown parameter to be determined or as a given constant. Basically, one can set a preliminary value for γ and solve

the feasibility problem for the given γ . The procedure can be repeated with decreasing values of γ until the problem becomes infeasible and no solution can be obtained for the parameters. By doing this a minimum upper bound for the L_2 -gain can be achieved.

In the next section, the obtained control design rules are implemented and evaluated for an urban network case study. As mentioned before, the network is represented by a high-level switched nonlinear model with perimeter control and switching between timing plans as control inputs.

7.5. CASE STUDY

In this section, we aim at designing a new control scheme for urban networks represented by the high-level models developed in Chapter 4 but without having exact knowledge about the traffic demands and at the same time with less computational effort.

Basically, we consider the hybrid MFD-based model of Chapter 4 as a switched nonlinear system. The main objective is to reduce the total time spent in the network formulated in the continuous-time as follows:

$$J = \int_0^T \left(\sum_{i=1}^R n_i(t) \right) dt, \quad (7.36)$$

with n_i (veh) the accumulation in each region i . Furthermore, we define the output of the system as the sum of the accumulations in all regions, as follows:

$$y(t) = [n_1(t), \dots, n_R(t)]^T. \quad (7.37)$$

In the robust control approach, we obtain the minimum upper bound γ for the L_2 -gain of the system, i.e.

$$\int_0^T \left(\sum_{i=1}^R n_i^2(t) \right) dt \leq \gamma^2 \int_0^T \|\omega(t)\|^2 dt, \quad \forall T \geq 0. \quad (7.38)$$

Comparing (7.36) and (7.38), we can conclude that minimizing γ will reduce the effects of disturbances (uncertain trip demands in the network) on the total time spent. Therefore, in the following, we design a robust switching law based on the proposed approach to deal with uncertain trip demands and to reduce congestion caused by them.

Moreover, since there are constraints on the perimeter control inputs, we use the quantization technique discussed in Section 7.2. The trip demands in the network are considered as disturbance signals. The main requirement of the proposed approach is that the disturbance is norm bounded and belongs to the class of square integrable functions. This assumption is valid for finite time intervals (e.g. the peak hours) in which the trip demands inside the urban network are bounded and have a finite average.

7.5.1. SET-UP

For an urban network divided into two regions; region 1, the periphery and region 2, the city center (as in Fig. 7.1), a two-state hybrid MFD-based model can be formulated as follows (based on the two-state model presented in [86]):

$$\dot{n}_1(t) = -G_{1,j}(n_1(t)) \cdot u(t) + \omega_1(t), \quad (7.39)$$

$$\dot{n}_2(t) = -G_{2,j}(n_2(t)) + G_{1,j}(n_1(t)) \cdot u(t) + \omega_2(t), \quad (7.40)$$

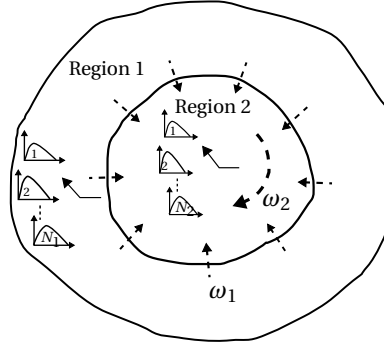


Figure 7.1: Schematic two-region urban network.

where $n_i(t)$, $i = 1, 2$, is the total number vehicles in region i at time t . Under the assumption that the average trip length within each region is constant with time, the trip completion flow $G_{i,j}(n_i(t))$ (veh/s) is defined as the rate of vehicles that reach their destinations [71]. Moreover, the signal timing plans for intersections inside each region can be altered. Consequently, instead of one MFD, a set of MFDs (each corresponds to a different timing plan) can be defined. Therefore, $G_{i,j}(n_i(t))$, with $j = 1, \dots, N_i$, constitute the MFDs for region i .

Using the perimeter control $u(t)$ may restrict the flow of vehicles from region 1, the periphery, to region 2, the city center. In this case study, we assume that the city center has two pre-defined timing plans and therefore two MFDs ($N_1 = 2$). Each MFD is modeled by a 3rd-order polynomial $G_{2,j}(n_2) = 1/3600 \cdot (a_{2,j}n_2^3 + b_{2,j}n_2^2 + c_{2,j}n_2)$ with coefficients $a_{2,1} = 1.4877 \cdot 10^{-7}$ ($1/(\text{veh}^2 \cdot \text{h})$), $b_{2,1} = -2.98 \cdot 10^{-3}$ ($1/(\text{veh} \cdot \text{h})$), $c_{2,1} = 15.091$ ($1/\text{h}$), $a_{2,2} = 2.57 \cdot 10^{-7}$ ($1/(\text{veh}^2 \cdot \text{h})$), $b_{2,2} = -4.47 \cdot 10^{-3}$ ($1/(\text{veh} \cdot \text{h})$), $c_{2,2} = 18.98$ ($1/\text{h}$). For the periphery, we assume that there exists only one timing plan and thus one MFD ($N_2 = 1$). The MFD of periphery is denoted by $G_1 = G_{1,1}$ and has $a_{1,1} = a_{2,1}$, $b_{1,1} = b_{2,1}$, $c_{1,1} = c_{2,1}$ as its parameters.

As discussed before, the perimeter control input is restricted to $[0, 1]$ and therefore we use the quantization technique presented in Section 7.2 in order to achieve a complete switching system as follows:

$$\dot{n}_1(t) = -G'_{1,j'}(n_1(t)) + \omega_1(t), \quad (7.41)$$

$$\dot{n}_2(t) = -G'_{2,j'}(n_2(t)) + G'_{1,j'}(n_1(t)) + \omega_2(t), \quad (7.42)$$

where the perimeter control input can take values from the set $\{0.1, 0.35, 0.65, 0.9\}$. The number of modes introduced by performing the quantization is $2 \cdot 4 = 8$ and therefore $j' \in \{1, \dots, 8\}$.

Here, we assume that the scenario simulates a morning peak in which a high trip demand ω_1 from the periphery (region 1) to the city center (region 2) exists while there is also a demand ω_2 for trips inside the center. Note that in our specific case, we assume that the demands from the center to the periphery and those for trips inside the periphery are relatively small and therefore negligible. Moreover, to take into account the uncertainty around the demands, we add a zero mean white Gaussian noise with variance 0.2 (veh^2/s^2) to the base profiles as shown in Figure 7.2 (a)-(b).

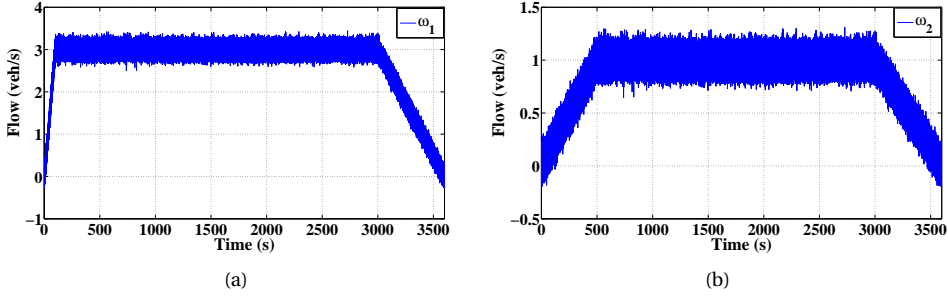


Figure 7.2: Trip demand profiles used in the simulation model, (a) trip demand from region 1 to region 2, (b) trip demands inside region 2.

7.5.2. RESULTS AND DISCUSSION

In order to determine the switching law σ , we use quadratic functions $V_i(n_i) = 1/2(\alpha_i n_i^2 + \beta_i n_i^2)$. Thus the switching rule is defined as

$$\sigma(t) = r(n_i(t)) = \arg \min_{i \in \{1, \dots, 8\}} 1/2(\alpha_i n_i^2 + \beta_i n_i^2). \quad (7.43)$$

The parameters α_i and β_i along with a feasible attenuation level γ are determined using (7.25) and the gridding technique described in Section 7.3. As for the grid size, we have assumed $\{n_1, n_2\} \in [0, 7000]$ and we have used steps of 200. The nonlinear feasibility problem is solved using the *fmincon* function inside the *Tomlab* toolbox of MATLAB. The obtained parameters are as follows:

$$\begin{aligned} (\alpha_i, \beta_i) \in & \{(3.8014, 2.9193), (6.5982, 4.3430), \\ & (9.9993, 5.7571), (5.4335, 6.2613), (7.2388, 3.2234), \\ & (4.5741, 0.2113), (8.4626, 0.2899), (4.8048, 1.0877)\}, \end{aligned}$$

with $\gamma = 0.8233 \cdot 3600$. The initial accumulations are $n_1(0) = 6200$ (veh), $n_2(0) = 5200$ (veh). The states are measured and plugged into the switching law (7.43) in order to find the active subsystem (corresponding to a specific MFD and perimeter value). The control inputs, perimeter control and switching between timing plans, are converted back from the switching signal σ' . The simulation model is (7.39)–(7.40) with noisy trip demands as illustrated in Fig. 7.2. The closed-looped system is simulated for one hour and results are depicted in Fig. 7.3. The performance of the robust switching control approach is compared with a greedy feedback control as well as a model predictive control scheme. The MPC controller is designed using the approach presented in Chapter 4. Note that for the prediction model, we use a discretized form of (7.39)–(7.40) with $T_s = 30$ s and $T_c = 60$ s. Moreover, the MPC controller is supplied by the information about the average time evolution of the trip demands, i.e. without the additive noise. Furthermore, the best performance of the MPC scheme is achieved with $N_p = 20$ and $N_c = 2$ (increasing N_p and N_c does not have considerable effects in this case). Moreover, the greedy feedback controller designed as follows. The perimeter input is set to $u = 0.1$ when $n_2 > n_{cr,2} = 3000$ (veh), and otherwise $u = 0.9$. Further, the MFD of the center is fixed either to $G_{2,1}$ or to $G_{2,2}$.

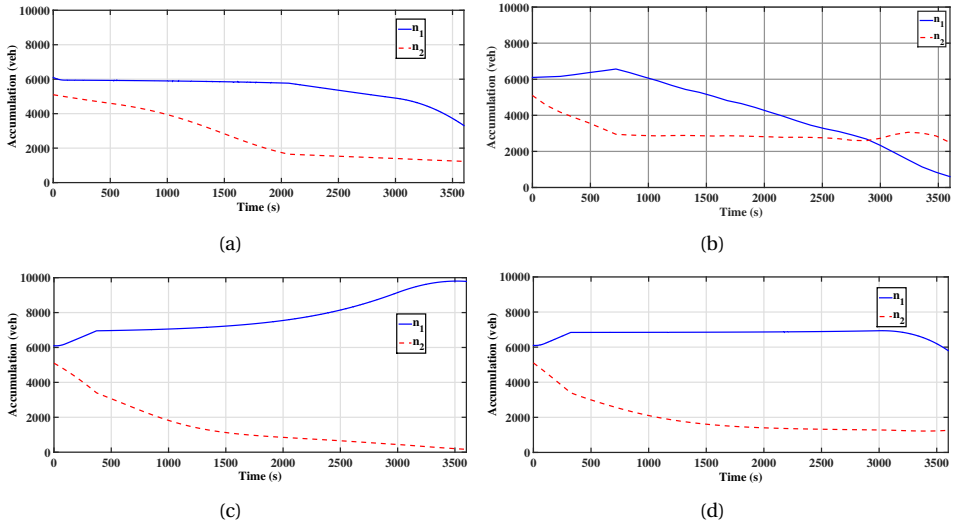


Figure 7.3: Closed-loop simulation results for different control schemes, (a) robust switching control, (b) MPC scheme, (c) greedy feedback control with MFD $G_{2,1}$, (d) greedy feedback control with MFD $G_{2,2}$.

It can be observed that the switching H_∞ control is able to prevent the gridlock condition and also significantly reduces the effects of the trip demands (disturbances). In one case of the greedy feedback controller, region 1 ends up in the gridlock situation (as the accumulations grow unboundedly in Fig. 7.3(c)). In other case of greedy controller, when timing plan 2 is chosen for the center, the accumulations eventually decrease by the end of simulation time. As can be inferred from Fig. 7.3(b), the performance of the MPC scheme is the best among them in terms of the total time spent (although there is a small increase in the accumulation of the periphery around the time 500 s). The main reason is that MPC has the average demand profile for the whole simulation period. However, the performance of the robust switching control scheme is considerable since it does not allow the accumulation in region 1 to grow beyond 6000 veh, and also since it does not use any information about the trip demands. Furthermore, the online computation of the robust control input is limited to 16 multiplications, 8 additions and a minimum operation. Therefore, there is a potential use of the proposed scheme for larger networks with more regions as it does not require online optimization.

The converted perimeter control input and switching between the two timing plans of the center are depicted in Fig. 7.4. Moreover, the L_2 -gain of the closed-loop system can be determined by setting the initial conditions to zero and by using (7.22) (the output of the system is defined as $y = [n_1, n_2]^T$). The achieved gain $\|y\|_{L_2} / \|\omega\|_{L_2}$ for the assumed demand profile is $0.1691 \cdot 3600$, which is lower than the upper bound $\gamma = 0.8233 \cdot 3600$ obtained from the optimization problem.

7.6. CONCLUDING REMARKS

Stabilization and H_∞ control of switched nonlinear systems with constrained feedback control input have been presented in this chapter. First, we have used a model trans-

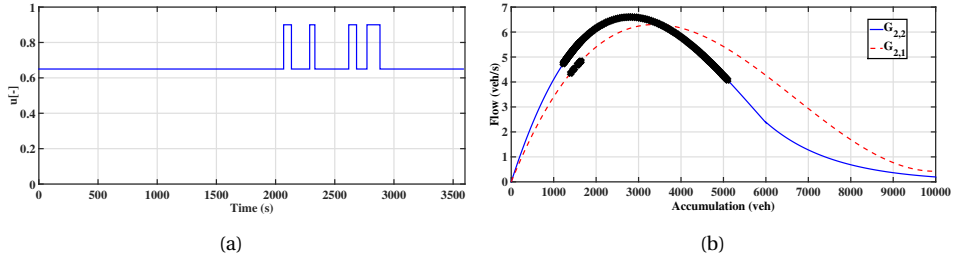


Figure 7.4: Closed-loop simulation with switching control, (a) perimeter control input converted back from the switching law, (b) switching between MFDs of region 2 obtained from the switching law σ .

formation in order to deal with the constraint on the control inputs. We have defined the L_2 -gain for switched nonlinear systems and next, we have presented an H_∞ switching control design procedure in order to achieve a desirable level of disturbance attenuation. Furthermore, the obtained results have been utilized for high-level control of urban networks modeled by a hybrid MFD representation. The total delay minimization problem in the network has been treated as a disturbance attenuation problem for the switched nonlinear model of the urban network. The obtained results have shown the effectiveness of the proposed robust control scheme in case of uncertain demand profiles. Moreover, as mentioned before, we have determined the Lyapunov functions required for the feedback switching law off-line and thus, the proposed method has a major advantage over e.g. MPC schemes both for the real-time implementation and for handling the uncertain demand profiles.

Nevertheless, the current approach is based on the determination of positive definite functions satisfying nonlinear inequality constraints. Finding appropriate functions for the general case of switched nonlinear systems could be very hard. In Chapters 9 we will present a different approach for formulating stability conditions for switched nonlinear systems that utilizes linear matrix inequality techniques.

8

ROBUST CONTROL FOR SECTOR-BOUNDED SWITCHED NONLINEAR SYSTEMS

This chapter presents stability analysis and robust H_∞ control for a particular class of switched systems characterized by nonlinear functions that belong to sector sets with arbitrary boundaries. The sector boundaries can have positive and/or negative slopes, and therefore, we cover the most general case in our approach. Using the special structure of the system but without making any additional assumptions (e.g. on the derivative of the nonlinear functions), and by proposing new multiple Lyapunov function candidates, we formulate the stability conditions and the control design procedure in the form of matrix inequalities. The proposed Lyapunov functions are more general than the quadratic functions previously proposed in the literature, as they incorporate the nonlinearities of the system and hence, lead to less conservative stability conditions. In order to stabilize the nonlinear switched system and further, to achieve a minimum upper bound for the L_2 -gain of the closed-loop controlled system, an optimization problem subject to bilinear matrix inequalities is established in order to determine the optimal matrices for the Lyapunov functions along with the robust state feedback gains. Moreover, using a special loop transformation to normalize the arbitrary sector bounds and other linear matrix inequality (LMI) techniques, we finally formulate a bi-level optimization problem that can be efficiently solved using a combination of a convex optimization algorithm and a line search method. This is a great advantage over the existing approaches for stability analysis and robust control of switched nonlinear systems. Furthermore, in order to show that the most general cases of the given class of switched systems can be treated with our approach and also to illustrate the performance of the proposed switching control scheme, two examples are presented.

8.1. INTRODUCTION

IN this chapter, we study a special case of switched systems comprising a set of nonlinear dynamical subsystems. In each subsystem, the evolution of the state is governed by linear combinations of nonlinear state-dependent functions. Furthermore, a state- and/or time-dependent switching signal determines the active subsystem at each time instant. The nonlinear functions are assumed to belong to sector sets with arbitrary (positive or negative, and possibly asymmetric) slopes for the sector boundaries. Thus, in the non-switched case, we cover more general cases of nonlinear functions compared e.g. to the Lur'e-type systems studied in [29, 81, 82, 172] and to the nonlinear systems that admit diagonal-type Lyapunov functions investigated in [4, 132].

In addition to the generalization of the nonlinear functions to arbitrary sector conditions, we have also added the switching between multiple subsystems each characterized with this type of nonlinear dynamics. This makes the analysis and control design problem even more challenging. To the best of our knowledge, the stability and robust control design problem for this class of switched systems with these general conditions has not been addressed in the literature.

This chapter contains three main contributions with respect to the state-of-the-art: 1) inclusion of sector bounds with arbitrary slopes for nonlinear functions (moreover, the nonlinear functions are no longer required to have an unbounded integral), 2) stability analysis for this class of switched systems under arbitrary switching using a less conservative approach based on multiple Lyapunov functions and the concept of average dwell time, 3) stabilization and robust disturbance attenuation of these systems using a bi-level convex optimization problem. In the following, we elaborate on these points.

For stability analysis under arbitrary switching, we propose a family of Lyapunov functions that incorporate both quadratic functions of the state and also the integrals of nonlinearities in the subsystems. Since the proposed Lyapunov candidate functions are general and include the nonlinear dynamics, this choice in general will lead to less conservative stability conditions compared to e.g. the use of quadratic functions (see [29, 39] for a specific non-switched case). Based on the concept of average dwell time [112], which occasionally allows fast switching, we formulate a feasibility problem based on matrix inequalities that are nonlinear in a single scalar variable only, in order to find a lower bound for the average dwell time. We further prove that the switched system is globally exponentially stable under arbitrary switching provided that the average time between consecutive switching time instants is larger than the obtained bound.

Next, we investigate the stabilization problem for the given class of switched systems in case of unstable modes and disturbances. Combining the proposed Lyapunov functions and their derivatives in order to obtain a single expression that can be used to design stabilizing control laws is challenging. This is because the Lyapunov functions include the integrals of nonlinear functions whereas in the time derivative of the Lyapunov functions, the nonlinear functions appear explicitly. However, using an assumption on the matrices of the Lyapunov functions along with some matrix operations, we formulate sufficient conditions for the design of robust switching control laws in the form of an optimization problem constrained by bilinear matrix inequalities. The optimization problem minimizes the upper bound on the L_2 -gain of the switched system and it gives the optimal state feedback gains and the matrices of the Lyapunov functions.

In order to further improve the efficiency of the design procedure, we exploit a transformation technique to normalize the sector boundaries and congruence transformations in order to re-arrange the matrix inequalities into linear ones. At the end, we obtain a bi-level optimization problem with a high-level problem that is non-convex only in a single scalar variable, while the low-level optimization problem is convex. Hence, we are able to solve the overall problem efficiently using a line search method along with a convex optimization method subject to LMI constraints. Hence, the overall problem can be efficiently solved using a line search method along with feasibility checking of LMIs. This is a great advantage over the existing approaches for stability analysis of switched nonlinear systems in the literature, which involve searching for Lyapunov functions without a pre-defined structure and/or solving multi-parametric optimization problems [35].

The chapter is organized as follows. In Section 8.2, we present the particular class of switched nonlinear systems under study. Section 8.3 presents stability conditions for the system under arbitrary switching. Section 8.4 discusses stability analysis with an average dwell time constraint. Next, we present the design of robust stabilizing controllers in Section 8.5. We then illustrate the performance of the proposed robust switching control scheme using two examples. Finally, the chapter concludes with a further discussion of the obtained results and open issues.

8.2. PROBLEM STATEMENT

Consider the following switched nonlinear system:

$$\dot{x}(t) = A_{\sigma(t)}x(t) + B_{\sigma(t)}u(t) + E_{\sigma(t)}f(x(t)) + H_{\sigma(t)}\omega(t), \quad (8.1)$$

$$u(t) = K_{\sigma(t)}x(t) + F_{\sigma(t)}f(x(t)), \quad (8.2)$$

$$y(t) = C_{\sigma(t)}g(x(t)), \quad (8.3)$$

with $x \in \mathbb{R}^n$ the state vector, $u \in \mathbb{R}^{n_u}$ the control input, $\omega \in \mathbb{R}^{n_\omega}$ the disturbance input, $y \in \mathbb{R}^{n_y}$ the output, and $f: \mathbb{R}^n \rightarrow \mathbb{R}^n: x_i \mapsto f_i(x_i)$, $g: \mathbb{R}^n \rightarrow \mathbb{R}^n: x_i \mapsto g_i(x_i)$ nonlinear vector functions. Moreover, the switching signal σ is defined as a piecewise constant function, $\sigma(\cdot): [0, +\infty) \rightarrow \{1, \dots, N\}$.

Assumption 8.1. *The scalar functions f_i are continuous and belong to the class \mathcal{S}_{c1} defined as follows:*

$$\mathcal{S}_{c1} = \{\phi: \mathbb{R} \rightarrow \mathbb{R} \mid \exists \alpha, \beta \in \mathbb{R}, \alpha < \beta, \text{ such that } (\phi(\zeta) - \alpha\zeta)(\phi(\zeta) - \beta\zeta) \leq 0, \phi(0) = 0, \forall \zeta \in \mathbb{R}\}. \quad (8.4)$$

Note that functions f_i are not required to lie only in the 1st and the 3rd quadrant as in [82], nor to have unbounded integrals as in [4, 132].

Assumption 8.2. *The scalar functions g_i are continuous and belong to the class \mathcal{S}_{c2} defined as follows:*

$$\mathcal{S}_{c2} = \{\psi: \mathbb{R} \rightarrow \mathbb{R} \mid \exists \delta \text{ such that } |\psi(\zeta)| \leq \delta|\zeta|, \forall \zeta \in \mathbb{R}\}. \quad (8.5)$$

In fact, \mathcal{S}_{c2} is a special case of the class \mathcal{S}_{c1} and functions that belong to the class \mathcal{S}_{c2} are bounded within a symmetric convex double cone with the origin as apex. Moreover, the nonlinear functions in system (8.1) can also be considered as state-dependent

disturbances. Therefore, specific applications in which this type of disturbances affect the system (e.g. cogging torque or no-current torque, unbalanced gravitational load and eccentricity are state-dependent disturbances affecting a motor control system), can be treated with our proposed analysis and control tools. For the non-switched and simplified version of system (8.1) formulated as follows:

$$\dot{x}(t) = Ef(x(t)). \quad (8.6)$$

The authors in [132] proved that (8.6) is absolutely stable if there exists a positive definite diagonal matrix $\Lambda = \text{diag}\{\lambda_i\}$, $\lambda_i > 0$, $\forall i \in \{1, \dots, n\}$, such that

$$V(x) = \sum_{i=1}^n \lambda_i \int_0^{x_i} f_i(\xi) d\xi \quad (8.7)$$

is a diagonal-type Lyapunov function for (8.6), provided that $x_i f_i(x_i) \geq 0$, $\forall i$.

However, stability of a composed switched system cannot be concluded from the stability of the subsystems [149]. According to [149], it is sufficient to construct a common Lyapunov function for a switched system in order to prove stability. Generally, finding a common Lyapunov function for the general case of switched nonlinear systems is a tedious task. In [4], stability analysis under arbitrary switching for system (8.1), with $A_\ell = 0$, $\forall \ell \in \{1, \dots, N\}$, and with $u, \omega \equiv 0$, using a common Lyapunov function of the form (8.7) is presented. However, extension of the results for arbitrary switching obtained in [4] to our more general model (8.1)–(8.3) and more important, to the stabilization and robust control problem is not possible. This is mainly because we need to combine and compare the values of the Lyapunov functions and their derivatives in order to compose a stabilizing control law and this is not feasible with the current formulation of the Lyapunov function (8.7) (due to the integral of the nonlinearities). One solution would be to use quadratic functions of the state. However, this choice would increase the conservatism in the stability analysis. Therefore, in the following, we use a different Lyapunov function that still contains the nonlinearities in the model and meanwhile, is extendable for the design of robust stabilizing switching laws. In the first stage, we propose a less conservative approach (compared to the common Lyapunov function method) for stability under arbitrary switching, using the concept of dwell time. Next, we extend the results for state-based switching and design of robust control laws. The resulting design conditions will be formulated in the form of matrix inequalities.

8

8.3. STABILITY ANALYSIS UNDER ARBITRARY SWITCHING

For the switched system (8.1) with $u(t), \omega(t) = 0 \forall t$, the following common Lyapunov function is proposed:

$$V(x) = x^T P x + 2 \sum_{i=1}^n \lambda_i \int_0^{x_i} f_i(\xi) d\xi. \quad (8.8)$$

For the Lyapunov functions (8.7) to be radially unbounded, the nonlinear functions f_i should have an unbounded integral, while in the new Lyapunov function (8.8) this is no longer required and thus, more general cases can be treated through this Lyapunov function. Note that asymptotic stability of all subsystems is a necessary condition for

stability under arbitrary switching. The time derivative of (8.8) along the trajectories of the switched system is obtained as follows (the time t is dropped for the sake of brevity):

$$\begin{aligned} \dot{V}(x) = & f^T(x)(\Lambda E_\sigma + E_\sigma^T \Lambda) f(x) + x^T (P E_\sigma + A_\sigma^T \Lambda) f(x) \\ & + f^T(x)(E_\sigma^T P + \Lambda A_\sigma) x + x^T (P A_\sigma + A_\sigma^T P) x, \end{aligned} \quad (8.9)$$

with $\Lambda = \text{diag}\{\lambda_i\}$. The derivative (8.9) for the active subsystem ℓ can be rewritten as

$$\dot{V}(x) = \begin{bmatrix} x \\ f(x) \end{bmatrix}^T \begin{bmatrix} P A_\ell + A_\ell^T P & P E_\ell + A_\ell^T \Lambda \\ E_\ell^T P + \Lambda A_\ell & \Lambda E_\ell + E_\ell^T \Lambda \end{bmatrix} \begin{bmatrix} x \\ f(x) \end{bmatrix}. \quad (8.10)$$

Now taking into account that the nonlinear functions f_i belong to the class \mathcal{S}_{c1} , the following theorem provides sufficient conditions for the asymptotic stability of (8.1) with $u, \omega \equiv 0$.

Theorem 8.1. *Assume there exists a symmetric matrix P , a positive diagonal matrix Λ , and a positive definite and diagonal matrix $\mathcal{F} = \text{diag}\{\tau_1, \dots, \tau_n\}$, such that the following LMIs¹:*

$$\begin{bmatrix} P A_\ell + A_\ell^T P - \mathcal{F} \mathcal{D}_\alpha \mathcal{D}_\beta & \star \\ E_\ell^T P + \Lambda A_\ell + \frac{1}{2} \mathcal{F} (\mathcal{D}_\alpha + \mathcal{D}_\beta) & \Lambda E_\ell + E_\ell^T \Lambda - \mathcal{F} \end{bmatrix} < 0, \quad \forall \ell \in \{1, \dots, N\}, \quad (8.11)$$

$$P + \mathcal{D}_\alpha \Lambda > 0, \quad (8.12)$$

with $\mathcal{D}_\alpha = \text{diag}\{\alpha_1, \dots, \alpha_n\}$ and $\mathcal{D}_\beta = \text{diag}\{\beta_1, \dots, \beta_n\}$ are feasible, then the switched system (8.1) with Assumption (8.1) and with $u, \omega \equiv 0$ will be asymptotically stable under arbitrary switching.

Proof. It is easy to verify that the sector condition (8.4), for the function f_i , can be written in the following quadratic form:

$$\begin{bmatrix} x_i \\ f_i(x_i) \end{bmatrix}^T \begin{bmatrix} \alpha_i \beta_i & -\frac{\alpha_i + \beta_i}{2} \\ -\frac{\alpha_i + \beta_i}{2} & 1 \end{bmatrix} \begin{bmatrix} x_i \\ f_i(x_i) \end{bmatrix} \leq 0. \quad (8.13)$$

The main idea is that the derivative (8.10) should be negative whenever (8.13) holds for all $i \in \{1, \dots, n\}$. Using the so-called S-procedure [22], the inequalities (8.10) and (8.13) can be combined, resulting in the LMI (8.11). Furthermore, we have for any $x_i \in \mathbb{R}$

$$\sum_{i=1}^n \lambda_i \int_0^{x_i} \alpha_i \xi d\xi \leq \sum_{i=1}^n \lambda_i \int_0^{x_i} f_i(\xi) d\xi \leq \sum_{i=1}^n \lambda_i \int_0^{x_i} \beta_i \xi d\xi. \quad (8.14)$$

Therefore, in order to guarantee that $V(x) > 0$, we need

$$x^T P x + x^T \mathcal{D}_\alpha \Lambda x > 0. \quad (8.15)$$

Hence, it is sufficient to have $P + \mathcal{D}_\alpha \Lambda$ positive definite as in (8.12). \square

Remark 8.1. *Note that since the nonlinear functions f_i are assumed to be continuous (cf. Assumption 8.1), the Lyapunov function (8.8) will be continuous for arbitrary switching patterns. This is a necessary condition for validity of the results presented in Theorem 8.1.*

¹The symbol \star is used to represent symmetric blocks.

8.4. STABILITY ANALYSIS WITH AVERAGE DWELL TIME

For the switched system (8.1) with $u(t), \omega(t) = 0 \forall t$, the following set of Lyapunov functions is proposed:

$$V_\ell(x) = x^T P_\ell x + 2 \sum_{i=1}^n \lambda_i^{(\ell)} \int_0^{x_i} f_i(\xi) d\xi, \quad \text{for } \ell = 1, \dots, N. \quad (8.16)$$

The following theorem provides sufficient conditions for exponential stability of (8.1) using the concepts of multiple Lyapunov functions [35] and the average dwell time [112].

Theorem 8.2. *Consider the system (8.1) with Assumption 8.1. Suppose there exist positive matrices $\Lambda_\ell = \text{diag}\{\lambda_i^{(\ell)}\}$, symmetric matrices P_ℓ , positive diagonal matrices \mathcal{T}_ℓ , for $\ell = 1, \dots, N$, and a positive scalar ε , such that*

$$\begin{bmatrix} P_\ell A_\ell + A_\ell^T P_\ell + \varepsilon(P_\ell + \Lambda_\ell \mathcal{D}_\beta) - \mathcal{T}_\ell \mathcal{D}_\alpha \mathcal{D}_\beta & \star \\ E_\ell^T P_\ell + \Lambda_\ell A_\ell + \frac{1}{2} \mathcal{T}_\ell (\mathcal{D}_\alpha + \mathcal{D}_\beta) & \Lambda_\ell E_\ell + E_\ell^T \Lambda_\ell - \mathcal{T}_\ell \end{bmatrix} < 0, \quad (8.17)$$

$$P_\ell + \Lambda_\ell \mathcal{D}_\alpha > 0, \quad \forall \ell \in \{1, \dots, N\}, \quad (8.18)$$

with $\mathcal{D}_\alpha = \text{diag}\{\alpha_i\}$, $\mathcal{D}_\beta = \text{diag}\{\beta_i\}$. System (8.1) with $u, \omega \equiv 0$ is globally exponentially stable under arbitrary switching, if the average dwell time of consecutive switching instants for any arbitrary interval (t_0, t) is bounded by

$$T_D(t_0, t) \geq \frac{1}{\varepsilon} \log \left(\max_{j, \ell \in \{1, \dots, N\}} \frac{b_{\max, j}}{a_{\min, \ell}} \right), \quad \forall t > t_0, \quad (8.19)$$

where $a_{\min, \ell}$ denotes the smallest singular value of $P_\ell + \Lambda_\ell \mathcal{D}_\alpha$ and $b_{\max, j}$ is the largest singular value of $P_j + \Lambda_j \mathcal{D}_\beta$.

Proof. Since $\lambda_i^{(\ell)} > 0$, we have

$$\sum_{i=1}^n \lambda_i^{(\ell)} \int_0^{x_i} \alpha_i \xi d\xi \leq \sum_{i=1}^n \lambda_i^{(\ell)} \int_0^{x_i} f_i(\xi) d\xi \leq \sum_{i=1}^n \lambda_i^{(\ell)} \int_0^{x_i} \beta_i \xi d\xi. \quad (8.20)$$

Therefore, for each Lyapunov function V_ℓ , the following inequalities hold:

$$a_{\min, \ell} \|x\|^2 \leq x^T (P_\ell + \Lambda_\ell \mathcal{D}_\alpha) x \leq V_\ell(x) \leq x^T (P_\ell + \Lambda_\ell \mathcal{D}_\beta) x \leq b_{\max, \ell} \|x\|^2. \quad (8.21)$$

Using the S-procedure [22], if (8.17) and (8.13) hold, we obtain

$$\underbrace{\begin{bmatrix} x \\ f(x) \end{bmatrix}^T \begin{bmatrix} P_\ell A_\ell + A_\ell^T P_\ell & P_\ell E_\ell + A_\ell^T \Lambda_\ell \\ E_\ell^T P_\ell + \Lambda_\ell A_\ell & \Lambda_\ell E_\ell + E_\ell^T \Lambda_\ell \end{bmatrix} \begin{bmatrix} x \\ f(x) \end{bmatrix}}_{\dot{V}_\ell(x)} < -\varepsilon x^T (P_\ell + \Lambda_\ell \mathcal{D}_\beta) x < -\varepsilon V_\ell(x). \quad (8.22)$$

Moreover, using (8.21), it can be easily shown that

$$V_\ell(x) \leq \eta V_j(x), \quad \forall x \in \mathbb{R}^n, \quad \forall j, \ell \in \{1, \dots, N\}, \quad (8.23)$$

with

$$\eta = \max_{j, \ell \in \{1, \dots, N\}} (b_{\max, j} / a_{\min, \ell}). \quad (8.24)$$

Now from (8.22) we obtain

$$V_{\sigma(t_k)}(x(t)) \leq e^{-\varepsilon(t-t_k)} V_{\sigma(t_k)}(x(t_k)), \quad \forall t \in [t_k, t_{k+1}), \quad (8.25)$$

with t_k the k -th switching time instant. Using (8.23) and by iteration, we get

$$\begin{aligned} V_{\sigma(t_k)}(x(t)) &\leq e^{-\varepsilon(t-t_k)} V_{\sigma(t_k)}(x(t_k)) \leq \\ &e^{-\varepsilon(t-t_k)} \eta V_{\sigma(t_{k-1})}(x(t_k)) \leq \dots \leq \eta^{N_\sigma(t, t_0)} e^{-\varepsilon(t-t_0)} V_{\sigma(t_0)}(x(t_0)), \end{aligned} \quad (8.26)$$

where $N_\sigma(t, t_0)$ denotes the number of switchings in (t_0, t) . Substituting

$$N_\sigma(t, t_0) \leq (t - t_0) / T_D, \quad (8.27)$$

with T_D the average dwell time between successive switching time instants, results in

$$V_{\sigma(t_k)}(x(t)) \leq e^{-(\varepsilon - \frac{\log \eta}{T_D})(t-t_0)} V_{\sigma(t_0)}(x(t_0)). \quad (8.28)$$

Hence, using (8.28) and (8.21), we obtain

$$\|x(t)\| \leq \frac{\max_{\ell \in \{1, \dots, N\}} b_{\max, \ell}}{\min_{j \in \{1, \dots, N\}} a_{\min, j}} e^{-\frac{1}{2}(\varepsilon - \frac{\log \eta}{T_D})(t-t_0)} \|x(t_0)\|. \quad (8.29)$$

Therefore, system (8.1) is globally exponentially stable for any switching pattern with $T_D(t_0, t)$ satisfying (8.19). \square

Remark 8.2. *If there exist common P and Λ matrices that satisfy the inequalities (8.17), it is easy to show that the bound (8.19) on the average dwell time reduces to $T_D \geq 0$, since (8.23) will hold for $\eta = 1$.*

Since (8.17) will be an LMI if the scalar variable ε is fixed, one can utilize an LMI optimization algorithm along with a line search method to find a feasible solution for (8.17)-(8.18). In fact, ε denotes the overall exponential decay rate of the Lyapunov functions. Therefore, it is expected that as the value of ε is increased, the inequalities (8.17)-(8.18) become infeasible from a certain point.

8.5. DESIGN OF ROBUST STABILIZING SWITCHING LAWS

In the previous sections, we have discussed the stability problem for switched systems (8.1)–(8.3) under given switching signals. In this section, we synthesize switching laws together with the control input u in order to stabilize the switched nonlinear system and moreover, to minimize the effects of disturbances on the output of the system. Therefore, from now on we assume that none of the subsystems of (8.1) is locally or globally asymptotically stable (otherwise, the solution for the stabilization problem would be trivial).

Consider the switched nonlinear system (8.1)–(8.3) composed of N subsystems. It is assumed that the state vector $x(t)$ is available for feedback for all $t \geq 0$. The switched system has the L_2 -gain bounded above by $\gamma > 0$ under some switching law σ if

$$\|y\|_{L_2[0, T]} \leq \gamma \|\omega\|_{L_2[0, T]} \quad (8.30)$$

for all nonzero ω that belong to the space of square integrable functions, i.e. the L_2 -space, and for the initial state $x(0) = 0$ (we assume this to illuminate the transient response resulting from nonzero initial states). The goal is to design a switching law σ of the form

$$\sigma(t) = r(x(t)), \quad (8.31)$$

with $r(\cdot) : \mathbb{R}^n \rightarrow \{1, \dots, N\}$ a piecewise constant function, such that the origin of the closed-loop system is globally asymptotically stable when $\omega(t) = 0, \forall t \geq 0$, and moreover, the desired upper bound γ for the L_2 -gain from ω to $y = C_\sigma g(x)$ on any finite time interval $[0, T]$ is achieved, i.e.

$$\int_0^T \left(\gamma^2 \|\omega(t)\|_2^2 - \|C_\sigma g(x)_{\sigma(t)}(x(t))\|_2^2 \right) dt \geq 0. \quad (8.32)$$

8.5.1. STABILIZATION USING MULTIPLE LYAPUNOV FUNCTIONS

A Lyapunov-like function is proposed as follows:

$$\mathcal{V}(x) = \min_{\ell=1, \dots, N} V_\ell(x), \quad (8.33)$$

with V_ℓ selected as

$$V_\ell(x) = x^T P_\ell x + 2 \sum_{i=1}^n \lambda_i \int_0^{x_i} f_i(\xi) d\xi. \quad (8.34)$$

Before proceeding with the main results, we define the subclass \mathcal{M} of Metzler matrices, with elements μ_{ij} and the following properties [35]:

$$\mu_{ij} \geq 0 \quad \forall i \neq j, \quad \sum_{i=1}^N \mu_{ij} = 0 \quad \forall j. \quad (8.35)$$

Theorem 8.3. *Assume there exist a matrix $M \in \mathcal{M}$, positive definite matrices P_ℓ , a positive diagonal matrix Λ , and positive diagonal matrices $\mathcal{T}_\ell = \text{diag}\{\tau_{1,\ell}, \dots, \tau_{n,\ell}\}$ satisfying the following inequalities:*

$$\begin{bmatrix} P_\ell A_\ell + A_\ell^T P_\ell - \mathcal{T}_\ell \mathcal{D}_\alpha \mathcal{D}_\beta + \sum_{j=1}^N \mu_{j\ell} P_j & \star \\ E_\ell^T P_\ell + \Lambda A_\ell + \frac{1}{2} \mathcal{T}_\ell (\mathcal{D}_\alpha + \mathcal{D}_\beta) & \Lambda E_\ell + E_\ell^T \Lambda - \mathcal{T}_\ell \end{bmatrix} < 0, \quad \forall \ell \in \{1, \dots, N\}, \quad (8.36)$$

$$P_\ell + \mathcal{D}_\alpha \Lambda > 0, \quad \forall \ell \in \{1, \dots, N\}, \quad (8.37)$$

with $\mathcal{D}_\alpha = \text{diag}\{\alpha_1, \dots, \alpha_n\}$ and $\mathcal{D}_\beta = \text{diag}\{\beta_1, \dots, \beta_n\}$, then the switching rule (8.31) with²

$$r(x(t)) = \arg \min_{\ell=1, \dots, N} V_\ell(x(t)) \quad (8.38)$$

makes the equilibrium point $x = 0$ of (8.1)–(8.3) (with $u, w \equiv 0$) globally asymptotically stable.

²Note that in (8.38), we take the minimum argument, in case of having multiple minima V_ℓ .

Proof. The Lyapunov function (8.33) is piecewise differentiable. Therefore, we use the so-called Dini derivative (see [35, 64]) formulated as follows:

$$\mathbf{D}^+(\mathcal{V}(x(t))) = \limsup_{\delta t \rightarrow 0^+} \frac{\mathcal{V}(x(t+\delta t)) - \mathcal{V}(x(t))}{\delta t}. \quad (8.39)$$

Assume that at an arbitrary time $t \geq 0$, the switching law is given by $\sigma(t) = r(x(t)) = \ell$ for some $\ell \in \mathcal{S}(x(t)) = \{\ell : \mathcal{V}(x(t)) = V_\ell(x(t))\}$. Hence, from (8.39) and (8.1), we have (using Theorem 1 of [142], see also [102])

$$\mathbf{D}^+(\mathcal{V}(x(t))) = \min_{i \in \mathcal{S}(x(t))} \left[\frac{\partial V_i}{\partial x} (A_\ell x + E_\ell f(x)) \right] \leq \frac{\partial V_\ell}{\partial x} (A_\ell x + E_\ell f(x)), \quad (8.40)$$

where ℓ denotes the index of the active subsystem determined from (8.38). Pre-multiplying (8.36) by $[x^\top, f^\top(x)]$ and post-multiplying by its transpose, we obtain

$$\begin{aligned} & \underbrace{\begin{bmatrix} x \\ f(x) \end{bmatrix}^\top \begin{bmatrix} P_\ell A_\ell + A_\ell^\top P_\ell & P_\ell E_\ell + A_\ell^\top \Lambda \\ E_\ell^\top P_\ell + \Lambda A_\ell & \Lambda E_\ell + E_\ell^\top \Lambda \end{bmatrix} \begin{bmatrix} x \\ f(x) \end{bmatrix}}_{\frac{\partial V_\ell}{\partial x} (A_\ell x + E_\ell f(x))} \\ & < \begin{bmatrix} x \\ f(x) \end{bmatrix}^\top \begin{bmatrix} \mathcal{F}_\ell \mathcal{D}_\alpha \mathcal{D}_\beta & -\frac{1}{2} \mathcal{F}_\ell (\mathcal{D}_\alpha + \mathcal{D}_\beta) \\ -\frac{1}{2} \mathcal{F}_\ell (\mathcal{D}_\alpha + \mathcal{D}_\beta) & \mathcal{F}_\ell \end{bmatrix} \begin{bmatrix} x \\ f(x) \end{bmatrix} - \sum_{j=1}^N \mu_{j\ell} x^\top P_j x, \\ & \ell \in \{1, \dots, N\}. \end{aligned} \quad (8.41)$$

Now taking into account the sector condition (8.13), using the fact that for the active subsystem ℓ , $V_\ell \leq V_j$, $\forall j \in \{1, \dots, N\} \setminus \{\ell\}$, we have

$$\mathbf{D}^+(\mathcal{V}(x(t))) \leq \frac{\partial V_\ell}{\partial x} (A_\ell x + E_\ell f(x)) < - \sum_{j=1}^N \mu_{j\ell} x^\top P_j x < -x^\top P_\ell x \sum_{j=1}^N \mu_{j\ell} = 0. \quad (8.42)$$

Note that the last equality holds since $\mu_{j\ell}$ are the elements of a Metzler matrix. Hence, the switching law (8.38) makes the equilibrium point $x = 0$ of the switched nonlinear system (8.1) with $u, \omega = 0$ globally asymptotically stable. \square

8.5.2. ROBUST H_∞ SWITCHING CONTROL DESIGN

Now assume that the disturbance input ω has a finite L_2 -norm as in (8.30). In the following, sufficient conditions for the design of a stabilizing state feedback control input together with a switching law are presented, in order to ensure an upper bound γ for the L_2 -gain (the actual L_2 -gain from the input ω to the output y of the system (8.1)–(8.3) would be smaller than or equal to γ). The main results are summarized in the following theorem.

Theorem 8.4. *Suppose there exist a Metzler matrix $M \in \mathcal{M}$ with elements μ_{ij} , positive definite matrices P_ℓ , a positive diagonal matrix Λ , and positive diagonal matrices $\mathcal{F}_\ell =$*

$\text{diag}\{\tau_{1,\ell}, \dots, \tau_{n,\ell}\}$ that give an optimal solution for the following problem:

$$\min_{\{P_\ell\}_{\ell=1}^N, \{K_\ell\}_{\ell=1}^N, \{F_\ell\}_{\ell=1}^N, \{T_\ell\}_{\ell=1}^N, \{\mu_{j\ell}\}_{j,\ell=1}^N, \Lambda, \rho} \quad (8.43)$$

subject to:

$$\begin{bmatrix} P_\ell(A_\ell + B_\ell K_\ell) + (A_\ell + B_\ell K_\ell)^\top P_\ell - \mathcal{F}_\ell \mathcal{D}_\alpha \mathcal{D}_\beta + \sum_{j=1}^N \mu_{j\ell} P_j & \star & \star & \star \\ (E_\ell + B_\ell F_\ell)^\top P_\ell + \Lambda(A_\ell + B_\ell K_\ell) + \frac{1}{2} \mathcal{F}_\ell (\mathcal{D}_\alpha + \mathcal{D}_\beta) & \Lambda(E_\ell + B_\ell F_\ell) + (E_\ell + B_\ell F_\ell)^\top \Lambda - \mathcal{F}_\ell & \star & \star \\ H_\ell^\top P_\ell & H_\ell^\top \Lambda & -\rho I & \star \\ \|C_\ell\|_{\mathbb{F}} \Delta & 0 & 0 & -I \end{bmatrix} < 0, \quad (8.44)$$

$$P_\ell + \mathcal{D}_\alpha \Lambda > 0, \quad P_\ell, \mathcal{F}_\ell, \Lambda > 0, \quad \rho > 0, \quad \forall \ell \in \{1, \dots, N\}, \quad (8.45)$$

then the control input

$$u(t) = K_\ell x(t) + F_\ell f(x(t)), \quad (8.46)$$

along with the min-switching law (8.38) make the closed-loop switched system (8.1)–(8.3) stable with the minimized upper bound $\gamma = \sqrt{\rho}$ for the L_2 -gain from ω to the output y .

Proof. Applying the Schur complement to (8.44) with respect to the fourth row and column, rearranging terms and pre-multiplying by $[x^\top, f^\top(x), \omega^\top]$ and post-multiplying by its transpose yields

$$\begin{aligned} & \underbrace{\begin{bmatrix} x \\ f(x) \end{bmatrix}^\top \begin{bmatrix} P_\ell(A_\ell + B_\ell K_\ell) + (A_\ell + B_\ell K_\ell)^\top P_\ell & \star \\ (E_\ell + B_\ell F_\ell)^\top P_\ell + \Lambda(A_\ell + B_\ell K_\ell) & \Lambda(E_\ell + B_\ell F_\ell) + (E_\ell + B_\ell F_\ell)^\top \Lambda \end{bmatrix} \begin{bmatrix} x \\ f(x) \end{bmatrix}}_{\frac{\partial V_\ell}{\partial x} (A_\ell x + B_\ell u + E_\ell f(x) + H_\ell \omega)} \\ & < \begin{bmatrix} x \\ f(x) \end{bmatrix}^\top \begin{bmatrix} \mathcal{F}_\ell \mathcal{D}_\alpha \mathcal{D}_\beta & \star \\ -\frac{1}{2} \mathcal{F}_\ell (\mathcal{D}_\alpha + \mathcal{D}_\beta) & \mathcal{F}_\ell \end{bmatrix} \begin{bmatrix} x \\ f(x) \end{bmatrix} - \sum_{j=1}^N \mu_{j\ell} x^\top P_j x - \|C_\ell\|_{\mathbb{F}}^2 x^\top \Delta^2 x + \rho \omega^\top \omega, \end{aligned} \quad (8.47)$$

with $\Delta = \text{diag}\{\delta_{i_1}, \dots, \delta_{i_n}\}$. Since (8.44) is valid for some $M \in \mathcal{M}$ and $V_j \geq V_\ell$ for all $j \in \{1, \dots, N\} \setminus \{\ell\}$, and based on the sector condition (8.13), we obtain

$$\begin{aligned} \mathbf{D}^+(\mathcal{V}(x(t))) & \leq \frac{\partial V_\ell}{\partial x} (A_\ell x + B_\ell u + E_\ell f(x) + H_\ell \omega) < - \sum_{j=1}^N \mu_{j\ell} x^\top P_j x - \|C_\ell\|_{\mathbb{F}}^2 x^\top \Delta^2 x + \rho \omega^\top \omega \\ & < - x^\top P_\ell x \underbrace{\sum_{j=1}^N \mu_{j\ell}}_{=0} - \|C_\ell\|_{\mathbb{F}}^2 x^\top \Delta^2 x + \rho \omega^\top \omega < -y^\top y + \rho \omega^\top \omega. \end{aligned} \quad (8.48)$$

The last inequality is justified using the following:

$$y^\top y = \|y\|_2^2 = \|C_{\sigma(t)} g(x)\|_2^2 \leq \|C_{\sigma(t)}\|_{\mathbb{F}}^2 \cdot \|g(x)\|_2^2 \leq \|C_{\sigma(t)}\|_{\mathbb{F}}^2 x^\top \Delta^2 x, \quad (8.49)$$

where the first inequality is obtained based on [79, (2.3.7) on page 57] and $\|\cdot\|_{\mathbb{F}}$ denotes the Frobenius norm. \square

Proposition 8.1. *The value $\gamma = \sqrt{\bar{\rho}}$ obtained from the optimization (8.43)–(8.45) is an upper bound for the L_2 -gain of the system (8.1)–(8.3). Hence, the actual closed-loop system would outperform the obtained upper bound for the L_2 -gain, since we have used the sector condition of Assumption 8.2.*

Remark 8.3. *In case $C_{\sigma(t)}$ is a square matrix, using the spectral norm of $C_{\sigma(t)}$ defined as*

$$\|C_{\sigma(t)}\|_2 = \sqrt{\lambda_{\max}(C_{\sigma(t)}^H C_{\sigma(t)})} \quad (8.50)$$

would result in a tighter bound compared to using the Frobenius norm as in (8.49). This can be easily shown using the fact that the spectral norm is less than or equal to the Frobenius norm [79].

Remark 8.4. *Asymptotic stability of (8.1) under switching law (8.38) is ensured even if sliding mode behavior occurs. In case of a sliding mode, the result of $\operatorname{argmin}_{\ell=1,\dots,N} V_\ell(x(t))$ might not be unique. However, using (8.42) (we assume $u, \omega \equiv 0$ for simplicity), it can be shown that the time derivative of the minimum Lyapunov function is strictly negative along the Filippov solution of the system. Assume that the cardinality of the set $\mathcal{S}(x)$ is larger than one, which means $\min_{\ell=1,\dots,N} V_\ell(x)$ is not unique. From the Lyapunov function (8.33) and the time-derivative (8.40) (assume $u, \omega \equiv 0$ for simplicity), a switch from any $\ell \in \mathcal{S}(x)$ to some $j \in \mathcal{S}(x)$ is allowed only if $\frac{\partial V_j}{\partial x}(A_\ell x + E_\ell f(x)) \leq \frac{\partial V_\ell}{\partial x}(A_\ell x + E_\ell f(x))$. However, we know from (8.42) that $\frac{\partial V_\ell}{\partial x}(A_\ell x + E_\ell f(x)) < 0$. We now show that $V_j, j \in \mathcal{S}(x)$, decreases along the corresponding Filippov solution. For the extended model of the switched system including the sliding motion, formulated as*

$$\dot{x}(t) = \left(\sum_{\ell \in \mathcal{S}(x)} \theta_\ell A_\ell \right) x + \left(\sum_{\ell \in \mathcal{S}(x)} \theta_\ell E_\ell \right) f(x), \quad 0 \leq \theta_\ell, \quad \sum_{\ell \in \mathcal{S}(x)} \theta_\ell = 1, \quad (8.51)$$

we have

$$\begin{aligned} \frac{\partial V_j}{\partial x} \left[\left(\sum_{\ell \in \mathcal{S}(x)} \theta_\ell A_\ell \right) x + \left(\sum_{\ell \in \mathcal{S}(x)} \theta_\ell E_\ell \right) f(x) \right] = \\ \sum_{\ell \in \mathcal{S}(x)} \theta_\ell \frac{\partial V_j}{\partial x} (A_\ell x + E_\ell f(x)) \leq \sum_{\ell \in \mathcal{S}(x)} \theta_\ell \frac{\partial V_\ell}{\partial x} (A_\ell x + E_\ell f(x)) < 0, \end{aligned}$$

where the first inequality holds from $\frac{\partial V_j}{\partial x}(A_\ell x + E_\ell f(x)) \leq \frac{\partial V_\ell}{\partial x}(A_\ell x + E_\ell f(x))$ under a sliding mode, and the last inequality is justified using

$$\begin{bmatrix} x \\ f(x) \end{bmatrix}^T \begin{bmatrix} P_\ell A_\ell + A_\ell^T P_\ell & \star \\ E_\ell^T P_\ell + \Lambda A_\ell & \Lambda E_\ell + E_\ell^T \Lambda \end{bmatrix} \begin{bmatrix} x \\ f(x) \end{bmatrix} + \sum_{j=1}^N \mu_j \ell^T P_j x < 0,$$

which readily shows that for each active subsystem ℓ the derivative of the Lyapunov function V_ℓ is negative along the trajectories of the subsystem ℓ (we follow the same reasoning as for (8.42), see also [102]). Hence, we conclude that the derivative of the positive-definite function $V_j = x^T P_j x + 2 \sum_{i=1}^n \lambda_i \int_0^{x_i} f_i(\xi) d\xi$ is strictly negative along the trajectories of (8.51).

The optimization problem (8.43)–(8.45) involves solving a Bilinear Matrix Inequality (BMI) problem, which is in general computationally hard. Essentially, we have to deal with two types of issues:

1. Multiplication of the unknown Metzler elements $\mu_{j\ell}$ by P_ℓ .
2. The term $\mathcal{T}_\ell \mathcal{D}_\alpha \mathcal{D}_\beta$ in the upper left component of the matrix inequality (8.44) would prevent using any congruence transformation to transform (8.44) into an LMI. For instance, the nonlinearity caused by the term $P_\ell B_\ell K_\ell$ can be avoided by pre- and post-multiplication with P_ℓ^{-1} (and of course by defining new variables). However, by doing this, a new nonlinear term $P_\ell^{-1} \mathcal{T}_\ell \mathcal{D}_\alpha \mathcal{D}_\beta P_\ell^{-1}$ would be introduced.

For the first issue, we can limit our search for Metzler matrices to the cases in which the diagonal elements μ_{ii} are all equal to each other (as is also done in [49, 73, 75]). Later on, this choice will help us to transform (8.44) into an LMI, although it is a more conservative approach, in general.

For the second issue, we use a transformation that brings the nonlinear functions f_i in (8.1) into the sector $[0, 1]$. Using this transformation, we can eliminate the term $\mathcal{T}_\ell \mathcal{D}_\alpha \mathcal{D}_\beta$ from the upper left component of (8.44). The transformed system, with nonlinear functions \tilde{f}_i bounded in the sector $[0, 1]$, has the following structure:

$$\dot{x}(t) = \bar{A}_{\sigma(t)} x(t) + B_{\sigma(t)} u(t) + \bar{E}_{\sigma(t)} \tilde{f}(x(t)) + H_{\sigma(t)} \omega(t), \quad (8.52)$$

$$u(t) = \bar{K}_{\sigma(t)} x(t) + \bar{F}_{\sigma(t)} f(x), \quad (8.53)$$

$$y(t) = C_{\sigma(t)} g(x(t)), \quad (8.54)$$

with the following system matrices:

$$\begin{aligned} \bar{A}_{\sigma(t)} &= A_{\sigma(t)} + E_{\sigma(t)} \mathcal{D}_\alpha, & \bar{E}_{\sigma(t)} &= E_{\sigma(t)} \Gamma, \\ \bar{K}_{\sigma(t)} &= K_{\sigma(t)} + F_{\sigma(t)} \mathcal{D}_\alpha, & \bar{F}_{\sigma(t)} &= F_{\sigma(t)} \Gamma, \end{aligned} \quad (8.55)$$

where $\mathcal{D}_\alpha = \text{diag}\{\alpha_1, \dots, \alpha_n\}$, $\Gamma = \text{diag}\{\beta_1 - \alpha_1, \dots, \beta_n - \alpha_n\}$, and \tilde{f}_i defined as

$$\tilde{f}_i(x_i) = \frac{1}{\beta_i - \alpha_i} \left(f_i(x_i) - \alpha_i x_i \right). \quad (8.56)$$

Moreover, the Lyapunov function (8.34) has to be adapted to the transformed system. Therefore, we have

$$\bar{V}_\ell(x) = x^\top \bar{P}_\ell x + 2 \sum_{i=1}^n \bar{\lambda}_i \int_0^{x_i} \tilde{f}_i(\xi) d\xi, \quad (8.57)$$

where

$$\bar{P}_\ell = P_\ell + \text{diag}\{\alpha_1 \lambda_1, \dots, \alpha_n \lambda_n\}, \quad (8.58)$$

$$\bar{\lambda}_i = \lambda_i (\beta_i - \alpha_i). \quad (8.59)$$

It should be noted that this transformation does not introduce any conservatism. The following theorem provides the design tools for robust H_∞ control of the transformed switched system (8.52)–(8.54).

Theorem 8.5. *Suppose there exist positive definite matrices Q_ℓ and S_ℓ , positive diagonal matrices Z and U_ℓ , matrices W_ℓ, Y_ℓ , and scalar $\bar{\mu} < 0$, such that the following problem:*

$$\min_{\{Q_\ell\}_{\ell=1}^N, \{W_\ell\}_{\ell=1}^N, \{Y_\ell\}_{\ell=1}^N, \{S_\ell\}_{\ell=1}^N, \{U_\ell\}_{\ell=1}^N, Z, \rho, \bar{\mu}} \rho \quad (8.60)$$

subject to:

$$\begin{bmatrix} \bar{A}_\ell Q_\ell + Q_\ell \bar{A}_\ell^T + B_\ell W_\ell + W_\ell^T B_\ell^T + \bar{\mu} Q_\ell & * & * & * & * \\ \bar{A}_\ell Q_\ell + B_\ell W_\ell + Y_\ell^T B_\ell^T + Z \bar{E}_\ell^T + S_\ell & B_\ell Y_\ell + \bar{E}_\ell Z + Z \bar{E}_\ell^T + Y_\ell^T B_\ell^T - U_\ell & * & * & * \\ H_\ell^T & H_\ell^T & -\rho I & * & * \\ \|C_\ell\|_{\mathbb{F}} \Delta Q_\ell & 0 & 0 & -I & * \\ -\bar{\mu} Q_\ell & 0 & 0 & 0 & \bar{\mu} Q_\ell \end{bmatrix} < 0, \quad (8.61)$$

$$\begin{bmatrix} Q_\ell & Q_\ell \\ Q_\ell & \mathcal{D}_{\alpha, (1)}^{-1} (\mathcal{D}_\beta - \mathcal{D}_\alpha) Z \end{bmatrix} > 0, \quad \forall \ell, j \in \{1, \dots, N\}, \ell \neq j \quad (8.62)$$

has an optimal solution, then the switching rule

$$\bar{\sigma}(t) = \bar{r}(x(t)) = \arg \min_{\ell=1, \dots, N} \bar{V}_\ell(x(t)), \quad (8.63)$$

with $\bar{P}_\ell = Q_\ell^{-1}$ and $\bar{\Lambda} = Z^{-1}$, along with the state feedback control law

$$u(t) = \bar{K}_\ell x(t) + \bar{F}_\ell \bar{f}(x(t)), \quad (8.64)$$

with $\bar{K}_\ell = W_\ell Q_\ell^{-1}$, $\bar{F}_\ell = Y_\ell Z^{-1}$, make the closed-loop switched system (8.52)–(8.54) globally asymptotically stable in the absence of disturbances, and further, guarantee the minimized upper bound $\gamma = \sqrt{\bar{\rho}}$ for the L_2 -gain.

Proof. We use a backward reasoning approach. First, we consider a Metzler matrix with equal diagonal elements, i.e. $\mu_{ii} = \bar{\mu}$, $\bar{\mu} < 0$. This implies that $\bar{\mu}^{-1} \sum_{j=1, j \neq \ell}^N \mu_{j\ell} = 1$ (note that only $\bar{\mu}$ is preserved in the final optimization problem (8.60)–(8.62)). Taking this into account, the Schur complement is performed to (8.61) with respect to the last row and column. Multiplying the result by $\mu_{j\ell}$, summing up for all $j \neq \ell$ and multiplying by $\bar{\mu}^{-1}$ will yield

$$\begin{bmatrix} \bar{A}_\ell Q_\ell + Q_\ell \bar{A}_\ell^T + B_\ell W_\ell + W_\ell^T B_\ell^T + \sum_{j=1, j \neq \ell}^N \mu_{j\ell} (Q_\ell Q_j^{-1} Q_\ell - Q_\ell) & * & * & * \\ \bar{A}_\ell Q_\ell + B_\ell W_\ell + Y_\ell^T B_\ell^T + Z \bar{E}_\ell^T + S_\ell & B_\ell Y_\ell + \bar{E}_\ell Z + Z \bar{E}_\ell^T + Y_\ell^T B_\ell^T - U_\ell & * & * \\ H_\ell^T & H_\ell^T & -\rho I & * \\ \|C_\ell\|_{\mathbb{F}} \Delta Q_\ell & 0 & 0 & -I \end{bmatrix} < 0, \quad \forall \ell \in \{1, \dots, N\}. \quad (8.65)$$

Now, we pre- and post-multiply (8.65) by the matrix $\text{diag}\{Q_\ell^{-1}, Z^{-1}, I, I\}$ with $Q_\ell^{-1} = \bar{P}_\ell$, $Z^{-1} = \bar{\Lambda}$, and next, we change the variables $W_\ell Q_\ell^{-1} = \bar{K}_\ell$, $Y_\ell Z^{-1} = \bar{F}_\ell$, $S_\ell Q_\ell^{-1} = 0.5 \bar{\mathcal{T}}_\ell$, and finally $U_\ell Z^{-1} = \bar{\mathcal{T}}_\ell$. Furthermore, we assign a new matrix $\bar{\mathcal{T}}_\ell$ to be equal to the positive diagonal matrix $\bar{\Lambda} \bar{\mathcal{T}}_\ell$. Applying again the Schur complement to the resulting matrix with respect to the fourth row and column, rearranging terms and pre-multiplying by

$[x^T, \bar{f}^T(x), \omega^T]$ and post-multiplying by its transpose yields

$$\begin{aligned} & \begin{bmatrix} x \\ \bar{f}(x) \\ \omega \end{bmatrix}^T \underbrace{\begin{bmatrix} \bar{P}_\ell(\bar{A}_\ell + B_\ell \bar{K}_\ell) + (\bar{A}_\ell + B_\ell \bar{K}_\ell)^T \bar{P}_\ell & \star & \star \\ (\bar{E}_\ell + B_\ell \bar{F}_\ell)^T \bar{P}_\ell + \bar{\Lambda}(\bar{A}_\ell + B_\ell \bar{K}_\ell) & \bar{\Lambda}(\bar{E}_\ell + B_\ell \bar{F}_\ell) + (\bar{E}_\ell + B_\ell \bar{F}_\ell)^T \bar{\Lambda} & \star \\ H_\ell^T \bar{P}_\ell & H_\ell^T \bar{\Lambda} & 0 \end{bmatrix}}_{\frac{\partial \bar{V}_\ell}{\partial x}(\bar{A}_\ell x + B_\ell u + \bar{E}_\ell \bar{f}(x) + H_\ell \omega)} \begin{bmatrix} x \\ \bar{f}(x) \\ \omega \end{bmatrix} \\ & < \begin{bmatrix} x \\ \bar{f}(x) \end{bmatrix} \begin{bmatrix} 0 & \star \\ -\frac{1}{2} \mathcal{T}_\ell & \mathcal{T}_\ell \end{bmatrix} \begin{bmatrix} x \\ \bar{f}(x) \end{bmatrix} - \sum_{j=1}^N \mu_j \ell x^T \bar{P}_j x - \|C_\ell\|_{\mathbb{F}}^2 x^T \Delta^2 x + \rho \omega^T \omega. \end{aligned} \quad (8.66)$$

Now the final matrix inequality has the form of (8.61), but with $\alpha_i = 0, \beta_i = 1$ for the transformed system.

The positive-definiteness of the Lyapunov functions (8.34) defined for the original system should be preserved under the proposed transformation. Pre- and post-multiplying (8.62) by the diagonal matrix $\text{diag}\{Q_\ell^{-1}, I\}$, and then performing the Schur complement to the result, we obtain

$$\bar{P}_\ell - \mathcal{D}_{\alpha,(1)}(\mathcal{D}_\beta - \mathcal{D}_\alpha)^{-1} \bar{\Lambda} > 0, \quad (8.67)$$

since $Q_\ell^{-1} = \bar{P}_\ell$ and $Z^{-1} = \bar{\Lambda}$. Now we use the fact that $\mathcal{D}_\alpha = \text{diag}\{\alpha_i\}$ can be written as subtraction of two positive definite diagonal matrices, i.e. $\mathcal{D}_\alpha = \mathcal{D}_{\alpha,(1)} - \mathcal{D}_{\alpha,(2)}$. Therefore, (8.67) guarantees

$$\bar{P}_\ell - \mathcal{D}_\alpha(\mathcal{D}_\beta - \mathcal{D}_\alpha)^{-1} \bar{\Lambda} > 0. \quad (8.68)$$

On the other hand, using (8.58)–(8.59), we get

$$0 < \bar{P}_\ell - \mathcal{D}_\alpha(\mathcal{D}_\beta - \mathcal{D}_\alpha)^{-1} \bar{\Lambda} = P_\ell + \mathcal{D}_\alpha \Lambda - \mathcal{D}_\alpha(\mathcal{D}_\beta - \mathcal{D}_\alpha)^{-1}(\mathcal{D}_\beta - \mathcal{D}_\alpha) \Lambda = P_\ell. \quad (8.69)$$

Finally, adding and subtracting the term $\mathcal{D}_\alpha \Lambda$ from the condition $Q_\ell^{-1} = \bar{P}_\ell > 0$, yields

$$0 < \bar{P}_\ell - \mathcal{D}_\alpha \Lambda + \mathcal{D}_\alpha \Lambda = P_\ell + \mathcal{D}_\alpha \Lambda. \quad (8.70)$$

Condition (8.70) has the form of (8.18) which ensures positive-definiteness of Lyapunov functions (8.34). \square

Remark 8.5. Note that if the variable $\bar{\mu}$ is fixed, the optimization problem (8.60)–(8.62) can be efficiently solved by any LMI solver. However, the optimal value of $\bar{\mu}$ corresponding to the minimum gain $\gamma = \sqrt{\bar{\rho}}$ can be obtained by a line search method together with feasibility checking of an LMI.

Proposition 8.2. The switching law σ determined by (8.38) with

$$\lambda_i = (Z^{-1})_{ii} \cdot (\beta_i - \alpha_i)^{-1}, \quad (8.71)$$

$$P_\ell = Q_\ell^{-1} - Z^{-1} \cdot \text{diag}\left\{\frac{\alpha_1}{\beta_1 - \alpha_1}, \dots, \frac{\alpha_n}{\beta_n - \alpha_n}\right\}, \quad (8.72)$$

together with the state feedback control law (8.2) with gains

$$F_\ell = \bar{F}_\ell \Gamma^{-1}, \quad K_\ell = \bar{K}_\ell - F_\ell \mathcal{D}_\alpha \quad (8.73)$$

make the closed-loop switched system (8.1)–(8.3) globally asymptotically stable for $\omega \equiv 0$, and guarantee the upper bound γ for the L_2 -gain (obtained from optimization (8.60)–(8.62)) for disturbance signals that belong to the L_2 space. The proof follows directly from the relations between the system matrices of the original and the transformed system.

8.6. CASE STUDIES

In order to illustrate the performance of the proposed robust switching control approach and also to emphasize that other methods in the literature are not able to cope with the more general cases we discussed in this chapter, we present two examples in this section.

8.6.1. EXAMPLE 1

We choose an example of the switched nonlinear system (8.1)–(8.3) with the following nonlinear functions:

$$f_1(x_1) = \begin{cases} |\sin(x_1)| & -\pi < x_1 < \pi \\ 0 & \text{otherwise} \end{cases} \quad (8.74)$$

$$f_2(x_2) = \begin{cases} 2x_2 & 0 \leq x_2 \\ 0.5x_2 & 0 > x_2 \end{cases} \quad (8.75)$$

and the system matrices

$$A_1 = \begin{bmatrix} 4 & 1 \\ 2.3 & 3 \end{bmatrix}, A_2 = \begin{bmatrix} -2 & 1 \\ 2 & 4 \end{bmatrix}, A_3 = \begin{bmatrix} 2 & -1 \\ -7 & 4 \end{bmatrix} \quad (8.76)$$

$$E_1 = \begin{bmatrix} 2 & 8 \\ -3 & 1 \end{bmatrix}, E_2 = \begin{bmatrix} -3 & 5 \\ 0 & 2 \end{bmatrix}, E_3 = \begin{bmatrix} 4 & 8 \\ -1 & 1 \end{bmatrix}, \quad (8.77)$$

and $H_\ell = I_{2 \times 2}$, $B_\ell = [1, 1]^T$, $C_\ell = [1, 1]$. Moreover, $g_i(x_i) = x_i$ and the disturbance signals are taken as $\omega_1(t) = \omega_2(t) = 100$, for $0 \leq t \leq 1$, and otherwise equal to zero. Note that none of the subsystems has matrices with negative eigenvalues and hence all are not stable. Moreover, the function f_1 does not have an unbounded integral as it is required for the methods in [132] and [4]. On the other hand, since the function f_2 consists of linear functions with different slopes, our approach (which is able to cope with arbitrary sector bounds) would be less conservative in tackling the stability and control problem. Now following the design procedure in Theorem 8.5 with sector bounds $(\alpha_1, \beta_1) = (-1, 1)$ and $(\alpha_2, \beta_2) = (0.5, 2)$, the state feedback control law (8.2) along with the switching rule (8.38) make the equilibrium $x = 0$ globally asymptotically stable in the absence of disturbance. Using a line search method and the convex optimization problem (8.60)–(8.62) (solved using the Yalmip toolbox and the SeDuMi solver), the best value obtained for γ is 0.1318. Moreover, the obtained matrices for the Lyapunov functions are

$$P_1 = \begin{bmatrix} 10.3307 & -10.3314 \\ -10.3314 & 10.3323 \end{bmatrix}, P_2 = \begin{bmatrix} 9.4144 & -9.4169 \\ -9.4169 & 9.4197 \end{bmatrix} \\ P_3 = \begin{bmatrix} 11.4676 & -11.4666 \\ -11.4666 & 11.4658 \end{bmatrix}, \Lambda = \begin{bmatrix} 0.5078 & 0 \\ 0 & 0.2979 \end{bmatrix}$$

Furthermore, the resulting feedback gain matrices are

$$K_1 = 10^4 \cdot [4.8258 \quad -5.9892], F_1 = [4.6502 \quad -5.2399] \\ K_2 = 10^4 \cdot [4.2731 \quad -5.0686], F_2 = [1.6438 \quad -3.3400] \\ K_3 = 10^5 \cdot [-1.2504 \quad 1.0872], F_3 = [2.3197 \quad -4.6176]$$

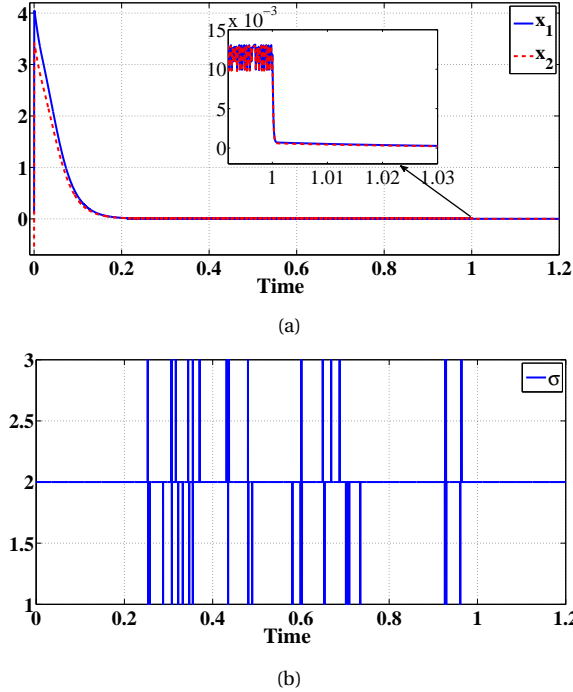


Figure 8.1: (a) State evolution of the closed-loop system, (b) Switching signal selecting the active subsystem

As depicted in Fig. 8.1, the designed switching control strategy is able to reduce the effects of severe disturbance signals influencing the system in the period $[0, 1]$ and furthermore, makes the closed-loop system stable. The response of the system contains oscillations with a very small amplitude, mainly because of function (8.74).

For the simulated example and the given disturbance inputs, the actual L_2 -gain calculated based on the simulation is 0.0529, which is indeed smaller than the upper bound $\gamma^* = 0.1318$.

8.6.2. EXAMPLE 2

In this section, the urban network case study discussed before in Section 7.5 of Chapter 7 is selected again. We will show that the MFD-based two-region model can be considered as a sector-bounded switched nonlinear system and therefore, we can take advantage of the proposed robust switching control design presented in this chapter.

SET-UP

First, we review the model's structure. For an urban network divided into two regions (as in Fig. 8.2): the periphery (region 1) and the city center (region 2), a hybrid MFD-based model is formulated as follows:

$$\dot{n}_1(t) = -G_{1,j}(n_1(t)) \cdot u(t) + \omega_1(t), \quad (8.78)$$

$$\dot{n}_2(t) = -G_{2,j}(n_2(t)) + G_{1,j}(n_1(t)) \cdot u(t) + \omega_2(t), \quad (8.79)$$

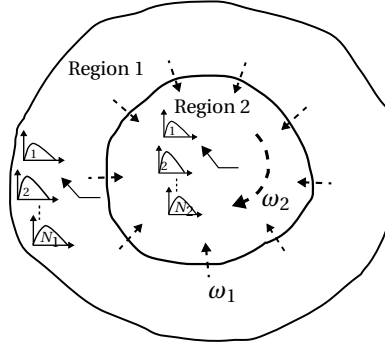


Figure 8.2: Schematic two-region urban network.

where $n_i(t)$, $i = 1, 2$, is the accumulation in region i at time t . The trip completion flow $G_{i,j}(n_i(t))$ (veh/s) is defined as the rate of vehicles reaching their destinations [71]. The timing plans for intersections inside each region can be altered. Consequently, instead of one MFD, a set of MFDs (each corresponding to a different timing plan) is defined. Therefore, $G_{i,j}$, with $j = 1, \dots, N_i$, constitute the MFDs for region i , with N_i the total number of MFDs (timing plans) defined for region i .

The perimeter control $u \in [0, 1]$ may restrict vehicles to transfer between regions (in our case, the flow of vehicles is restricted from region 1, the periphery, to region 2, the city center). The perimeter control can be realized by e.g. coordinating green and red durations of signalized intersections placed on the border between two regions.

We assume that each of the regions has three timing plans and therefore three MFDs ($N_1 = N_2 = 3$). Each MFD is modeled by an exponential function $G_{i,j}(n_2) = 1/3600 \cdot a_{i,j} \cdot n_i \cdot \exp(-1/2 \cdot (n_i/n_{i,cr,j})^2)$, $i \in \{1, 2\}$, $j \in \{1, \dots, 3\}$. The parameters used in our simulation are as follows:

$$G_{1,j}: a_{1,1} = 17.8 \text{ (1/h)}, a_{1,2} = 9.75 \text{ (1/h)}, a_{1,3} = 13 \text{ (1/h)}, n_{1,cr,j} = 3500 \text{ (veh)}$$

$$G_{2,j}: a_{2,j} = a_{1,j}/1.3, n_{2,cr,j} = n_{1,cr,j}/1.2$$

Furthermore, the perimeter control input u is assumed as to be a quantized input that can take values from the set $\{0.1, 0.3, 0.5, 0.7, 0.9\}$.

By quantizing the perimeter control input, the MFD-based model (8.78)–(8.79) can be reformulated in the format of the switched system (8.1)–(8.3). The quantized perimeter input introduces 5 modes. Each region is assumed to have 3 MFDs. Therefore, the total number of modes (subsystems) will be $3 \times 3 \times 5 = 45$. The resulting system matrices are as follows (we only mention E_1 ; for other subsystems the structure of the E matrix is the same, only the MFD coefficients $a_{i,j}$ and the value for the perimeter control input differ.):

$$A_\ell = 0, B_\ell = 0, H_\ell = \begin{bmatrix} 1 & 0 \\ 0 & 1 \end{bmatrix}, C_\ell = \begin{bmatrix} 1 & 0 \\ 0 & 1 \end{bmatrix}, \quad (8.80)$$

$$E_1 = \begin{bmatrix} -0.1 \cdot a_{1,1}/3600 & 0 \\ 0.1 \cdot a_{1,1}/3600 & -a_{2,1}/3600 \end{bmatrix}, \dots \quad (8.81)$$

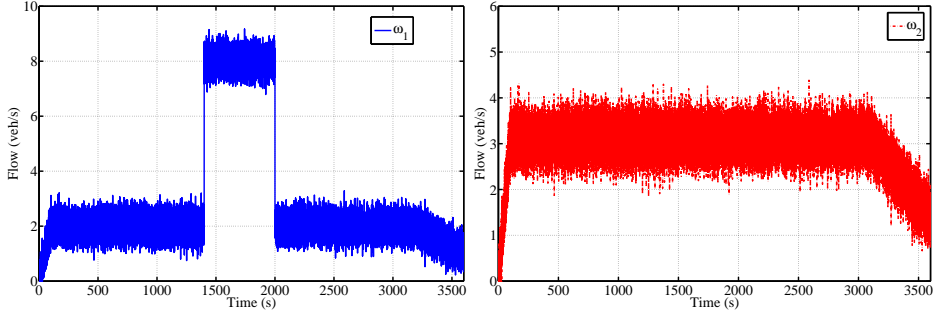


Figure 8.3: Trip demands: region 1 to 2 (ω_1), and inside region 2 (ω_2).

The sector bounded nonlinear function $f = [f_1, f_2]^T$ is

$$f = \left[n_1 \cdot \exp\left(-0.5\left(\frac{n_1}{n_{1,cr}}\right)^2\right), n_2 \cdot \exp\left(-0.5\left(\frac{n_2}{n_{2,cr}}\right)^2\right) \right]^T. \quad (8.82)$$

For the sector slopes we take $(\alpha_1, \beta_1) = (0.0168, 0.607)$ for f_1 and $(\alpha_2, \beta_2) = (0.0028, 0.655)$ for f_2 . Moreover, the output function g in (8.3) is $[n_1, n_2]^T$.

The assumed trip demands are depicted in Fig. 8.3. The uncertainty in the demands is modeled using zero mean white Gaussian noise with variance $0.2 \text{ (veh}^2/\text{s}^2)$ added to the average profiles. Moreover, we have included a sudden jump in ω_2 to evaluate the robustness of our control approach.

RESULTS AND DISCUSSION

The matrices of the Lyapunov functions along with the minimum upper bound for the L_2 -gain are determined *offline* by solving (8.60)–(8.62) using the Yalmip toolbox and the SeDuMi solver. For simulation, we use the model (8.78)–(8.79) along with the noisy demand profiles depicted in Fig. 8.3. The accumulations are measured and plugged into the switching law (8.38) to determine the active subsystem (and subsequently, to obtain the specific MFD and the proper perimeter control input). The converted control inputs are applied to the simulation model (used to represent the real traffic network). The obtained results are depicted in Fig. 8.4. As can be inferred from Fig. 8.4(a), the switching control stabilizes the system and also significantly reduce the effects of the trip demands (disturbances).

Moreover, in order to demonstrate the effectiveness of the proposed control strategy, the results are compared with two control strategies. In the first one, a greedy feedback controller is designed as follows: if the accumulation of the center is higher than the critical one, the perimeter control input is set to the minimum and otherwise to the maximum. Nine combinations are possible based on the number of MFDs defined for each region. In all cases, one or both regions end up in the gridlock situation. In Fig. 8.4(b), we have illustrated the performance of the greedy controller with MFDs $G_{1,1}$ and $G_{2,1}$ fixed for each region, respectively. In the second control strategy, we implement an MPC scheme based on the method presented in Chapter 4. For the prediction model, we use a discretized form of (8.78)–(8.79) with $T_s = 30 \text{ s}$ and $T_c = 60 \text{ s}$. Moreover, the MPC controller is supplied by the information about the average time evolution of the trip demands, i.e. without the additive noise and *without* the sudden jump.

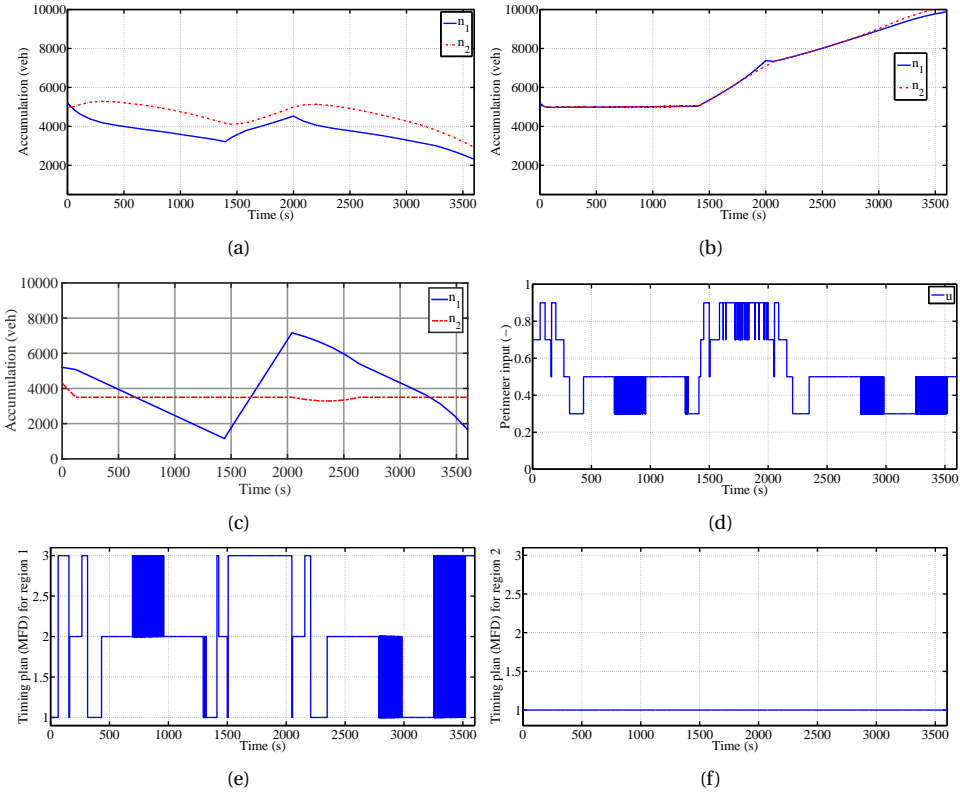


Figure 8.4: Accumulations: (a) Robust switching control, (b) greedy feedback controller, (c) MPC scheme. Converted control inputs from the designed switching signal: (d) perimeter signal, (e) switching between MFDs of region 1, (f) switching between MFDs of region 2.

As can be inferred from Fig. 8.4(a) and (c), the performance of the MPC scheme is better than the robust controller before the sudden jump in the trip demand ω_1 . However, since MPC does not have information about the jump, the congestion builds up again until the demand flow reduces to the lower level. Note that in the robust control case, there is also increase in the accumulations but it is less than in the MPC case. Furthermore, the best performance of the MPC scheme is achieved with $N_p = 30$ and $N_c = 2$ (further increasing N_p and N_c does not have considerable effects in this case).

Furthermore, the robust control strategy is computationally efficient (compared to MPC), as it only requires computing 45 Lyapunov functions and determining the index of the active sub-system during the simulation period. Moreover, setting the initial accumulations to zero, the actual L_2 -gain is $0.1237 \cdot 3600$ which is lower than the theoretical upper bound $0.1418 \cdot 3600$ obtained by solving optimization problem (8.60)–(8.62).

8.7. CONCLUDING REMARKS

In this chapter, we have considered stability analysis and H_∞ control for a class of switched nonlinear systems with general point symmetric sector conditions and with

arbitrary sector slopes. Combining multiple Lyapunov functions that contain both quadratic functions of the state and integrals of the nonlinearities of the system, we have formulated stability conditions under arbitrary switching in the form of matrix inequalities. Furthermore, the design of robust stabilizing controllers is proposed as a bi-level optimization problem where the high-level problem is non-convex in a single scalar variable only and the low-level problem is convex. This is a great advantage in contrast to the general case for switched nonlinear systems, which is based on searching for Lyapunov functions without a pre-defined structure and which involves solving multi-parametric optimization problems.

Possible extensions to the current work are 1) introducing different sector bounds for different quadrants to better characterize the sector-bounded nonlinear functions and to reduce the conservatism even more, 2) investigating the possibility of using polynomial Lyapunov functions [33] for stability analysis, and 3) calculating the largest sector bounds that ensure stability.

9

STABILIZATION AND ROBUST CONTROL FOR MIXED SWITCHING AFFINE SYSTEMS

This chapter presents stability analysis and robust H_∞ control for a general class of switched systems characterized by nonlinear functions. The proposed approach consists in approximating the switched nonlinear system with a switched affine system that has a mixture of controlled and autonomous switching behavior. Utilizing a joint polyhedral partitioning approach, we propose a stabilizing switching law based on quadratic Lyapunov functions and with taking into account the autonomous switching between polyhedral regions. In order to ensure the decrease of the overall Lyapunov function, we propose two approaches. The first method consists in guaranteeing continuity of the Lyapunov function over the boundaries of polyhedral regions. The second approach is based on relaxing the continuity requirement by using additional matrix inequalities. The second approach is less conservative but has more variables and matrix inequalities than the first method. If one scalar variable is fixed, the stabilization conditions will have the form of linear matrix inequalities (LMIs). Moreover, we extend the two proposed methods for robust H_∞ control. The design procedures result in bi-level optimization problems that are nonconvex only in a single scalar variable while the lower-level problems are convex. Furthermore, we present sufficient conditions for stabilizing the original switched nonlinear system using the proposed switching schemes. Finally, through several worked examples, we demonstrate the performance of the proposed stabilization and robust control methods.

9.1. INTRODUCTION

As discussed in the previous chapters, in contrast to the switched linear case, there is no concrete procedure for stability analysis and control of general nonlinear systems. Stability analysis for switched nonlinear systems has been investigated for particular cases only, e.g. for switched nonlinear systems with generalized homogeneous mappings [244], for a class of switched nonlinear systems with nonminimum phase modes [236], and for sector-bounded switched nonlinear systems [4, 93], as presented in Chapter 8. In [35, 55], a multiple Lyapunov functions approach is proposed for stability analysis under arbitrary switching and design of stabilizing controllers. However, as stated in [35], the difficult part is to search for suitable Lyapunov functions. Even if one manages to find a proper structure for the Lyapunov function candidates, the design procedure would in general involve solving multi-parametric optimization problems subject to nonlinear inequality constraints that have multiplication of matrices and state variables.

Therefore, in this chapter we aim at tackling the stability problem for switched nonlinear systems with smooth nonlinear functions using a different and novel framework. The main idea is to approximate each nonlinear subsystem with a piecewise affine function. In this way, we obtain a switched system composed of piecewise affine subsystems and a controllable switching signal that orchestrates the switching between PWA subsystems. Note that there also exists an autonomous type of switching between these affine functions of each PWA subsystem. This autonomous switching makes the stability analysis and control of such system a tedious task.

This chapter has four main contributions. The first contribution is the design of a stabilizing switching law for the mixed switched affine system. The design conditions are in the form of linear matrix inequalities. Compared to the existing min switching techniques [73, 74], which are based on the Metzler matrices, the proposed approach is less conservative. The key feature is to replace the elements of a Metzler matrix with matrix variables. This however comes at the price of introducing more variables in the stability conditions. The second contribution is to relax the continuity of the Lyapunov functions over the boundaries of partitions (which is essential for the methods proposed in [197, 204]) using additional linear matrix inequalities. The third contribution is the design of robust switching and state feedback controllers for reducing the effects of disturbances. The design procedure is formulated as a bi-level optimization problem that consists of line search on the higher level along with a convex optimization problem on the lower level. Finally, the last main contribution is to present sufficient conditions for which the proposed switching control schemes would be able to stabilize the original switched nonlinear system.

Stabilization of the mixed switched affine system is performed using multiple quadratic Lyapunov functions and a min switching strategy. However, as mentioned in [197], the decrease of the overall Lyapunov function should be ensured in order to obtain global asymptotic stability. To this aim, [197] parameterized the Lyapunov functions using matrices that define the boundary between polyhedral regions. In this way, the overall piecewise quadratic Lyapunov function will by construction be continuous over the boundaries of regions. Instead of doing that, in this work, we propose two approaches to either enforce continuity of the Lyapunov function on the boundary between regions, or to guarantee decrease of the overall Lyapunov function. In the first

approach, we use additional equality constraints to impose continuity over boundaries. This makes the design of robust state feedback controllers easy, since we do not limit the matrices of the Lyapunov function to take a particular structure [99, 197, 204]. In the second approach, we propose less conservative conditions in which the continuity of the Lyapunov function over the boundaries of the polyhedral regions is relaxed and instead, through additional inequality constraints, the decrease of the overall Lyapunov function is ensured.

Next, we further extend these two approaches to the joint design of stabilizing switching laws and state feedback controllers to attenuate the effects of disturbances on the switched system. Using linear matrix inequality (LMI) techniques, we formulate the design conditions in the form of an optimization problem that is non-convex in a single scalar variable only. The optimization problem can be recast as a convex optimization problem along with a line search on the single scalar variable.

Finally, the connection of the control scheme and the original switched nonlinear system is discussed. Since the design conditions are developed based on the approximated switched affine system, there might be a performance deterioration or even instability if the proposed controllers are connected to the switched nonlinear system. Therefore, sufficient conditions to guarantee stability of the original switched nonlinear system are determined based on the accuracy of the approximated switched affine system.

The chapter is organized as follows. In Section 9.2, we discuss the switched nonlinear system and the way it is approximated by a switched affine system with integrated autonomous and controlled switching. Section 9.3 presents two procedures for the design of stabilizing switching rules. In Section 9.4, we formulate the robust H_∞ control of the switched affine system. Stabilization of the original switched nonlinear system using the proposed switching control schemes is discussed in Section 9.5. Next, through several worked examples in Section 9.6, we illustrate the performance of the proposed stabilization and robust control methods. The chapter concludes with further discussion of the obtained results and remained challenges.

9.2. PROBLEM STATEMENT

Consider the following switched nonlinear system

$$\dot{x}(t) = f_{\sigma(t)}(x(t)) + G_{\sigma(t)}u(t) + H_{\sigma(t)}\omega(t), \quad (9.1)$$

$$y(t) = C_{\sigma(t)}x(t), \quad (9.2)$$

with $x \in \mathbb{R}^n$ the state, $u \in \mathbb{R}^{n_u}$ the control input, $\omega \in \mathbb{R}^{n_\omega}$ the disturbance input, and $y \in \mathbb{R}^{n_y}$ the output of the system. The switching signal is denoted by $\sigma(\cdot)$, which is assumed to be piecewise constant over time. The variable $\sigma(t)$ takes values from a pre-defined index set. In other words, for each value that $\sigma(t)$ assumes, the state space model (9.1)–(9.2) is governed by different vector functions f_i from the following set:

$$f_{\sigma(t)} \in \{f_1, \dots, f_N\} \quad (9.3)$$

A function $\phi : \Omega \rightarrow \mathbb{R}^m$ is PWA if there exists a polyhedral partition $\{\Omega_i\}_{i \in \mathcal{I}}$ ($\cup_{i \in \mathcal{I}} \Omega_i = \Omega$, $\Omega_i \neq \emptyset$, $\text{int}(\Omega_i) \cap \text{int}(\Omega_j) = \emptyset$, $\forall i \neq j$) of $\Omega \subseteq \mathbb{R}^n$ such that ϕ is affine on each polyhedron Ω_i . By considering a sufficiently large number of regions, one can smoothly ap-

proximate nonlinear functions f_i by PWA functions with arbitrary accuracy. The piecewise affine (PWA) approximation of f_i will have the following form:

$$f_i(x) \cong (A_{i,\ell} \cdot x + b_{i,\ell}), \quad \text{if } x \in \mathcal{X}_{i,\ell}, \quad (9.4)$$

with $A_{i,\ell} (n \times n)$ and $b_{i,\ell} (n \times 1)$, $\mathcal{X}_{i,\ell}$ the corresponding polyhedron, and $\ell \in \mathcal{M}_i = \{1, \dots, M_i\}$, with M_i the number of polyhedral partitions for the function f_i .

Now the switched system (9.1) can be approximated by the following switched affine system:

$$\dot{x}(t) = A_{\sigma(t),\ell} x(t) + b_{\sigma(t),\ell} + G_{\sigma(t)} u(t) + H_{\sigma(t)} \omega(t), \quad (9.5)$$

$$y(t) = C_{\sigma(t)} x(t), \quad \text{if } x \in \mathcal{X}_{\sigma(t),\ell}, \quad (9.6)$$

where the controlled switching signal σ takes values from the set $\mathcal{N} = \{1, \dots, N\}$, with N the total number of affine subsystems.

Note that two types of switching are integrated in (9.5), one associated with switching between affine functions describing the dynamics of each PWA subsystem i ; this type of switching is therefore uncontrolled, and the other one is the controlled switching between subsystems driven by σ . In the following sections, the focus is first on the stabilization and robust control of (9.5) and next, on connecting the obtained results to the stability problem for the original switched nonlinear system (9.1). Before proceeding, two useful lemmas from the literature are presented.

Lemma 9.1 (Finsler Lemma [128, 208]). *Let $x \in \mathbb{R}^n$, $Q \in \mathbb{R}^{n \times n}$ and $B \in \mathbb{R}^{m \times n}$ such that $\text{rank}(B) < n$. The following statements are equivalent:*

- $x^T Q x < 0, \quad \forall x \neq 0 \text{ such that } Bx = 0$
- $B^\perp{}^T Q B^\perp < 0$
- $\exists \lambda \in \mathbb{R} : Q - \lambda B^T B < 0$
- $\exists \zeta \in \mathbb{R}^{n \times m} : Q + \zeta B + B^T \zeta^T < 0$

where $B^\perp = 0$ is a basis for the null space of B , which means that each $x \neq 0$ such that $Bx = 0$ can be obtained as $x = B^\perp z$, for some $z \neq 0$.

Lemma 9.2 (Matrix Inversion Lemma [180]). *It can be easily proved that:*

$$(\mathcal{A} - \mathcal{B}\mathcal{D}^{-1}\mathcal{C})^{-1} = \mathcal{A}^{-1} + \mathcal{A}^{-1}\mathcal{B}(\mathcal{D} - \mathcal{C}\mathcal{A}^{-1}\mathcal{B})^{-1}\mathcal{C}\mathcal{A}^{-1} \quad (9.7)$$

for matrices $\mathcal{A}, \mathcal{B}, \mathcal{C}, \mathcal{D}$ with compatible dimensions and provided that all the inverses exist (see page 147 of [180] for the proof).

9.3. STABILIZATION USING STATE-BASED SWITCHING

The main aim is to drive the state of system (9.5), with $u, \omega \equiv 0$, to a desired state x_r . Given the desired state x_r and the switched system (9.5), the error system can be formulated as follows:

$$\dot{e}(t) = A_{\sigma(t),\ell} e(t) + q_{\sigma(t),\ell} + G_{\sigma(t)} u(t) + H_{\sigma(t)} \omega(t), \quad (9.8)$$

$$y_e(t) = C_{\sigma(t)} e(t), \quad \text{if } e \in \mathcal{E}_{\sigma(t),\ell} \quad (9.9)$$

$$e(t) = x(t) - x_r, \quad q_{\sigma(t),\ell} = b_{\sigma(t),\ell} + A_{\sigma(t),\ell} x_r.$$

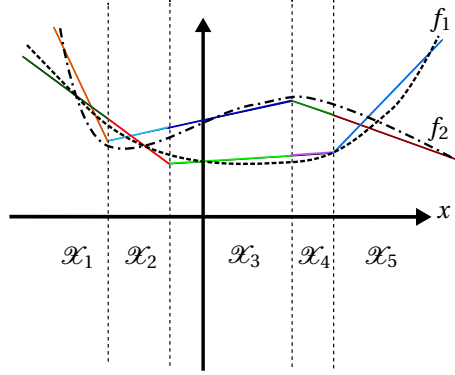


Figure 9.1: Example of the piecewise affine approximation of two nonlinear functions f_1 and f_2 .

Now the aim is re-defined as to design a switching rule that asymptotically steers the state of the error system to the origin.

Before proceeding with the main results, a joint partitioning of the state space is presented that helps with the design procedure. The main motivation is that the functions f_i in (9.1) may not all be approximated using the same number of affine functions and also, not with the same polyhedral regions. Therefore, as depicted in Fig. 9.1, even if the number of affine pieces is not the same for all nonlinear functions, we can split the affine functions in such a way that the number of affine functions will be identical for all nonlinear functions f_i and moreover, the polyhedral regions will be common for all piecewise affine subsystems. For instance, in Fig. 9.1, 5 polyhedral regions are defined and the number of affine functions approximating each nonlinear function f_i is extended to 5 in order to provide a common partitioning of the state space for all subsystems (note that each nonlinear function f_i is originally approximated by 3 affine functions but in order to create a common partition of the state space with same boundaries for both functions, the number of affine functions (and regions) is extended to 5). Since we provide a common partitioning for all subsystems, from now we use \mathcal{E}_ℓ instead of $\mathcal{E}_{\sigma(t),\ell}$.

Each polyhedral region \mathcal{E}_ℓ is characterized by:

$$F_\ell e + f_\ell \geq 0, \quad \text{iff } e \in \mathcal{E}_\ell, \tag{9.10}$$

where the inequality is element-wise. Further, (9.10) can be reformulated as follows:

$$\bar{F}_\ell \begin{bmatrix} e \\ 1 \end{bmatrix} \geq 0, \quad \bar{F}_\ell = [F_\ell \quad f_\ell]. \tag{9.11}$$

Furthermore, the boundary hyperplane for each pair of neighboring regions \mathcal{E}_ℓ and $\mathcal{E}_{\ell'}$ is represented by

$$h_{\ell\ell'}^\top e + g_{\ell\ell'} = 0 \Leftrightarrow \underbrace{\begin{bmatrix} h_{\ell\ell'}^\top & g_{\ell\ell'} \end{bmatrix}}_{\bar{h}_{\ell\ell'}^\top} \begin{bmatrix} e \\ 1 \end{bmatrix} = 0 \tag{9.12}$$

Moreover, for each polyhedral region $\mathcal{E}_\ell, \ell \in \mathcal{M} = \{1, \dots, M\}$, with M the total number of polyhedral regions (number of affine functions associated to each subsystem), the following auxiliary functions are defined:

$$V_{i,\ell}(e) = \begin{bmatrix} e \\ 1 \end{bmatrix}^T \underbrace{\begin{bmatrix} P_{i,\ell} & \star \\ s_{i,\ell}^T & r_{i,\ell} \end{bmatrix}}_{\tilde{P}_{i,\ell}} \underbrace{\begin{bmatrix} e \\ 1 \end{bmatrix}}_{\tilde{e}}, \quad \forall i \in \mathcal{N}, \forall \ell \in \mathcal{M}, \quad (9.13)$$

with $P_{i,\ell} \in \mathbb{R}^{n \times n}$ symmetric, $s_{i,\ell} \in \mathbb{R}^n$, and $r_{i,\ell} \in \mathbb{R}$. For each \mathcal{E}_ℓ , a Lyapunov function is proposed as follows:

$$\mathcal{V}_\ell(e) = \min_{i \in \mathcal{N}} V_{i,\ell}(e). \quad (9.14)$$

The following theorem presents the design procedure for a stabilizing switching rule that brings the state of the error system (9.8) to the origin, provided that at least for one subsystem $q_{i,\ell} = 0$ in the polyhedral regions containing the origin. This means that the desired state x_r is an (unstable or stable) equilibrium of at least one of the subsystems of (9.5).

Theorem 9.1. *Assume there exists at least one subsystem \hat{i} with $q_{\hat{i}} = 0$ in regions containing the origin. Moreover, suppose there exist symmetric matrices $P_{i,\ell}$ and $\mathcal{T}_{i,j,\ell}$, vectors $s_{i,\ell}, \zeta_{\ell\ell'}$, scalars $r_{i,\ell}$, and symmetric matrices U_ℓ, Z_ℓ with nonnegative elements that satisfy*

$$\begin{bmatrix} P_{i,\ell} A_{i,\ell} + A_{i,\ell}^T P_{i,\ell} & \star \\ s_{i,\ell}^T A_{i,\ell} + q_{i,\ell}^T P_{i,\ell} & q_{i,\ell}^T s_{i,\ell} + s_{i,\ell}^T q_{i,\ell} \end{bmatrix} - \sum_{j \in \mathcal{N}, j \neq i} \mathcal{T}_{i,j,\ell} + \tilde{F}_\ell^T U_\ell \tilde{F}_\ell < 0, \\ \forall (i, \ell) \in \{(i, \ell) \in \mathcal{N} \times \mathcal{M} \mid i \neq \hat{i}\} \cup \{(\hat{i}, \ell) \in \mathcal{N} \times \mathcal{M} \mid 0 \notin \mathcal{E}_\ell\}, \quad (9.15)$$

$$P_{i,\ell} A_{i,\ell} + A_{i,\ell}^T P_{i,\ell} - \sum_{j \in \mathcal{N}, j \neq \hat{i}} \mathcal{T}_{i,j,\ell} + F_\ell^T U_\ell F_\ell < 0, \quad \forall \ell \in \mathcal{M} : 0 \in \mathcal{E}_\ell, \quad (9.16)$$

$$\mathcal{T}_{i,j,\ell} < \mu_{\min} \cdot \left(\begin{bmatrix} P_{i,\ell} & \star \\ s_{i,\ell}^T & r_{i,\ell} \end{bmatrix} - \begin{bmatrix} P_{j,\ell} & \star \\ s_{j,\ell}^T & r_{j,\ell} \end{bmatrix} \right), \quad \forall i, j \in \mathcal{N}, i \neq j, \forall \ell \in \mathcal{M}, \quad (9.17)$$

$$\begin{bmatrix} P_{i,\ell} & \star \\ s_{i,\ell}^T & r_{i,\ell} \end{bmatrix} - \tilde{F}_\ell^T Z_\ell \tilde{F}_\ell > 0, \quad \forall i \in \mathcal{N}, \ell \in \mathcal{M}, \quad (9.18)$$

$$s_{\hat{i},\ell} = 0, \quad \forall \ell \in \mathcal{M} : 0 \in \mathcal{E}_\ell, \quad (9.19)$$

$$r_{\hat{i},\ell} < r_{j,\ell}, \quad \forall j \in \mathcal{N}, j \neq \hat{i}, \quad \forall \ell \in \mathcal{M} : 0 \in \mathcal{E}_\ell, \quad (9.20)$$

$$\begin{bmatrix} P_{i,\ell} & \star \\ s_{i,\ell}^T & r_{i,\ell} \end{bmatrix} = \begin{bmatrix} P_{i,\ell'} & \star \\ s_{i,\ell'}^T & r_{i,\ell'} \end{bmatrix} + \bar{h}_{\ell\ell'} \zeta_{\ell\ell'}^T + \zeta_{\ell\ell'} \bar{h}_{\ell\ell'}^T, \\ \forall \ell, \ell' \in \mathcal{M} : \mathcal{E}_\ell \cap \mathcal{E}_{\ell'} \neq \emptyset, \quad \forall i \in \mathcal{N}, \quad (9.21)$$

for a given positive scalar $\mu_{\min} > 0$. Then the switching rule¹

$$\sigma(t) = \arg \min_{i \in \mathcal{N}} V_{i,\ell}(e(t)), \quad \text{if } e(t) \in \mathcal{E}_\ell, \quad (9.22)$$

with $V_{i,\ell}$ defined as in (9.13), will asymptotically bring the state of the error system (9.8), with $u, \omega \equiv 0$, to the origin.

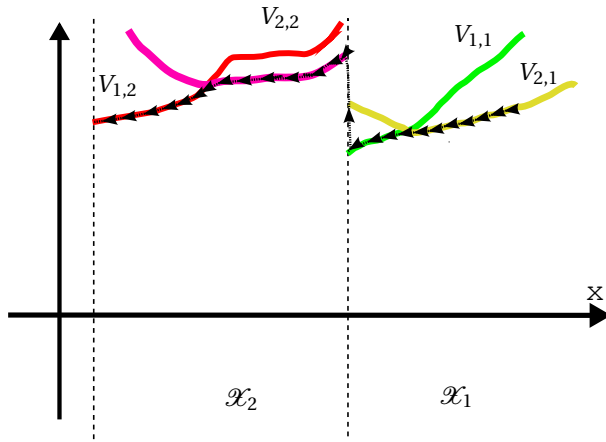


Figure 9.2: Example of increase in the Lyapunov function at the boundary between regions. The overall switched affine system might then become unstable.

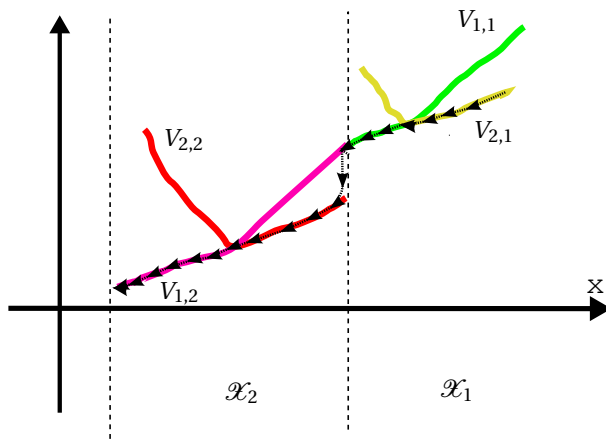


Figure 9.3: Example of preventing an increase in the overall Lyapunov function. At the boundary between regions \mathcal{X}_1 and \mathcal{X}_2 , the values of Lyapunov functions $V_{1,1}$ and $V_{1,2}$ coincide. Right after switching to region \mathcal{X}_2 , the switching rule (9.22) determines the minimum of the Lyapunov functions and switches to the corresponding subsystem.

Proof. Suppose that at an arbitrary time instant $t \geq 0$ and based on the polyhedral region ℓ in which the state of the error system resides, the switching law is given by $\sigma(t) = r(e(t)) = i$ for some $i \in \mathcal{I}_\ell(e) = \{i : \mathcal{V}_\ell(e) = V_{i,\ell}(e)\}$. Hence, following the definition of the Dini derivative [35, 64], for our error system (9.8), we have

$$\mathbf{D}^+(\mathcal{V}_\ell(e)) = \min_{j \in \mathcal{I}_\ell(e(t))} \left[\frac{\partial V_{j,\ell}}{\partial e} (A_{j,\ell}e + q_{j,\ell}) \right] \leq \frac{\partial V_{i,\ell}}{\partial e} (A_{i,\ell}e + q_{i,\ell}), \quad (9.23)$$

where i denotes the index of the active subsystem in region ℓ determined from (9.22). Pre-multiplying (9.15) by $[e^T, 1]$ and post-multiplying by its transpose, using (9.17) and also the fact that for the polyhedral region ℓ , (9.11) holds, and U_ℓ has nonnegative entries, we obtain

$$\underbrace{\begin{bmatrix} e \\ 1 \end{bmatrix}^T \begin{bmatrix} P_{i,\ell} A_{i,\ell} + A_{i,\ell}^T P_{i,\ell} & \star \\ s_{i,\ell}^T A_{i,\ell} + q_{i,\ell}^T P_{i,\ell} & q_{i,\ell}^T s_{i,\ell} + s_{i,\ell}^T q_{i,\ell} \end{bmatrix} \begin{bmatrix} e \\ 1 \end{bmatrix}}_{\frac{\partial V_{i,\ell}}{\partial e} (A_{i,\ell}e + q_{i,\ell})} < \sum_{j \in \mathcal{N}, j \neq i} \begin{bmatrix} e \\ 1 \end{bmatrix}^T \mathcal{T}_{i,j} \begin{bmatrix} e \\ 1 \end{bmatrix} - \begin{bmatrix} e \\ 1 \end{bmatrix}^T \bar{F}_\ell^T U_\ell \bar{F}_\ell \begin{bmatrix} e \\ 1 \end{bmatrix} < \begin{bmatrix} e \\ 1 \end{bmatrix}^T \sum_{j \in \mathcal{N}, j \neq i} \mu_{\min} \begin{bmatrix} P_{i,\ell} - P_{j,\ell} & \star \\ s_{i,\ell}^T - s_{j,\ell}^T & r_{i,\ell} - r_{j,\ell} \end{bmatrix} \begin{bmatrix} e \\ 1 \end{bmatrix} \quad (9.24)$$

Now since for the active subsystem i , $V_{i,\ell} \leq V_{j,\ell}, \forall j \neq i, j \in \{1, \dots, N\}$, the last inequality in (9.24) is less than zero, which means that the derivative of the Lyapunov function $V_{i,\ell}$ along the trajectory of the subsystem i in the polyhedral region ℓ is negative. The same procedure is applied to (9.16). Note that (9.16) provides the same condition as in (9.15) but with illuminating the rows and columns with zero elements. This condition guarantees that the derivative of the Lyapunov function $V_{i,\ell}$ would be zero only when the state e is zero and the value of the Lyapunov function is less than the other Lyapunov functions. Note that using the conditions (9.19) and (9.20) we ensure that the minimum of the overall Lyapunov function occurs at the origin and the derivative of the active Lyapunov function at the origin is zero.

Moreover, the Lyapunov functions (9.13) are not required to be positive definite in the entire space but only in the active polyhedral region. This is ensured using constraint (9.18) and it can be easily proved using (9.11).

In order to have global asymptotic stability, the decrease of the Lyapunov function inside the polyhedral regions is not enough. As depicted in Fig. 9.2, the overall Lyapunov function may increase over time and the state of the error system may then grow unboundedly. Therefore, we should connect the Lyapunov functions in neighboring polyhedral regions in such a way that the decrease in the overall Lyapunov function is ensured. One way to tackle this problem is to equalize the values of the Lyapunov functions \mathcal{V}_ℓ and $\mathcal{V}_{\ell'}$ for the boundary hyperplane of neighboring regions \mathcal{E}_ℓ and $\mathcal{E}_{\ell'}$. Note that at the boundary between polyhedral regions an uncontrolled switching between affine functions of the same subsystem i occurs². Therefore, we only need to connect the Lyapunov

¹Note that in (9.22), we take the minimum argument, in case there are multiple minima $V_{i,\ell}$.

²Note that the uncontrolled switching may occur between affine functions of the same subsystem, since we redefine and unify the partitions for all subsystems.

punov functions associated with each subsystem i at the boundary between neighboring regions ℓ and ℓ' . Hence, we need

$$\bar{e}^T \bar{P}_{i,\ell} \bar{e} = \bar{e}^T \bar{P}_{i,\ell'} \bar{e}, \quad \forall e: \bar{h}_{\ell\ell'}^T \bar{e} = 0 \quad (9.25)$$

In order to recast (9.25) as an LMI, we define auxiliary vectors $\zeta_{\ell\ell'}$ and combine the two equalities in (9.25) in the following way:

$$\bar{e}^T \bar{P}_{i,\ell} \bar{e} = \bar{e}^T \bar{P}_{i,\ell'} \bar{e} + \bar{e}^T \bar{h}_{\ell\ell'} \zeta_{\ell\ell'}^T \bar{e} + \bar{e}^T \zeta_{\ell\ell'} \bar{h}_{\ell\ell'}^T \bar{e}. \quad (9.26)$$

Since (9.26) should hold for all e , we can instead check the feasibility of the equality (9.21). \square

Remark 9.1. Note that in case there are multiple subsystems of (9.8) that have an equilibrium at the origin, we assign the index \hat{i} to one of them arbitrarily and check the feasibility of the conditions in Theorem 9.1. In case the conditions are found to be infeasible, we can assign the index \hat{i} to another subsystem and repeat the procedure.

Remark 9.2. In order to solve the LMIs (9.15)–(9.21), one should set a value for μ_{\min} . In fact, μ_{\min} is acting like a bound on the elements of a Metzler matrix. Instead of constraining the diagonal elements of a Metzler matrix to be identical (as is suggested in [35, 73]), we fix a lower bound for all the elements and moreover, we introduce auxiliary matrix variables $\mathcal{F}_{i,j,\ell}$. These two steps will make the approach less conservative. Hence, in order to solve the feasibility problem (9.15)–(9.21), one can set a value for μ_{\min} and next, solve the resulting LMIs.

Constraint (9.21) could be conservative in the sense that subsystem i in region ℓ might not become active right before the uncontrolled switching at the boundary between regions ℓ and ℓ' . Therefore, the following theorem is proposed in which constraint (9.21) is removed and instead, we impose constraints on the Lyapunov functions of the *active* subsystems at the boundary between polyhedral regions.

Theorem 9.2. Assume there exist symmetric matrices $P_{i,\ell}$, $\mathcal{F}_{i,j,\ell}$, $\mathcal{R}_{i,j,\ell}$, vectors $s_{i,\ell}$, $\zeta_{\ell\ell'}$, scalars $r_{i,\ell}$, $\beta_{\min} > 0$, $\mu_{\min} > 0$, and symmetric matrices U_ℓ , Z_ℓ with nonnegative elements that satisfy (9.15)–(9.20) and the following matrix inequalities:

$$\bar{P}_{i,\ell'} - \bar{P}_{j,\ell} - \mathcal{R}_{i,j,\ell} + \bar{h}_{\ell\ell'} \zeta_{\ell\ell'}^T + \zeta_{\ell\ell'} \bar{h}_{\ell\ell'}^T \leq 0, \quad (9.27)$$

$$\mathcal{R}_{i,j,\ell} < \beta_{\min} (\bar{P}_{i,\ell} - \bar{P}_{j,\ell}), \quad (9.28)$$

$$\forall i, j \in \mathcal{N}, i \neq j, \quad \forall \ell, \ell' \in \mathcal{M}: \mathcal{E}_\ell \cap \mathcal{E}_{\ell'} \neq \emptyset,$$

then the switching rule (9.22) with $V_{i,\ell}$ defined as in (9.13), will asymptotically bring the state of the error system (9.8) to the origin.

Proof. We consider a transition from region \mathcal{E}_ℓ to region $\mathcal{E}_{\ell'}$. Pre- and post-multiplying (9.27) and (9.28) by \bar{e}^T and by its transpose respectively, will result in

$$\begin{aligned} V_{i,\ell'} - V_{j,\ell} + \underbrace{\bar{e}^T \bar{h}_{\ell\ell'} \zeta_{\ell\ell'}^T \bar{e} + \bar{e}^T \zeta_{\ell\ell'} \bar{h}_{\ell\ell'}^T \bar{e}}_{=0, \text{ if } e \in \mathcal{E}_\ell \cap \mathcal{E}_{\ell'}} \bar{e} &\leq \bar{e}^T \mathcal{R}_{i,j,\ell} \bar{e} < \beta_{\min} (V_{i,\ell} - V_{j,\ell}), \quad \forall \ell, \ell' \in \mathcal{M}: \mathcal{E}_\ell \cap \mathcal{E}_{\ell'} \neq \emptyset \end{aligned} \quad (9.29)$$

Now if at the boundary between regions \mathcal{E}_ℓ and $\mathcal{E}_{\ell'}$, subsystem i is active, which means

$$\beta_{\min}(V_{i,\ell} - V_{j,\ell}) \leq 0, \quad \forall j \in \mathcal{N}, \quad (9.30)$$

then, due to (9.29), $V_{i,\ell'} \leq V_{j,\ell}$, $\forall j \in \mathcal{N}$. Hence, the value of the Lyapunov function $V_{i,\ell'}$ for the subsequent polyhedral region $\mathcal{E}_{\ell'}$ would be

$$V_{i,\ell'} \leq \min_{j \in \mathcal{N}, j \neq i} V_{j,\ell} \quad (9.31)$$

The same reasoning holds for moving from region $\mathcal{E}_{\ell'}$ to \mathcal{E}_ℓ . In contrast to condition (9.21), conditions (9.27)–(9.28) impose constraints only on the values of the Lyapunov functions of the *active* subsystems at the boundaries and moreover, these values no longer need to coincide with the ones of the respective subsystems in the previous regions.

In the end, based on (9.31) we can conclude that the overall Lyapunov function for the error system (9.8) will be decreasing and therefore, the error state would asymptotically approaches zero using the switching strategy (9.22). \square

Remark 9.3. *With fixed scalar variables μ_{\min} and β_{\min} , conditions (9.15)–(9.18) and (9.27)–(9.28) will become LMIs. Therefore, the overall feasibility problem can be solved using LMI solvers along with line search on μ_{\min} and β_{\min} .*

Remark 9.4. *The previous results are developed without taking into account the possible sliding modes inside polyhedral regions and/or on the boundaries. For inside the polyhedral regions we prove that even if a sliding mode occurs (as a result of switching between subsystems) it will be always stable. It can be shown that the time-derivative of the minimum Lyapunov function is strictly negative along the Filippov solution of the system (similar to the approach in Remark 2 of [73]), as follows ($0 \leq \theta_{i,\ell}$, $\sum_{i \in \mathcal{N}} \theta_{i,\ell} = 1$):*

$$\frac{\partial V_{j,\ell}}{\partial e} \sum_{i \in \mathcal{N}} \theta_{i,\ell} (A_{i,\ell} e + q_{i,\ell}) \leq \sum_{i \in \mathcal{N}} \theta_{i,\ell} \frac{\partial V_{i,\ell}}{\partial e} (A_{i,\ell} e + q_{i,\ell}) < 0, \quad \text{for } e \in \mathcal{E}_\ell, \quad (9.32)$$

where the last inequality is justified using the same reasoning as in (9.23) and (9.24), and the first inequality holds from the fact that under sliding mode a switching from subsystem j to subsystem i is allowed only if

$$\frac{\partial V_{j,\ell}}{\partial e} (A_{i,\ell} e + q_{i,\ell}) \leq \frac{\partial V_{i,\ell}}{\partial e} (A_{i,\ell} e + q_{i,\ell}). \quad (9.33)$$

However, if there exist attractive sliding modes on the boundaries of polyhedral regions, they should be taken into account in the stability analysis as it is also studied in [126] for PWA systems. Similar to the approach of [126], if there exists a sliding set \mathcal{S} of the following general form:

$$\mathcal{S} = \{e \mid \Phi \bar{e} \geq 0 \wedge \Psi \bar{e} = 0\}, \quad (9.34)$$

with Φ and Ψ the matrices characterizing the sliding set, then for neighboring polyhedral regions \mathcal{E}_ℓ and $\mathcal{E}_{\ell'}$ with $\mathcal{E}_\ell \cap \mathcal{S} \neq \emptyset$, $\mathcal{E}_{\ell'} \cap \mathcal{S} \neq \emptyset$, we need to have

$$\frac{\partial V_{i,\ell}}{\partial e} (A_{i,\ell'} e + q_{i,\ell'}) < 0, \quad \forall e \in \mathcal{S}, \quad \forall i \in \mathcal{N}, \quad (9.35)$$

in order to ensure the stability of the Filippov solutions. Since the uncontrolled switching at the boundaries occurs only for the affine functions of the same subsystem, therefore in (9.35) we require the negativeness of $V_{i,\ell}$ only on the trajectories of the same subsystem i in the neighboring region ℓ' . Using the S -procedure and the Finsler Lemma, the following LMIs can be established:

$$\bar{P}_{i,\ell} \bar{A}_{i,\ell'} + \bar{A}_{i,\ell'}^T \bar{P}_{i,\ell} + \Phi^T \Lambda_{i,\ell,\ell'} \Phi + \eta_{i,\ell,\ell'} \Psi^T \Psi < 0, \quad \forall i \in \mathcal{N}, \forall \ell, \ell' \in \mathcal{M}, \quad (9.36)$$

with $\Lambda_{i,\ell,\ell'}$ symmetric matrices with nonnegative elements, and $\eta_{i,\ell,\ell'}$ scalar multipliers.

9.4. ROBUST SWITCHING CONTROL DESIGN FOR L_2 -GAIN MINIMIZATION

In the previous section, we have discussed the stabilization problem for the switched system (9.8)–(9.9) using only the controlled switching signal σ . In this section, we synthesize switching laws together with the state feedback control input u in order to asymptotically stabilize the error system and moreover, to minimize the effects of the disturbance ω on the output y_e (note that the extension of Theorems 9.1 and 9.2 for robust H_∞ control of (9.5) using only the switching signal σ would be straightforward and it is skipped for presentation in this chapter).

We assume that the disturbance vector ω belongs to the space of square integrable functions, i.e. the L_2 space. The switched system is said to have L_2 -gain bounded above by $\gamma > 0$ under some switching law σ if the L_2 -norm of the output is bounded by $\|y_e\|_{L_2[0,T]} \leq \gamma \|\omega\|_{L_2[0,T]}$ for all nonzero ω that belong to the L_2 -space and for initial condition $x(0) = 0$ (to eliminate the transient response caused by nonzero initial conditions). The following two theorems provide the design procedure to achieve the goals mentioned above. Note that the desired state x_r does not have to be an equilibrium of any of the subsystems.

Note that in the following theorems we use the augmented system matrices and vectors defined as follows [197]:

$$\bar{A}_{i,\ell} = \begin{bmatrix} A_{i,\ell} & q_{i,\ell} \\ 0_{1 \times n} & 0 \end{bmatrix}, \quad \bar{G}_i = \begin{bmatrix} G_i \\ 0_{1 \times n_u} \end{bmatrix}, \quad \bar{H}_i = \begin{bmatrix} H_i \\ 0_{1 \times n_\omega} \end{bmatrix}, \quad \bar{C}_i = [C_i \quad 0_{n_y \times 1}] \quad (9.37)$$

Theorem 9.3. Assume there exist symmetric matrices $Q_{i,\ell}$, $\mathcal{T}_{i,j,\ell}$, positive definite matrices W_ℓ, R_ℓ with nonpositive off-diagonal elements, and scalars $\lambda_{\ell\ell'}$ such that the convex optimization problem

$$\begin{aligned} & \min \gamma & (9.38) \\ & \text{s.t.} \\ & \left[\begin{array}{ccc} \bar{A}_{i,\ell} Q_{i,\ell} + Q_{i,\ell} \bar{A}_{i,\ell}^T + \bar{G}_i Y_{i,\ell} + Y_{i,\ell}^T \bar{G}_i^T - \sum_{j \in \mathcal{N}, j \neq i} \mathcal{T}_{i,j,\ell} & \star & \star & \star \\ & \bar{H}_i^T & -\gamma I & \star & \star \\ & \bar{C}_i Q_{i,\ell} & 0 & -I & \star \\ & \bar{F}_\ell Q_{i,\ell} & 0 & 0 & -W_\ell \end{array} \right] < 0, \\ & \forall (i, \ell) \in \{(i, \ell) \in \mathcal{N} \times \mathcal{M} \mid i \neq \hat{i}\} \cup \{(\hat{i}, \ell) \in \mathcal{N} \times \mathcal{M} \mid 0 \notin \mathcal{E}_\ell\}, & (9.39) \end{aligned}$$

$$\begin{bmatrix} A_{\hat{i},\ell}Q_{\hat{i},\ell} + Q_{\hat{i},\ell}A_{\hat{i},\ell}^T + G_{\hat{i}}Y_{\hat{i},\ell} + Y_{\hat{i},\ell}^T G_{\hat{i}}^T - \sum_{j \in \mathcal{N}, j \neq \hat{i}} \mathcal{T}_{\hat{i},j,\ell} & \star & \star & \star \\ & H_{\hat{i}}^T & & \\ & C_{\hat{i}} & & \\ & F_{\ell}Q_{\hat{i},\ell} & & \end{bmatrix} < 0, \quad \forall \ell \in \mathcal{M} : 0 \in \mathcal{E}_{\ell}, \quad (9.40)$$

$$\begin{bmatrix} Q_{i,\ell} - \mu_{\min}^{-1} \mathcal{T}_{i,j,\ell} & \star \\ Q_{i,\ell} & Q_{j,\ell} \end{bmatrix} > 0, \quad \forall i, j \in \mathcal{N}, i \neq j, \forall \ell \in \mathcal{M}, \quad (9.41)$$

$$\begin{bmatrix} Q_{i,\ell} & \star \\ \bar{F}_{\ell}Q_{i,\ell} & R_{\ell} \end{bmatrix} > 0, \quad \forall i \in \mathcal{N}, \forall \ell \in \mathcal{M}, \quad (9.42)$$

$$\begin{bmatrix} Q_{i,\ell} & \star \\ F_{\ell}Q_{i,\ell} & R_{\ell} \end{bmatrix} > 0, \quad \forall \ell \in \mathcal{M} : 0 \in \mathcal{E}_{\ell}, \quad (9.43)$$

$$\begin{bmatrix} Q_{i,\ell'} - Q_{i,\ell} & \star \\ \bar{h}_{\ell'\ell}^T Q_{i,\ell} & -(\lambda_{\ell'\ell} - \bar{h}_{\ell'\ell}^T Q_{i,\ell} \bar{h}_{\ell'\ell}) \end{bmatrix} \geq 0, \quad (9.44)$$

$$\begin{bmatrix} Q_{i,\ell'} & \star & \star \\ Q_{i,\ell'} & Q_{i,\ell} & \star \\ \bar{h}_{\ell'\ell}^T Q_{i,\ell'} & 0 & \lambda_{\ell'\ell} \end{bmatrix} \geq 0, \quad \forall \ell, \ell' \in \mathcal{M} : \mathcal{E}_{\ell} \cap \mathcal{E}_{\ell'} \neq \emptyset, \quad \forall i \in \mathcal{N}, \quad (9.45)$$

$$\begin{aligned} W_{\ell}, R_{\ell} > 0, (W_{\ell})_{ij} \leq 0, (R_{\ell})_{ij} \leq 0, & \quad \forall i, j \in \mathcal{N}, i \neq j, \forall \ell \in \mathcal{M}, \\ Q_{i,\ell} > 0, \mu_{\min} > 0, \lambda_{\ell'\ell} > 0, \gamma > 0, & \quad \forall i \in \mathcal{N}, \forall \ell, \ell' \in \mathcal{M}, \ell \neq \ell' \end{aligned}$$

with \hat{i} the index of an arbitrary selected subsystem, has an optimal solution $\gamma^* > 0$ for a given positive scalar $\mu_{\min} > 0$, then the switching rule (9.22) with matrices

$$\bar{P}_{i,\ell} = Q_{i,\ell}^{-1}, \quad \forall (i, \ell) \in \{(i, \ell) \in \mathcal{N} \times \mathcal{M} | i \neq \hat{i}\} \cup \{(\hat{i}, \ell) \in \mathcal{N} \times \mathcal{M} | 0 \notin \mathcal{E}_{\ell}\} \quad (9.46)$$

and

$$P_{\hat{i},\ell} = Q_{\hat{i},\ell}^{-1}, \quad \forall \ell \in \mathcal{M} : 0 \in \mathcal{E}_{\ell}, \quad (9.47)$$

with $V_{\hat{i},\ell}(e) = e^T P_{\hat{i},\ell} e$, and the state feedback control laws $u_{i,\ell} = K_{i,\ell} \bar{e}$ with gains

$$K_{i,\ell} = Y_{i,\ell} Q_{i,\ell}^{-1}, \quad \forall (i, \ell) \in \{(i, \ell) \in \mathcal{N} \times \mathcal{M} | i \neq \hat{i}\} \cup \{(\hat{i}, \ell) \in \mathcal{N} \times \mathcal{M} | 0 \notin \mathcal{E}_{\ell}\} \quad (9.48)$$

and

$$u_{\hat{i},\ell} = Y_{\hat{i},\ell} Q_{\hat{i},\ell}^{-1} e + k_{\hat{i},\ell}, \quad \forall \ell \in \mathcal{M} : 0 \in \mathcal{E}_{\ell}, \quad (9.49)$$

with $k_{\hat{i},\ell}$ a solution of $q_{\hat{i},\ell} + G_{\hat{i},\ell} k_{\hat{i},\ell} = 0$, stabilize the system (9.8)–(9.9) and moreover ensure an upper bound $\sqrt{\gamma^*}$ for the L_2 -gain of the system from the disturbance input w to the output y_e .

Proof. First, the Schur complement is performed on (9.41) with respect to the second row and column. Next, the result is multiplied from both sides by $Q_{i,\ell}^{-1} = \bar{P}_{i,\ell}$ and $Q_{j,\ell}^{-1}$ is replaced by $\bar{P}_{j,\ell}$. This yields

$$\bar{P}_{i,\ell} \mathcal{T}_{i,j,\ell} \bar{P}_{i,\ell} < \mu_{\min} (\bar{P}_{i,\ell} - \bar{P}_{j,\ell}). \quad (9.50)$$

Similarly, by performing the Schur complement and substituting the matrices in (9.42) we obtain (9.18) with $R_\ell^{-1} = Z_\ell$ (note that in case the subsystem i^* is involved and $\ell : 0 \in \mathcal{E}_\ell$, then sizes of the matrices must be adjusted by appropriate addition of zero elements in rows and columns). Note that the inverse of R_ℓ is a matrix with nonnegative elements (which is necessary for the condition (9.18)), since R_ℓ is a positive definite matrix with nonpositive off-diagonal elements (The inverse of a real symmetric positive definite matrix with nonpositive off-diagonal elements, as known as a Stieltjes matrix, is a nonsingular matrix with nonnegative elements [79]).

On the other hand, we perform the Schur complement on (9.39) 2 times, each time with respect to the last row and column. Next, we pre- and post-multiply the result by $Q_{i,\ell}^{-1} = \bar{P}_{i,\ell}$, change the variables $Y_{i,\ell} Q_{i,\ell}^{-1} = K_{i,\ell}$, rearrange the terms, and finally multiply both sides by $[\bar{e}^T, \omega^T]$ and its transpose. Using (9.50) and (9.10), we obtain

$$\begin{aligned} & \begin{bmatrix} \bar{e} \\ \omega \end{bmatrix}^T \begin{bmatrix} \bar{P}_{i,\ell}(\bar{A}_{i,\ell} + \bar{G}_i K_{i,\ell}) + (\bar{A}_{i,\ell} + \bar{G}_i K_{i,\ell})^T \bar{P}_{i,\ell} & \star \\ \bar{H}_i^T \bar{P}_{i,\ell} & 0 \end{bmatrix} \begin{bmatrix} \bar{e} \\ \omega \end{bmatrix} \\ & < \sum_{j \in \mathcal{N}, j \neq i} \bar{e}^T \mathcal{F}_{i,j,\ell} \bar{e} - \bar{e}^T \bar{F}_\ell^T W_\ell^{-1} \bar{F}_\ell \bar{e} - y_e^T y_e + \gamma \omega^T \omega \\ & < \mu_{\min} \sum_{j \in \mathcal{N}, j \neq i} (V_{i,\ell} - V_{j,\ell}) - y_e^T y_e + \gamma \omega^T \omega. \end{aligned} \quad (9.51)$$

Since for the active subsystem i in region ℓ , $V_{i,\ell} \leq V_{j,\ell}$, $\forall j \in \mathcal{N}$, we finally have

$$\mathbf{D}^+(\mathcal{V}_\ell(e(t))) < -y_e^T y_e + \gamma \omega^T \omega. \quad (9.52)$$

The same procedure is applied to (9.40). Note that since we select the constant part $k_{i,\ell}$ of the feedback input as a solution of $q_{i,\ell} + G_{i,\ell} k_{i,\ell} = 0$, the affine part of the system dynamics is vanished and therefore, the derivative of $V_{i,\ell}$ along the trajectories of the closed-loop system \hat{i} will be $e^T P_{i,\ell} (A_{i,\ell} + G_{i,\ell} Y_{i,\ell} Q_{i,\ell}^{-1}) + (A_{i,\ell} + G_{i,\ell} Y_{i,\ell} Q_{i,\ell}^{-1})^T P_{i,\ell} e$, where $P_{i,\ell} = Q_{i,\ell}^{-1}$.

Moreover, we show that the continuity of the overall Lyapunov function is preserved through the conditions (9.44) and (9.45). Applying the Schur complement to the last row and column of (9.44) and using Lemma 9.2 results in (note that in case the subsystem i^* is involved and $\ell : 0 \in \mathcal{E}_\ell$, then sizes of the matrices must be adjusted by appropriate addition of zero elements in rows and columns)

$$\begin{aligned} & Q_{i,\ell'} - Q_{i,\ell} + Q_{i,\ell} \bar{h}_{\ell\ell'} (\lambda_{\ell\ell'} - \bar{h}_{\ell\ell'}^T Q_{i,\ell} \bar{h}_{\ell\ell'})^{-1} \bar{h}_{\ell\ell'}^T Q_{i,\ell} \geq 0 \\ & \Rightarrow Q_{i,\ell'} + Q_{i,\ell} \left(\underbrace{-Q_{i,\ell}^{-1}}_{\mathcal{A}^{-1}} + \underbrace{Q_{i,\ell}^{-1} Q_{i,\ell} \bar{h}_{\ell\ell'}}_{\mathcal{B}} \left(\underbrace{\lambda_{\ell\ell'} - \bar{h}_{\ell\ell'}^T Q_{i,\ell} Q_{i,\ell}^{-1} Q_{i,\ell} \bar{h}_{\ell\ell'}}_{\mathcal{D}^{-1}} \right)^{-1} \underbrace{\bar{h}_{\ell\ell'}^T Q_{i,\ell} Q_{i,\ell}^{-1}}_{\mathcal{C}} \right) Q_{i,\ell} \geq 0 \\ & \xrightarrow{\text{Lemma 9.2}} Q_{i,\ell'} + Q_{i,\ell} \left(-Q_{i,\ell} - Q_{i,\ell} \bar{h}_{\ell\ell'} \lambda_{\ell\ell'} \bar{h}_{\ell\ell'}^T Q_{i,\ell} \right)^{-1} Q_{i,\ell} \geq 0 \\ & \Rightarrow Q_{i,\ell'} - Q_{i,\ell} \left(Q_{i,\ell} + Q_{i,\ell} \bar{h}_{\ell\ell'} \lambda_{\ell\ell'}^{-1} \bar{h}_{\ell\ell'}^T Q_{i,\ell} \right)^{-1} Q_{i,\ell} \geq 0 \\ & \Rightarrow \begin{bmatrix} Q_{i,\ell} + Q_{i,\ell} \bar{h}_{\ell\ell'} \lambda_{\ell\ell'}^{-1} \bar{h}_{\ell\ell'}^T Q_{i,\ell} & Q_{i,\ell} \\ Q_{i,\ell} & Q_{i,\ell'} \end{bmatrix} \geq 0 \\ & \Rightarrow Q_{i,\ell} + Q_{i,\ell} \bar{h}_{\ell\ell'} \lambda_{\ell\ell'}^{-1} \bar{h}_{\ell\ell'}^T Q_{i,\ell} - Q_{i,\ell} Q_{i,\ell'}^{-1} Q_{i,\ell} \geq 0 \end{aligned} \quad (9.53)$$

Pre- and post-multiplying (9.53) by $Q_{i,\ell}^{-1} = \bar{P}_{i,\ell}$ yields

$$\bar{P}_{i,\ell'} - \bar{P}_{i,\ell} - \lambda_{\ell\ell'}^{-1} \bar{h}_{\ell\ell'} \bar{h}_{\ell\ell'}^T \leq 0. \quad (9.54)$$

Now pre- and post-multiplying the result by \bar{e}^T and its transpose and using Lemma 9.1, we obtain

$$V_{i,\ell'} \leq V_{i,\ell} \quad \text{when} \quad \bar{h}_{\ell\ell'}^T \bar{e} = 0. \quad (9.55)$$

On the other hand, applying the Schur complement twice to (9.45) with respect to the last column and row, and then pre- and post-multiplying the result by $Q_{i,\ell'}^{-1} = \bar{P}_{i,\ell'}$ and assigning $Q_{i,\ell}^{-1} = \bar{P}_{i,\ell}$ yields (note that in case the subsystem i^* is involved and $\ell : 0 \in \mathcal{E}_\ell$, then sizes of the matrices must be adjusted by appropriate addition of zero elements in rows and columns)

$$\bar{P}_{i,\ell'} - \bar{P}_{i,\ell} - \lambda_{\ell\ell'}^{-1} \bar{h}_{\ell\ell'} \bar{h}_{\ell\ell'}^T \geq 0. \quad (9.56)$$

Now pre- and post-multiplying (9.56) by \bar{e}^T and its transpose and using the Finsler Lemma, results

$$V_{i,\ell'} \geq V_{i,\ell} \quad \text{when} \quad \bar{h}_{\ell\ell'}^T \bar{e} = 0. \quad (9.57)$$

Finally, (9.55) and (9.57) imply that the values of the Lyapunov functions $V_{i,\ell}$ and $V_{i,\ell'}$ should coincide at the boundary between the neighboring regions \mathcal{E}_ℓ and $\mathcal{E}_{\ell'}$.

The overall Lyapunov function is continuous over the boundaries between the polyhedral regions. Moreover, in the origin, the Lyapunov function has its minimum value, i.e. $V_{\hat{i},\ell}(0) = 0$ and the derivative the Lyapunov function is also zero because the state feedback input $u_{\hat{i},\ell}$ makes the closed loop subsystem linear ($q_{\hat{i},\ell} + G_{\hat{i},\ell} k_{\hat{i},\ell} = 0$). Further, it is assumed that the initial state is zero and $V(e(0)) = 0$. The reason for this assumption is to eliminate the transient response of the system due to nonzero initial conditions. Now since asymptotic stability implies $V(e(\infty)) = 0$, using (9.52) we obtain $\|y_e\|_2 \leq \gamma \|\omega\|_2$. \square

Remark 9.5. *In order to obtain the lowest value for γ , one can assign the index \hat{i} each time to one subsystem, solves the optimization problem in Theorem 9.3 based on this selection, and in the end, compare the minimum values γ^* obtained from solving the optimization problems and use the corresponding solution for state feedback and switching laws.*

Remark 9.6. *The optimization problem (9.38)–(9.45) can be recast as a bi-level optimization problem in which on the higher level a line search on μ_{\min} is performed, while on the lower level a convex optimization problem subject to LMI constraints (with fixed μ_{\min}) is solved.*

The next theorem presents a less conservative approach to ensure the overall decrease in the Lyapunov function. This comes at the price of adding more conditions that involve bilinear matrix inequalities and gridding on one variable.

Theorem 9.4. *Assume there exist symmetric matrices $Q_{i,\ell}$, $\mathcal{T}_{i,j,\ell}$, $\mathcal{S}_{i,j,\ell}$, positive definite matrices W_ℓ, R_ℓ with nonpositive off-diagonal elements, and scalars $\lambda_{\ell\ell'}$, $\mu_{\min} > 0$,*

$\beta_{\min} > 0$, such that the optimization problem (9.38)–(9.42) with additional constraints formulated as follows:

$$\begin{bmatrix} \beta_{\min} Q_{i,\ell} & \star & \star \\ Q_{i,\ell} & \beta_{\min}^{-1} Q_{i,\ell} & \star \\ 0 & \beta_{\min}^{-1} Q_{j,\ell} & \mathcal{S}_{i,j,\ell} + \beta_{\min}^{-1} Q_{j,\ell} \end{bmatrix} > 0, \quad (9.58)$$

$$\begin{bmatrix} Q_{j,\ell} & \star & \star & \star \\ \bar{h}_{\ell\ell'}^{-1} Q_{j,\ell} & \lambda_{\ell\ell'} & \star & \star \\ Q_{j,\ell} & 0 & Q_{i,\ell'} & \star \\ 0 & 0 & Q_{i,\ell'} & Q_{i,\ell'} - \mathcal{S}_{i,j,\ell} \end{bmatrix} > 0, \quad (9.59)$$

$$\forall i, j \in \mathcal{N}, i \neq j, \quad \forall \ell, \ell' \in \mathcal{M} : \mathcal{E}_\ell \cap \mathcal{E}_{\ell'} \neq \emptyset$$

has an optimal solution $\gamma^* > 0$, then the switching rule (9.22) with matrices

$$\bar{P}_{i,\ell} = Q_{i,\ell}^{-1}, \quad \forall (i, \ell) \in \{(i, \ell) \in \mathcal{N} \times \mathcal{M} \mid i \neq \hat{i}\} \cup \{(\hat{i}, \ell) \in \mathcal{N} \times \mathcal{M} \mid 0 \notin \mathcal{E}_\ell\} \quad (9.60)$$

and

$$P_{\hat{i},\ell} = Q_{\hat{i},\ell}^{-1}, \quad \forall \ell \in \mathcal{M} : 0 \in \mathcal{E}_\ell, \quad (9.61)$$

with $V_{\hat{i},\ell}(e) = e^T P_{\hat{i},\ell} e$, and the state feedback control laws $u_{i,\ell} = K_{i,\ell} \bar{e}$ with gains

$$K_{i,\ell} = Y_{i,\ell} Q_{i,\ell}^{-1}, \quad \forall (i, \ell) \in \{(i, \ell) \in \mathcal{N} \times \mathcal{M} \mid i \neq \hat{i}\} \cup \{(\hat{i}, \ell) \in \mathcal{N} \times \mathcal{M} \mid 0 \notin \mathcal{E}_\ell\} \quad (9.62)$$

and

$$u_{\hat{i},\ell} = Y_{\hat{i},\ell} Q_{\hat{i},\ell}^{-1} e + k_{\hat{i},\ell}, \quad \forall \ell \in \mathcal{M} : 0 \in \mathcal{E}_\ell, \quad (9.63)$$

with $k_{\hat{i},\ell}$ a solution of $q_{\hat{i},\ell} + G_{\hat{i},\ell} k_{\hat{i},\ell} = 0$, stabilize the system (9.8)–(9.9) and moreover ensure an upper bound $\sqrt{\gamma^*}$ for the L_2 -gain of the system from the disturbance input ω to the output y_e .

Proof. First, we apply the Schur complement to (9.58) with respect to the last row and column, as follows (note that in case the subsystem i^* is involved and $\ell : 0 \in \mathcal{E}_\ell$, then sizes of the matrices must be adjusted by appropriate addition of zero elements in rows and columns):

$$\begin{bmatrix} \beta_{\min} Q_{i,\ell} & \star \\ Q_{i,\ell} & \beta_{\min}^{-1} Q_{i,\ell} - \beta_{\min}^{-1} Q_{j,\ell} (\mathcal{S}_{i,j,\ell} + \beta_{\min}^{-1} Q_{j,\ell})^{-1} \beta_{\min}^{-1} Q_{j,\ell} \end{bmatrix} > 0. \quad (9.64)$$

Next, using Lemma 9.2 the following reformulation of (9.64) is obtained

$$\begin{bmatrix} \beta_{\min} Q_{i,\ell} & \star \\ Q_{i,\ell} & (\beta_{\min} Q_{j,\ell}^{-1} + \mathcal{S}_{i,j,\ell}^{-1})^{-1} \end{bmatrix} > 0. \quad (9.65)$$

Performing the Schur complement once more with respect to the second row and column, and multiplying the result by $Q_{i,\ell}^{-1} = \bar{P}_{i,\ell}$ and substituting $Q_{j,\ell}^{-1} = \bar{P}_{j,\ell}$, $\mathcal{S}_{i,j,\ell}^{-1} = \mathcal{R}_{i,j,\ell}$ yields

$$\beta_{\min} (\bar{P}_{i,\ell} - \bar{P}_{j,\ell}) - \mathcal{R}_{i,j,\ell} > 0. \quad (9.66)$$

On the other hand, applying the Schur complement to (9.59) with respect to the last row and column, multiplying the resulting matrices and adding to the first matrix yields (note that in case the subsystem i^* is involved and $\ell : 0 \in \mathcal{E}_\ell$, then sizes of the matrices must be adjusted by appropriate addition of zero elements in rows and columns)

$$\begin{bmatrix} Q_{j,\ell} & \star & \star \\ \bar{h}_{\ell\ell'}^T Q_{j,\ell} & \lambda_{\ell\ell'} & \star \\ Q_{j,\ell} & 0 & Q_{i,\ell'} - Q_{i,\ell'}(Q_{i,\ell'} - \mathcal{S}_{i,j,\ell})^{-1}Q_{i,\ell'} \end{bmatrix} > 0. \quad (9.67)$$

Using Lemma 9.2, (9.67) can be reformulated as follows:

$$\begin{bmatrix} Q_{j,\ell} & \star & \star \\ \bar{h}_{\ell\ell'}^T Q_{j,\ell} & \lambda_{\ell\ell'} & \star \\ Q_{j,\ell} & 0 & (Q_{i,\ell'}^{-1} - \mathcal{S}_{i,j,\ell}^{-1})^{-1} \end{bmatrix} > 0. \quad (9.68)$$

Now performing the Schur complement twice with respect to the last row and column, and multiplying the result by $Q_{j,\ell}^{-1} = \bar{P}_{j,\ell}$ and substituting $Q_{i,\ell'}^{-1} = \bar{P}_{i,\ell'}$, $\mathcal{S}_{i,j,\ell}^{-1} = \mathcal{R}_{i,j,\ell}$, we obtain

$$\bar{P}_{j,\ell} - \bar{P}_{i,\ell'} + \mathcal{R}_{i,j,\ell} - \lambda_{\ell\ell'}^{-1} \bar{h}_{\ell\ell'} \bar{h}_{\ell\ell'}^T > 0. \quad (9.69)$$

Conditions (9.66) and (9.69) are of the same form as of conditions (9.27)–(9.28) in Theorem 9.2. The only difference is that here we use scalar multipliers $\lambda_{\ell\ell'}$ instead of matrix multipliers $\zeta_{\ell\ell'}$ (see Lemma 9.1). Therefore, following the proof of Theorem 9.2 we can conclude that the overall Lyapunov function will decrease over time. \square

Remark 9.7. Fixing the scalar variables μ_{\min} and β_{\min} , the optimization problem stated in Theorem 9.4 will become a convex optimization problem subject to LMI constraints. Therefore, the overall optimization problem can be solved using convex optimization methods along with line searches on μ_{\min} and β_{\min} .

9.5. STABILIZATION OF THE ORIGINAL SWITCHED NONLINEAR SYSTEM

In this section, we discuss the stability of the switched nonlinear system (9.1) using the switching law designed based on the approximated switched affine system (9.5). For simplicity and without loss of generality we assume that $x_r = 0$. The approximation error can be defined as follows:

$$\epsilon_i(x) = f_i(x) - (A_{i,\ell}x + b_{i,\ell}) \quad \text{if } x \in \mathcal{X}_\ell, \forall i \in \mathcal{N}. \quad (9.70)$$

Suppose that the original switched nonlinear system (9.1) is controlled by the switching law (9.22). Therefore when $\sigma(t) = i$, the dynamics of (9.1) is governed by f_i . Hence, the derivative of the Lyapunov function (9.14) along the trajectories of (9.1) is

$$\dot{V}_\ell = \begin{bmatrix} f_i(x) \\ 0 \end{bmatrix}^T \begin{bmatrix} P_{i,\ell} & \star \\ s_{i,\ell}^T & r_{i,\ell} \end{bmatrix} \begin{bmatrix} x \\ 1 \end{bmatrix} + \begin{bmatrix} x \\ 1 \end{bmatrix}^T \begin{bmatrix} P_{i,\ell} & \star \\ s_{i,\ell}^T & r_{i,\ell} \end{bmatrix} \begin{bmatrix} f_i(x) \\ 0 \end{bmatrix} \quad (9.71)$$

for $x \in \mathcal{X}_\ell$ (note that since the continuity of V_ℓ on the boundaries of the polyhedral regions is preserved under conditions of Theorem 9.1, we only consider the behavior of V_ℓ and \dot{V}_ℓ inside the polyhedral regions). Replacing $f_i(x)$ by $\epsilon_i(x) + A_{i,\ell}x + b_{i,\ell}$ yields

$$\dot{V}_\ell = \begin{bmatrix} x \\ 1 \end{bmatrix}^T \begin{bmatrix} A_{i,\ell}^T P_{i,\ell} + P_{i,\ell} A_{i,\ell} & \star \\ b_{i,\ell}^T P_{i,\ell} + s_{i,\ell}^T A_{i,\ell} & 2b_{i,\ell}^T s_{i,\ell} \end{bmatrix} \begin{bmatrix} x \\ 1 \end{bmatrix} + 2 \begin{bmatrix} x \\ 1 \end{bmatrix}^T \begin{bmatrix} P_{i,\ell} & \star \\ s_{i,\ell}^T & r_{i,\ell} \end{bmatrix} \begin{bmatrix} \epsilon_i(x) \\ 0 \end{bmatrix}. \quad (9.72)$$

Now since the inequalities in (9.15) of Theorem 9.1 are strict, there should exist a positive scalar variable denoted by α such that

$$\begin{bmatrix} P_{i,\ell} A_{i,\ell} + A_{i,\ell}^T P_{i,\ell} & \star \\ b_{i,\ell}^T P_{i,\ell} + s_{i,\ell}^T A_{i,\ell} & 2b_{i,\ell}^T s_{i,\ell} \end{bmatrix} - \sum_{j \in \mathcal{N}, j \neq i} \mathcal{T}_{i,j,\ell} + \bar{F}_\ell^T U_\ell \bar{F}_\ell < -\alpha I, \quad \forall i, j \in \mathcal{N}, i \neq j, \forall \ell \in \mathcal{M}. \quad (9.73)$$

Now if (9.73) holds, we obtain

$$\begin{bmatrix} x \\ 1 \end{bmatrix}^T \begin{bmatrix} P_{i,\ell} A_{i,\ell} + A_{i,\ell}^T P_{i,\ell} & \star \\ b_{i,\ell}^T P_{i,\ell} + s_{i,\ell}^T A_{i,\ell} & 2b_{i,\ell}^T s_{i,\ell} \end{bmatrix} \begin{bmatrix} x \\ 1 \end{bmatrix} < -\alpha \|\bar{x}\|_2^2 \quad (9.74)$$

for the active subsystem i in (9.5). Therefore, for (9.72) we have

$$\dot{V}_\ell < -\alpha \|\bar{x}\|_2^2 + 2 \begin{bmatrix} x \\ 1 \end{bmatrix}^T \begin{bmatrix} P_{i,\ell} & \star \\ s_{i,\ell}^T & r_{i,\ell} \end{bmatrix} \begin{bmatrix} \epsilon_i(x) \\ 0 \end{bmatrix} \quad (9.75)$$

for $x \in \mathcal{X}_\ell$. Therefore, in order to have $\dot{V}_\ell < 0$ for the switched nonlinear system, we need to have

$$2 \begin{bmatrix} x \\ 1 \end{bmatrix}^T \begin{bmatrix} P_{i,\ell} & \star \\ s_{i,\ell}^T & r_{i,\ell} \end{bmatrix} \begin{bmatrix} \epsilon_i(x) \\ 0 \end{bmatrix} < \alpha \|\bar{x}\|_2^2. \quad (9.76)$$

The following proposition provides the sufficient condition for stabilization of the switched nonlinear system (9.1) using switching law (9.22).

Proposition 9.1. *Assume there exist matrices $P_{i,\ell}$ and $\mathcal{T}_{i,j,\ell}$, vectors $s_{i,\ell}, \zeta_{\ell\ell}$, scalars $r_{i,\ell}, \alpha > 0$ and symmetric matrices U_ℓ, Z_ℓ with nonnegative elements that satisfy (9.17)–(9.21) and (9.73) for a given positive scalar $\mu_{\min} > 0$. Then the switching rule (9.22) asymptotically stabilizes (9.1) provided that the norm of the PWA approximation error is bounded by*

$$\|\epsilon_i(x)\|_2 < \frac{\alpha \|\bar{x}\|_2}{2a_{\max}(\bar{P}_{i,\ell})}, \quad \forall i \in \mathcal{N}, \text{ for } x \in \mathcal{X}_\ell, \quad (9.77)$$

where $a_{\max}(\bar{P}_{i,\ell})$ denotes the largest singular value of $\bar{P}_{i,\ell}$.

Proof. First, it can be easily proved that

$$\bar{x}^T \bar{P}_{i,\ell} \begin{bmatrix} \epsilon_i(x) \\ 0 \end{bmatrix} \leq \|\bar{x}\|_2 a_{\max}(\bar{P}_{i,\ell}) \|\epsilon_i(x)\|_2. \quad (9.78)$$

Therefore, using (9.77) we obtain

$$2\bar{x}^T \bar{P}_{i,\ell} \begin{bmatrix} \epsilon_i(x) \\ 0 \end{bmatrix} \leq 2\|\bar{x}\|_2 a_{\max}(\bar{P}_{i,\ell}) \|\epsilon_i(x)\|_2 \leq \alpha \|\bar{x}\|_2^2, \quad (9.79)$$

which yields $\dot{V}_\ell < 0$ as in (9.75) and hence, asymptotic stability of the switched nonlinear system (9.1) is ensured. \square

Remark 9.8. *As can be inferred from (9.77), the upper bound on the approximation error $\epsilon_i(x)$ depends on the maximum singular values of the $\bar{P}_{i,\ell}$ matrices. Therefore, the upper bound on the approximation error can be further relaxed if a search for $\bar{P}_{i,\ell}$ matrices that satisfy (9.17)–(9.21) and (9.73), and with minimized maximum singular values is performed. Furthermore, a similar extension can be performed for the results of Section 9.4 for robust H_∞ control of the switched nonlinear system (9.1)–(9.2).*

9.6. CASE STUDIES

In this section, three examples are presented to evaluate and compare the performance of the stabilizing approaches proposed in Section 9.3 and Section 9.4. In the first example, the conditions of Theorem 9.1 are used to design a stabilizing switching law. In the second example, with the same system description but with an additional state feedback control input and disturbance signals, we use Theorem 9.3 to design a robust switching control scheme. In the last example, we consider the urban traffic model used in Sections 7.5 and 8.6, reformulate it, and then design a robust switching controller based on Theorem 9.2.

9.6.1. EXAMPLE 1

In this example, we use the conditions presented in Theorem 9.1 to design a stabilizing switching controller. We directly use the error model (9.8) with the following matrices:

$$F_1 = -F_3 = \begin{bmatrix} -1 & 1 \\ 1 & 1 \end{bmatrix}, \quad F_2 = -F_4 = \begin{bmatrix} 1 & -1 \\ 1 & 1 \end{bmatrix}, \\ \bar{h}_{12} = \bar{h}_{34} = [1 \quad -1]^T, \quad \bar{h}_{23} = \bar{h}_{41} = [1 \quad 1]^T,$$

Region 1 :

$$A_{1,1} = \begin{bmatrix} 3 & 1 \\ -5 & -8 \end{bmatrix}, \quad A_{2,1} = \begin{bmatrix} -2 & 6 \\ 2 & 9 \end{bmatrix}, \quad A_{3,1} = \begin{bmatrix} 4 & 4 \\ -2 & 3 \end{bmatrix},$$

Region 2 :

$$A_{1,2} = \begin{bmatrix} 2 & 5 \\ -1 & -3 \end{bmatrix}, \quad A_{2,2} = \begin{bmatrix} -4 & 1 \\ -2 & 6 \end{bmatrix}, \quad A_{3,2} = \begin{bmatrix} 2.5 & 7 \\ 2 & -9 \end{bmatrix},$$

Region 3 :

$$A_{1,3} = \begin{bmatrix} 5 & 3 \\ -2 & -4 \end{bmatrix}, \quad A_{2,3} = \begin{bmatrix} 3 & -1 \\ 4 & 2 \end{bmatrix}, \quad A_{3,3} = \begin{bmatrix} 2 & -3 \\ -1 & -4 \end{bmatrix},$$

Region 4 :

$$A_{1,4} = \begin{bmatrix} 6 & -2 \\ -4 & 5 \end{bmatrix}, \quad A_{2,4} = \begin{bmatrix} -5 & 1 \\ -2 & 3 \end{bmatrix}, \quad A_{3,4} = \begin{bmatrix} -1 & -3 \\ 2 & 8 \end{bmatrix}.$$

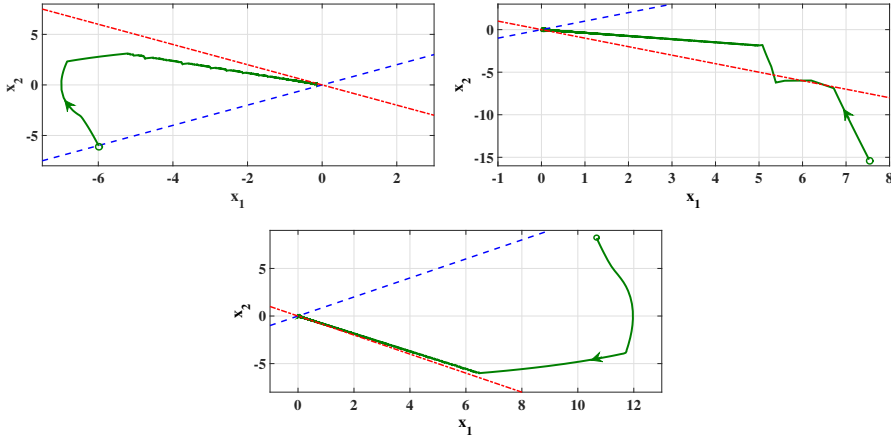


Figure 9.4: Example 9.6.1: Simulation of the closed-loop system for different initial states. The dashed blue and red lines represent the boundaries between regions.

Note that none of the subsystems is stable. Using line search and the Yalmip toolbox (with the SeDuMi solver), the feasibility problem (9.15)–(9.21) is solved and the following matrices are obtained for the switching rule (9.22):

$$\begin{aligned}
 P_{1,1} &= \begin{bmatrix} 0.2854 & -0.1497 \\ -0.1497 & 0.5810 \end{bmatrix}, & P_{1,2} &= \begin{bmatrix} 0.0587 & 0.0823 \\ 0.0823 & 0.3513 \end{bmatrix}, \\
 P_{2,1} &= \begin{bmatrix} 0.2821 & -0.1472 \\ -0.1472 & 0.5934 \end{bmatrix}, & P_{2,2} &= \begin{bmatrix} 0.0581 & 0.0820 \\ 0.0820 & 0.3551 \end{bmatrix}, \\
 P_{3,1} &= \begin{bmatrix} 0.2852 & -0.1486 \\ -0.1486 & 0.5843 \end{bmatrix}, & P_{3,2} &= \begin{bmatrix} 0.0590 & 0.0827 \\ 0.0827 & 0.3488 \end{bmatrix}, \\
 P_{1,3} &= \begin{bmatrix} -2.5457 & 0.3938 \\ 0.3938 & 3.5848 \end{bmatrix}, & P_{1,4} &= \begin{bmatrix} 3.0332 & 0.1662 \\ 0.1662 & -1.5240 \end{bmatrix}, \\
 P_{2,3} &= \begin{bmatrix} -2.5563 & 0.4027 \\ 0.4027 & 3.6083 \end{bmatrix}, & P_{2,4} &= \begin{bmatrix} 2.9895 & 0.1710 \\ 0.1710 & -1.4888 \end{bmatrix}, \\
 P_{3,3} &= \begin{bmatrix} -2.5553 & 0.3921 \\ 0.3921 & 3.5788 \end{bmatrix}, & P_{3,4} &= \begin{bmatrix} 3.0063 & 0.1578 \\ 0.1578 & -1.5287 \end{bmatrix}.
 \end{aligned}$$

As depicted in Fig. 9.4, the designed switching control strategy is able to steer the error state to the origin for different initial conditions. Moreover, Fig. 9.5 illustrates the overall Lyapunov function (obtained by taking the minimum of the Lyapunov functions in each region).

9.6.2. EXAMPLE 2

In this example we use Theorem 9.3 to design a robust control scheme for the system presented in Example 9.6.1, but now with an additional state feedback control $u = K_{i,\ell}x$

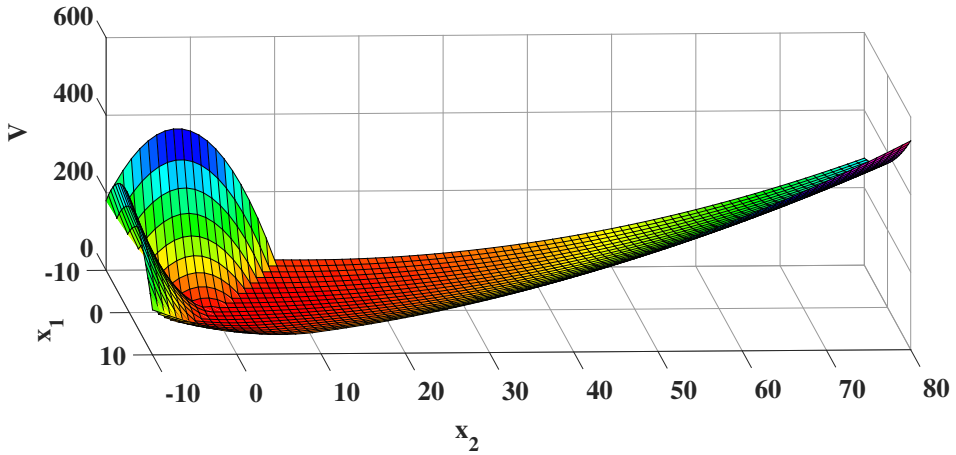


Figure 9.5: Example 9.6.1: Plot of the overall Lyapunov function; note that its continuity is preserved over boundaries of the regions.

and a disturbance signal ω with system matrices $G_i = [1, 1]^T$ and $H_i = C_i = I_2$. The Lyapunov matrices and the feedback gains are determined using the optimization problem (9.38)–(9.45) with line search on μ_{\min} (from 0 to 200, with steps of 1). The obtained value of μ_{\min} corresponding to the minimum upper bound on the L_2 -gain is 184.

$$P_{1,1} = \begin{bmatrix} 0.7911 & 0.7904 \\ 0.7904 & 0.7910 \end{bmatrix}, P_{1,2} = \begin{bmatrix} 0.7755 & 0.7748 \\ 0.7748 & 0.7752 \end{bmatrix},$$

$$P_{2,1} = \begin{bmatrix} 0.8088 & 0.8082 \\ 0.8082 & 0.8089 \end{bmatrix}, P_{2,2} = \begin{bmatrix} 0.7890 & 0.7885 \\ 0.7885 & 0.7891 \end{bmatrix},$$

$$P_{3,1} = \begin{bmatrix} 0.7998 & 0.7991 \\ 0.7991 & 0.7997 \end{bmatrix}, P_{3,2} = \begin{bmatrix} 0.7817 & 0.7809 \\ 0.7809 & 0.7812 \end{bmatrix},$$

$$P_{1,3} = \begin{bmatrix} 8.0485 & -8.0465 \\ -8.0465 & 8.0446 \end{bmatrix}, P_{1,4} = \begin{bmatrix} 9.5119 & -9.5121 \\ -9.5121 & 9.5124 \end{bmatrix},$$

$$P_{2,3} = \begin{bmatrix} 7.9614 & -7.9584 \\ -7.9584 & 7.9556 \end{bmatrix}, P_{2,4} = \begin{bmatrix} 8.6968 & -8.6983 \\ -8.6983 & 8.6999 \end{bmatrix},$$

$$P_{3,3} = \begin{bmatrix} 7.8345 & -7.8312 \\ -7.8312 & 7.8282 \end{bmatrix}, P_{3,4} = \begin{bmatrix} 9.3655 & -9.3663 \\ -9.3663 & 9.3671 \end{bmatrix},$$

$$K_{1,1} = [-7397 \quad -7389], K_{1,2} = [-7322 \quad -7318],$$

$$K_{2,1} = [-7245 \quad -7249], K_{2,2} = [-7517 \quad -7520],$$

$$K_{3,1} = [-7323 \quad -7317], K_{3,2} = [-7761 \quad -7756],$$

$$K_{1,3} = [-121831 \quad 108113], K_{1,4} = [53567 \quad -81067],$$

$$K_{2,3} = [-168194 \quad 154613], K_{2,4} = [696943 \quad -725951],$$

$$K_{3,3} = [-216848 \quad 203056], K_{3,4} = [215898 \quad -240181].$$

The switching control scheme is able to stabilize the system and further significantly attenuate the impact of the disturbance on the output of the system. Simulation results for a particular disturbance input are presented in Fig. 9.6(a)-(d). The calculated L_2 -gain for the closed-loop system is 0.00382, while the minimum upper bound for the L_2 -gain obtained by solving the optimization problem (9.38)–(9.45) is 0.21814.

9.6.3. EXAMPLE 3

In this example, we again consider the MFD-based urban traffic model discussed in Sections 7.5 and 8.6. Using the proposed switching control strategies for mixed switching affine system, we aim at designing a robust H_∞ controller for this nonlinear system. First, we review the model's description.

SET-UP

As also discussed in Chapters 7 and 8, for an urban network divided into two regions: the city center (region 2) and the periphery (region 1), the following macroscopic model is proposed [86, 91, 92]:

$$\dot{n}_1(t) = -G_1(n_1(t)) \cdot u(t) + \omega_1(t), \quad (9.80)$$

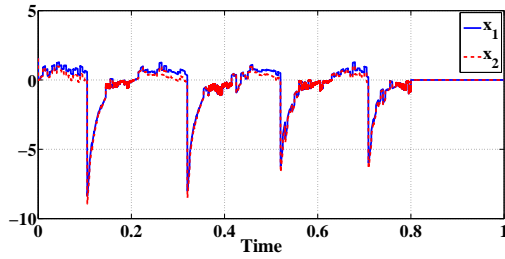
$$\dot{n}_2(t) = -G_2(n_2(t)) + G_1(n_1(t)) \cdot u(t) + \omega_2(t), \quad (9.81)$$

with $n_i(t)$ (veh) the accumulation in region i at time t . The trip completion flow $G_i(n_i(t))$ (veh/s) is defined as the rate of vehicles reaching their destinations and is approximated by an exponential function $G_i(n_i) = 1/3600 \cdot a_i \cdot n_i \cdot \exp(-1/2 \cdot (n_i/n_{i,cr})^2)$, $i \in \{1, 2\}$, with $a_1 = 16.95$, $a_2 = 15.83$. Further, the perimeter control $u \in [0, 1]$ may restrict vehicles to transfer between regions (in our case, the flow of vehicles is restricted from the periphery to the city center). The perimeter control can be realized by e.g. coordinating green and red durations of signalized intersections placed on the border between two regions. Moreover, trips generated in the network are denoted by ω_i (veh/s) and considered as disturbances affecting the system. The assumed profile for trip demands are depicted in Fig. 9.8. The uncertainty in the demands is modeled using zero mean white Gaussian noise with variance 0.2 (veh²/s²) added to the average profiles.

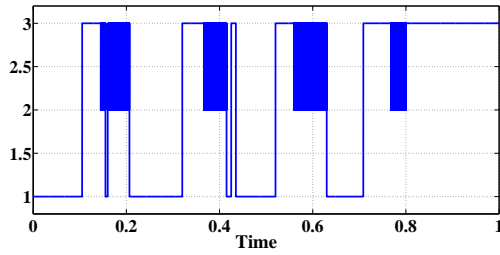
The exponential functions G_i can be approximated by PWA functions, as illustrated in Fig. 9.7. The result will be a PWA system with four partitions in the state space defined based on the critical accumulations $n_{i,cr}$.

Furthermore, our investigations in Chapter 4 showed that the evolution of flows is not very sensitive to small changes in the perimeter signal. Therefore, we assume that u can take values from the finite set $\{0.1, 0.35, 0.65, 0.9\}$. Doing this along with approximating the trip flow functions will result in a switched affine system with mixed controlled and uncontrolled switching behavior and with the following system matrices:

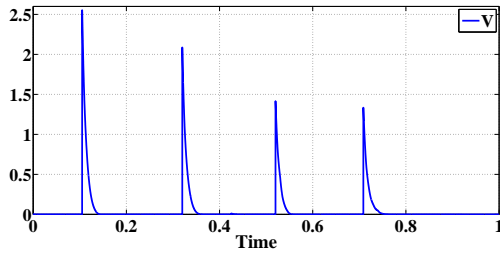
$$F_1 = \begin{bmatrix} 1 & 0 \\ 0 & 1 \end{bmatrix}, F_2 = \begin{bmatrix} 1 & 0 & -n_{1,cr} \\ 0 & -1 & n_{2,cr} \\ 0 & 1 & 0 \\ -1 & 0 & n_{1,jam} \end{bmatrix},$$



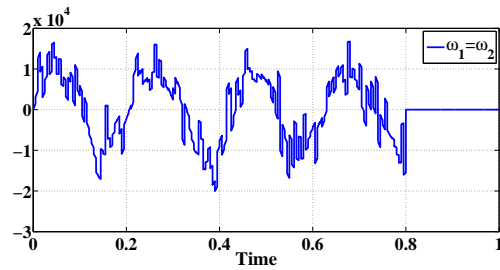
(a)



(b)



(c)



(d)

Figure 9.6: Example 9.6.2: (a) state trajectories over time, (b) switching signal σ over time (switching between subsystems), (c) overall Lyapunov function, (d) disturbance signals.

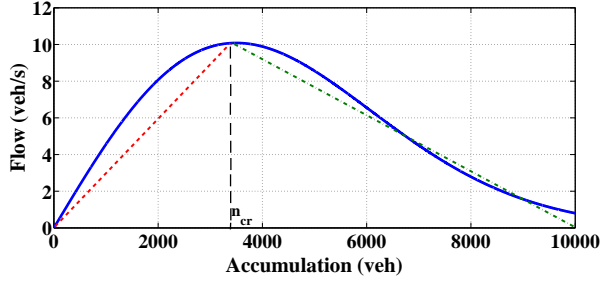


Figure 9.7: Example 9.6.3: Piecewise affine approximation of the trip completion flow function G_i .

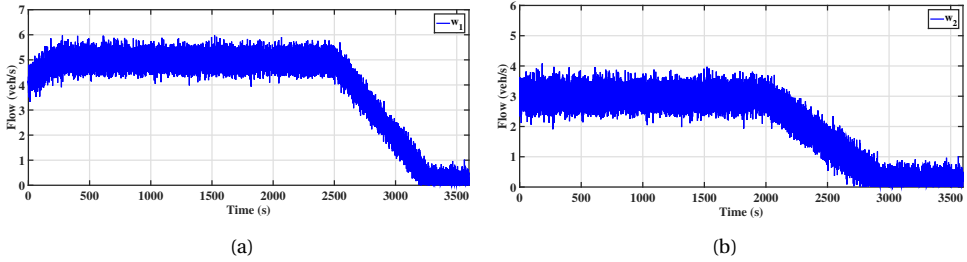


Figure 9.8: Example 9.6.3: trip demands, (a) from region 1 to 2, (b) inside region 2.

$$F_3 = \begin{bmatrix} -1 & 0 & n_{1,cr} \\ 0 & 1 & -n_{2,cr} \\ 1 & 0 & 0 \\ 0 & -1 & n_{2,jam} \end{bmatrix}, F_4 = \begin{bmatrix} 1 & 0 & -n_{1,cr} \\ 0 & 1 & -n_{2,cr} \\ -1 & 0 & n_{1,jam} \\ 0 & -1 & n_{2,jam} \end{bmatrix},$$

$$\bar{h}_{12} = \bar{h}_{34} = \begin{bmatrix} 1 & 0 & -n_{1,cr} \end{bmatrix}^T,$$

$$\bar{h}_{13} = \bar{h}_{24} = \begin{bmatrix} 0 & 1 & -n_{2,cr} \end{bmatrix}^T,$$

$$A_{i,1} = \begin{bmatrix} -u_i \cdot \frac{10}{n_{1,cr}} & 0 \\ u_i \cdot \frac{10}{n_{1,cr}} & -\frac{7}{n_{2,cr}} \end{bmatrix}, b_{i,1} = \begin{bmatrix} 0 \\ 0 \end{bmatrix},$$

$$A_{i,2} = \begin{bmatrix} u_i \cdot \frac{8}{n_{1,jam} - n_{1,cr}} & 0 \\ -u_i \cdot \frac{8}{n_{1,jam} - n_{1,cr}} & -\frac{7}{n_{2,cr}} \end{bmatrix}, b_{i,2} = \begin{bmatrix} -u_i \cdot 16.22 \\ u_i \cdot 16.22 \end{bmatrix},$$

$$A_{i,3} = \begin{bmatrix} -u_i \cdot \frac{10}{n_{1,cr}} & 0 \\ u_i \cdot \frac{10}{n_{1,cr}} & \frac{5}{n_{2,jam} - n_{2,cr}} \end{bmatrix}, b_{i,3} = \begin{bmatrix} 0 \\ -10.75 \end{bmatrix},$$

$$A_{i,4} = \begin{bmatrix} u_i \cdot \frac{8}{n_{1,jam} - n_{1,cr}} & 0 \\ -u_i \cdot \frac{8}{n_{1,jam} - n_{1,cr}} & \frac{5}{n_{2,jam} - n_{2,cr}} \end{bmatrix}, b_{i,4} = \begin{bmatrix} -u_i \cdot 16.22 \\ u_i \cdot 16.22 - 10.75 \end{bmatrix},$$

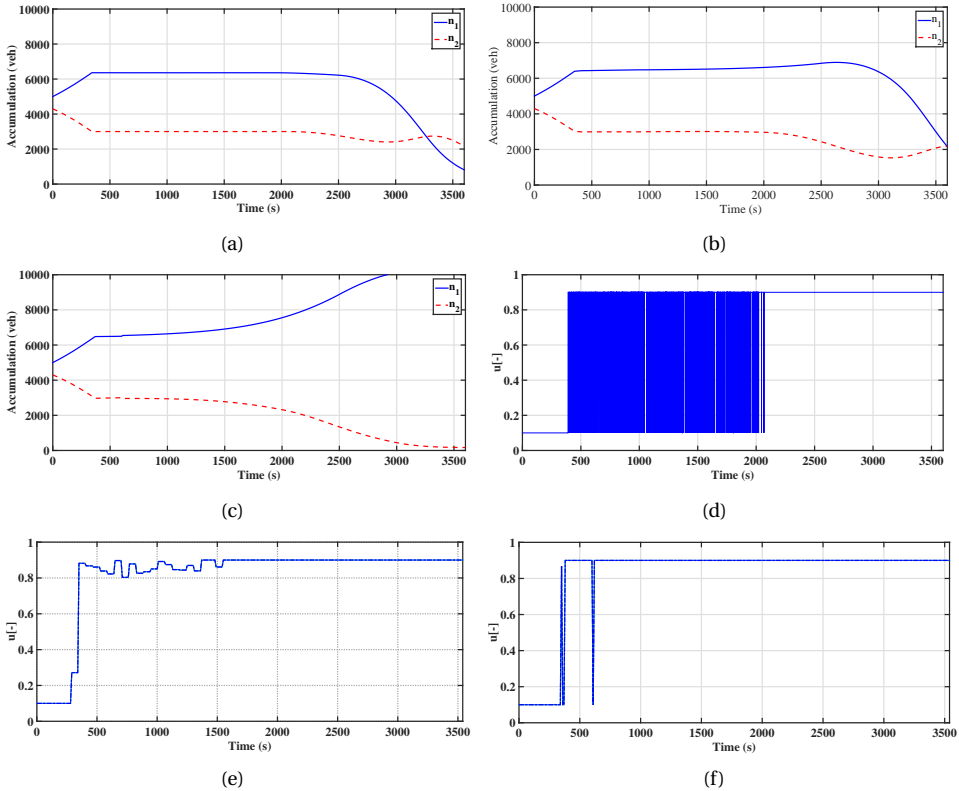


Figure 9.9: Example 9.6.3, Accumulations: (a) robust control, (b) MPC method, (c) greedy feedback control. Perimeter control input: (d) robust switching scheme, (e) MPC scheme, (f) greedy control.

with $n_{1,cr} = 3500$ (veh), $n_{2,cr} = 3000$ (veh), $n_{1,jam} = 10000$ (veh), $n_{2,jam} = 9000$ (veh) and $u_i \in \{0.1, 0.35, 0.65, 0.9\}$.

RESULTS AND DISCUSSION

The matrices of the Lyapunov functions along with the minimum upper bound of the L_2 -gain are determined using an extended version of conditions in Theorem 9.2 (the conditions of Theorem 9.1 were found infeasible for this example) for robust H_∞ control (since there is no state feedback controller u , the extension is quite straightforward and the presentation is skipped in this chapter). Note that we use the LMI solver SeDuMi and the Yalmip toolbox along with line search on μ_{min} and β_{min} (from 0 to 200 for each, with steps of 1). We implement a tri-level optimization problem where in the highest level, line search on μ_{min} is performed. On the middle level, gridding on β_{min} is carried out. And on the lowest level, the minimization of γ subject to LMI constraints (with fixed μ_{min} and β_{min}) is performed. The obtained values for μ_{min} and β_{min} corresponding to the minimum achieved γ , are 159 and 10, respectively.

The Lyapunov matrices are presented in Box I.

For simulation, we use the model (9.80)–(9.81) along with the noisy demand profiles depicted in Fig. 9.8. The measured accumulations are supplied to (9.22) to determine

$$\begin{aligned}
P_{1,1} &= \begin{bmatrix} 15.8293 & 2.1235 \\ 2.1235 & 4.5335 \end{bmatrix}, P_{2,1} = \begin{bmatrix} 15.8000 & 2.1260 \\ 2.1260 & 4.5335 \end{bmatrix}, P_{3,1} = \begin{bmatrix} 15.7649 & 2.1291 \\ 2.1291 & 4.5335 \end{bmatrix}, P_{4,1} = \begin{bmatrix} 15.7358 & 2.1317 \\ 2.1317 & 4.5334 \end{bmatrix}, \\
P_{1,2} &= \begin{bmatrix} 3.9867 \cdot 10^{-5} & 8.4224 \cdot 10^{-5} & 0.7128 \\ 8.4224 \cdot 10^{-5} & 5.3187 \cdot 10^{-5} & -0.6935 \\ 0.7128 & -0.6935 & 32.7528 \end{bmatrix}, P_{2,2} = \begin{bmatrix} 3.9820 \cdot 10^{-5} & 8.4245 \cdot 10^{-5} & 0.7139 \\ 8.4245 \cdot 10^{-5} & 5.3190 \cdot 10^{-5} & -0.6937 \\ 0.7139 & -0.6937 & 16.3897 \end{bmatrix}, \\
P_{3,2} &= \begin{bmatrix} 3.9779 \cdot 10^{-5} & 8.4272 \cdot 10^{-5} & 0.7151 \\ 8.4272 \cdot 10^{-5} & 5.3190 \cdot 10^{-5} & -0.6939 \\ 0.7151 & -0.6939 & -2.2494 \end{bmatrix}, P_{4,2} = \begin{bmatrix} 3.9828 \cdot 10^{-5} & 8.4306 \cdot 10^{-5} & 0.7154 \\ 8.4306 \cdot 10^{-5} & 5.3190 \cdot 10^{-5} & -0.6942 \\ 0.7154 & -0.6942 & -12.4139 \end{bmatrix}, \\
P_{1,3} &= \begin{bmatrix} 9.8171 \cdot 10^{-7} & 5.7418 \cdot 10^{-7} & -5.4657 \cdot 10^{-4} \\ 5.7418 \cdot 10^{-7} & 2.7229 \cdot 10^{-7} & 1.7718 \cdot 10^{-3} \\ -5.4657 \cdot 10^{-4} & 1.7718 \cdot 10^{-3} & 3.8305 \end{bmatrix}, P_{1,4} = \begin{bmatrix} -8.6688 \cdot 10^{-6} & 9.2617 \cdot 10^{-6} & 1.3909 \cdot 10^{-2} \\ 9.2617 \cdot 10^{-6} & -1.1040 \cdot 10^{-5} & 1.2609 \cdot 10^{-2} \\ 1.3909 \cdot 10^{-2} & 1.2609 \cdot 10^{-2} & 2.1053 \end{bmatrix}, \\
P_{2,3} &= \begin{bmatrix} 9.8085 \cdot 10^{-7} & 5.7385 \cdot 10^{-7} & -5.4408 \cdot 10^{-4} \\ 5.7385 \cdot 10^{-7} & 2.7229 \cdot 10^{-7} & 1.7718 \cdot 10^{-3} \\ -5.4408 \cdot 10^{-4} & 1.7718 \cdot 10^{-3} & 3.8306 \end{bmatrix}, P_{2,4} = \begin{bmatrix} -8.6925 \cdot 10^{-6} & 9.2750 \cdot 10^{-6} & 1.4019 \cdot 10^{-2} \\ 9.2750 \cdot 10^{-6} & -1.1039 \cdot 10^{-5} & 1.2486 \cdot 10^{-2} \\ 1.4019 \cdot 10^{-2} & 1.2486 \cdot 10^{-2} & 2.0895 \end{bmatrix}, \\
P_{3,3} &= \begin{bmatrix} 9.7980 \cdot 10^{-7} & 5.7347 \cdot 10^{-7} & -5.4113 \cdot 10^{-4} \\ 5.7347 \cdot 10^{-7} & 2.7229 \cdot 10^{-7} & 1.7718 \cdot 10^{-3} \\ -5.4113 \cdot 10^{-4} & 1.7718 \cdot 10^{-3} & 3.8306 \end{bmatrix}, P_{3,4} = \begin{bmatrix} -8.7211 \cdot 10^{-6} & 9.2911 \cdot 10^{-6} & 1.4151 \cdot 10^{-2} \\ 9.2911 \cdot 10^{-6} & -1.1039 \cdot 10^{-5} & 1.2338 \cdot 10^{-2} \\ 1.4151 \cdot 10^{-2} & 1.2338 \cdot 10^{-2} & 2.0632 \end{bmatrix}, \\
P_{4,3} &= \begin{bmatrix} 9.7886 \cdot 10^{-7} & 5.7316 \cdot 10^{-7} & -5.3873 \cdot 10^{-4} \\ 5.7316 \cdot 10^{-7} & 2.7228 \cdot 10^{-7} & 1.7718 \cdot 10^{-3} \\ -5.3873 \cdot 10^{-4} & 1.7718 \cdot 10^{-3} & 3.8304 \end{bmatrix}, P_{4,4} = \begin{bmatrix} -8.7452 \cdot 10^{-6} & 9.3046 \cdot 10^{-6} & 1.4263 \cdot 10^{-2} \\ 9.3046 \cdot 10^{-6} & -1.1039 \cdot 10^{-5} & 1.2214 \cdot 10^{-2} \\ 1.4263 \cdot 10^{-2} & 1.2214 \cdot 10^{-2} & 2.0362 \end{bmatrix}.
\end{aligned}$$

Box I. The obtained matrices for the Lyapunov functions.

the active subsystem (to obtain the proper perimeter input). The results are depicted in Fig. 9.9. As inferred from Fig. 9.9(a), the switching control resolves the initial congestion in the network and also significantly reduces the effects of the high-level trip demands. Moreover, the robust control method is compared with an MPC perimeter control scheme and a greedy feedback control strategy. As for MPC, the prediction model is selected as the discretized form of (9.80)–(9.81) with $T_s = 30$ s and $T_c = 60$ s. Moreover, the MPC controller is supplied by the information about the average time evolution of the trip demands, without the additive noise. Further, the prediction horizon and the control horizon are selected as $N_p = 20$ and $N_c = 2$ (increasing N_p and N_c had little effects in this scenario). The greedy feedback controller designed as follows. The perimeter input is set to $u = 0.1$ when $n_2 > n_{2,cr} = 3000$ (veh), and otherwise $u = 0.9$.

As can be observed from Fig. 9.9(b), MPC is able to prevent gridlock and moreover, reduce congestion in both regions. Although MPC scheme is supplied by an estimation of the demand, its performance is slightly worse (the accumulation in region 1 increases in the middle of the simulation period) than that of the robust switching method. Moreover, the greedy feedback controller is not able to prevent gridlock, as can be seen in Fig. 9.9(c). The perimeter controller inputs obtained from the three methods are depicted in Fig. 9.9(d)–(f).

Finally, setting the initial accumulations to zero, the actual L_2 -gain is $0.0881 \cdot 3600$,

which is lower than the upper bound $0.1332 \cdot 3600$ obtained by solving the optimization problem.

9.7. CONCLUDING REMARKS

Stability analysis and design of stabilizing controllers for switched affine systems with mixed switching types have been presented. The switched system has both autonomous and controlled switching included in the model. To tackle the stabilization and robust disturbance attenuation problem for such a system, first we have proposed a joint polyhedral partitioning of the entire state space and then multiple state-based switching rules defined for each polyhedral region. Further, the continuity of the Lyapunov functions on the boundaries of the regions was relaxed and less conservative results have been presented. Moreover, the proposed design conditions have been developed in the form optimization problems that are nonconvex only in scalar variables. Finally, we have presented sufficient conditions for stabilizing switched nonlinear systems using the proposed control schemes. Simulation results for different systems have shown that the proposed switching control schemes are able asymptotically stabilize the system. Furthermore, we have demonstrated that the proposed control schemes can be used for control of nonlinear systems. As a possible extension of the current work, we can further reducing the conservatism using a joint time-based and state-based switching strategy and the concept of average dwell-time [6, 53, 112].

10

CONCLUSIONS AND RECOMMENDATIONS

In this thesis, we have presented efficient model predictive control schemes to reduce congestion and to improve the travel time in both freeway and urban traffic networks. Further, we have proposed robust stabilizing switching control strategies for switched nonlinear systems. Several examples and case studies have shown the effectiveness of our proposed optimal and robust control schemes. In this final chapter, we first summarize the main results from the previous chapters, after which we will present several suggestions and recommendations on topics that can be interesting for further research.

10.1. CONCLUSIONS

THE main contributions of the work presented in this dissertation can be summarized as follows:

- **Extension of the Link Transmission Model for traffic control**
In order to achieve an efficient model-based predictive control scheme for freeway networks, we have extended the Link Transmission Model, to include the effects of the traffic measures, ramp metering and variable speed limits.
- **Integrated hybrid perimeter and timing plans control for large-scale urban networks**
We have proposed a hybrid model predictive control scheme for large-scale multi-region urban networks. In this scheme, we have provided the opportunity to control *inside* urban regions, rather than only at the boundaries. This has been realized using a new hybrid multi-region network model and via switching between timing plans of urban intersections.
- **Efficient robust H_∞ control of sector-bounded switched nonlinear systems via bi-level optimization**
For switched nonlinear systems with nonlinearities bounded in sector sets with arbitrary slopes, we have developed a robust H_∞ switching control scheme. We

have formulated the design procedure as a bi-level optimization problem that can be efficiently solved using a line search method along with a convex optimization method subject to linear matrix inequality constraints.

- **Robust stabilization of switched affine systems with mixed switching behavior**

We have proposed stabilizing and robust H_∞ control schemes for switched affine systems with mixed controlled and autonomous switching behavior. In order to reduce the conservatism, we have relaxed the continuity of the overall Lyapunov function using linear matrix inequality techniques.

OTHER HIGHLIGHTS

Extensive discussions and concluding remarks on the conducted research in this thesis have been presented in the previous chapters. Here we briefly present some highlights.

In the first part of this thesis, we have focused on reducing the complexity of modeling and control of large-scale freeway and urban networks. Particularly, in order to reduce the computation time required to solve the online optimization problems, we have used some approximations and model transformation techniques in order to formulate mixed integer linear optimization problems. Simulation results in Chapters 3 and 4 have shown that the computational effort for solving the mixed integer linear optimization problems is significantly lower than in the nonlinear optimization problem case and hence, they are more suitable for real-time traffic control. Furthermore, we have also proposed a hierarchical predictive scheme that efficiently solves the dynamic route guidance problem for large-scale urban networks in a regional fashion.

In the second part, we have presented three main approaches to design robust stabilizing controllers for switched nonlinear systems: 1) a direct approach that uses the nonlinear functions for control synthesis, 2) a more efficient approach that uses sector bounds on the nonlinear functions to design controllers and also to find sufficient conditions for asymptotic stability under arbitrary switching with average dwell time constraint, and 3) a method that reduces the conservatism of the second approach even more, via approximating the switched nonlinear system by a switched affine system and uses the approximate system as basis for robust control design. In the second and third approaches, we have achieved a structured design procedure that can be efficiently performed using convex optimization methods. The main advantages of all three approaches are 1) the offline *design* of the switching laws and the feedback control inputs that limits the online computation to simple multiplications and min operations, 2) minimization of the effects of disturbances on the output of the system without having exact knowledge of the evolution over time of the disturbances.

10.2. RECOMMENDATIONS FOR FUTURE RESEARCH

In this section, we present open problems that still have to be tackled along with some additional directions for future research.

10.2.1. FREEWAY NETWORK MODELING AND CONTROL USING THE LINK TRANSMISSION MODEL

The Link Transmission Model (LTM) provides an efficient modeling approach for large-scale freeway networks due to its special link and node modeling structure. With our proposed extensions, we have prepared the LTM for use as a prediction model in the framework of MPC. However, the modeling abilities of the LTM can be still improved.

- **Multi-rate LTM**

Although the LTM allows large sample times in general, the network layout at certain parts (in particular the mainstream road between successive off-ramps/on-ramps) needs to be represented by relatively short links, which forces us to take shorter sampling periods (the sample time should be selected such that no vehicle entering a link reaches the downstream end in less than one sampling period). Therefore, in order to further increase the efficiency of modeling, we propose to investigate the possibility of having multiple sampling periods in the LTM.

- **Modeling capacity drop**

The traffic scenarios in which capacity drop occurs and influences the traffic flows cannot yet be accurately modeled by the LTM. Therefore, further extension of the LTM to integrate the effects of the capacity drop case is recommended. One conceptual idea is to have state-dependent capacity parameters in the LTM. However, this would need additional conditions that should be designed such that the advantages of the LTM are not deteriorated.

- **Evaluation of variable speed limit modeling using real data**

The evaluation of the theoretical extensions of the LTM, particularly integrating the effects of variable speed limits control in the model, must be performed using data collected from freeway networks equipped with variable speed limit signs.

- **Field implementation**

More extensive micro-simulations with different traffic scenarios and network layouts are required to better evaluate our proposed ramp metering and variable speed limits control scheme using the LTM. After this stage, we propose to perform the field implementation of the proposed modeling and control scheme. This will shed more light on the performance of this approach under real traffic conditions.

10.2.2. MACROSCOPIC MODELING AND HYBRID PREDICTIVE CONTROL OF URBAN NETWORKS

Proper network partitioning, use of MFD-based models, and a hierarchical control scheme help to reduce the computational complexity of control and coordination of large-scale urban networks. However, there are still several open problems and research directions to investigate.

- **Mutual interaction of perimeter and timing plans controllers**

Generally, the perimeter and the switching controllers may affect the performance of each other. However, in sufficiently large subnetworks these mutual impacts can be neglected, as in our modeling approach. Nevertheless, more research can be allocated to identify and model the impacts of perimeter control and switching between timing plans on each other.

- **Estimation of traffic states**

While the total accumulations in a subnetwork can be measured using GPS data or other sensing tools, it is not easy to estimate the destination-dependent accumulations. One solution is to use the information from the in-car navigation systems. However, this may trigger controversy related to the privacy concerns. As an alternative solution, we propose to estimate and extract the destination-dependent accumulations from the total accumulations. However, we have to take into account the hybrid nature of the closed-loop traffic system and also difference types of noises that exist in the system. Possible solutions to investigate are particle filtering approaches, identification and estimation methods for hybrid systems and machine learning techniques.

- **Micro-simulation and field implementation of the MFD-based control scheme**

Implementing the proposed control approaches using micro-simulation software packages would shed more light on how the control schemes change the spatial distribution of congestion in the network and how the two types of controllers may interact. In this process, proper realization of the optimal perimeter control inputs using local traffic signal controllers along with designing effective timing plans that correspond to well-defined desired MFDs is important. As a next step, field implementation of the proposed predictive control strategies should be considered.

- **Characterizing the effects of route choice on the MFD**

In our proposed route guidance scheme, we have assumed that manipulating the splitting rates for flows of vehicles heading to a certain destination region is performed mostly in the areas close to the borders between regions in order to keep the MFDs unaltered. This assumption can be relaxed by defining multiple MFDs for each region to include the effects of manipulating destination-dependent flows. Characterizing the effects of the route choice on the MFDs and obtaining high-level models that incorporate these effects is an interesting research direction.

- **Integrating user preferences in the route guidance**

As an extension to the proposed approach, we can incorporate the preferences of the drivers and their desired routes in the optimization procedure used to determine the traffic flow splitting rates. Game-theoretic approaches can be employed to include the preferences of drivers in the design process and also to influence their decisions.

- **Designing lower-level local controllers**

In the current work, we have focused on the higher level of the route guidance

scheme. We have assumed that there exist local traffic signal controllers, dynamic route information panels (DRIPs), and in-car navigation devices that help to realize the optimal distribution of destination-dependent flows. The design of the lower level controllers that realize the optimal splitting rates is retained as future work.

10.2.3. STABILITY ANALYSIS AND ROBUST CONTROL SYNTHESIS FOR SWITCHED NONLINEAR SYSTEMS

In this part, we present some ideas for improving the performance of the proposed methodologies and also for extending to other cases of switched systems.

- **Reducing conservatism by using tighter sector sets**

Introducing different sector bounds for different quadrants with arbitrary slopes would better characterize the sector-bounded nonlinear functions and would also reduce more the conservatism. Maintaining the efficiency of the design approach and formulating or approximating the stability conditions as linear matrix inequalities is the main aim. Combining linear matrix inequality techniques, linear annihilators, and the Finsler Lemma may be useful to solve this problem.

- **Combining dwell time constraint with state-based switching**

To reduce the conservatism of the proposed stabilizing methods, we can integrate time-based and state-based switching such that admissible increases in the value of the overall Lyapunov function at the switching time instants would be allowed. Designing such a switching scheme for (sector-bounded) switched nonlinear systems and meanwhile, maintaining the efficiency of the procedure is challenging. As a starting point, one can try to derive bounds on the decay rates of the Lyapunov functions between consecutive switching instants using the sector slopes.

- **Relaxing the decrease of the Lyapunov function over boundaries using dwell time constraints**

To stabilize switched affine systems with mixed switching types, the value of the overall Lyapunov function does not need to decrease over the boundaries of the polyhedral regions. Using a dwell time constraint on the controlled switching, we can allow the Lyapunov function to grow inside and at the boundaries of regions. However, the automatic switching that occurs at the boundaries makes the development of such a dwell time constrained switching scheme difficult. Estimating and imposing a minimum time duration that the system composed of several subsystems is allowed to stay in one polyhedral region is a possible solution direction.

- **Using other robust performance criteria**

In our robust control approaches we have considered the H_∞ performance criterion mainly because it is suitable for our particular traffic application. However, extension of the proposed methods for other criteria such as the H_2 performance index which maintains the efficiency of the design procedures is worthwhile to explore.

- **Control synthesis for discrete-time switched nonlinear systems**

In this thesis, we have focused on the continuous-time switched nonlinear sys-

tems, while as a future direction, we can look into the robust control design problem for the discrete-time counterpart.

ADDITIONAL DIRECTIONS FOR FUTURE RESEARCH

As a final outlook, we present some more general research directions.

- **Distributed mixed integer linear programming**
 The macroscopic modeling approach and the reformulation of the optimization problems have contributed to the computational efficiency of the proposed traffic control approaches. However, if the scale of the network becomes too large, the centralized MPC scheme will not be real-time feasible. One solution is to decompose the centralized MILP optimization problem and to solve it in a distributed way. However, efficiently decomposing the centralized MILP problem, coordinating the subproblems, and characterizing the degree of suboptimality of the solution are among the challenges.
- **Combining MPC and robust H_∞ control**
 We suggest to combine the robust H_∞ control method and the MPC scheme. The conceptual approach is as follows. The MPC controller uses the prediction model along with the nominal time profile of the disturbance to optimally compute the control inputs. Meanwhile, the actual perturbation around the nominal disturbance is measured and supplied to the robust H_∞ controller. The robust controller is designed such that it minimizes the L_2 -gain from the perturbation of the disturbance to the output of the system. Design of such control system for our case of switched nonlinear systems would be interesting to investigate.
- **Robust control of switched systems using Integral Quadratic Constraints (IQCs)**
 An IQC is an integral inequality describing the relation between input/output signals of a system, in a structured and unified form. The IQC description provides a structural approach to characterize and to analyze uncertain dynamics, time-varying parameters, disturbances, nonlinearities, and combinations of them. IQC-based stability analysis and robust control often lead to efficient and relatively smaller size convex optimization problems. Therefore, we propose to investigate the possibility of using the IQC-based stability analysis and control synthesis for switched systems. In particular, for switched nonlinear systems, IQC may provide more efficient control design approaches with less inequality constraints for large number of subsystems. However, due to the multiple dynamics governing the switched system and the controlled/uncontrolled switching behavior, applying the IQC theories may need significant theoretical extensions.
- **Stochastic control for switched nonlinear systems**
 Using the stochastic properties of disturbance signals affecting the switched system, we can design stochastic optimal controllers. Although this is a challenging theoretical problem but the resulting methods would be less conservative than the robust control approach.
- **Distributed coordinated robust switching control**
 For large-scale applications of switched systems, e.g. urban networks with multiple regions and several timing plans or large-scale smart power networks with

considerable number of power converters, we would need to extend our robust switching control approach to a distributed and coordinated switching scheme. The problem is to design coordinated switching controllers for interconnected switched systems in order to achieve a global performance.

- **Application of our macroscopic modeling and control approaches in other large-scale networks**

Since the conservation law holds for many infrastructure networks such as water management systems, logistic systems, communication networks, smart grids, and even future traffic networks which may involve combined road and air traffic with perhaps private flying vehicles, we can extend our macroscopic modeling and hierarchical management schemes to design efficient control strategies for other large-scale networks.

BIBLIOGRAPHY

BIBLIOGRAPHY

- [1] K. Aboudolas, M. Papageorgiou, and E. Kosmatopoulos, "Store-and-forward based methods for the signal control problem in large-scale congested urban road networks," *Transportation Research Part C*, vol. 17, no. 2, pp. 163–174, 2009.
- [2] K. Aboudolas, M. Papageorgiou, A. Kouvelas, and E. Kosmatopoulos, "A rolling-horizon quadratic-programming approach to the signal control problem in large-scale congested urban road networks," *Transportation Research Part C*, vol. 18, pp. 680–694, 2010.
- [3] K. Aboudolas and N. Geroliminis, "Perimeter and boundary flow control in multi-reservoir heterogeneous networks," *Transportation Research Part B*, vol. 55, pp. 265–281, 2013.
- [4] A. Y. Aleksandrov, Y. Chen, A. V. Platonov, and L. Zhang, "Stability analysis for a class of switched nonlinear systems," *Automatica*, vol. 47, no. 10, pp. 2286–2291, 2011.
- [5] A. Alessandri, A. Di Febbraro, A. Ferrara, and E. Punta, "Nonlinear optimization for freeway control using variable-speed signaling," *IEEE Transactions on Vehicular Technology*, vol. 48, no. 6, pp. 2042–2052, 1999.
- [6] L. Allerhand and U. Shaked, "Robust stability and stabilization of linear switched systems with dwell time," *IEEE Transactions on Automatic Control*, vol. 56, no. 2, pp. 381–386, 2011.
- [7] A. Atamtürk and M. W. P. Savelsbergh, "Integer-programming software systems," *Annals of Operation Research*, vol. 140, no. 1, pp. 67–124, 2005.
- [8] S. Azuma, J. Imura, and T. Sugie, "Lebesgue piecewise affine approximation of nonlinear systems," *Nonlinear Analysis: Hybrid Systems*, vol. 4, no. 1, pp. 92–102, 2010.
- [9] J. Barcelo and J. Casas, "Dynamic network simulation with AIMSUN," in *Simulation Approaches in Transportation Analysis*, ser. Operations Research/Computer Science Interfaces Series, R. Kitamura and M. Kuwahara, Eds. New York, USA: Springer, 2005, vol. 31, pp. 57–98.
- [10] A. Barisone, D. Giglio, R. Minciardi, and R. Poggi, "A macroscopic traffic model for real-time optimization of signalized urban areas," in *Proceedings of the 41st IEEE Conference on Decision and Control*, Las Vegas, USA, 2002, pp. 900–903.
- [11] L. Baskar, B. De Schutter, and J. Hellendoorn, "Hierarchical model-based predictive control for intelligent vehicle highway systems: Regional controllers," in *Proceedings of the 13th International IEEE Conference on Intelligent Transportation Systems (ITSC 2010)*, Madeira Island, Portugal, 2010, pp. 249–254.
- [12] T. Bellemans, B. De Schutter, and B. De Moor, "Model predictive control for ramp metering of motorway traffic: A case study," *Control Engineering Practice*, vol. 14, no. 7, pp. 757–767, 2006.

- [13] A. Bemporad, F. Borrelli, and M. Morari, "Model predictive control based on linear programming—the explicit solution," *IEEE Transactions on Automatic Control*, vol. 47, no. 12, pp. 1974–1985, 2002.
- [14] A. Bemporad, G. Ferrari-Trecate, and M. Morari, "Observability and controllability of piecewise affine and hybrid systems," *IEEE Transactions on Automatic Control*, vol. 45, no. 10, pp. 1864–1876, 2000.
- [15] A. Bemporad and M. Morari, "Control of systems integrating logic, dynamics, and constraints," *Automatica*, vol. 35, no. 3, pp. 407–427, 1999.
- [16] A. Berman and R. J. Plemmons, *Nonnegative Matrices in the Mathematical Sciences*. New York, USA: SIAM, 1994.
- [17] C. Bielefeldt and F. Busch, "MOTION—a new on-line traffic signal network control system," in *Proceedings of the 7th International Conference on Road Traffic Monitoring and Control*, London, United Kingdom, 1994, pp. 55–59.
- [18] K. Bogenberger, S. Vukanovic, and H. Keller, "ACCEZZ—adaptive fuzzy algorithms for traffic responsive and coordinated ramp metering," in *Proceedings of the Applications of Advanced Technology in Transportation*, Boston, USA, 2002, pp. 94–99.
- [19] F. Boillot, J. Blossville, J. Lesort, V. Motyka, M. Papageorgiou, and S. Sellam, "Optimal signal control of urban traffic networks," in *Proceedings of the Conference on Road Traffic Monitoring and Control*, Washington DC, USA, 1992, pp. 75–79.
- [20] F. Boillot, S. Midenet, and J. C. Pierrelee, "The real-time urban traffic control system CRONOS: Algorithm and experiments," *Transportation Research Part C*, vol. 14, no. 1, pp. 18–38, 2006.
- [21] B. Borchers and J. E. Mitchell, "A computational comparison of branch and bound and outer approximation algorithms for 0-1 mixed integer nonlinear programs," *Computers and Operations Research*, vol. 24, pp. 699–701, 1996.
- [22] S. Boyd, L. E. Ghaoui, E. Feron, and V. Balakrishnan, *Linear Matrix Inequalities in Systems and Control Theory*. Philadelphia, USA: SIAM, 1994.
- [23] M. S. Branicky, "Multiple Lyapunov functions and other analysis tools for switched and hybrid systems," *IEEE Transactions on Automatic Control*, vol. 43, no. 4, pp. 475–482, 1998.
- [24] E. Bredensteiner and K. Bennett, "Multicategory classification by support vector machines," *Computational Optimizations and Applications*, vol. 12, no. 1–3, pp. 53–79, 1999.
- [25] C. Briat and A. Seuret, "Affine characterizations of minimal and mode-dependent dwell-times for uncertain linear switched systems," *IEEE Transactions on Automatic Control*, vol. 58, no. 5, pp. 1304–1310, 2013.
- [26] R. W. Brockett, "Asymptotic stability and feedback stabilization," in *Differential Geometric Control Theory*, R. W. Brockett, R. S. Millman, and H. J. Sussmann, Eds. Boston, USA: Birkhäuser, 1983, pp. 181–191.

- [27] C. Buisson and C. Ladier, "Exploring the impact of homogeneity of traffic measurements on the existence of macroscopic fundamental diagrams," *Transportation Research Record*, no. 2124, pp. 127–136, 2009.
- [28] R. C. Carlson, I. Papamichail, and M. Papageorgiou, "Integrated feedback ramp metering and mainstream traffic flow control on motorways using variable speed limits," *Transportation Research Part C*, vol. 46, pp. 209–221, 2014.
- [29] E. Castelan, S. Tarbouriech, and I. Queinnec, "Control design for a class of nonlinear continuous-time systems," *Automatica*, vol. 44, no. 8, pp. 2034–2039, 2008.
- [30] T. Chang and G. Sun, "Modeling and optimization of an oversaturated signalized network," *Transportation Research Part B*, vol. 38, no. 6, pp. 687–707, 2004.
- [31] D. Cheng, L. Guo, Y. Lin, and Y. Wang, "Stabilization of switched linear systems," *IEEE Transactions on Automatic Control*, vol. 50, no. 5, pp. 661–666, 2005.
- [32] S. Cheng, M. A. Epelman, and R. L. Smith, "CoSIGN: A parallel algorithm for coordinated traffic signal control," *IEEE Transactions on Intelligent Transportation Systems*, vol. 7, no. 4, pp. 551–564, 2006.
- [33] G. Chesi, P. Colaneri, J. Geromel, R. Middleton, and R. Shorten, "A nonconservative lmi condition for stability of switched systems with guaranteed dwell time," *IEEE Transactions on Automatic Control*, vol. 57, no. 5, pp. 1297–1302, 2012.
- [34] M. C. Choy, D. Srinivasan, and R. L. Cheu, "Cooperative hybrid agent architecture for real-time traffic signal control," *IEEE Transactions on Systems, Man, and Cybernetics, Part A: Systems and Humans*, vol. 33, no. 5, pp. 597–607, 2003.
- [35] P. Colaneri, J. C. Geromel, and A. Astolfi, "Stabilization of continuous-time switched nonlinear systems," *Systems & Control Letters*, vol. 57, no. 1, pp. 95–103, 2008.
- [36] Z. Cong, B. De Schutter, and R. Babuška, "A new ant colony routing approach with a trade-off between system and user optimum," in *Proceedings of the 14th International IEEE Conference on Intelligent Transportation Systems (ITSC 2011)*, Washington DC, USA, 2011, pp. 1369–1374.
- [37] D. Corona, A. Giua, and C. Seatzu, "Stabilization of switched systems via optimal control," *Nonlinear Analysis: Hybrid Systems*, vol. 11, no. 1, pp. 1–10, 2014.
- [38] F. A. Cuzzola and M. Morari, "An LMI approach for H_∞ analysis and control of discrete-time piecewise affine systems," *International Journal of Control*, vol. 75, no. 16–17, pp. 1293–1301, 2002.
- [39] J. G. da Silva Jr., E. Castelan, J. Corso, and D. Eckhard, "Dynamic output feedback stabilization for systems with sector-bounded nonlinearities and saturating actuators," *Journal of the Franklin Institute*, vol. 350, no. 3, pp. 464 – 484, 2013.
- [40] J. Daafouz, P. Riedinger, and C. Iung, "Stability analysis and control synthesis for switched systems: A switched Lyapunov function approach," *IEEE Transactions on Automatic Control*, vol. 47, no. 11, pp. 1883–1887, 2002.

- [41] C. Daganzo, "The cell transmission model: A simple dynamic representation of freeway traffic," *Transportation Research B*, vol. 28, no. 4, pp. 269–287, 1994.
- [42] C. Daganzo, "The cell transmission model, part II: Network traffic," *Transportation Research B*, vol. 29, no. 1, pp. 79–94, 1995.
- [43] C. Daganzo, "Urban gridlock: Macroscopic modeling and mitigation approaches," *Transportation Research Part B*, vol. 41, no. 1, pp. 49–62, 2007.
- [44] C. Daganzo, V. Gayah, and E. J. Gonzales, "Macroscopic relations of urban traffic variables: Bifurcations, multivaluedness and instability," *Transportation Research Part B*, vol. 45, no. 1, pp. 278–288, 2011.
- [45] C. Daganzo and N. Geroliminis, "An analytical approximation for the macroscopic fundamental diagram of urban traffic," *Transportation Research Part B*, vol. 42, no. 9, pp. 771–781, 2008.
- [46] W. Dayawansa and C. F. Martin, "A converse Lyapunov theorem for a class of dynamical systems which undergo switching," *IEEE Transactions on Automatic Control*, vol. 44, no. 4, pp. 751–760, 1999.
- [47] L. B. de Oliveira and E. Camponogara, "Multi-agent model predictive control of signaling split in urban traffic networks," *Transportation Research Part C*, vol. 18, no. 1, pp. 120–139, 2010.
- [48] B. De Schutter, S. Hoogendoorn, H. Schuurman, and S. Stramigioli, "A multi-agent case-based traffic control scenario evaluation system," in *Proceedings of the IEEE 6th International Conference on Intelligent Transportation Systems*, Shanghai, China, 2003, pp. 678–683.
- [49] G. Deaecto and J. Geromel, " H_∞ control for continuous-time switched linear systems," *Journal of Dynamic Systems, Measurement, and Control*, vol. 132, no. 4, pp. 04 101 311–04 101 317, 2010.
- [50] G. S. Deaecto, J. C. Geromel, and J. Daafouz, "Dynamic output feedback control of switched linear systems," *Automatica*, vol. 47, no. 8, pp. 1713–1720, 2011.
- [51] R. A. Decarlo, M. S. Branicky, S. Pettersson, B. Lennartson, and P. J. Antsaklis, "Perspectives and results on the stability and stabilizability of hybrid systems," *Proceedings of IEEE: Special Issue Hybrid Systems*, vol. 88, pp. 1069–1082, 2000.
- [52] M. Dotoli, M. P. Fanti, and C. Meloni, "A signal timing plan formulation for urban traffic control," *Control Engineering Practice*, vol. 14, no. 11, pp. 1297–1311, 2006.
- [53] C. Duan and F. Wu, "Analysis and control of switched linear systems via dwell-time min-switching," *Systems & Control Letters*, vol. 70, pp. 8–16, 2014.
- [54] C. Duan and F. Wu, "Analysis and control of switched linear systems via modified Lyapunov-Metzler inequalities," *International Journal of Robust and Nonlinear Control*, vol. 24, no. 5, pp. 276–294, 2014.

- [55] N. H. El-Farra, P. Mhaskar, and P. Christofides, "Output feedback control of switched nonlinear systems using multiple Lyapunov functions," *Systems & Control Letters*, vol. 54, no. 12, pp. 1163–1182, 2005.
- [56] L. Fang, H. Lin, and P. J. Antsaklis, "Stabilization and performance analysis for a class of switched systems," in *Proceedings of the 43rd IEEE Decision and Control Conference*, Paradise Island, Bahamas, 2004, pp. 3265–3270.
- [57] J. Farges, J. Henry, and J. Tufal, "The PRODYN real-time traffic algorithm," in *Proceedings of the 4th IFAC Symposium of Transportation Systems*, Baden, Germany, 1983, pp. 307–312.
- [58] M. Fellendorf and P. Vortisch, "Microscopic traffic flow simulator vissim," in *Fundamentals of Traffic Simulation*, ser. International Series in Operations Research and Management Science, J. Barceló, Ed. New York, USA: Springer, 2010, vol. 145, pp. 63–93.
- [59] A. Ferrara, S. Sacone, and S. Siri, "Supervisory model predictive control for freeway traffic systems," in *Proceedings of IEEE 52nd Annual Conference on Decision and Control (CDC)*, Florence, Italy, 2013, pp. 905–910.
- [60] G. Ferrari-Trecate, M. Muselli, D. Liberati, and M. Morari, "A clustering technique for the identification of piecewise affine systems," *Automatica*, vol. 39, no. 2, pp. 205–217, 2003.
- [61] A. F. Filippov, *Differential Equations with Discontinuous Right Hand Side*. Norwell, USA: Kluwer Academic, 1988.
- [62] R. Fletcher, *Practical Methods of Optimization, Volume 1: Unconstrained Optimization*. Chichester, England: John Wiley and Sons, 1980.
- [63] J. Frejo and E. Camacho, "Global versus local MPC algorithms in freeway traffic control with ramp metering and variable speed limits," *IEEE Transactions on Intelligent Transportation Systems*, vol. 13, no. 4, pp. 1556–1565, 2012.
- [64] K. Garg, *Theory of Differentiation: A Unified Theory of Differentiation via New Derivate Theorems and New Derivatives*. New York, USA: Wiley-Interscience, 1998.
- [65] N. H. Gartner, F. J. Pooran, and C. M. Andrews, "Implementation of the OPAC adaptive control strategy in a traffic signal network," in *Proceedings of the 4th International IEEE Conference on Intelligent Transportation Systems*, Oakland, USA, 2001, pp. 195–200.
- [66] N. Gartner, "Simulation study of OPAC: A demand-responsive strategy for traffic signal control," *Transportation and Traffic Theory*, vol. 12, pp. 233–250, 1983.
- [67] N. Geroliminis, N. Zheng, and K. Aboudolas, "A three-dimensional macroscopic fundamental diagram for mixed bi-modal urban networks," *Transportation Research Part C*, vol. 42, no. 3, pp. 168–181, 2014.

- [68] N. Geroliminis and B. Boyaci, "The effect of variability of urban systems characteristics in the network capacity," *Transportation Research Part B*, vol. 46, no. 10, pp. 1607–1623, 2012.
- [69] N. Geroliminis and C. Daganzo, "Macroscopic modeling of traffic in cities," in *Proceedings of the 86th Annual Meeting of the Transportation Research Board*, no. 07-0413, Washington DC, USA, 2007, pp. 1–21.
- [70] N. Geroliminis and C. F. Daganzo, "Existence of urban-scale macroscopic fundamental diagrams: some experimental findings," *Transportation Research Part B*, vol. 42, no. 9, pp. 759–770, 2008.
- [71] N. Geroliminis, J. Haddad, and M. Ramezani, "Optimal perimeter control for two urban regions with macroscopic fundamental diagrams: A model predictive approach," *IEEE Transactions on Intelligent Transportation Systems*, vol. 14, no. 1, pp. 348–359, 2013.
- [72] N. Geroliminis and J. Sun, "Properties of a well-defined macroscopic fundamental diagram for urban traffic," *Transportation Research Part B*, vol. 45, no. 3, pp. 605–617, 2011.
- [73] J. Geromel and P. Colaneri, "Stability and stabilization of continuous-time switched linear systems," *SIAM Journal on Control and Optimization*, vol. 45, no. 5, pp. 1915–1930, 2006.
- [74] J. Geromel, G. Deaecto, and J. Daafouz, "Suboptimal switching control consistency analysis for switched linear systems," *IEEE Transactions on Automatic Control*, vol. 58, no. 7, pp. 1857–1861, 2013.
- [75] J. C. Geromel and G. S. Deaecto, "Switched state feedback control for continuous-time uncertain systems," *Automatica*, vol. 45, no. 2, pp. 593–597, 2009.
- [76] J. Geromel, P. Colaneri, and P. Bolzern, "Dynamic output feedback control of switched linear systems," *IEEE Transactions on Automatic Control*, vol. 53, no. 3, pp. 720–733, 2008.
- [77] J. W. Godfrey, "The mechanism of a road network," *Traffic Engineering and Control*, vol. 11, no. 7, pp. 323–327, 1969.
- [78] R. Goebel, R. Sanfelice, and A. Teel, "Hybrid dynamical systems," *IEEE Control Systems Magazine*, vol. 29, no. 2, pp. 28–93, 2009.
- [79] G. Golub and C. Van Loan, *Matrix Computations*, 2nd ed. Baltimore, Maryland: The John Hopkins University Press, 1989.
- [80] G. Gomes and R. Horowitz, "Optimal freeway ramp metering using the asymmetric cell transmission model," *Transportation Research Part C*, vol. 14, no. 4, pp. 244–262, 2006.
- [81] C. A. C. Gonzaga, M. Jungers, and J. Daafouz, "Stability analysis and stabilization of switched nonlinear systems," *International Journal of Control*, vol. 85, no. 7, pp. 822–829, 2012.

- [82] C. A. C. Gonzaga, M. Jungers, and J. Daafouz, "Stability analysis of discrete-time Lur'e systems," *Automatica*, vol. 48, no. 10, pp. 2277–2283, 2012.
- [83] N. Groot, B. De Schutter, and H. Hellendoorn, "Toward system-optimal routing in traffic networks: A reverse stackelberg game approach," *IEEE Transactions on Intelligent Transportation Systems*, pp. 1–12, 2014.
- [84] J. Haddad, B. De Schutter, D. Mahalel, I. Ioslovich, and P.-O. Gutman, "Optimal steady-state control for isolated traffic intersections," *IEEE Transactions on Automatic Control*, vol. 55, no. 11, pp. 2612–617, 2010.
- [85] J. Haddad and A. Shraiber, "Robust perimeter control design for an urban region," *Transportation Research Part B*, vol. 68, no. 6, pp. 315–332, 2014.
- [86] J. Haddad and N. Geroliminis, "On the stability of traffic perimeter control in two-region urban cities," *Transportation Research Part B*, vol. 46, no. 1, pp. 1159–1176, 2012.
- [87] J. Haddad, M. Ramezani, and N. Geroliminis, "Cooperative traffic control of a mixed network with two urban regions and a freeway," *Transportation Research Part B*, vol. 54, no. 8, pp. 17–36, 2013.
- [88] M. Hajiahmadi, R. Corthout, C. Tampère, B. De Schutter, and H. Hellendoorn, "Variable speed limit control based on the extended link transmission model," *Transportation Research Record*, no. 2390, pp. 11–19, 2013.
- [89] M. Hajiahmadi, B. De Schutter, and H. Hellendoorn, "Control of traffic networks using the link transmission model and mixed integer linear programming," in *Proceedings of the 1st European Symposium on Quantitative Methods in Transportation Systems*, Lausanne, Switzerland, 2012.
- [90] M. Hajiahmadi, B. De Schutter, and H. Hellendoorn, "Model predictive traffic control: A mixed-logical dynamic approach based on the link transmission model," in *Proceedings of the 13th IFAC Symposium on Control in Transportation Systems (CTS'2012)*, Sofia, Bulgaria, 2012, pp. 144–149.
- [91] M. Hajiahmadi, B. De Schutter, and H. Hellendoorn, "Robust H_∞ control for switched nonlinear systems with application to high-level urban traffic control," in *Proceedings of the 52nd IEEE Conference on Decision and Control*, Florence, Italy, 2013, pp. 899–904.
- [92] M. Hajiahmadi, B. De Schutter, and H. Hellendoorn, "Robust H_∞ control of a class of switched nonlinear systems with application to macroscopic urban traffic control," in *Proceedings of the 53rd IEEE Conference on Decision and Control*, Los Angeles, USA, 2014, pp. 1727–1732.
- [93] M. Hajiahmadi, B. De Schutter, and H. Hellendoorn, "Stabilization and robust H_∞ control for sector-bounded switched nonlinear systems," *Automatica*, vol. 50, no. 10, pp. 2726–2731, 2014.

- [94] M. Hajiahmadi, B. De Schutter, and H. Hellendoorn, "Stabilization and robust H_∞ control for mixed switching affine systems," *IEEE Transactions on Automatic Control*, accepted, 2015.
- [95] M. Hajiahmadi, J. Haddad, B. De Schutter, and N. Geroliminis, "Optimal hybrid macroscopic traffic control for urban regions: Perimeter and switching signal plans controllers," in *Proceedings of the 12th European Control Conference*, Zürich, Switzerland, 2013, pp. 3000–3005.
- [96] M. Hajiahmadi, J. Haddad, B. De Schutter, and N. Geroliminis, "Optimal hybrid perimeter and switching plans control for urban traffic networks," *IEEE Transactions on Control Systems Technology*, vol. 23, no. 2, pp. 464–478, 2015.
- [97] M. Hajiahmadi, V. L. Knoop, B. De Schutter, and H. Hellendoorn, "Optimal dynamic route guidance: A model predictive approach using the macroscopic fundamental diagram," in *Proceedings of the 16th IEEE Conference on Intelligent Transportation Systems*, The Hague, The Netherlands, 2013, pp. 1022–1028.
- [98] M. Hajiahmadi, G. van de Weg, C. Tampère, R. Corthout, A. Hegyi, B. De Schutter, and H. Hellendoorn, "Integrated predictive control of freeway networks using the extended link transmission model," *IEEE Transactions on Intelligent Transportation Systems*, accepted, 2015.
- [99] A. Hassibi and S. Boyd, "Quadratic stabilization and control of piecewise-linear systems," in *Proceedings of the 1998 American Control Conference*, 1998, pp. 3659–3664.
- [100] F. Hayes-Roth, "Rule-based systems," *Communications of the ACM*, vol. 28, no. 9, pp. 921–932, 1985.
- [101] W. Heemels, M. Lazar, N. van de Wouw, and A. Pavlov, "Observer-based control of discrete-time piecewise affine systems: Exploiting continuity twice," in *Proceedings of the IEEE Conference on Decision and Control*, Cancun, Mexico, December 2008, pp. 4675–4680.
- [102] W. Heemels and S. Weiland, "Input-to-state stability and interconnections of discontinuous dynamical systems," *Automatica*, vol. 44, pp. 3079–3086, December 2008.
- [103] A. Hegyi, *Model Predictive Control for Integrating Traffic Control Measures*. Delft, The Netherlands: Ph.D. dissertation, Delft University of Technology, 2004.
- [104] A. Hegyi, B. De Schutter, and H. Hellendoorn, "Model predictive control for optimal coordination of ramp metering and variable speed limits," *Transportation Research Part C*, vol. 13, no. 3, pp. 185–209, 2005.
- [105] D. Helbing, "Improved fluid-dynamic model for vehicular traffic," *Physical Review E*, vol. 51, no. 4, pp. 3164–3169, 1995.
- [106] D. Helbing, "Gas-kinetic derivation of Navier-Stokes-like traffic equations," *Physical Review*, vol. 53, no. 3, pp. 2366–2381, 1996.

- [107] D. Helbing, "Derivation of a fundamental diagram for urban traffic flow," *The European Physical Journal B*, vol. 70, no. 2, pp. 229–241, 2009.
- [108] D. Helbing, A. Hennecke, V. Shvetsov, and M. Treiber, "Micro- and macro-simulation of freeway traffic," *Mathematical and Computer Modeling*, vol. 35, no. 6, pp. 517–547, 2002.
- [109] R. Herman and I. Prigogine, "A two-fluid approach to town traffic," *Science*, vol. 204, no. 4389, pp. 148–151, 1979.
- [110] J. Hespanha and A. Morse, "Stability of switched systems with average dwell-time," in *Proceedings of the 38th IEEE Control and Decision Conference*, Phoenix, USA, 1999, pp. 2655–2660.
- [111] J. P. Hespanha, " \mathcal{L}_2 -induced gains of switched linear systems," in *Unsolved Problems in Mathematical Systems & Control Theory*, V. D. Blondel and A. Megretski, Eds. Princeton, USA: Princeton University Press, 2003, pp. 131–133.
- [112] J. P. Hespanha, "Uniform stability of switched linear systems: Extensions of LaSalle's invariance principle," *IEEE Transactions on Automatic Control*, vol. 49, no. 4, pp. 470–482, 2004.
- [113] J. P. Hespanha and A. S. Morse, "Switching between stabilizing controllers," *Automatica*, vol. 38, no. 11, pp. 1905–1907, 2002.
- [114] T. Heung, T. Ho, and Y. Fung, "Coordinated road-junction traffic control by dynamic programming," *IEEE Transactions on Intelligent Transportation Systems*, vol. 6, no. 3, pp. 341–350, 2005.
- [115] W. Himpe, R. Corthout, C. M. Tampère, and B. Immers, "An implicit solution scheme for the link transmission model," in *Proceedings of the 16th IEEE Intelligent Transportation Systems Conference*, The Hague, The Netherlands, 2013, pp. 572–577.
- [116] S. Hoogendoorn and P. Bovy, "State-of-the-art of vehicular traffic flow modelling," *Proceedings of the Institution of Mechanical Engineers, Part I: Journal of Systems and Control Engineering*, vol. 215, no. 4, pp. 283–303, 2001.
- [117] S. Hoogendoorn, B. De Schutter, and H. Schuurman, "Decision support in dynamic traffic management, Real-time scenario evaluation," *European Journal of Transport and Infrastructure Research*, vol. 3, no. 1, pp. 21–38, 2003.
- [118] T. Hu, L. Ma, and Z. Lin, "Stabilization of switched systems via composite quadratic functions," *IEEE Transactions on Automatic Control*, vol. 53, no. 11, pp. 2571–2585, 2008.
- [119] H. Ye, A. N. Michel, and L. Hou, "Stability theory for hybrid dynamical systems," *IEEE Transactions on Automatic Control*, vol. 43, no. 4, pp. 461–474, 1998.
- [120] H. Ishii, T. Basar, and R. Tempo, "Randomized algorithms for synthesis of switching rules for multimodal systems," *IEEE Transactions on Automatic Control*, vol. 50, no. 6, pp. 754–767, 2005.

- [121] A. Isidori, *Nonlinear Control Systems*. Berlin, Germany: Springer-Verlag, 1995.
- [122] B. N. Janson, "Dynamic traffic assignment for urban road networks," *Transportation Research Part B*, vol. 25B, no. 2/3, pp. 143–161, 1991.
- [123] Y. Ji and N. Geroliminis, "On the spatial partitioning of urban transportation networks," *Transportation Research Part B*, vol. 46, no. 10, pp. 1639–1656, 2012.
- [124] Z. Ji, X. Guo, L. Wang, and G. Xie, "Robust H_∞ control and stabilization of uncertain switched linear systems: A multiple Lyapunov functions approach," *Transactions of the ASME Journal of Dynamic Systems, Measurement and Control*, vol. 128, pp. 696–700, 2006.
- [125] W. Jin and H. Zhang, "On the distribution schemes for determining flows through a merge," *Transportation Research B*, vol. 37, no. 6, pp. 521–540, 2003.
- [126] M. Johansson, *Piecewise Linear Control Systems*. Berlin Heidelberg, Germany: Springer-Verlag, 2003.
- [127] M. Jungers, C. A. C. Gonzaga, and J. Daafouz, "Min-switching local stabilization for discrete-time switching systems with nonlinear modes," *Nonlinear Analysis: Hybrid Systems*, vol. 9, no. 1, pp. 18–26, 2013.
- [128] T. Kailath, *Linear Systems*. Englewood Cliffs, USA: Prentice Hall International, 1998.
- [129] M. Kamal, M. Mukai, J. Murata, and T. Kawabe, "Model predictive control of vehicles on urban roads for improved fuel economy," *IEEE Transactions on Control Systems Technology*, vol. 21, no. 3, pp. 831–841, 2013.
- [130] O. Karabacak, "Dwell time and average dwell time methods based on the cycle ratio of the switching graph," *Systems & Control Letters*, vol. 62, no. 11, pp. 1032–1037, 2013.
- [131] H. Kashani and G. Saridis, "Intelligent control for urban traffic systems," *Automatica*, vol. 19, no. 2, pp. 191–197, 1983.
- [132] E. Kazkurewicz and A. Bhaya, *Matrix Diagonal Stability in Systems and Computation*. Boston, USA: Birkhäuser, 1999.
- [133] B. S. Kerner and P. Konhauser, "Cluster effect in initially homogeneous traffic flow," *Physical Review E*, vol. 48, no. 3, pp. 2335–2338, 1993.
- [134] M. Keyvan-Ekbatani, A. Kouvelas, I. Papamichail, and M. Papageorgiou, "Exploiting the fundamental diagram of urban networks for feedback-based gating," *Transportation Research Part B*, vol. 46, no. 10, pp. 1393–1403, 2012.
- [135] M. Keyvan-Ekbatani, M. Papageorgiou, and I. Papamichail, "Urban congestion gating control based on reduced operational network fundamental diagrams," *Transportation Research Part C*, vol. 33, no. 4, pp. 74–87, 2013.

- [136] V. L. Knoop, S. Hoogendoorn, and J. W. C. van Lint, "Routing strategies based on the macroscopic fundamental diagram," in *Proceedings of the 91th Annual Meeting of the Transportation Research Board*, no. 12-0227, Washington DC, USA, 2012, pp. 1–10.
- [137] E. Kosmatopoulos, M. Papageorgiou, A. Vakouli, and A. Kouvelas, "Adaptive fine-tuning of nonlinear control systems with application to the urban traffic control strategy TUC," *IEEE Transactions on Control Systems Technology*, vol. 15, no. 6, pp. 991–1002, 2007.
- [138] A. Kotsialos, M. Papageorgiou, M. Mangeas, and H. Haj-Salem, "Coordinated and integrated control of motorway networks via nonlinear optimal control," *Transportation Research Part C*, vol. 10, no. 1, pp. 65–84, 2002.
- [139] A. Kotsialos and M. Papageorgiou, "Efficiency and equity properties of freeway network-wide ramp metering with AMOC," *Transportation Research Part C*, vol. 12, no. 6, pp. 401–420, 2004.
- [140] A. Kotsialos and M. Papageorgiou, "Nonlinear optimal control applied to coordinated ramp metering," *IEEE Transactions on Control Systems Technology*, vol. 12, no. 6, pp. 920–932, 2004.
- [141] A. Kotsialos, M. Papageorgiou, C. Diakaki, Y. Pavlis, and F. Middelham, "Traffic flow modeling of large-scale motorway networks using the macroscopic modeling tool METANET," *IEEE Transactions on Intelligent Transportation Systems*, vol. 3, no. 4, pp. 282–292, 2002.
- [142] L. Lasdon, *Optimization Theory for Large Systems*. New York, USA: Macmillan, 1970.
- [143] J. Lebacque, "The Godunov scheme and what it means for first order traffic flow models," in *Proceedings of the 13th International Symposium of Transportation and Traffic Theory (ISTTT)*, Lyon, France, 1996, pp. 621–644.
- [144] L. Leclercq, V. Knoop, F. Marczak, and S. Hoogendoorn, "Capacity drop at merges: New analytical investigations," in *Proceedings of the 17th International IEEE Conference on Intelligent Transportation Systems*, Qindao, China, 2014, pp. 1129–1134.
- [145] L. Leclercq, N. Chiabaut, and B. Trinquier, "Macroscopic fundamental diagrams: A cross-comparison of estimation methods," *Transportation Research Part B*, vol. 62, pp. 1–12, 2014.
- [146] H. Lenz, R. Sollacher, and M. Lang, "Nonlinear speed-control for a continuum theory of traffic flow," in *Proceedings of the 14th IFAC World Congress*, Beijing, China, 1999, pp. 67–72.
- [147] L.-L. Li, J. Zhao, and G. Dimirovski, "Robust H_∞ control for a class of uncertain switched nonlinear systems using constructive approach," in *Proceedings of the 2008 American Control Conference*, Seattle, USA, 2008, pp. 5068–5073.

- [148] Y. Li, J. Xu, and L. Shen, "A perimeter control strategy for oversaturated network preventing queue spillback," *Procedia–Social and Behavioral Sciences*, vol. 43, no. 8, pp. 418–427, 2012.
- [149] D. Liberzon, *Switching in Systems and Control*. Boston, USA: Birkhäuser, 2003.
- [150] D. Liberzon and A. Morse, "Basic problems in stability and design of switched systems," *IEEE Control Systems Magazine*, vol. 19, no. 5, pp. 59–70, 1999.
- [151] M. Lighthill and G. Whitman, "On kinematic waves II: A traffic flow theory on long crowded roads," *Proceedings of the Royal Society of London Series A*, vol. 229, no. 1178, pp. 317–345, 1995.
- [152] H. Lin and P. Antsaklis, "Stability and stabilizability of switched linear systems: A survey of recent results," *IEEE Transactions on Automatic Control*, vol. 54, no. 2, pp. 308–322, 2009.
- [153] S. Lin, B. De Schutter, A. Hegyi, Y. Xi, and H. Hellendoorn, "On a spatiotemporally discrete urban traffic model," *IET Intelligent Transport Systems*, vol. 8, no. 3, pp. 219–231, 2014.
- [154] S. Lin, B. De Schutter, Y. Xi, and H. Hellendoorn, "Fast model predictive control for urban road networks via MILP," *IEEE Transactions on Intelligent Transportation Systems*, vol. 12, no. 3, pp. 846–856, 2011.
- [155] S. Liu, B. De Schutter, and H. Hellendoorn, "Multi-class traffic flow and emission control for freeway networks," in *Proceedings of the 16th IEEE Intelligent Transportation Systems Conference*, The Hague, The Netherlands, 2013, pp. 2223–2228.
- [156] H. K. Lo, "A cell-based traffic control formulation: Strategies and benefits of dynamic timing plans," *Transportation Science*, vol. 35, no. 2, pp. 148–164, 2001.
- [157] H. Lo, E. Chang, and Y. Chan, "Dynamic network traffic control," *Transportation Research Part A*, vol. 35, no. 8, pp. 721–744, 2001.
- [158] F. Long, S. Fei, Z. Fu, S. Zheng, and W. Wei, " H_∞ control and stabilization of switched linear systems with linear fractional uncertainties via output feedback," *Nonlinear Analysis: Hybrid Systems*, vol. 2, no. 1, pp. 18–27, 2008.
- [159] P. Lowrie, "The Sydney coordinated adaptive traffic system: Principles, methodology, algorithms," in *Proceedings of the International Conference on Road Traffic Signalling*, London, United Kingdom, 1982, pp. 67–70.
- [160] J. Maciejowski, *Predictive Control with Constraints*. Harlow, England: Prentice Hall, 2002.
- [161] H. Mahmassani, J. Williams, and R. Herman, "Performance of urban traffic networks," in *Proceedings of the 10th International Symposium on Transportation and Traffic Theory*, N. Gartner and N. Wilson, Eds. Amsterdam, The Netherlands: Elsevier, 1987, pp. 1–20.

- [162] H. Majid, M. Hajiahmadi, B. De Schutter, H. Abouaïssa, and D. Jolly, "Distributed model predictive control of freeway traffic networks: A serial partially cooperative approach," in *Proceedings of the 17th International IEEE Conference on Intelligent Transportation Systems*, Qingdao, China, 2014, pp. 1876–1881.
- [163] J. L. Mancilla-Aguilar and R. A. Garcia, "A converse Lyapunov theorem for nonlinear switched systems," *Systems & Control Letters*, vol. 41, no. 1, pp. 67–71, 2000.
- [164] V. Mauro and C. Di Taranto, "Utopia," in *Proceedings of the 2nd IFAC-IFIP-IFORS Symposium on Traffic Control and Transportation Systems*, Paris, France, 1989, pp. 575–597.
- [165] A. May, *Traffic Flow Fundamentals*. Englewood Cliffs, USA: Prentice Hall, 1990.
- [166] A. Mazlounian, N. Geroliminis, and D. Helbing, "The spatial variability of vehicle densities as determinant of urban network capacity," *Philosophical Transactions of the Royal Society A: Mathematical, Physical and Engineering Sciences*, vol. 368, no. 1928, pp. 4627–4647, 2010.
- [167] R. D. McKelvey and A. McLennan, *Handbook of Computational Economics*. Amsterdam, The Netherlands: Elsevier, 1996, ch. Computation of equilibria in finite games, pp. 87–142.
- [168] A. Messmer and M. Papageorgiou, "METANET: A macroscopic simulation program for motorway networks," *Traffic Engineering and Control*, vol. 31, no. 9, pp. 466–470, 1990.
- [169] E. Mojica-Nava, N. Quijano, N. Rakoto-Ravalontsalama, and A. Gauthier, "A polynomial approach for stability analysis of switched systems," *Systems & Control Letters*, vol. 59, pp. 98–104, 2010.
- [170] A. P. Molchanov and E. Pyatnitskiy, "Criteria of asymptotic stability of differential and difference inclusions encountered in control theory," *Systems & Control Letters*, vol. 13, no. 1, pp. 59–64, 1989.
- [171] D. Monderer and L. Shapley, "Fictitious play property for games with identical interests," *Journal of Economic Theory*, vol. 68, no. 1, pp. 258–265, 1996.
- [172] V. Montagner, R. Oliveira, T. Calliero, R. Borges, P. Peres, and C. Prieur, "Robust absolute stability and nonlinear state feedback stabilization based on polynomial Lur'e functions," *Nonlinear Analysis: Theory, Methods, and Applications*, vol. 70, no. 5, pp. 1803–1812, 2009.
- [173] A. S. Morse, "Supervisory control of families of linear set-point controllers—part 1: exact matching," *IEEE Transactions on Automatic Control*, vol. 41, no. 10, pp. 1413–1431, 1996.
- [174] K. Nagel, "Microscopic traffic modeling on parallel high performance computers," *Parallel Computing*, vol. 20, no. 1, pp. 125–146, 1994.
- [175] K. Nagel, "Particle hopping models and traffic flow theory," *Physical Review E*, vol. 53, no. 5, pp. 4655–4672, 1996.

- [176] K. S. Narendra and J. Balakrishnan, "A common Lyapunov function for stable LTI systems with commuting A-matrices," *IEEE Transactions on Automatic Control*, vol. 39, no. 12, pp. 2469–2471, 1994.
- [177] G. Newell, "A simplified theory of kinematic waves in highway traffic, part III: Multi-destination flows," *Transportation Research Part B*, vol. 27, no. 4, pp. 281–313, 1993.
- [178] D. Ni and J. Leonard, "A simplified kinematic wave model at a merge bottleneck," *Applied Mathematical Modelling*, vol. 29, no. 11, pp. 1045–1072, 2005.
- [179] B. Niu and J. Zhao, "Robust H_∞ control for a class of switched nonlinear cascade systems via multiple Lyapunov functions approach," *Applied Mathematics and Computation*, vol. 218, no. 11, pp. 6330–6339, 2012.
- [180] B. Noble, *Applied Linear Algebra*. Englewood Cliffs, USA: Prentice Hall, 1969.
- [181] J. Ortigosa, M. Menendez, and H. Tapia, "Study on the number and location of measurement points for an MFD perimeter control scheme: a case study of Zürich," *EURO Journal on Transportation and Logistics*, vol. 1, no. 3, pp. 245–266, 2013.
- [182] M. Papageorgiou, "Some remarks on macroscopic traffic flow modelling," *Transportation Research Part A*, vol. 32, no. 5, pp. 323–329, 1998.
- [183] M. Papageorgiou, C. Diakaki, V. Dinopoulou, A. Kotsialos, and Y. Wang, "Review of road traffic control strategies," *Proceedings of the IEEE*, vol. 91, no. 12, pp. 2043–2067, 2003.
- [184] M. Papageorgiou, H. Hadj-Salem, and J. M. Blosseville, "ALINEA: A local feedback control law for on-ramp metering," *Transportation Research Record*, no. 1320, pp. 58–64, 1991.
- [185] M. Papageorgiou, "Dynamic modeling, assignment, and route guidance in traffic networks," *Transportation Research Part B*, vol. 24B, no. 6, pp. 471–495, 1990.
- [186] I. Papamichail and M. Papageorgiou, "Traffic-responsive linked ramp-metering control," *IEEE Transactions on Intelligent Transportation Systems*, vol. 9, no. 1, pp. 111–121, 2008.
- [187] I. Papamichail, A. Kotsialos, I. Margonis, and M. Papageorgiou, "Coordinated ramp metering for freeway networks – a model-predictive hierarchical control approach," *Transportation Research Part C*, vol. 18, no. 3, pp. 311–331, 2010.
- [188] Y. Pavlis and W. Recker, "A mathematical logic approach for the transformation of the linear conditional piecewise functions of dispersion-and-store and cell transmission traffic flow models into linear mixed-integer form," *Transportation Science*, vol. 43, no. 1, pp. 98–116, 2009.
- [189] H. Payne, "Models of freeway traffic and control," *Mathematical Models of Public Systems*, vol. 9, no. 4, pp. 225–235, 1975.

- [190] S. Peeta and A. Ziliaskopoulos, "Foundations of dynamic traffic assignment: The past, the present and the future," *Networks and Spatial Economics*, vol. 1, no. 3/4, pp. 233–265, 2001.
- [191] S. Pettersson, "Synthesis of switched linear systems," in *Proceedings of 42nd IEEE Decision and Control Conference*, Maui, USA, 2003, pp. 5283–5288.
- [192] S. Pettersson and B. Lennartson, "Hybrid system stability and robustness verification using linear matrix inequalities," *International Journal of Control*, vol. 75, no. 16, pp. 1335–1355, 2002.
- [193] W. Philips, "A kinetic model for traffic flow with continuum implications," *Transportation Planning and Technology*, vol. 5, no. 3, pp. 131–138, 1979.
- [194] L. Pipes, "An operational analysis of traffic dynamics," *Journal of Applied Physics*, vol. 24, no. 3, pp. 274–281, 1953.
- [195] D. Pisarski and C. Canudas de Wit, "Optimal balancing of road traffic density distributions for the Cell Transmission Model," in *Proceedings of IEEE 51st Annual Conference on Decision and Control*, Maui, USA, 2012, pp. 6969–6974.
- [196] T. Ranney, "Psychological factors that influence car-following and car-following model development," *Transportation Research Part F*, vol. 2, no. 4, pp. 213–219, 1999.
- [197] A. Rantzer and M. Johansson, "Piecewise linear quadratic optimal control," *IEEE Transactions on Automatic Control*, vol. 45, no. 4, pp. 629–637, 2000.
- [198] J. Rawlings and D. Mayne, *Model Predictive Control: Theory and Design*. Madison, USA: Nob Hill Publishing, 2009.
- [199] S. Ray, *Graph Theory with Algorithms and Its Applications*. New Delhi, India: Springer, 2013.
- [200] P. Richard, "Shock waves on the highway," *Operation Research*, vol. 4, no. 1, pp. 42–51, 1956.
- [201] S. G. Ritchie, "A knowledge-based decision support architecture for advanced traffic management," *Transportation Research Part A*, vol. 24, no. 1, pp. 27–37, 1990.
- [202] D. Robertson, "TRANSYT: A traffic network study tool," Road Research Laboratory, Crowthorne, United Kingdom, Tech. Rep. 253, 1969.
- [203] D. Robertson and R. Bretherton, "Optimizing networks of traffic signals in real time - the SCOOT method," *IEEE Transactions on Vehicular Technology*, vol. 40, no. 1, pp. 11–15, 1991.
- [204] L. Rodrigues and J. P. How, "Observer-based control of piecewise-affine systems," *Journal of Control*, vol. 76, no. 5, pp. 459–477, 2003.
- [205] S. Russell and P. Norvig., *Artificial Intelligence: A Modern Approach*. Englewood Cliffs, USA: Prentice-Hall, 2003.

- [206] M. Saberi and H. Mahmassani, "Exploring properties of network-wide flow-density relations in a freeway network," in *Proceedings of the 91th Annual Meeting of the Transportation Research Board*, no. 12-2203, Washington DC, USA, 2012, pp. 153–163.
- [207] T. Saumtally, J. Lebacque, and H. Haj-Salem, "Static traffic assignment with side constraints in a dense orthotropic network," *Procedia–Social and Behavioral Sciences*, vol. 20, no. 1, pp. 465–474, 2011.
- [208] C. C. Scharlau, M. C. de Oliveira, A. Trofino, and T. J. Dezuó, "Switching rule design for affine switched systems using a max-type composition rule," *Systems & Control Letters*, vol. 68, pp. 1–8, 2014.
- [209] C. Scherer, P. Gahinet, and M. Chilali, "Multi-objective output feedback control via LMI optimization," *IEEE Transactions on Automatic Control*, vol. 42, no. 2, pp. 896–911, 1997.
- [210] S. Sen and K. Head, "Controlled optimization of phases at an intersection," *Transportation Science*, vol. 31, no. 1, pp. 5–17, 1997.
- [211] A. Skabardonis and N. Geroliminis, "Real-time monitoring and control on signalized arterials," *Journal of Intelligent Transportation Systems*, vol. 12, no. 2, pp. 64–74, 2008.
- [212] E. Skafidas, R. J. Evans, A. V. Savkin, and I. R. Petersen, "Stability results for switched controller systems," *Automatica*, vol. 35, no. 4, pp. 553–564, 1999.
- [213] S. Smulders, "Control of freeway traffic flow by variable speed signs," *Transportation Research Part B*, vol. 24, no. 2, pp. 111–132, 1990.
- [214] S. Smulders, "Modeling and simulation of freeway traffic flow," Centre for Mathematics and Computer Science, Amsterdam, Netherlands, Report OS-R8615, 1986.
- [215] S. Smulders, "Modeling and filtering of freeway traffic flow," in *Proceedings of the 10th International Symposium of Transportation and Traffic Theory*, N. Gartner and N. Wilson, Eds. New York, USA: Elsevier, 1987, pp. 139–158.
- [216] S. Smulders, "Control of freeway traffic flow," Ph.D. dissertation, University of Twente, Enschede, Netherlands, 1989.
- [217] E. Sontag, "Nonlinear regulations: The piecewise linear approach," *IEEE Transactions on Automatic Control*, vol. 26, no. 2, pp. 346–357, 1981.
- [218] Z. Sun, S. S. Ge, and T. H. Lee, "Controllability and reachability criteria for switched linear systems," *Automatica*, vol. 38, no. 5, pp. 775–786, 2002.
- [219] H. Taale and F. Middelham, "Ten years of ramp-metering in The Netherlands," in *Proceedings of the 10th International Conference on Road Transport Information and Control*, London, United Kingdom, 2000, pp. 106–110.

- [220] C. Tampère, R. Corthout, D. Cattrysse, and L. H. Immers, "A generic class of first order node models for dynamic macroscopic simulation of traffic flows," *Transportation Research Part B*, vol. 45, no. 1, pp. 289–309, 2011.
- [221] H. Thanh-Trung, S. Ge, and L. T. Heng, "Persistent dwell-time switched nonlinear systems: Variation paradigm and gauge design," *IEEE Transactions on Automatic Control*, vol. 55, no. 2, pp. 321–327, 2010.
- [222] J. Van Antwerp and R. Braatz, "A tutorial on linear and bilinear matrix inequalities," *Journal of Process Control*, vol. 10, no. 1, pp. 363–385, 2000.
- [223] M. van den Berg, A. Hegyi, B. De Schutter, and J. Hellendoorn, "Integrated traffic control for mixed urban and freeway networks: A model predictive control approach," *European Journal of Transport and Infrastructure Research*, vol. 7, no. 3, pp. 223–250, 2007.
- [224] E. van der Hoogen and S. Smulders, "Control by variable speed signs: Results of the dutch experiment," in *Proceedings of the 7th IEE International Conference on Road Traffic Monitoring and Control*, London, Engeland, 1994, pp. 145–149.
- [225] A. van der Schaft, *L₂-Gain and Passivity Techniques in Nonlinear Control*. New York, USA: Springer, 2000.
- [226] J. W. C. van Lint, S. P. Hoogendoorn, and M. Schreuder, "Faslane: A new multiclass first-order traffic flow model," *Transportation Research Record*, no. 2088, pp. 177–187, 2008.
- [227] J. H. van Schuppen, "Routing of freeway traffic – a state space model and routing problems," in *Proceedings of the 30th IEEE Conference on Decision and Control*, New York, USA, 1991, pp. 2194–2195.
- [228] J. H. van Schuppen, "Routing control of motorway networks," in *Coordinated control strategies*. Hague Consulting Group, 1997.
- [229] D. van Zwieten, E. Lefeber, and W. Heemels, "Observer design for a class of piecewise affine hybrid systems," in *Proceedings of Hybrid Systems: Computation and Control (HSCC)*, Philadelphia, USA, 2013, pp. 153–162.
- [230] F. Viti and C. M. Tampère, "Dynamic traffic assignment: recent advances and new theories towards real time applications and realistic travel behaviour," in *New Developments in Transport Planning*. Edward Elgar Publishing, 2010.
- [231] Y. Wang and S. Boyd, "Fast model predictive control using online optimization," *IEEE Transactions on Control Systems Technology*, vol. 18, no. 2, pp. 267–278, 2010.
- [232] F. V. Webster, "Traffic signal settings," Road Research Laboratory, London, United Kingdom, Tech. Rep. 30, 1958.
- [233] M. A. Wicks, P. Peleties, and R. A. DeCarlo, "Switched controller design for the quadratic stabilization of a pair of unstable linear systems," *European Journal of Control*, vol. 4, no. 2, pp. 140–147, 1998.

- [234] H. Williams, *Model Building in Mathematical Programming*. New York, USA: Wiley, 1993.
- [235] H. Yang, B. Jiang, and V. Cocquempot, "A survey of results and perspective on stabilization of switched nonlinear systems with unstable modes," *Nonlinear Analysis: Hybrid Systems*, vol. 13, no. 2, pp. 45–60, 2014.
- [236] H. Yang, B. Jiang, and H. Zhang, "Stabilization of non-minimum phase switched nonlinear systems with application to multi-agent systems," *Systems & Control Letters*, vol. 61, no. 10, pp. 1023–1031, 2012.
- [237] T. Yoshii, Y. Yonezawa, and R. Kitamura, "Evaluation of an area metering control method using the macroscopic fundamental diagram," in *Proceedings of the 12th World Conference of Transportation Research*, Lisbon, Portugal, 2010, pp. 1–12.
- [238] I. Yperman, *The Link Transmission Model for Dynamic Network Loading*. Leuven, Belgium: Ph.D. dissertation, Katholieke Universiteit Leuven, 2007.
- [239] I. Yperman, S. Logghe, C. M. Tampère, and B. Immers, "The multi-commodity link transmission model for dynamic network loading," in *Proceedings of the 85th Annual Meeting of the Transportation Research Board*, no. 06-1062, Washington DC, USA, 2006, pp. 1–24.
- [240] E. Yurtseven, W. Heemels, and M. Camlibel, "Disturbance decoupling of switched linear systems," *Systems & Control Letters*, vol. 61, no. 1, pp. 69–78, 2012.
- [241] S. Zegeye, B. De Schutter, J. Hellendoorn, E. Breunese, and A. Hegyi, "A predictive traffic controller for sustainable mobility using parameterized control policies," *IEEE Transactions on Intelligent Transportation Systems*, vol. 13, no. 3, pp. 1420–1429, 2012.
- [242] J. Zhang, Z. Han, F. Zhu, and J. Huang, "Stability and stabilization of positive switched systems with mode-dependent average dwell time," *Nonlinear Analysis: Hybrid Systems*, vol. 9, no. 8, pp. 42–55, 2013.
- [243] X. Zhang, Y. Gao, and Z.-Q. Xia, "Stabilization of switched systems with polytopic uncertainties via composite quadratic functions," *Nonlinear Analysis: Hybrid Systems*, vol. 11, pp. 71–83, 2014.
- [244] J. Zhao and G. Dimirovski, "Quadratic stability of a class of switched nonlinear systems," *IEEE Transactions on Automatic Control*, vol. 49, no. 4, pp. 574–578, 2004.
- [245] J. Zhao and D. J. Hill, "On stability, L_2 -gain and H_∞ control for switched systems," *Automatica*, vol. 44, no. 5, pp. 1220–1232, 2008.

SUMMARY

In this thesis, we develop optimal and robust control techniques for hybrid systems. The thesis has two main parts, 1) traffic flow modeling and design of predictive control schemes for large-scale freeway and urban networks, 2) stability analysis and robust stabilization of switched nonlinear systems.

In the first part, we focus on traffic flow modeling and control from a macroscopic point of view. For freeway networks, we extend the recently developed Link Transmission Model for on-ramp metering and for variable speed limit control. For urban networks, we propose a high-level hybrid multi-region model. In this modeling framework, an urban network is partitioned into multiple subnetworks and it is controlled by limiting the flows of vehicles between subnetworks and moreover, by switching between signal timing plans of intersections inside each subnetwork. Using the proposed models in the freeway and urban traffic frameworks, we develop model predictive control (MPC) schemes in order to attenuate congestion and to decrease the total travel times. Since the obtained models are nonlinear and hybrid in the sense that both continuous and discrete dynamics exist in the model, suitable approximation techniques are proposed in order to transform the models into systems of linear equations and inequalities with mixed real and integer variables. Utilizing the transformed models, we formulate mixed integer linear optimization problems and integrate them in the MPC framework. Finally, as the last main contribution of the first part, we provide a solution for the problem of route guidance in large-scale urban networks. Utilizing another high-level multi-region model, we propose a bi-level optimal dynamic route guidance scheme in which we aggregate the origins and destinations in the entire network towards regional-based origin-destinations. At the higher level, optimal regional routes are determined based on the predictions provided by the multi-region model. At the lower level, the local controllers realize the optimal routes obtained from the higher level by altering the split fractions of vehicles traveling between neighboring regions. Overall, the obtained results regarding freeway and urban network control and route guidance show considerable performance and computational efficiency of the proposed schemes.

In the second part of the thesis, we investigate the stability analysis and the design of robust stabilizing controllers for switched nonlinear systems. As a connection to first part, the hybrid traffic flow models developed before can be also interpreted as switched systems. A switched nonlinear system comprises of several nonlinear dynamical subsystems and a switching signal that orchestrates the switching between subsystems. In this part of the thesis, we present three main contributions for stability analysis and stabilization of switched nonlinear systems. First, we propose a robust H_∞ switching controller for switched system with constrained control input. Next, for switched systems with nonlinear functions bounded in asymmetric sector bounds, we present stability analysis under arbitrary switching with average dwell time and furthermore, we formulate the design of robust stabilizing switching laws as an optimization problem that can be solved using a line search method along with a convex optimization algorithm. As

the last main contribution, we propose methods on stabilization and robust control for a general class of switched systems that can be approximated by switched affine systems with mixed controlled and autonomous switching behavior. We present two approaches for the design of robust stabilizing switching laws with a trade-off between computational effort and conservatism. As for the design procedure, we develop bi-level optimization problems that can be solved using line search methods along with convex optimization algorithms. Furthermore, we provide sufficient conditions for stabilizing the original switched nonlinear system using the proposed switching schemes. To evaluate the performance of all control schemes proposed in this part of the thesis, we present several case studies. Overall, the major advantages of the proposed robust switching control approaches are the efficiency in obtaining the parameters of controllers using convex optimization algorithms, and also fast and real-time control, which is crucial for our particular traffic applications.

SAMENVATTING

In dit proefschrift ontwikkelen we optimale en robuuste regeltechnieken voor hybride systemen. Het proefschrift bestaat uit twee hoofdbestanddelen, 1) het modeleren van verkeersstromen en het ontwerp van voorspellende regelaars voor grootschalige snelweg- en stedelijke netwerken, 2) stabiliteitsanalyse en robuuste stabilisatie van schakelende niet-lineaire systemen.

In het eerste deel leggen we de focus op het modeleren en regelen van de verkeersstromen vanuit een macroscopisch oogpunt. Voor snelwegnetwerken breiden we het recent ontwikkelde *Link Transmission Model* uit met toeritdosering en met variabele snelheidslimieten. Voor stedelijke netwerken stellen we een hoog-niveau hybride multi-regio model voor. In dit modelleringskader is een stedelijk netwerk verdeeld in verschillende subnetwerken en wordt het geregeld door het beperken van de stromen van voertuigen tussen de subnetwerken alsmede door het schakelen tussen tijdsplanningen van verkeerslichten op kruispunten binnen elk subnetwerk. Door gebruik te maken van de voorgestelde modellen voor snelweg- en stedelijk verkeer, ontwikkelen we modelgebaseerde voorspellende regeling (in het Engels: Model Predictive Control (MPC)) schema's met als doel files te verminderen en de totale reistijden te verkorten. Doordat de verworven modellen niet-lineair en hybride zijn, in de zin dat continue en discrete dynamica deel uitmaken van het model, worden er geschik benaderingsmethodes voorgesteld met als doel de modellen om te zetten in systemen met lineaire vergelijkingen en ongelijkheden met reële en gehele variabelen. Gebruikmakend van de benaderende modellen formuleren we lineaire problemen met reële en gehele variabelen en integreren die in het MPC kader. De laatste bijdrage van het eerste deel is de oplossing die we voorstellen voor het probleem van routegeleiding in grootschalige stedelijke netwerken. Gebruikmakend van een hoog-niveau multi-regio model stellen we een twee-laags optimaal dynamisch routegeleidingsconcept voor waarin we de herkomsten en bestemmingen in het gehele netwerk vertalen naar herkomsten en bestemmingen op regioniveau. Op hoger niveau worden de optimale regionale routes bepaald aan de hand van de voorspellingen geleverd door het multi-regio model. Op lager niveau realiseren de lokale regelaars de optimale routes die bepaald zijn op het hogere niveau door het aanpassen van de verdeling van de fracties van de voertuigen tussen aangrenzende regio's. Met betrekking tot de regeling van snelweg- en stedelijke netwerken en de routegeleiding tonen over het geheel genomen de behaalde resultaten de zeer goede prestaties en de rekenkundige efficiëntie van de voorgestelde methodes aan.

In het tweede deel van dit proefschrift onderzoeken we de stabiliteitsanalyse en het ontwerp van robuuste stabiliserende regelaars voor schakelende niet-lineaire systemen. Het verband met het eerste deel van het proefschrift bestaat eruit dat de hybride verkeersstroommodellen die daar ontwikkeld zijn gezien kunnen worden als geschakeld systemen. Een geschakeld niet-lineair systeem bestaat uit verschillende niet-lineaire dynamische deelsystemen en een schakelsignaal dat het schakelen tussen deelsystemen orkestreert. In dit deel van het proefschrift presenteren we drie belangrijke bij-

dragen aan de stabiliteitsanalyse en stabilisatie van schakelende niet-lineaire systemen. Als eerste stellen we een robuuste H_∞ schakelende regelaar voor schakelende systemen met een begrensde regelingang voor. Daarna stellen we, voor schakelende systemen met niet-lineaire functies begrensd door asymmetrische sectorgrenzen, stabiliteitsanalyses voor willekeurige schakelgedrag met een gemiddelde verblijftijd voor en verder formuleren we het ontwerp van robuuste stabiliserende schakelregels als een optimalisatie probleem dat kan worden opgelost door gebruik te maken van een lijnzoekmethode in combinatie met een convex optimalisatie-algoritme. Als laatste bijdrage stellen we methodes voor voor de stabilisatie en robuuste regeling van een algemene groep schakelende systemen die benaderd kan worden door schakelende affine systemen met een mengeling van geregeld en autonoom schakelend gedrag. We presenteren twee methodes voor het ontwerp van robuuste stabiliserende schakelregels met een afweging tussen rekenkundige inspanning en conservatisme. Als ontwerpprocedure ontwikkelen we twee-laags optimalisatieproblemen die opgelost kunnen worden met bisectiezoekmethodes in combinatie met convexe optimalisatie-algoritmes. Bovendien geven we voldoende voorwaarden voor de stabilisatie van het originele schakelende niet-lineaire systeem gebruikmakend van de voorgestelde schakelmethodes. Om de prestaties van alle, in dit deel van het proefschrift voorgestelde regeltechniekmethodes te evalueren presenteren we een aantal casussen. Over het geheel genomen zijn de grootste voordelen van de voorgestelde robuust schakelende regelmethodes de efficiëntie in het bepalen van de parameters van de regelaars door gebruik te maken van convexe optimalisatie-algoritmes, en ook de snelle en in reële tijd uitvoerbare regeling, wat van cruciaal belang is in de door ons beschouwde verkeerstoepassingen.

LIST OF PUBLICATIONS

JOURNAL ARTICLES

1. M. Hajiahmadi, B. De Schutter, H. Hellendoorn. *Stabilization and Robust H_∞ Control for Sector-bounded Switched Nonlinear Systems*, Automatica 50(10), pp. 2726–2731, 2014.
2. M. Hajiahmadi, J. Haddad, B. De Schutter, N. Geroliminis. *Optimal Hybrid Perimeter and Switching Plans Control for Urban Traffic Networks*, IEEE Transactions on Control Systems Technology, 23(2), pp. 464–478, 2015.
3. M. Hajiahmadi, B. De Schutter, H. Hellendoorn. *Stabilization and Robust H_∞ Control for Mixed Switching Affine Systems*, IEEE Transactions on Automatic Control, accepted, 2015.
4. M. Hajiahmadi, G. S. van de Weg, C. Tampère, R. Corthout, A. Hegyi, B. De Schutter, H. Hellendoorn. *Integrated Predictive Control of Freeway Networks Using the Extended Link Transmission Model*, IEEE Transactions on Intelligent Transportation Systems, accepted, 2015.
5. M. Hajiahmadi, R. Corthout, C. Tampère, B. De Schutter, H. Hellendoorn. *Variable Speed Limits Control Based on the Extended Link Transmission Model*, Transportation Research Record 2390(1), pp. 11–19, 2013.
6. M. Hajiahmadi, B. De Schutter, H. Hellendoorn. *Robust Switching Control Strategies for High-level Urban Networks Control*, International Journal of Robust and Nonlinear Control, submitted, 2014.
7. M. Hajiahmadi, V. L. Knoop, B. De Schutter, H. Hellendoorn. *Optimal Dynamic Route Guidance for Large-scale Urban Networks*, IEEE Transactions on Intelligent Transportation Systems, submitted, 2015.

CONFERENCE PAPERS

1. M. Hajiahmadi, B. De Schutter, H. Hellendoorn. *Robust H_∞ Control of a Class of Switched Nonlinear Systems with Application to Macroscopic Urban Traffic Control*, in Proceedings of the 53rd IEEE Conference on Decision and Control, pp. 1727–1732, Los Angeles, California, USA, Dec. 2014.
2. H. Majid, M. Hajiahmadi, B. De Schutter, H. Abouaissa, D. Jolly. *Distributed Model Predictive Control of Freeway Networks: A Serial Partially Cooperative Approach*, in Proceedings of the 17th IEEE Conference on Intelligent Transportation Systems, pp. 1876–1881, Qingdao, China, Oct. 2014.
3. M. Hajiahmadi, B. De Schutter, H. Hellendoorn. *Robust H_∞ Control for Switched Nonlinear Systems with Application to High-level Urban Traffic Control*, in Proceedings of the 52nd IEEE Conference on Decision and Control, pp. 899–904, Florence, Italy, Dec. 2013.

4. M. Hajiahmadi, V. L. Knoop, B. De Schutter, H. Hellendoorn. *Optimal Dynamic Route Guidance: A Model Predictive Approach Using the Macroscopic Fundamental Diagram*, in Proceedings of the 16th IEEE Conference on Intelligent Transportation Systems, pp. 1022–1028, The Hague, The Netherlands, Oct. 2013.
5. M. Hajiahmadi, J. Haddad, B. De Schutter, N. Geroliminis. *Optimal Hybrid Macroscopic Traffic Control for Urban Regions: Perimeter and Switching Signal Plans Controllers*, in Proceedings of the 12th European Control Conference, pp. 3000–3005, Zürich, Switzerland, July 2013.
6. M. Hajiahmadi, R. Corthout, C. Tampère, B. De Schutter, H. Hellendoorn. *Variable Speed Limits Control Based on the Extended Link Transmission Model*, in Proceedings of the 92nd Annual Meeting of the Transportation Research Board, paper 13-0409, Washington, DC, USA, Jan. 2013.
7. M. Hajiahmadi, B. De Schutter, H. Hellendoorn. *Model Predictive Traffic Control: A Mixed-logical Dynamic Approach Based on the Link Transmission Model*, in Proceedings of the 13th IFAC Symposium on Control in Transportation Systems, pp. 144–149, Sofia, Bulgaria, Sep. 2012.
8. M. Rinaldi, L. Capisani, A. Ferrara, A. Nunez, M. Hajiahmadi, B. De Schutter. *Distributed Identification of the Cell Transmission Traffic Model: A Case Study*, in Proceedings of the American Control Conference, pp. 6545–6550, Montréal, Canada, June 2012.

CURRICULUM VITÆ

Mohammad Hajiahmadi was born on November 22, 1985 in Isfahan, Iran. He finished his pre-university education at the National Organization for Development of Exceptional Talents (NODET) in Iran. In 2008, Mohammad obtained the BSc degree in Electrical Engineering at Isfahan University of Technology, Isfahan, Iran with honors. Next, he got admitted to the MSc program of the Electrical Engineering Department of Amirkabir University of Technology (Tehran Polytechnic), Tehran, Iran and he obtained his MSc degree in 2011.

Since May 2011, Mohammad has been employed as a PhD candidate at the Delft Center for Systems and Control, Delft University of Technology, under the supervision of Prof. De Schutter and Prof. Hans Hellendoorn. At the end of his first year, he obtained the certificate of the Dutch Institute of Systems and Control (DISC). His research has been focused on developing efficient optimal and robust control strategies for hybrid and switched systems with application to control of large-scale traffic networks. During his PhD program, he had the opportunity to visit the Urban Transport Systems Laboratory of École Polytechnique Fédéral de Lausanne and collaborate with Prof. Nikolas Geroliminis and Dr. Jack Haddad. Moreover, he had several short visits to the group of Prof. Chris M.J. Tampère at the Katholieke Universiteit Leuven.

